

RADIATION DAMAGE IN INORGANIC SOLIDS  
- SPECTROSCOPIC INVESTIGATIONS OF  
STRUCTURE AND MECHANISM

by

R. S. EACHUS

A Thesis submitted to the University of Leicester  
for the Degree of Doctor of Philosophy  
in the Faculty of Science  
April 1969

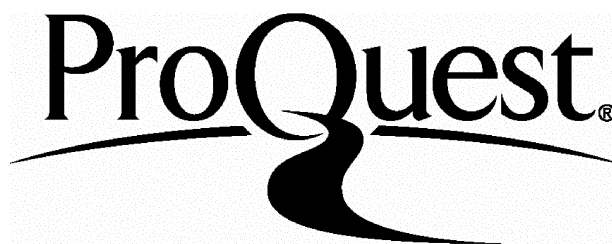
ProQuest Number: U622482

All rights reserved

INFORMATION TO ALL USERS

The quality of this reproduction is dependent upon the quality of the copy submitted.

In the unlikely event that the author did not send a complete manuscript and there are missing pages, these will be noted. Also, if material had to be removed, a note will indicate the deletion.



ProQuest U622482

Published by ProQuest LLC(2015). Copyright of the Dissertation is held by the Author.

All rights reserved.

This work is protected against unauthorized copying under Title 17, United States Code.  
Microform Edition © ProQuest LLC.

ProQuest LLC  
789 East Eisenhower Parkway  
P.O. Box 1346  
Ann Arbor, MI 48106-1346

X753012110

*Thesis*

*361521*

*2-10-1969*

*X. The author*



STATEMENT

The work described in this thesis was carried out by the author in the Department of Chemistry of the University of Leicester during the period October 1966 to April 1969.

No part of this thesis is concurrently being submitted for any other degree.

*R. S. Eachus.*

April, 1969.

TO MY PARENTS

## ACKNOWLEDGEMENTS

I should like to record my gratitude to the many people who have helped to make this thesis possible.

To Professor M.C.R. Symons for his constant help and guidance throughout the course of this work.

To Mr. J.A. Brivati for his assistance in matters of instrumentation.

To Dr. S. Subramanian with whom the work outlined in Part II was carried out jointly.

To Dr. D.J.A. Tinling for many helpful discussions and his constructive criticism after reading the manuscript.

To the Science Research Council for financial support.

Finally, I would also like to thank my wife for her constant moral support and for preparing the typescript.

-----

## ABSTRACT

### PART I

A number of interesting inorganic radicals have been prepared by exposing polycrystalline materials doped with suitable anions to high energy radiation.

The species  $(\text{NaH})^+$ ,  $\text{BO}_3^{2-}$ ,  $\text{NO}_3^{2-}$ ,  $\text{ClO}_3^{2-}$ , and  $\text{ClO}_4^{2-}$  are discussed in detail in Chapters III, IV and V. The data derived from their ESR and electronic spectra are used both as an aid in identification and as a probe of their electronic and molecular structures.

### PART II

The magnetic and optical properties of six paramagnetic species ( $\text{ClO}_3$ ,  $\text{ClO}_3^{2-}$ ,  $\text{ClO}_2$ ,  $(\text{Cl}-\text{ClO}_2)^-$ ,  $\text{Cl}_2^-$  and  $\text{O}_3^-$ ), produced by the  $\gamma$ -irradiation of  $\text{KClO}_3$ , are discussed in detail in Chapter VI. Their configurations in the chlorate lattice are deduced, and a tentative mechanism for radiation damage in  $\text{KClO}_3$  is formulated.

There is substantial evidence for the existence of the free radical  $\text{ClOO}$  from kinetic studies in the gas phase. Chapter III describes how this species was isolated in  $\text{KClO}_4$  and frozen 90%  $\text{H}_2\text{SO}_4$  matrices from the UV-photolysis of trapped  $\text{ClO}_2$  radicals. In these environments the 'peroxy-chlorine' species slowly isomerises back to  $\text{ClO}_2$  and a

mechanism for this interconversion process is suggested.

### PART III

Trapped silver atoms are known to be formed when glasses containing argentous ions are exposed to high energy radiation. In Chapter VIII A we outline the identification of several inequivalent silver-containing centres, including trapped silver atoms,  $\text{AgH}^+$  cations and aquated silver atoms, in frozen aqueous  $\text{H}_2\text{SO}_4$  and show how the natures of the radiolysis products were dependent upon the acid concentration of the matrix. Furthermore, the species  $(\text{AgOR})^+$  have been detected in irradiated alcoholic solutions containing  $\text{Ag}^+$  ions.

The thermally initiated decomposition of these silver radicals has been followed by ESR and optical spectroscopy in Chapters VIII B. In both acid and alcoholic environments, radical annihilation must proceed via aggregation and the polynuclear species  $\text{Ag}_2^+$ ,  $(\text{Ag}_2\text{H})^{2+}$  and  $\text{Ag}_4^{n+}$  have been identified as intermediates in this process.

Wherever possible the cadmium analogues of the silver radicals have been prepared to facilitate a comparison of their magnetic properties and structures.

## CONTENTS

### CHAPTER I

#### General Introduction

A. Aspects of Electron Spin Resonance Spectroscopy .. .. .	2
B. Instrumentation .. .. .	13

### PART I

#### STABILISED RADICALS IN PRECIPITATED POWDERS

### CHAPTER II

<u>Introduction to Part I</u>	18
-------------------------------	----

### CHAPTER III

#### The Alkali Metal Ion - Hydrogen Atom Centre in Barium Sulphate

Experimental Procedure .. .. .	23
Discussion .. .. .	27
Mechanism of Formation .. .. .	35

### CHAPTER IV

#### Tetra-Atomic Oxides and Oxyions of the Non-Metals

Experimental Procedure .. .. .	37
<u>Section A</u> - The $\text{BO}_3^{2-}$ Anion and Related Species with 23 Valence-Electrons	
Experimental Results .. .. .	38

Discussion .. .. .	45
Mechanism of Formation .. .. .	55
<u>Section B</u> - The $\text{NO}_3^{2-}$ Anion and Related Species with 25 Valence-Electrons	
Experimental Results .. .. .	57
Discussion .. .. .	60
Mechanism of Radiation Damage in Nitrate-Doped Calcite .. .. .	70
<u>Section C</u> - The 27 Valence-Electron Species $\text{ClO}_3^{2-}$	
Experimental Results .. .. .	70
Discussion .. .. .	74
Mechanism of Radiation Damage .. .. .	81

CHAPTER V

The 33 Valence-Electron  $\text{ClO}_4^{2-}$  Anion and Related  
Species

Experimental Procedure and Results .. .. .	83
Discussion .. .. .	87
Mechanism of Formation .. .. .	103

PART II

SPECTROSCOPIC INVESTIGATIONS OF RADIATION DAMAGE IN  
 $\text{KClO}_3$  and  $\text{KClO}_4$

CHAPTER VI

Radiation Damage in Potassium Chlorate

Experimental Procedure	..	..	..	..	..	107
Experimental Results	..	..	..	..	..	111
Discussion	..	..	..	..	..	139
Mechanism of Radiation Damage in $KClO_3$	..	..				163

## CHAPTER VII

### Radiation Damage in Potassium Perchlorate

Experimental Procedure	..	..	..	..	..	170
Experimental Results	..	..	..	..	..	175
Discussion	..	..	..	..	..	196
Aspects of Radiation Damage in $KClO_4$	..	..				210

## PART III

### TRAPPED SILVER AND CADMIUM RADICALS IN GLASSY MATRICES

## CHAPTER VIII

### Section A - The Matrix Isolation of Silver and Cadmium Species in Unusual Valency States

Experimental Procedure	..	..	..	..	..	216
Experimental Results	..	..	..	..	..	218
Discussion	..	..	..	..	..	239
Mechanism of Formation	..	..	..	..	..	261

### Section B - Polynuclear Silver and Cadmium Species in Alcoholic and Aqueous Acid Glasses

Experimental Results	..	..	..	..	..	264
Discussion	..	..	..	..	..	282

REFERENCES	..	..	..	..	..	294
------------	----	----	----	----	----	-----

CHAPTER I

GENERAL INTRODUCTION

## GENERAL INTRODUCTION

This thesis is a detailed report of a research project in which the electron spin resonance (ESR) technique has been applied to the problem of identifying radicals which remain trapped in a variety of inorganic crystalline and amorphous solids after they have been produced by exposing the materials to high energy radiation ( $\gamma$ -rays). Three main objectives formed the basis for this investigation:-

a) To prepare specific radicals by the irradiation of suitable host materials doped with diamagnetic impurity anions, these radicals having been chosen to test some of the predictions of the "Molecular Orbital" and "Valence Bond" theories.

In Part I we illustrate how the unpaired electron can act as a probe of a radical's electronic structure and geometry, and how the wealth of information obtained from its ESR spectrum may be utilised.

b) To monitor the radiation-induced chemical decomposition of crystalline inorganic solids.

In general, the products of radiation damage trapped in inorganic materials lie in a limited number of precisely defined orientations which are

related by the crystal symmetry. In Part II information about the nature and orientation of the radiolysis products in  $\text{KClO}_3$  and  $\text{KClO}_4$  is coupled with a certain amount of chemical expectation so that general conclusions can be drawn regarding the mechanism of radiation damage in these materials.

c) To employ high energy radiation for the preparation of paramagnetic atoms and mono-, di- and polymeric cations in frozen mineral acid and alcoholic solvents.

In Part III we show how, in these vitreous matrices, the unpaired electron probes the environment of the radical-product, which is essentially that of the parent cation.

#### A. ASPECTS OF ELECTRON SPIN RESONANCE SPECTROSCOPY

Because of the publication of several recent comprehensive reviews,<sup>1-10</sup> no attempt will be made in this introductory section to outline the fundamental theory underlying the ESR experiment. Furthermore, we are not concerned here with the many interpretive problems involved in the analysis of complex ESR spectra, for these have been treated in depth elsewhere.<sup>11</sup> Instead, a brief review is given of the methods involved in the extrac-

tion of structural information from the spin-resonance parameters of inorganic radicals.

1. The Evaluation of the Principal Values of the g- and A-Tensors

a) From single-crystal studies

The ESR spectrum of a radical trapped in an arbitrary orientation, with respect to the applied magnetic field direction, in an irradiated single crystal can be described by the following spin-Hamiltonian

$$\begin{aligned} \mathcal{H} = & \beta (g_{xx} H_x S_x + g_{yy} H_y S_y + g_{zz} H_z S_z) \\ & + a_{xx} I_x S_x + a_{yy} I_y S_y + a_{zz} I_z S_z \quad \dots\dots(1) \end{aligned}$$

where  $(g_{xx}, g_{yy}, g_{zz})$  and  $(a_{xx}, a_{yy}, a_{zz})$  are the principal values of the g- and A-tensors, and  $S_x, I_x, H_x$  refer to the x-components of the electron spin operator, nuclear spin operator and the magnetic field. The symbol  $\beta$  represents the Bohr magneton. When the ESR experiment is performed using a single crystal, it is usual to rotate the crystal in turn about three mutually perpendicular axes. The principal values of both the g- and A-tensors and their direction cosines relative to the

crystal axes can then be deduced from the observed angular variations of the  $g$ - and  $A$ -factors. Detailed descriptions of the techniques involved and convenient methods of processing the experimental information are given by Geusic and Brown,<sup>12</sup> Pryce,<sup>13</sup> Weil and Anderson,<sup>14</sup> and Schonland.<sup>15</sup> The method used to evaluate the spin-resonance data included in Chapters VI and VII for radicals trapped in  $KClO_3$  and  $KClO_4$  follows closely that of Schonland, and has been fully described elsewhere.<sup>16</sup>

b) From powder spectra

Studies of radicals in single crystals are invariably lengthy and tedious, and when the primary object of the investigation is the identification of trapped paramagnetic species the procedure is not always necessary. It is generally more convenient, and certainly much simpler, to study the radicals randomly oriented in polycrystalline and glassy materials. Under these conditions the pertinent spin-resonance information can be derived by a comparison of the observed ESR spectrum with a number of theoretical line shapes computed for commonly occurring conditions. For example, Figure I.1A shows the ESR spectrum ascribed to nitrogen dioxide trapped in a polycrystalline sample of  $\gamma$ -irradiated  $NaNO_3$ . The ESR parameters of the  $NO_2$  radical can readily be deduced from a comparison of this

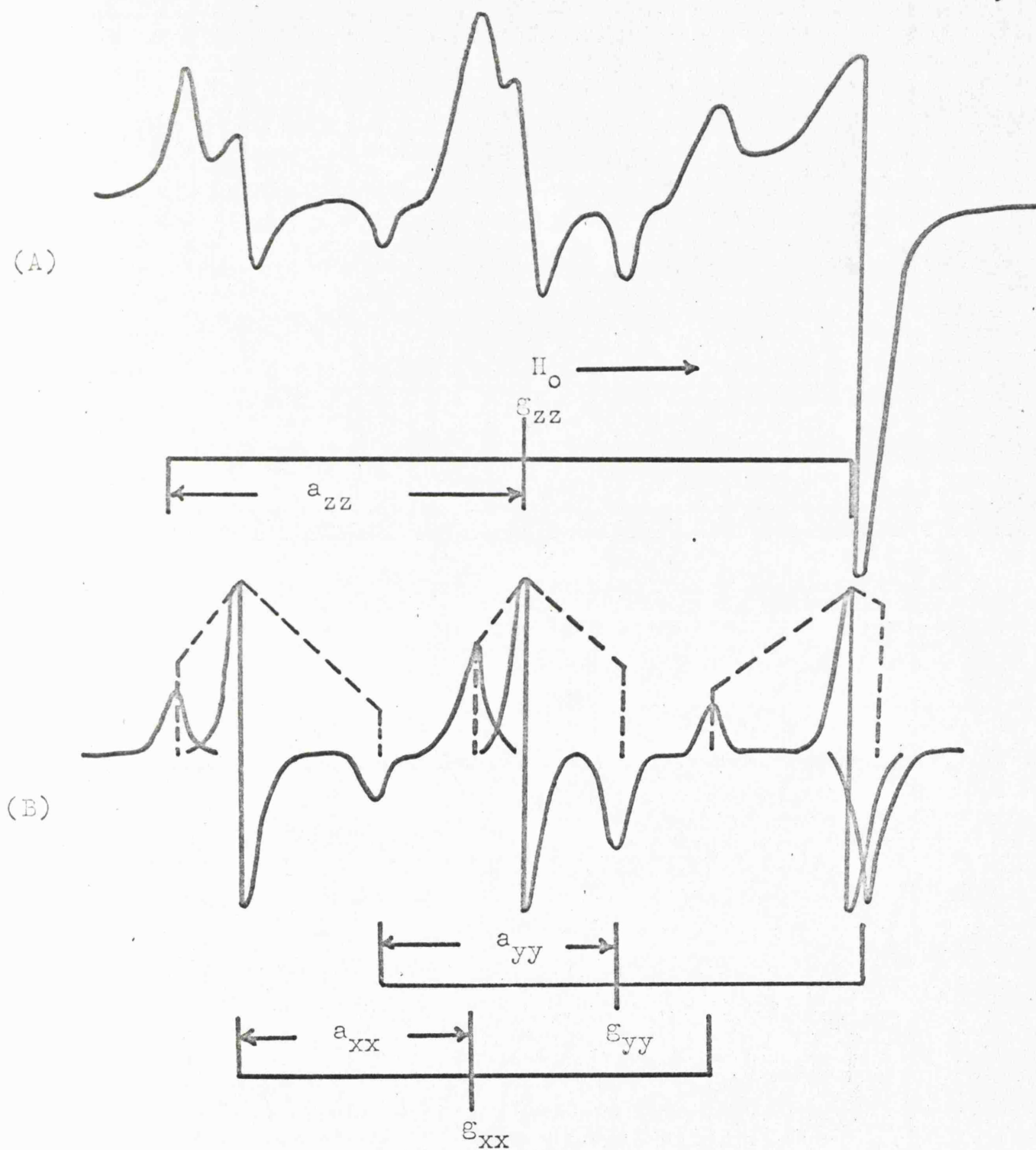


Figure I.1. (A) The experimental ESR spectrum of  $\text{NO}_2$  in polycrystalline  $\text{NaNO}_3$  for comparison with (B) The theoretical ESR line shape for a species containing a single magnetic nucleus ( $I = 1$ ) and possessing anisotropic  $g$ - and  $A$ -tensors.

spectrum with the theoretical line shape (Figure I.1B) for a species containing a single interacting magnetic nucleus ( $I = 1$ ) and possessing completely anisotropic g- and A-tensors.<sup>17</sup>

Although the evaluation of the experimental spin-resonance parameters from a study of single crystals is generally more satisfactory, pitfalls in analysis do occur, particularly when there are several magnetically non-equivalent trapping sites in the crystal unit cell. In these circumstances, the data derived from powder measurements act as a useful check on the interpretation of the single-crystal results.

## 2. Information from the Hyperfine Tensor

The experimental tensor ( $a_{xx}, a_{yy}, a_{zz}$ ) representing the total hyperfine interaction between the unpaired electron and a given nucleus may be resolved into isotropic and anisotropic components as follows

$$\begin{vmatrix} a_{xx} \\ a_{yy} \\ a_{zz} \end{vmatrix} = A_{iso} \begin{vmatrix} 1 \\ 1 \\ 1 \end{vmatrix} + \begin{vmatrix} B_{xx} \\ B_{yy} \\ B_{zz} \end{vmatrix} \dots\dots(2)$$

### a) The isotropic hyperfine tensor

The isotropic part of the hyperfine tensor stems

solely from the presence of unpaired electron spin-density at the nucleus. This can arise in one of three ways

- i) from spin-density directly in an ns-orbital,
  - ii) from a configurational interaction which admixes excited states with appreciable s-character into a ground-state which has no s-orbital contribution,
- or iii) from polarisation of inner s-electrons by unpaired electron density in outer s-, p-, d- or f-orbitals.

The hyperfine coupling between an electron in an ns-orbital and the nucleus at the centre of that orbital is given by

$$A_{\text{iso}} = a_{\text{ns}}^2 \left( \frac{8\pi}{3} \right) g_N \beta_N |\psi_{\text{ns}}(0)|^2 \text{ gauss} \quad \dots\dots(3)$$

where  $a_{\text{ns}}^2$  is the spin-population of the ns-orbital and  $\psi_{\text{ns}}(0)$  is the value of the ns-wavefunction at the nucleus. Thus, we can estimate the orbital population of the ns-orbital ( $a_{\text{ns}}^2$ ) quite simply from a comparison of the experimental ( $A_{\text{iso}}$ ) value with the theoretical value ( $A_{\text{iso}}^0$ ) calculated from an atomic wavefunction for an electron occupying the ns-orbital.

It is convenient to classify radicals as  $\sigma$  or  $\pi$ , the

major distinction being that in the former there is a direct contribution from an s atomic orbital to the molecular orbital containing the unpaired electron, resulting in an appreciable isotropic hyperfine coupling.<sup>18</sup> In contrast, for  $\pi$ -radicals there is usually only a small residual isotropic coupling which arises from spin-polarisation of valence electrons, particularly those involved in  $\sigma$ -bonding.

b) The anisotropic hyperfine tensor

If d-orbitals are assumed not to contribute appreciably to the molecular orbital containing the unpaired electron, then by analogous arguments to those outlined above, the anisotropic component of the hyperfine tensor may lead directly to the np-orbital population. (This neglect of d-orbital involvement may not be justified, however, except, of course, for radicals of the first row elements).

The contribution of unpaired spin in a p-orbital to the anisotropic hyperfine tensor when the external field is applied along the symmetry axis is given by the expression

$$2B = a_{np}^2 \left(\frac{4}{5}\right) g_N \beta_N \langle r^{-3} \rangle_{np} \text{ gauss} \quad \dots\dots(4)$$

where  $\langle r^{-3} \rangle_{np}$  is the average value of  $r^{-3}$ , r being the

distance of the nucleus from the electron in the np-orbital, and  $a_{np}^2$  is the electronic population of the orbital. We can estimate  $a_{np}^2$  from a comparison of the experimental  $2B$  value with the theoretical value ( $2B^0$ ), calculated from the free-atom value of  $\langle r^{-3} \rangle$  and taking  $a_{np}^2$  as unity.

Anisotropic couplings of an order of magnitude smaller than those stemming directly from np-density can arise from the dipolar coupling of a magnetic nucleus and an unpaired electron in an orbital on a neighbouring atom. When the distance between the unpaired electron and the interacting nucleus is greater than  $1.5\text{\AA}$  these indirect couplings can be satisfactorily estimated, to first-order, by a simple point-dipole approximation. However, when this separation approaches  $1.5\text{\AA}$  it is necessary to use the more realistic approach of McConnell and Strathdee.<sup>19</sup>

Thus, the isotropic and anisotropic components of the hyperfine tensor, representing the interaction of the unpaired electron with a single magnetic nucleus, can yield estimates of both the s- and p-character of the molecular orbital of the electron at that nucleus (provided that d-orbital contributions to this molecular orbital are neglected). It is now possible to deduce the

hybridisation ratio  $\lambda$  (where  $\lambda^2 = a_p^2/a_s^2$ ) which is related to the bond angles in certain radicals through Coulson's orthogonality relationships.<sup>20</sup> Values of bond angles calculated from spin-resonance data generally agree well with those obtained by more conventional techniques, which is indeed remarkable in view of the drastic assumptions involved in the method of population analysis that we have outlined.

The relevant parameters ( $|\Psi_{ns}(0)|^2$ ,  $\langle r^{-3} \rangle_{np}$ ,  $A_{iso}^0$  and  $2B^0$ ) required for the assessment of orbital population for a variety of atoms are collated in Table I.1.

### 3. Information from the g-tensor

Although the hyperfine coupling tensor is the most helpful piece of information derived from an ESR spectrum, the g-tensor is also informative. Anisotropy in g-tensors is often readily detected in the ESR experiment and reflects the incomplete quenching of the orbital motion of the unpaired electron. This residual orbital angular momentum results from a mixing of the molecular orbital containing the unpaired electron with other molecular orbitals. Consequently, the g-factor in an arbitrary direction may be greater or less than the free-spin value (2.0023) for, in general, there are competing excited states that can combine with the ground state of

TABLE I.1. Atomic Parameters and Nuclear Hyperfine Coupling Constants <sup>a</sup>

Nucleus	Natural Abundance %	Spin (I)	$ \Psi_{ns}(0) ^2$ (a.u.)	$\langle r^{-3} \rangle_{np}$ (a.u.)	$A_{iso}^0$ (gauss)	$2B^0$	Ref.
<sup>1</sup> H	99.984	1/2	-	-	508	-	23
<sup>2</sup> H	0.0156	1	-	-	78	-	23
<sup>10</sup> B	18.83	3	-	-	242	13	24
<sup>11</sup> B	81.17	3/2	1.408 (2s)	0.775 (2p)	725	38	24
<sup>13</sup> C	1.108	1/2	2.767 (2s)	1.692 (2p)	1130	66	24
<sup>14</sup> N	99.635	1	4.770 (2s)	3.101 (2p)	552	34	24
<sup>19</sup> F	100	1/2	11.966 (2s)	7.546 (2p)	17,200	1084	24
<sup>23</sup> Na	100	3/2	-	-	317	-	23
<sup>31</sup> P	100	1/2	5.625 (3s)	3.319 (3p)	3636	206	25

TABLE I.1. (Continued)

$^{33}\text{S}$	0.74	3/2	7.919 (3s)	4.814 (3p)	975	56	25
$^{35}\text{Cl}$	75.4	3/2	10.644 (3s)	6.710 (3p)	1680	100	25
$^{37}\text{Cl}$	24.6	3/2	-	-	1395	84	25
$^{39}\text{K}$	93.08	3/2	-	-	83	-	23
$^{41}\text{K}$	6.91	3/2	-	-	45	-	23
$^{43}\text{Ca}$	0.13	7/2	-	-	-	-	-
$^{75}\text{As}$	100	3/2	12.5606 (4s)	6.9871 (4p)	3430	183	26
$^{107}\text{Ag}$	51.90	1/2	-	-	612	-	22
$^{109}\text{Ag}$	48.10	1/2	-	-	706	-	22
$^{111}\text{Cd}$	12.86	1/2	-	-	5137	-	27
$^{113}\text{Cd}$	12.34	1/2	-	-	5374	-	$27\frac{1}{2}$

a. The values of  $|\psi_{ns}(0)|^2$  and  $\langle r^{-3} \rangle_{np}$  are those calculated by Morton et.al. from the wavefunctions of the authors in the references.

the radical. Those which involve the excitation of the magnetic electron to an outer vacant level give a negative contribution, and those which involve excitation of an inner electron into the half-filled orbital give a positive contribution to the g-factor. Hence, the g-tensor gives us valuable information about the symmetry of the radical and the proximity of magnetically coupled excited states. A more detailed exposition of these points is given in reference 11.

## B. INSTRUMENTATION

### 1. Electron Spin Resonance Measurements

The electron spin resonance spectra, at 9.3 Gc/s, of polycrystalline and glassy samples were obtained using a commercial X-band Varian V4502-03 high resolution spectrometer with 100 kc/s field modulation. The method employed for the calibration of the magnetic field has been described in detail elsewhere,<sup>21</sup> and the estimated accuracy of the g-values and hyperfine coupling constants measured in this way are  $\pm 0.0004$  (in 2.0000) and  $\pm 0.03$  gauss respectively. Measurements at 77°K were made with the paramagnetic samples immersed in liquid nitrogen in a quartz Dewar which could be inserted directly into the spectrometer cavity. Measurements at temperatures between 77° and 295°K were made using a variable-temperature

accessory designed and constructed in these laboratories; the absolute temperature of the sample could be controlled within  $\pm 0.5^\circ\text{K}$ . Spectra at  $4.2^\circ\text{K}$  were obtained employing a Varian V4545B liquid helium accessory and superheterodyne detection. Powder spectra were occasionally measured at 34.0 Gc/s on a Q-band spectrometer which employed superheterodyne detection. Single-crystal spectra at  $77^\circ$  and  $295^\circ\text{K}$  were obtained on an X-band spectrometer on which the magnetic field was calibrated against a proton NMR magnetometer. Both of these instruments have been fully described elsewhere.<sup>21,22</sup>

Measurements at 3.1 Gc/s were carried out on an S-band spectrometer which incorporated a three port circulator, one arm of which was connected to an E.M.I. reflex klystron which had a power output of 150 mW. This arm also included an attenuator for varying the power and a wavemeter for measuring the microwave frequency. The second arm of the circulator was connected to the spectrometer cavity via a matching variable impedance, and the third arm was coupled to the crystal detector. . 100 kc/s modulation of the magnetic field was used to sample the slope of the electron resonance absorption line. The rectangular cavity oscillated in the  $H_{013}$  mode and the 100 kc/s modulation was introduced internally by means of

two single-turn coils positioned in a Helmholtz configuration for maximum homogeneity.

The D.C. magnetic-field was provided by a Newport Instruments Type A electromagnet with 4-in pole pieces fitted with 7-in pole tips, The maximum field available was 3,500 gauss. The magnetic field was non-linear with current because of the saturation of the magnetic yoke and was therefore, monitored with a Hall probe the output from which straddled the X-axis of an XY-recorder. Consequently the chart was linear with field. The signal from the crystal detector was amplified at 100 kc/s, phase-sensitive detected, passed through a noise filter and finally fed into the recorder.

To increase the sensitivity of the spectrometer a 64 channel averaging computer was available. For measurements at 77°K samples were immersed in liquid nitrogen in a quartz Dewar which could be directly inserted into the cavity, and for measurements within the range 140° to 450°K a variable-temperature accessory incorporating a tungsten resistance thermometer was used.

All of these spectrometers, except the first, were designed and constructed by Mr. J.A. Brivati.

## 2. Optical Absorption Measurements

Electronic spectra within the range 50,000 - 8,000  $\text{cm}^{-1}$

were measured on a Unicam SP700 'Double-Beam' Recording Spectrophotometer. The optical spectra of vitreous samples between 77°K and room temperature were obtained using a variable-temperature cell which was designed and constructed in these laboratories. The absolute temperature of the sample was monitored with a precalibrated copper-constantan thermocouple with direct digital readout.

Single-crystal optical absorption studies were carried out with the crystals mounted in an adjustable sample-holder, and the optimum conditions for the measurement of spectra were obtained using a variable iris-attenuator placed in the reference beam of the spectrophotometer.

### 3. Reflectance Spectra

The diffuse and total reflectance spectra of finely powdered materials were obtained using a Beckman DK2A Ratio Recording Spectrophotometer with 24500 Reflectance Photometer Attachment. All Spectra were measured at room temperature against a reference sample of lithium fluoride or magnesium oxide.

### 4. Infra-red Spectra

A Perkin Elmer 225 grating infra-red spectrophotometer with a low temperature accessory was used for the measurement of IR spectra of frozen solutions.

## 5. Methods of Irradiation

Irradiations with  $^{60}\text{Co}$   $\gamma$ -rays were carried out in a 'Gammacell-200' supplied by Atomic Energy of Canada Ltd., which produced an effective dose rate of approximately 0.15 Mrads per hour. Irradiations at  $77^\circ\text{K}$  were accomplished with the samples immersed in liquid nitrogen in a pyrex Dewar which was designed to fit close to the radiation source. Photolysis with  $3650\text{\AA}$  radiation was carried out with a high-pressure mercury arc lamp, and photolysis at  $77^\circ\text{K}$  was accomplished by placing the sample in a quartz tail-piece of a Dewar filled with liquid nitrogen.

PART I

STABILISED RADICALS IN PRECIPITATED POWDERS

CHAPTER II

INTRODUCTION TO PART I

## INTRODUCTION TO PART I

In Part I of this thesis we report the preparation of some interesting inorganic radicals by  $\gamma$ -irradiation of polycrystalline matrices containing impurity ions. These doped powders were produced by coprecipitating the microcomponent with a large excess of a suitable host material, particularly calcium carbonate or barium sulphate. The ESR and electronic spectra of such radicals were used both as an aid to their identification and as a probe into their electronic structure and geometry.

The initial act in the radiation damage of inorganic diamagnetic solids is commonly electron ejection. If the ejected 'conduction' electron is trapped in some manner at a distance from the parent cation, and if the latter distorts to inhibit hole migration, then paramagnetic species result and can often be studied by ESR. In general these 'centres' are stable only at low temperatures and readily decompose when the substrate is annealed. In the absence of impurity or defect sites the electron and the hole-centre may recombine to produce an excited parent molecule which often decomposes before it has time to drop to the ground state. A suitable impurity ion at a lattice site in the solid can act as a competing trapping site for the electron, and the result-

ing radical may have a high thermal stability. This stability will be enhanced if the configuration and charge of the paramagnetic impurity centre are compatible with the host lattice. For example, as we shall see later, the most stable oxyanion radicals trapped in an  $M^{II}XO_3$  lattice are almost certain to have the  $XO_3^{2-}$  structure.

The coprecipitation technique has several substantial advantages over conventional methods of obtaining dilute solid-solutions of the impurity ions that are precursors to tri-, tetra- and penta-atomic radicals in ionic crystals. In particular, one can often coprecipitate either salts that do not form mixed crystals with the host when grown by slow evaporation from solution, or salts that decompose at elevated temperatures obviating melt-growth techniques. A fundamental understanding of the coprecipitation phenomenon is necessary before it is possible to anticipate which impurity ions will be incorporated into a particular precipitated matrix. We begin, therefore, with a brief review of those factors which influence this process.<sup>29</sup>

#### COPRECIPITATION

Coprecipitation of an impurity with the host material probably occurs either by the adsorption of the microcomponent onto the host or by the formation of a solid solution.

The concentration of the microcomponent is determined by:

a) The relative sizes and charges of the coprecipitant and host lattice ions.

A low concentration of coprecipitant ions will occur if their inclusion in the host necessitates a significant lattice distortion. This distortion may be relieved however, if the impurity ions aggregate to form neutral molecules or clusters within the matrix.

b) The structural relationship between the host lattice and the coprecipitant salt.

The highest concentrations of impurity ions are obtained when the materials are isomorphous. This also seems to indicate that molecular units rather than individual ions are incorporated into the host lattice.

The rapid direct mixing of reagents in high concentration to form precipitates is the least reproducible method of inducing coprecipitation. However, this method does have the advantage that it often leads to a loss of selectivity by the host, and a concomitant increase in concentration of impurity ions. The solid state diffusion process may then be sufficiently rapid to render the solid

phase homogeneous, the rate of diffusion increasing markedly when the precipitate is annealed close to its melting point. When the substrate forms as a colloidal precipitate, impurity ions in the solution can be adsorbed onto the solid surface. These foreign ions may then be incorporated into the substrate lattice, mainly at the 'inner' surface of each precipitate particle. This mechanism is particularly important because coprecipitation may occur with the formation of an adsorption compound even though the microcomponent ions are structurally incompatible with the host lattice.

There is no apparent reason why liquids should not be coprecipitated with solids, and indeed solvent molecules have been found in close association with the host lattice (a) as part of the solvation structure in the normal crystal lattice, (b) as part of the crystal structure, (c) incorporated with the coprecipitated foreign ions, and (d) occluded and entrapped at microscopic sites.

For the following reasons we have used calcium carbonate (calcite) and barium sulphate extensively as host matrices for the coprecipitation of impurity ions.

- a) Both salts form as colloidal precipitates from aqueous media at temperatures close to the boiling

points of the solutions. Thus impurity ions whose structure may not be compatible with either of these lattices may still be coprecipitated as adsorption compounds. If the powders are then annealed at high temperatures, ion diffusion occurs, rendering the solid phases homogeneous.

- b) Neither salt contains abundant magnetic nuclei (see Table I.1) so that there is no line broadening in the ESR spectra of trapped radicals through superhyperfine interactions with the matrix.
- c) Both salts are very insoluble in water.
- d) The ESR spectra of the radicals formed by the  $\gamma$ -irradiation of both pure  $\text{CaCO}_3$  and  $\text{BaSO}_4$  are relatively simple, consisting of broad featureless absorptions centred close to the free-spin g-factor. Consequently, they do not complicate the analysis of ESR spectra arising from trapped radicals.

CHAPTER III

THE ALKALI METAL ION - HYDROGEN ATOM CENTRE

IN BARIUM SULPHATE

## THE ALKALI METAL ION - HYDROGEN ATOM CENTRE IN BARIUM SULPHATE

The exposure of precipitated barium sulphate to  $\gamma$ -rays led to the formation of hydrogen atoms which were subsequently trapped at a variety of sites in the host lattice. One such trapped-atom centre, stable at 77°K, exhibited hyperfine coupling to a second nucleus.

### EXPERIMENTAL PROCEDURE

All reagents used were AnalaR grade purified further by recrystallisation from aqueous solution. Barium sulphate powders doped with impurity ions were prepared by precipitation at 370°K from aqueous solutions of barium chloride containing approximately 10% of the microcomponent salt, and the suspension was allowed to digest at 353°K overnight. Samples of the doped powder were dried at 420°K for 24 hours prior to their exposure to  $\gamma$ -radiation doses ranging from 0.5 to 30 Mrads, at both liquid nitrogen and room temperatures.

### EXPERIMENTAL RESULTS

When barium sulphate was precipitated from aqueous solutions containing sodium ions, and then vacuum dried, powdered, and  $\gamma$ -irradiated at 77°K, its ESR spectrum at this temperature and a microwave power level of 10 mW showed the presence of three paramagnetic defect centres

(Figure III.1). The most abundant radical, characterised by an intense featureless absorption centred close to the free-spin g-factor, also resulted when fused barium sulphate was  $\gamma$ -irradiated at 77°K. This centre probably originated from the radiation damage of sulphate anions. However, we were unable to detect hyperfine interactions involving  $^{33}\text{S}$  ( $^{33}\text{S}$ ;  $I = 3/2$ , 0.74% isotopic abundance) and therefore, could not unambiguously identify this species. We shall label this centre the "sulphate" radical for the purpose of this account. At 77°K and 100 mW, features from the "sulphate" radical and the second paramagnetic centre, labelled B in Figure III.1, were almost completely saturated whilst those of A, a pair of axially symmetric quartets (Figure III.2) separated by approximately 511 gauss, had increased both in resolution and intensity. An increase in concentration of radical A occurred when the barium sulphate was precipitated in the presence of singly charged anions such as nitrate, chlorate or perchlorate.

When potassium ions were incorporated into the sulphate lattice an analogous species to A was formed, but the hyperfine features from this centre were less well resolved and it was only possible to obtain

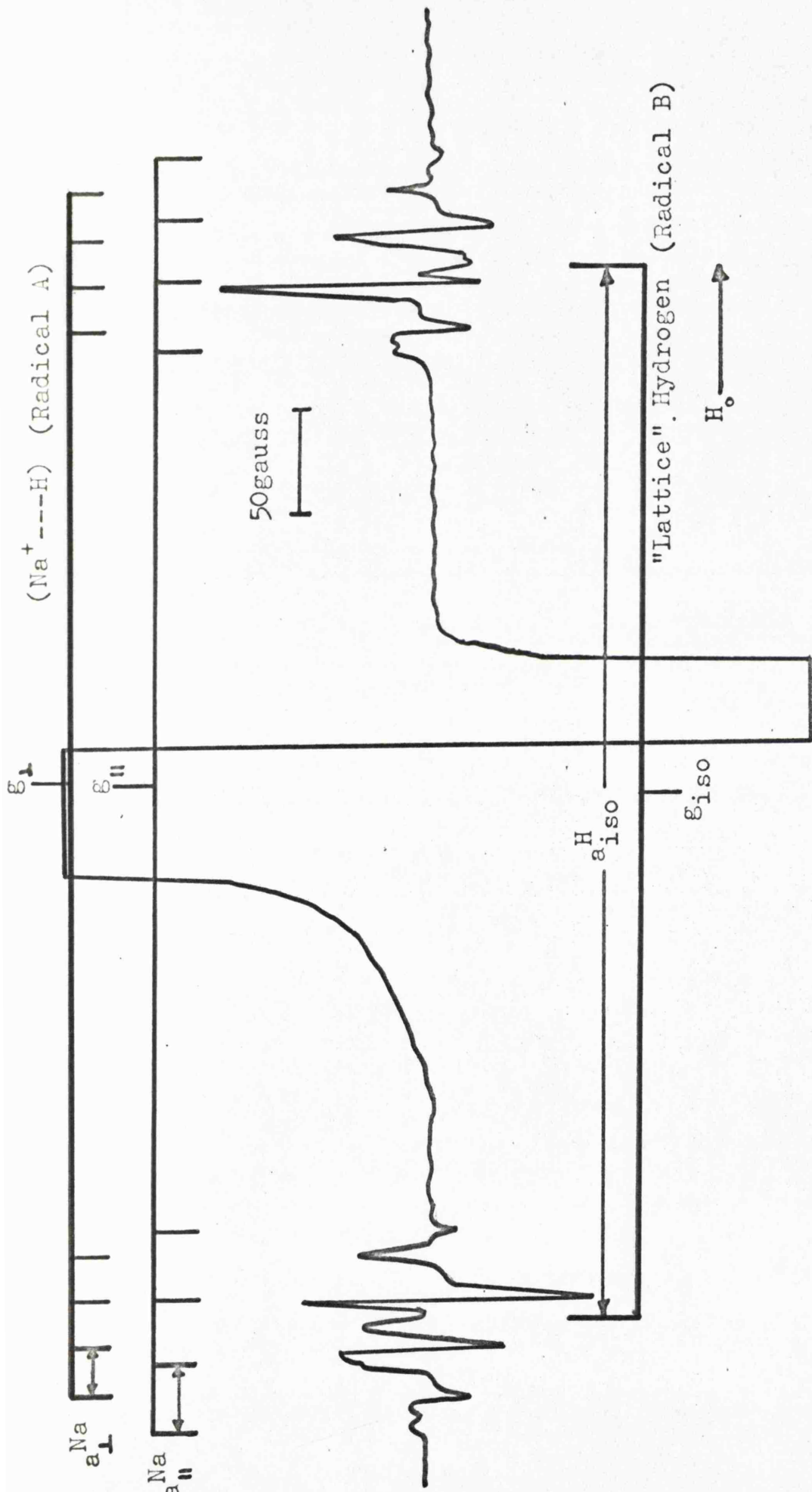


Figure III.1. The ESR spectrum of irradiated, precipitated  $\text{BaSO}_4$  measured at  $77^\circ\text{K}$ .

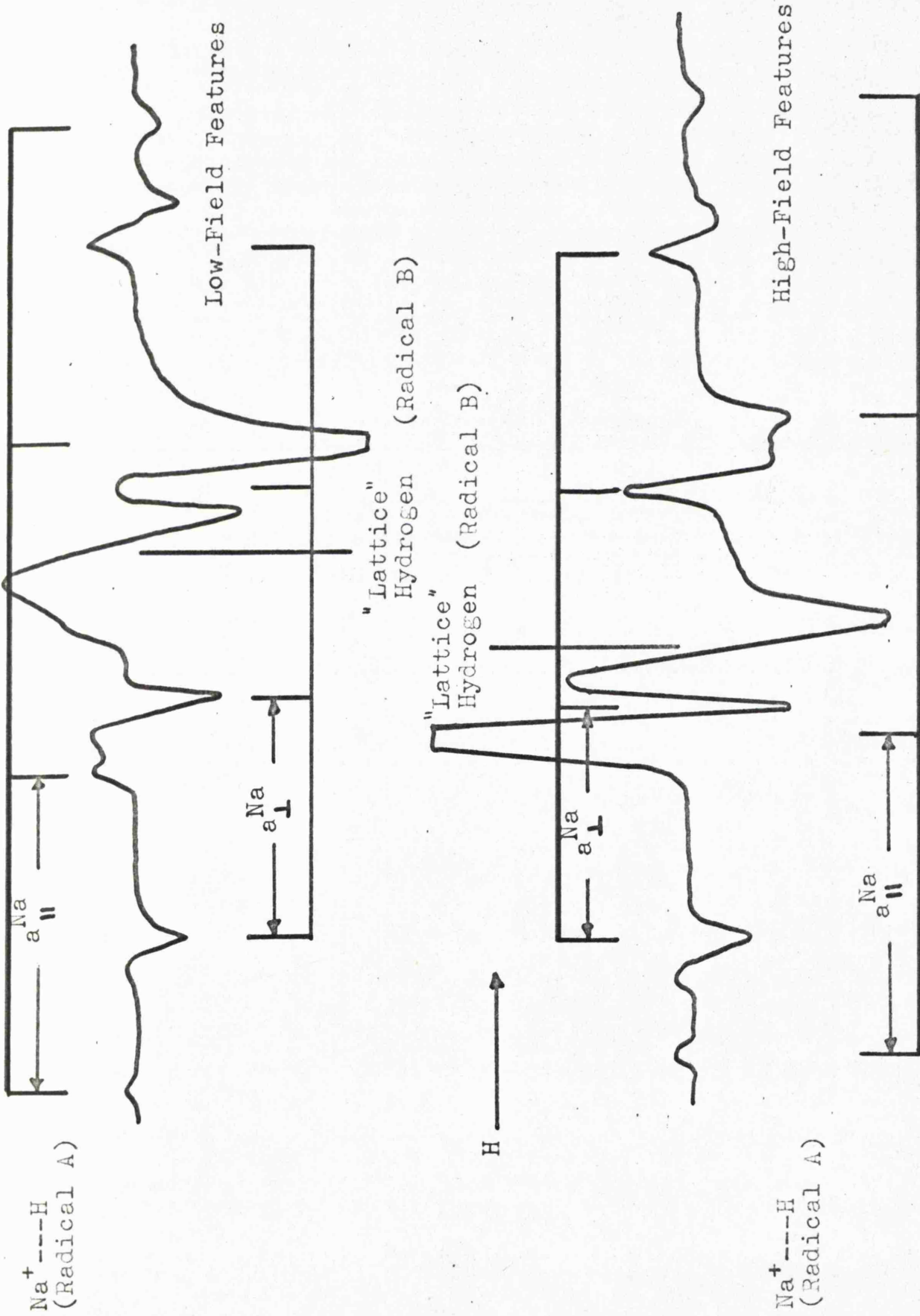


Figure III.2. The low-field and high-field components of the (Na<sup>+</sup>---H) and "lattice" hydrogen ESR spectra in BaSO<sub>4</sub> measured at 77°K

perpendicular hyperfine splitting constants from the outermost features of the quartets. Figure III.3 shows the ESR spectrum at 77°K and 100 mW of irradiated barium sulphate, precipitated by the addition of sodium sulphate solution to barium chloride in D<sub>2</sub>O. The original principal doublet splitting of 511 gauss of radical A has collapsed to a triplet of approximately 79 gauss separation.

Features from radical A decayed when the sample was annealed to about 220°K; there was a parallel increase in intensity of the ESR signal from B. Recooling to 77°K did not regenerate A.

## DISCUSSION

### 1. The Identification of Radical A

For the following reasons radical A is almost certainly the alkali metal ion - hydrogen atom adduct (Na<sup>+</sup>---H):

- a) The major doublet splitting of 511 gauss must arise from the interaction of the unpaired electron with a single proton (<sup>1</sup>H; I = ½, 99.98% isotopic abundance). Deuterium substitution resulted in the expected major triplet splitting of 79 gauss arising from the coupling of the unpaired electron with the <sup>2</sup>H nucleus (<sup>2</sup>H; I = 1).<sup>11</sup>

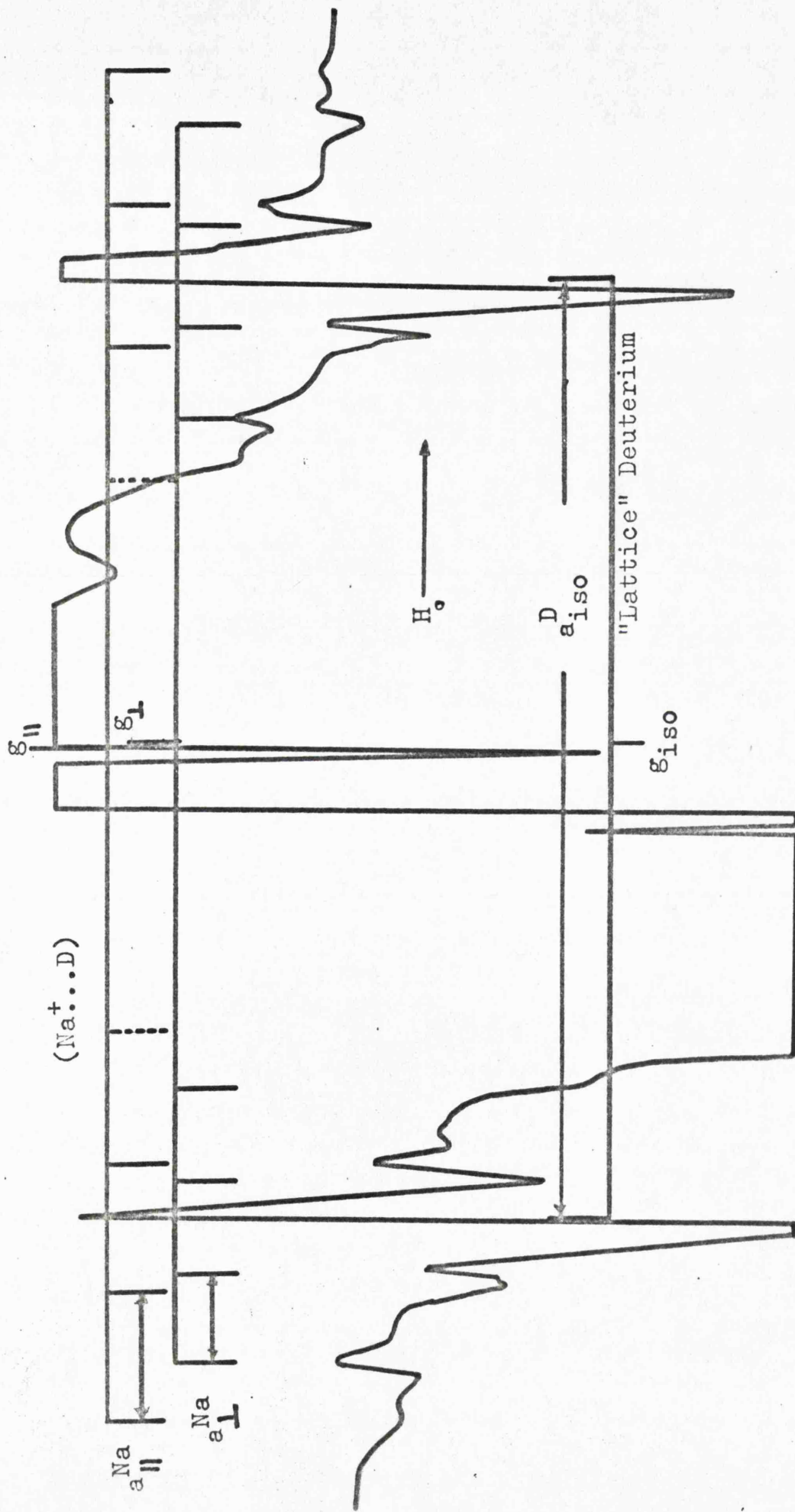


Figure III.2.

The ESR spectrum of the  $(Na^+ \dots D)$  and "Lattice" deuterium centres in  $BaSO_4$  measured at  $77^\circ K$  and 100 mW.

b) The secondary, axially symmetric splitting arises through hyperfine coupling to a  $\text{Na}^+$  ion. ( $^{23}\text{Na}$ ,  $I = 3/2$ , 100% isotopic abundance). A marked reduction in this subsidiary splitting occurred when potassium ions ( $^{39}\text{K}$ ;  $I = 3/2$ , 93.08% isotopic abundance) replaced  $\text{Na}^+$  ions in the sulphate lattice. This is not surprising in view of the smaller nuclear magnetic moment of potassium compared to sodium.<sup>11</sup> We have ruled out the possibility that this splitting arises through coupling to a  $^{35}\text{Cl}$  nucleus ( $I = 3/2$ , 74.6% isotopic abundance) of a chloride ion for two reasons. Firstly, we were unable to detect features arising from the corresponding  $^{37}\text{Cl}$  nucleus ( $I = 3/2$ , 24.6% isotopic abundance) and secondly, we obtained exactly the same ESR spectrum from an irradiated sample of barium sulphate precipitated from a solution of barium nitrate, in the complete absence of chloride. The low natural abundance of the magnetic  $^{135}\text{Ba}$ ,  $^{137}\text{Ba}$  nuclei ( $I = 3/2$ ; 6.6 and 11.3% isotopic abundance) makes it unlikely that these isotopes are responsible for this subsidiary interaction.

c) The intensity of the ESR spectrum of this

radical increased markedly when the sulphate was precipitated in the presence of anions such as  $\text{NO}_3^-$ ,  $\text{ClO}_3^-$  and  $\text{ClO}_4^-$ . In order to maintain charge neutrality the inclusion of singly charged anions into the sulphate lattice requires a concomitant increase in the concentration of sodium ions as impurity.

## 2. The Identification of Radical B

The ESR spectrum of radical B is characteristic of a species containing a single magnetic nucleus of spin  $\frac{1}{2}$ . It is not unreasonable to assume this species to be a hydrogen atom trapped at a barium or sulphate ion site in the lattice, labelled "lattice" hydrogen for convenience, since the spin-resonance parameters of this centre are similar to those reported for hydrogen atoms in the gas phase.<sup>30</sup> When the host lattice was precipitated from  $\text{D}_2\text{O}$ , radiation damage resulted in the formation of the corresponding trapped deuterium atom.

The results obtained for radicals A and B are included in Table III.1.

## 3. The Structure of the ( $\text{Na}^+ \text{---} \text{H}$ ) Centre

The alkali metal ion - hydrogen atom centre is thought to arise from the trapping of a hydrogen atom,

TABLE III.1. Electron Spin Resonance Parameters for the (Na<sup>+</sup>---H) Centre and Related Species.

Radical	$g_{\parallel}$	$g_{\perp}$	$g_{av}$	$B_{\parallel}$	$B_{\perp}$	$A_{iso}$	$B_{\parallel}$	$B_{\perp}$	$A_{iso}$	Hydrogen Hyperfine Splittings (in gauss)	$a_s^2$ on metal	Ref.
H atoms in the gas phase			2.00226									30
B "Lattice" Hydrogen centre in BaSO <sub>4</sub>			2.0015									c
A (Na <sup>+</sup> ---H)	2.0012	2.0013	2.0013	4.2	-2.1	17.2	+1.7	-0.8	511.5	0.054		c
(K <sup>+</sup> ---H) b.		2.0016				$a_{\perp}^K = 4.0$		$a_{\perp} \approx 500$		$\sim 0.05$		c
(Na <sup>+</sup> ---D) b.		2.0032				$a_{\perp}^{Na} = 16.2$		$a_{\perp}^D \approx 79$				c

a. Corrected to 2nd-order by application of the Breit-Rabi equation.<sup>58</sup>

b. Only the perpendicular features have been resolved.

c. This work.

if not at a sodium site itself, then at a barium or sulphate site close to a sodium ion.

The anisotropic hyperfine tensor representing the interaction of the unpaired electron with the single sodium nucleus must have the form  $(2B, -B, -B)$ . From a crude point-dipole approximation, assuming the distance between the interacting dipoles is a measure of the  $(\text{Na}^+ \text{---} \text{H})$  'bond length,' we calculate  $R$  in Figure III.4 to be  $1.5\text{\AA}$ . This can be compared to the bond length of  $1.8\text{\AA}$  for sodium hydride in the gas phase.<sup>30</sup> Since  $|A_{\parallel}^{\text{Na}}|$  is greater than  $|A_{\perp}^{\text{Na}}|$  and  $2B$  is necessarily positive, then  $A_{\text{iso}}^{\text{Na}}$  must be positive and almost certainly results from the direct delocalisation of the unpaired electron into the sodium  $3s$ -orbital, giving a spin-density of  $0.054$ . However, the proton coupling shows no evidence for such delocalisation, being, in fact, slightly greater than that of hydrogen atoms in the gas phase.<sup>30</sup> This apparently anomalous increase in the proton hyperfine coupling can be satisfactorily explained in terms of the theory proposed by Adrian<sup>31</sup>, and later developed by Jen and coworkers<sup>32</sup>, to account for the effect of the matrix upon the wavefunction's of trapped atoms. They suggest that the perturbation of the trapped atom wavefunction's by the matrix can be

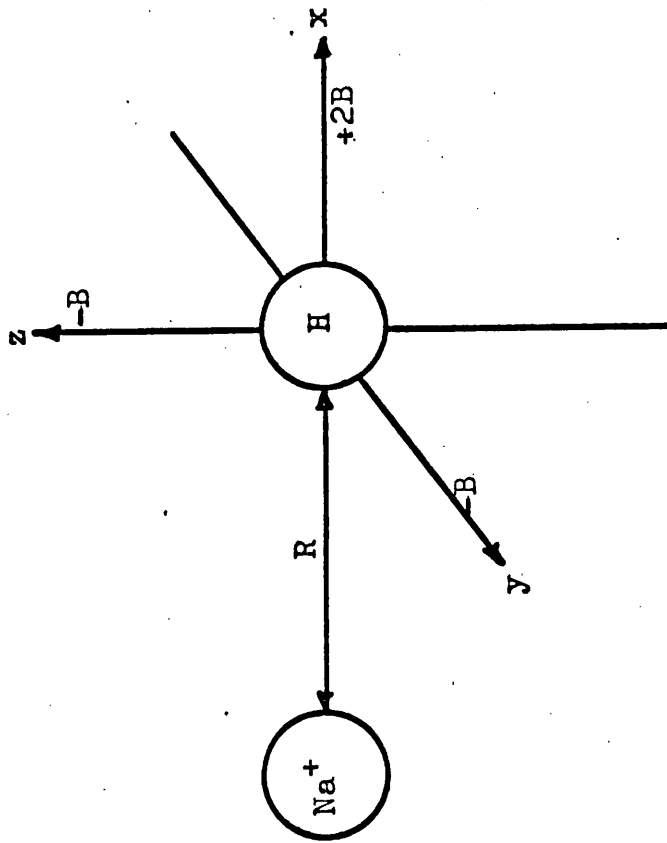


Figure III.4. The ( $\text{Na}^+ \text{---} \text{H}$ ) centre in a  $\text{BaSO}_4$  lattice.

envisaged as the sum of several opposing effects, principally:

- a) The van der Waal's (dispersion) forces between two interacting particles, which will tend to maximise the interaction energy by expanding the wavefunction's of the particles.
- b) Pauli exclusion forces, which operate when the particle separation is small, and which effectively result in a shrinkage of the wavefunction's of the interacting particles away from each other. This interaction will also admix some of the wavefunction's of the matrix particles with those of the trapped atom.

Hence, for the ( $\text{Na}^+ \text{---} \text{H}$ ) species, mechanism a) would lead to an overall reduction in the proton hyperfine coupling from the free atom value, whilst b) would give rise to an increased proton coupling and superhyperfine splitting from the 'matrix' sodium ion. The absolute magnitudes of g-value shifts brought about by such matrix perturbations are less readily predicted, but they must always be negative.<sup>11</sup> If our basic model of a hydrogen atom trapped at a distance of approximately  $1-2\text{\AA}$  from a sodium ion in the sulphate lattice is correct, then our experimental results

suggest that the effects of mechanism b) outweigh those of mechanism a).

#### 4. The Structure of the "Lattice" Hydrogen Centre

The ( $\text{Na}^+ \text{---H}$ ) centre was irreversibly converted to "lattice" hydrogen when the barium sulphate host lattice was annealed at  $220^\circ\text{K}$ , indicating the higher thermal stability of the latter centre. By analogy with the bonding scheme proposed for hydrogen atoms trapped at basic anion sites in a variety of irradiated phosphates,<sup>33</sup> we suggest that the proton of the "lattice" hydrogen centre forms a  $\sigma$ -bond to a basic oxygen of the sulphate anion. The extra electron is then accommodated in the corresponding  $\sigma^*$ -level. Since the  $\sigma$ -level is concentrated principally on oxygen the  $\sigma^*$ -level is mainly on hydrogen and therefore, the spin-resonance parameters for this centre closely resemble those of a free hydrogen atom.

#### MECHANISM OF FORMATION

To explain the formation of two inequivalent hydrogen species we have to propose the existence of two distinct and competing trapping sites in the sulphate lattice. X-ray studies of barium sulphate precipitated from aqueous solution have suggested that water coprecipitates with the salt and exists as a solid-solution in

the lattice, a group of three water molecules replacing a  $\text{BaSO}_4$  unit.<sup>34</sup> Analogously, alkali metal ions and solvent molecules may be concurrently coprecipitated if the size of the combined guest and solvate ion is appropriate. The lithium ion is known to carry one molecule of water into the precipitated sulphate lattice.<sup>35</sup>

If conduction electrons resulting from the radiation damage of the host lattice ions are subsequently trapped at defect sites containing an alkali metal ion and a water molecule, then there is a high probability that hydrogen atoms, formed on dissociative electron capture by  $\text{H}_2\text{O}$ , will be trapped at an alkali metal ion site. Alternatively, if these generated electrons are trapped at defect sites containing only coprecipitated solvent, then the resulting hydrogen atoms may be trapped at a sulphate anion site.

CHAPTER IV

TETRA-ATOMIC OXIDES AND OXYIONS OF THE NON-METALS

## TETRA-ATOMIC OXIDES AND OXYIONS OF THE NON-METALS

In this chapter we report the formation of a variety of tetra-atomic oxides and oxyanions of the first and second row elements when calcium carbonate powders doped with suitable impurity ions were exposed to high energy radiation. The radicals are classified according to the number of valence-electrons they possess.

We have assumed that the influence of the carbonate environment upon the properties of the trapped radicals is negligible and have compared their observed spin-resonance and molecular parameters with those of well-substantiated isoelectronic molecules and ions.

### EXPERIMENTAL PROCEDURE

Samples of calcium carbonate powders doped with suitable impurity ions were prepared by precipitation from aqueous solutions of AnalaR grade calcium chloride, containing approximately 10% of the microcomponent salt, at temperatures close to the boiling point of the solutions. Samples of the doped carbonate were dried at 420°K for 24 hours prior to their exposure to  $\gamma$ -radiation doses ranging from 0.5 to 30 Mrads.

Samples for diffuse reflectance measurements were powdered in a vibration-mill for several hours prior to

their irradiation.

## SECTION A

### THE $\text{BO}_3^{2-}$ ANION AND RELATED SPECIES WITH 23 VALENCE-ELECTRONS

#### EXPERIMENTAL RESULTS

##### 1. ESR Spectra

Exposure of calcite doped with borate ions to  $\gamma$ -radiation at 77°K resulted in the formation of the radicals  $\text{CO}_3^{3-}$  and  $\text{CO}_3^-$ .<sup>36</sup> On annealing, these radicals decayed with the subsequent formation of two further paramagnetic species, X and Y in Figure IV.1. Radical X was also formed when pure calcium carbonate was irradiated at room temperature and it has been previously identified as the  $\text{CO}_2^-$  radical-anion.<sup>37</sup> At 300°K and 10 mW microwave power the hyperfine features of Y were somewhat obscured by the intense g-features of the  $\text{CO}_2^-$  radical-ion, but it was possible to associate four broad lines ( $\Delta H_{\text{ms}} \cong 7$  gauss) with this centre. However, at 77°K and 100 mW microwave power considerable saturation of the ESR features from the  $\text{CO}_2^-$  centre occurred, whilst those of radical Y were considerably better resolved (see Figure IV.2). Under these conditions it was possible to analyse the ESR spectrum of Y in terms of a species having axially symmetric g- and A-tensors. Irradiation

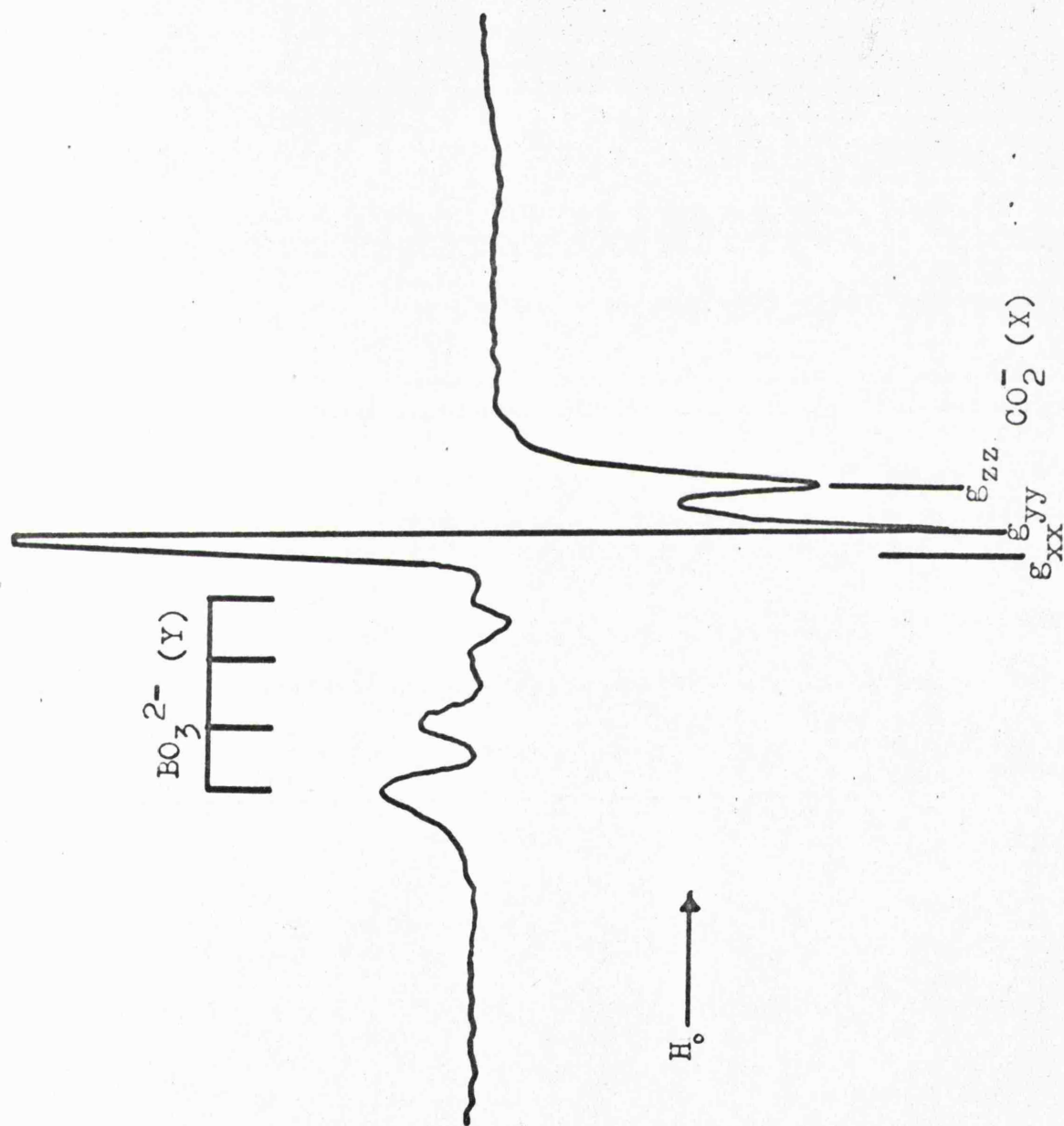


Figure IV.1. ESR spectrum of irradiated, borate-doped calcite measured at  $300^\circ\text{K}$  and 10 mW.

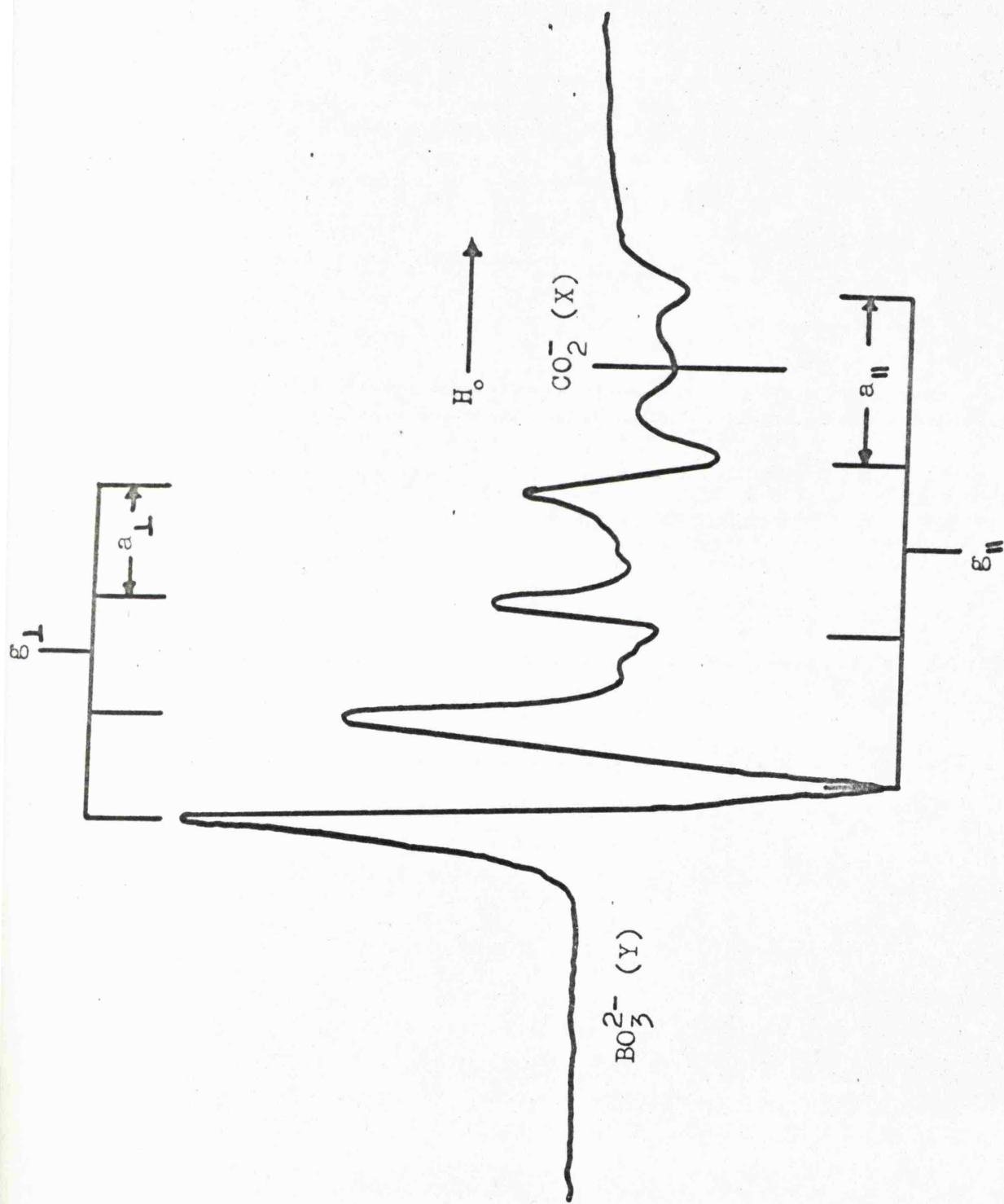


Figure IV.2. ESR spectrum of irradiated, borate-doped calcite measured at  $77^{\circ}\text{K}$  and 100 mW.

of calcite doped with both borate and nitrate resulted in the production of radical Y and  $\text{NO}_3^{2-38}$  (see Figure IV.3). The presence of nitrate impurity centres in calcite is known to inhibit the formation of the  $\text{CO}_2^-$  radical-anion (see Chapter IV.B). The spin-resonance features of the  $\text{NO}_3^{2-}|\text{CO}_3^{2-}|$  centre\* were completely saturated at high microwave power levels and low temperatures (Figure IV.4) therefore, we were able to confirm our analysis of the ESR spectrum of radical Y under these conditions without the ambiguity brought about by the presence of the  $\text{CO}_2^-$  anion. A further confirmation of our analysis was obtained by measuring the spectrum of radical Y at 8 mm wavelength. (Figure IV.5).

Radical Y was extremely stable in the calcite lattice and only decayed when the doped powder was heated to  $420^\circ\text{K}$  for several days. Precipitation of borate doped calcium carbonate from deuterium oxide did not affect the ESR spectrum of the radicals produced by  $\gamma$ -irradiation.

## 2. Electronic Spectra

The doped carbonate, which was deep blue after exposure to  $\gamma$ -rays, exhibited an intense asymmetric

\* The convention adopted in this and subsequent accounts will denote by  $\text{NO}_3^{2-}|\text{CO}_3^{2-}|$  a  $\text{NO}_3^{2-}$  ion occupying a normal carbonate ion position in carbonate crystals.

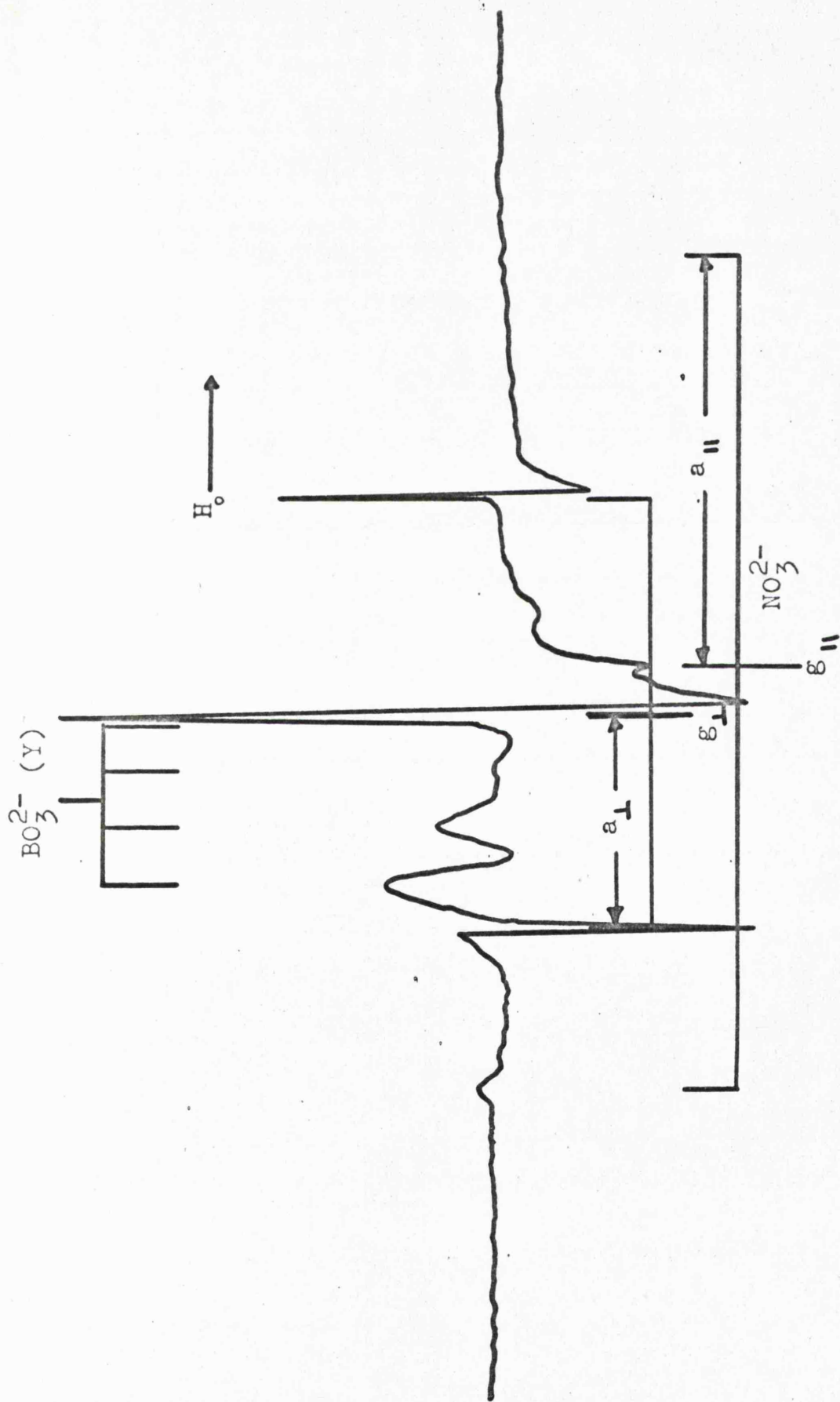


Figure IV.3. ESR spectrum of irradiated calcite doped with nitrate and borate measured at  $300^{\circ}\text{K}$  and 10 mW.

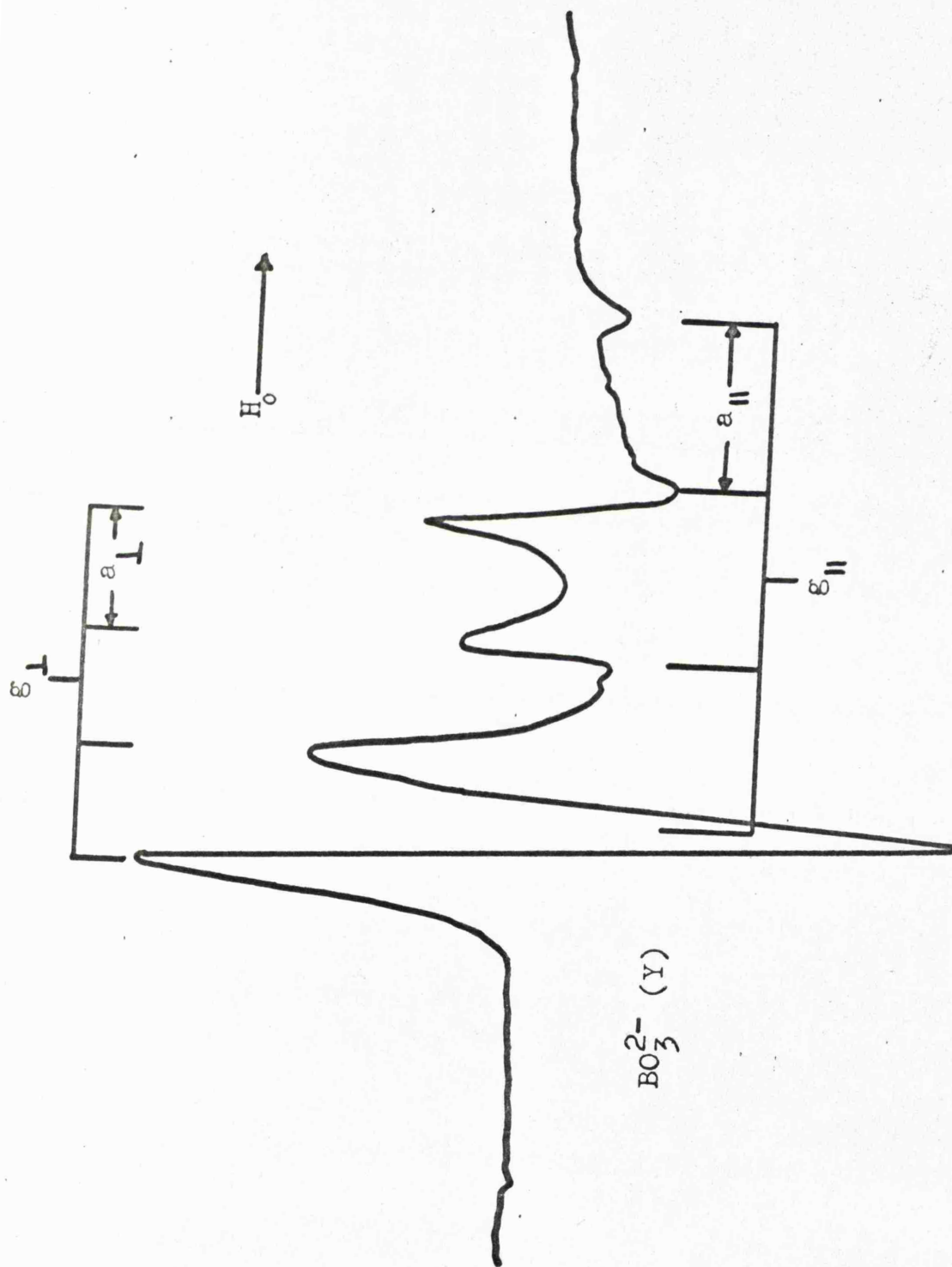


Figure IV.4. ESR spectrum of irradiated calcite doped with nitrate and borate measured at  $77^\circ\text{K}$  and 100 mW.

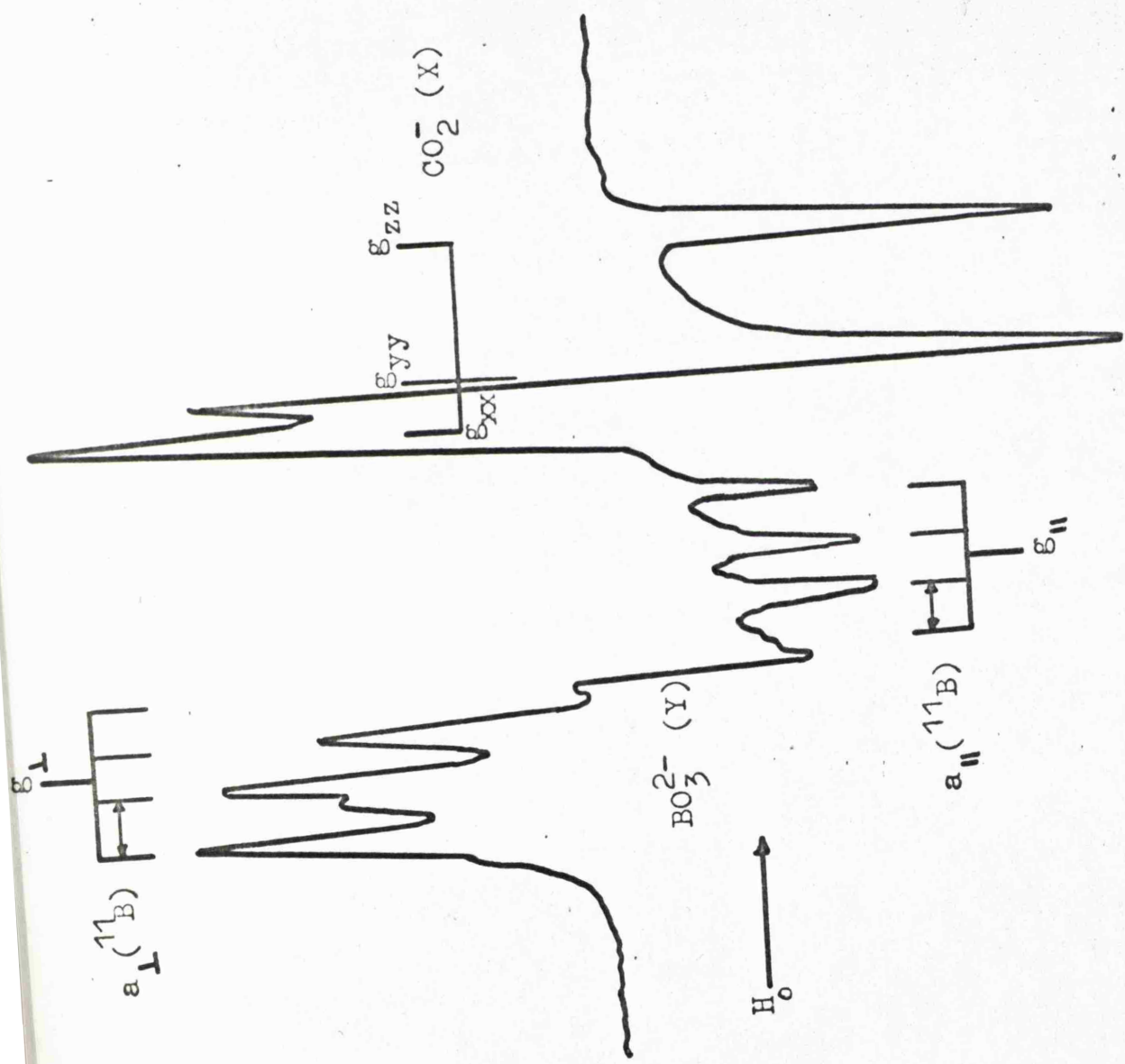


Figure IV.5.

ESR spectrum of borate-doped calcite measured at 300°K and 34 Gc/s.

absorption with a maximum intensity at approximately 630 nm ( $15,880 \text{ cm}^{-1}$ ) in the diffuse reflectance spectrum, measured at room temperature (see Figure IV.6). No such band developed in pure calcite upon irradiation and so we assign this absorption to radical Y.

## DISCUSSION

### 1. The Identification of Radical Y

There are several reasons for suggesting that radical Y, formed on irradiation of calcium carbonate doped with borate, is  $\text{BO}_3^{2-}$ .

a) The ESR spectrum of Y is characteristic of an axially symmetric species containing a single nucleus of spin  $3/2$ . It is not unreasonable to assume this nucleus to be  $^{11}\text{B}$  ( $I = 3/2$ ; 81.17% isotopic abundance). The spin-resonance lines for this centre are rather broad ( $\Delta H_{\text{ms}} \cong 7$  gauss) possibly due to the presence of unresolved hyperfine features from  $^{10}\text{B}$  nuclei ( $I = 3$ ; 18.83% isotopic abundance). The spin populations for the boron 2s- and 2p-orbitals can now be derived from the theoretical values for spin populations of unity. If we assume that both the parallel and perpendicular hyperfine coupling constants have the same sign, this gives values of 0.014

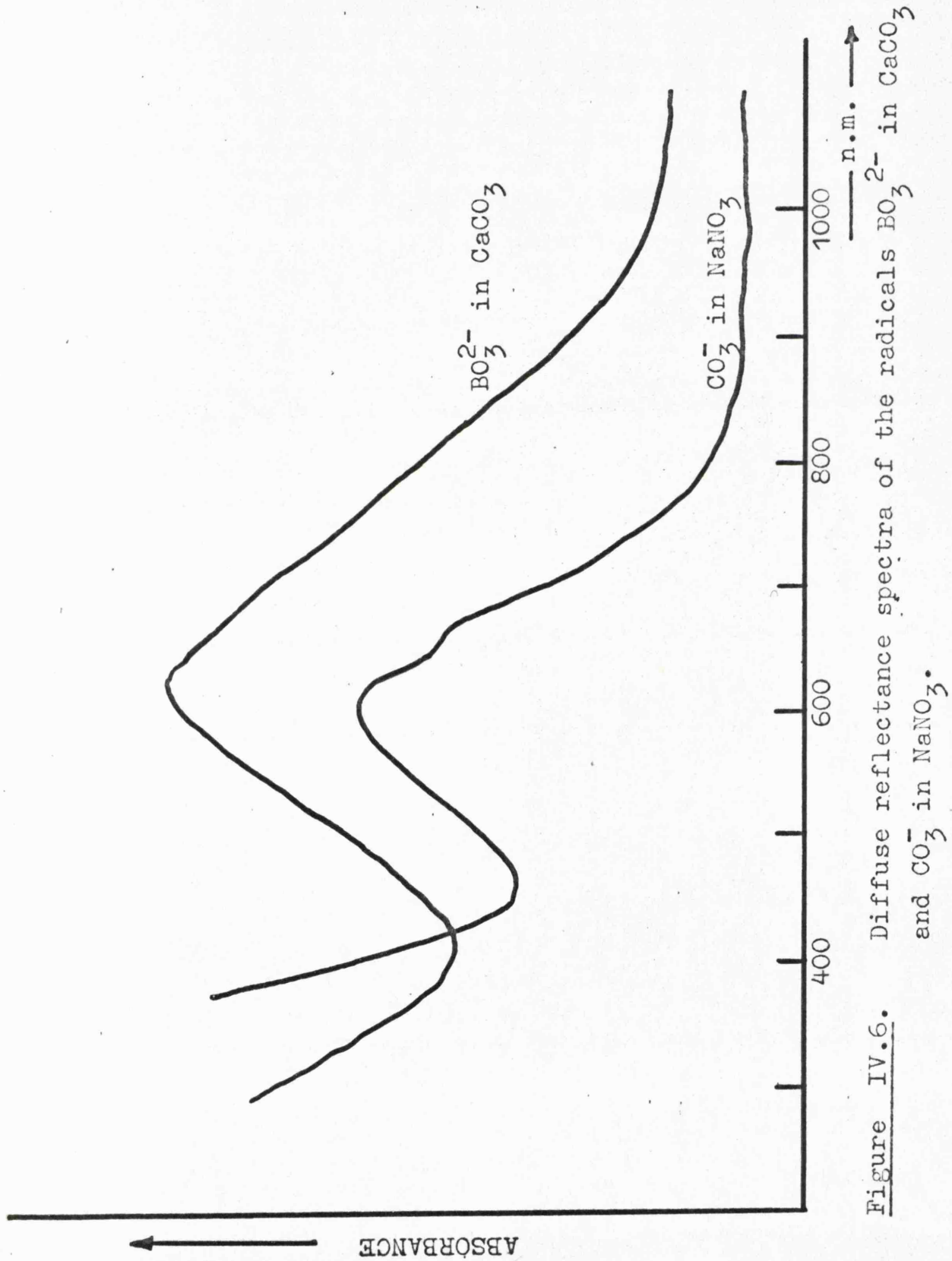


Figure IV.6. Diffuse reflectance spectra of the radicals  $\text{BO}_3^{2-}$  in  $\text{CaCO}_3$  and  $\text{CO}_3^{2-}$  in  $\text{NaNO}_3$ .

for the 2s-orbital and 0.071 for the 2p-orbital and a 2p/2s-ratio of 5.3. The values of 0.002 for the 2s-orbital and 0.38 for the 2p-orbital, obtained from the alternative sign combination, correspond to a 2p/2s-ratio of 193. This is improbably large even for an electron confined entirely to the 2p-orbital of boron, when the 2s-density due to polarisation is expected to be of the order 1-2%. Therefore, we ignore the latter sign combination for the hyperfine coupling constants.

A comparison of the spin-resonance data and the derived molecular parameters for Y with those of the  $\text{CO}_3^{2-}$ <sup>36</sup> and  $\text{NO}_3^{2-}$ <sup>39</sup> radicals, (see Tables IV.1 & 2) supports our assignment of this centre to their isoelectronic analogue, the  $\text{BO}_3^{2-}$  radical-ion.

b) Radical Y is an electron deficient species. This is demonstrated by the results of the competition reaction with nitrate ions. The nitrate ion acts as a very efficient electron trap in the calcite lattice leading to the formation of the stable  $\text{NO}_3^{2-}|\text{CO}_3^{2-}|$  centre (Chapter IV.B). It is so effective that it completely inhibits the production of the  $\text{CO}_2^-$  radical-ion formed, in the absence of impurities, upon dissociative electron capture by

TABLE IV.1. The Electron Spin Resonance Data of the  $\text{BO}_3^{2-}$ ,  $\text{CO}_3^-$  and  $\text{NO}_3^-$  Radicals.

Radical Matrix	g-tensor			Hyperfine tensor in gauss				Ref.	
	$g_{xx}$	$g_{yy}$	$g_{zz}$	$g_{av}$	$B_{xx}$	$B_{yy}$	$B_{zz}$		$A_{iso}$
$\text{BO}_3^{2-}$ (Y) $\text{CaCO}_3$	2.0080	2.0127	2.0127	2.0111	-2.8	+1.4	+1.4	- 9.8	a
$\text{CO}_3^-$ $\text{CaCO}_3$	2.0051	2.0162	2.0162	2.0125	-2.5	+1.25	+1.25	-10.6	36
$\text{KHCO}_3$	2.0086	2.0184	2.0184	2.0151	-2	+1	+1	-11	39
$\text{NO}_3^-$ Urea Nitrate	2.0066	2.0140	2.0203	2.0136	-	-	-	-	39
$\text{KNO}_3$	2.0031	2.0232	2.0232	2.0165	-0.57	0.28	0.28	- 3.74	41
$^{13}\text{C}$ molecular sieve	$g_{iso} =$	$2.019$			$A_{iso} =$	$-5.9$			44

a. This work.

TABLE IV.2. Molecular Parameters for the  $\text{BO}_3^{2-}$ ,  $\text{CO}_3^-$   
and  $\text{NO}_3$  Radicals.

		$a_s^2$	$a_p^2$	2p/2s	$a_s^2 + a_p^2$
$\text{BO}_3^{2-}$	$\text{CaCO}_3$	-0.014	-0.071	5.3	-0.085
$\text{CO}_3^-$	$\text{CaCO}_3$	-0.009	-0.038	4.1	-0.047
	$\text{KHCO}_3$	-0.01	-0.030	3.0	-0.040
$\text{NO}_3$	Urea Nitrate	-	-	-	-
	$\text{KNO}_3$	-0.007	-0.017	2.4	-0.024
	13x molecular sieve	-0.010			

the radiation-produced  $\text{CO}_3^- | \text{CO}_3^{2-} |$  hole centre. Both radical Y and  $\text{NO}_3^{2-}$  were formed when calcite doped with nitrate and borate was exposed to  $\gamma$ -rays. The production of Y was unaffected by the presence of an effective electron trap, suggesting that it was formed by hole trapping at a borate impurity anion site.

c) The remarkable thermal stability of Y in calcite would suggest that it has the  $\text{XO}_3^{2-}$  structure, maintaining overall charge-neutrality within the host lattice.

d) The optical absorption spectra of the  $\text{CO}_3^-$  and  $\text{NO}_3$  radicals have been reported previously, and the relevant data are given in Table IV.3. These isoelectronic radicals have absorption bands in the region 500-700 nm ( $20,000-14,000 \text{ cm}^{-1}$ ) depending on the matrix in which they are studied. Hence, the presence of a strong asymmetric absorption at 630 nm ( $15,880 \text{ cm}^{-1}$ ) in the diffuse reflectance spectrum of Y in calcite lends further support to our assignment.

e) The borate doped calcite sample was precipitated from an aqueous solution containing 10% orthoboric acid. Any other radical structure,

TABLE IV.3. Optical Absorption Parameters for the  $\text{BO}_3^{2-}$ ,  $\text{CO}_3^-$  and

$\text{NO}_3^-$  Radicals

Radical	Matrix	Absorption maxima	Ref.
$\text{NO}_3^-$	Nitrogen at 20°K	629 n.m. (15,900 $\text{cm}^{-1}$ )	45
		666 n.m. (15,000 $\text{cm}^{-1}$ )	
	Urea Nitrate	610 n.m. (16,400 $\text{cm}^{-1}$ )	39
$\text{CO}_3^-$	Gas Phase	624 n.m. (16,050 $\text{cm}^{-1}$ )	46
		600 n.m. (16,670 $\text{cm}^{-1}$ )	
	in $\text{CO}_3^{2-}$ doped $\text{NaNO}_3$ $\gamma$ -irradiated at 300°K	With a shoulder at 650 n.m. (15,400 $\text{cm}^{-1}$ )	a
		650 n.m. (15,400 $\text{cm}^{-1}$ )	36
$\text{BO}_3^{2-}$	$\text{KHCO}_3$	535 n.m. (18,700 $\text{cm}^{-1}$ )	39
	$\text{CaCO}_3$	630 n.m. (15,900 $\text{cm}^{-1}$ )	a

a. This work

whose formation from an anion derived from orthoboric acid seems plausible on chemical grounds; would be expected to have larger  $^{11}\text{B}$  coupling constants. This is true of such species as  $\text{BO}_3^{4-}$  and  $\text{BO}_2^{2-}$ ; and radicals of the form  $\text{HBO}_3^-$ ,  $\text{H}_2\text{BO}_3$ ,  $\text{H}_2\text{BO}_2$ ,  $\text{HBO}^-$  and  $\text{H}_2\text{BO}$  would be expected to have appreciable coupling to their hydrogen atoms.

## 2. The Structure of $\text{BO}_3^{2-}$

Figure IV.7 is the Walsh correlation diagram for  $\text{AB}_3$  tetra-atomic radicals.<sup>40</sup>  $\text{BO}_3^{2-}$  is a 23-valence electron radical and therefore, from the diagram, we predict that the unpaired electron occupies a non-bonding  $a_2'$ -molecular orbital, constructed entirely from the in-plane 2p-orbitals of oxygen, and that the molecule will be planar as there is no strain to be relieved by distortion. The magnetic interaction with the boron nucleus must arise through spin-polarisation of the  $\sigma$ -bonding electrons giving rise to a small dipolar coupling of the form  $(-2B, B, B)$  together with a small negative isotropic coupling. The isoelectronic radicals  $\text{CO}_3^-$  and  $\text{NO}_3$  have been reported to be either planar having  $D_{3h}$  symmetry,<sup>36,41</sup> or to exhibit an in-plane distortion.<sup>39</sup> Chantry and coworkers<sup>39</sup> postulated that this distortion was inherent but it has since been suggested that in fact it is

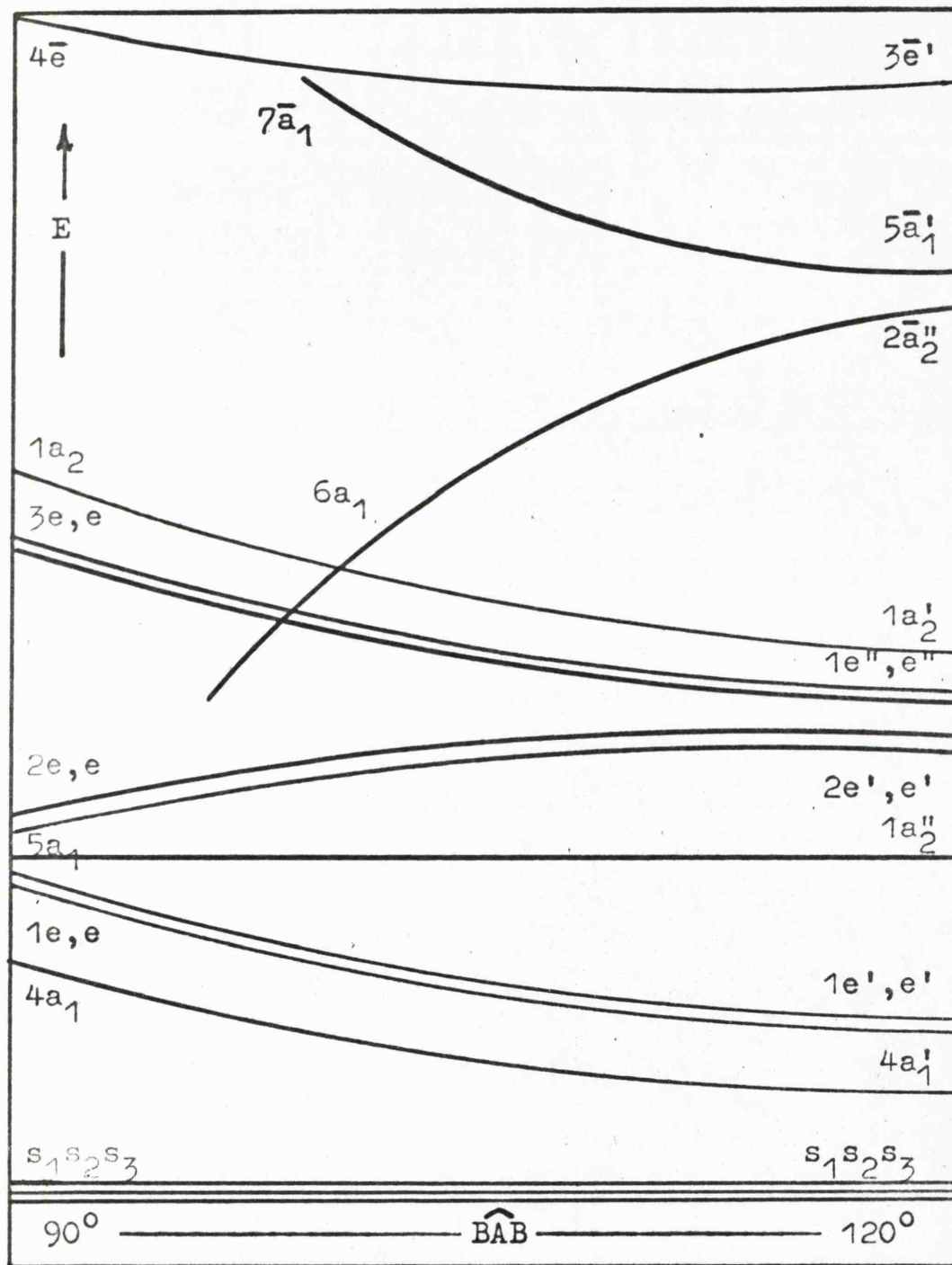


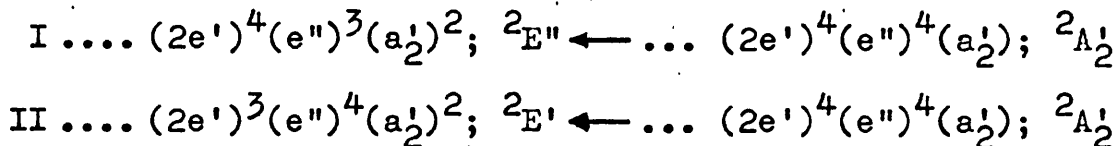
Figure IV.7. The Walsh orbital-correlation diagram for  $AB_3$  radicals and molecules.

environmentally induced.<sup>11</sup> Similar environmental effects have been observed for the  $\text{NO}_3^{2-}$  radical-anion (Chapter V.). The small hyperfine coupling constants and broad resonance features of the ESR spectrum of  $\text{BO}_3^{2-}$  at 3 cm wavelength make it impossible to detect any deviation from axial symmetry for this radical. However, at 8 mm wavelength it is quite clear that no such distortion has occurred.

The in-plane g-factor ( $g_{\perp}$ ) is considerably greater than the free-spin value. This positive g-shift must arise through magnetic coupling of the  $a_2'$ -level and the close but lower-lying  $e''$ -level. The  $g_{\parallel}$ -value is expected to be slightly less than free spin due to coupling of the  $a_2'$ -level and the higher lying  $\bar{a}_1'$ -orbital, although the experimentally determined value is somewhat greater than 2.0023.

### 3. The Electronic Spectrum of the $\text{BO}_3^{2-}$ Anion

For 23 valence-electron  $\text{AO}_3$  oxy-radicals having  $D_{3h}$ -symmetry, there are four low lying excited configurations and corresponding transitions:



Transition I, polarised perpendicular to the molecular plane, is forbidden, whilst transition II is

strongly allowed and polarised in the plane of the radical. The observed asymmetric band in the reflectance spectrum of  $\text{BO}_3^{2-}$  ( $\lambda_{\text{max}} = 630 \text{ nm}, 15,880 \text{ cm}^{-1}$ ) is assigned to the transition  ${}^2\text{E}' \leftarrow {}^2\text{A}'_2$ , by analogy with the results of Chantry et. al.<sup>39</sup> for the isoelectronic  $\text{CO}_3^-$  and  $\text{NO}_3$  radicals. This transition occurs between molecular orbitals that are mixtures of oxygen 2p-atomic orbitals with no central atom character and therefore we expect, and indeed find, only slight shifting of absorption maxima for the series  $\text{BO}_3^{2-}$ ,  $\text{CO}_3^-$  and  $\text{NO}_3$ .

#### MECHANISM OF FORMATION

The boron electron-deficient species  $\text{BO}_3^{2-}$  can be formed by hole trapping at a  $\text{BO}_3^{3-}$  anion site or by direct radiation damage of a protonated borate species, resulting in the loss of a hydrogen atom. The latter process can be dismissed since no  $\text{BO}_3^{2-}$  radicals, which are detectable by ESR, were produced when a doped calcite sample was irradiated for several days at 77°K.  $\text{BO}_3^{2-}$  radicals did form, however, when the sample was annealed at approximately 220°K, there being a direct resonant-hole transfer from the  $\text{CO}_3^-$  radicals to the impurity anion sites.

Since there have been no previous reports of the

existence of  $\text{BO}_3^{3-}$  anions in solution, it is difficult to envisage how such anions were trapped in the calcite lattice. For the  $\text{CO}_3^{2-}$  and  $\text{NO}_3^-$  ions in solution two optical absorption bands have been detected - a weak band near 300 nm ( $33,300 \text{ cm}^{-1}$ ) and a rather intense absorption close to 200 nm ( $50,000 \text{ cm}^{-1}$ ). The high energy absorption has been assigned to a  $n-\pi^*$  transition of symmetry  ${}^1\text{E}' \leftarrow {}^1\text{A}_1'$ , whilst the band close to 300 nm ( $33,300 \text{ cm}^{-1}$ ) is the forbidden  $\pi-\pi^*$  transition of electronic symmetry  ${}^1\text{A}_1'' \leftarrow {}^1\text{A}_1'$ .<sup>42</sup> One would expect the  $\text{BO}_3^{3-}$  anion in solution to have optical absorption bands in the same regions. We have been unable to detect these absorptions in aqueous orthoboric acid solutions, even at temperatures close to the boiling point of the solutions. It should be remembered, however, that precipitation of the doped calcium carbonate sample occurred from a solution containing a high concentration of calcium chloride. The addition of neutral salts such as  $\text{CaCl}_2$ ,  $\text{BaCl}_2$ ,  $\text{SrCl}_2$ ,  $\text{K}_2\text{SO}_4$  and  $\text{KNO}_3$ , to solutions of orthoboric acid is known to result in a marked increase in its pH.<sup>43</sup> A solution of orthoboric acid in 5.4 M  $\text{CaCl}_2$  has a pH of 4.5 compared to 10.5 for a pure solution of the acid. The pH of the solution of calcium chloride and orthoboric acid from which the precipitated powders were prepared varied from 3.5 at

300°K to 1.8 at 368°K. This increased ionisation of the acid at elevated temperatures and high salt concentrations may well explain the inclusion of isolated  $\text{BO}_3^{3-}$  anions in the precipitated calcite lattice.

## SECTION B

### THE $\text{NO}_3^{2-}$ ANION AND RELATED SPECIES WITH 25 VALENCE-ELECTRONS

#### EXPERIMENTAL RESULTS

The presence of impurity ions in doped samples of calcium carbonate was confirmed by infrared spectroscopy. The IR absorption bands attributable to trapped nitrate ions were well resolved, even at 300°K, indicating that  $\text{NO}_3^-$  ions occupy vacant carbonate ion positions in the calcite lattice.

The exposure of polycrystalline samples of nitrate-doped calcite to  $\gamma$ -rays at 77°K resulted in the formation of the  $\text{CO}_3^{3-}$  and  $\text{CO}_3^-$  radicals,<sup>36</sup> and a third unidentified paramagnetic species, labelled (a) in Figure IV.8, giving rise to a weak ESR absorption at  $g = 2.0088$ . When the powder was annealed the spectrum altered significantly. At 120°K features from the  $\text{CO}_3^{3-}$  and  $\text{CO}_3^-$  radicals were reduced in intensity, whereas there was an increase in intensity of features from (a) and two new centres, labelled X and Y in Figure IV.9. At 300°K only X and a second unidentified

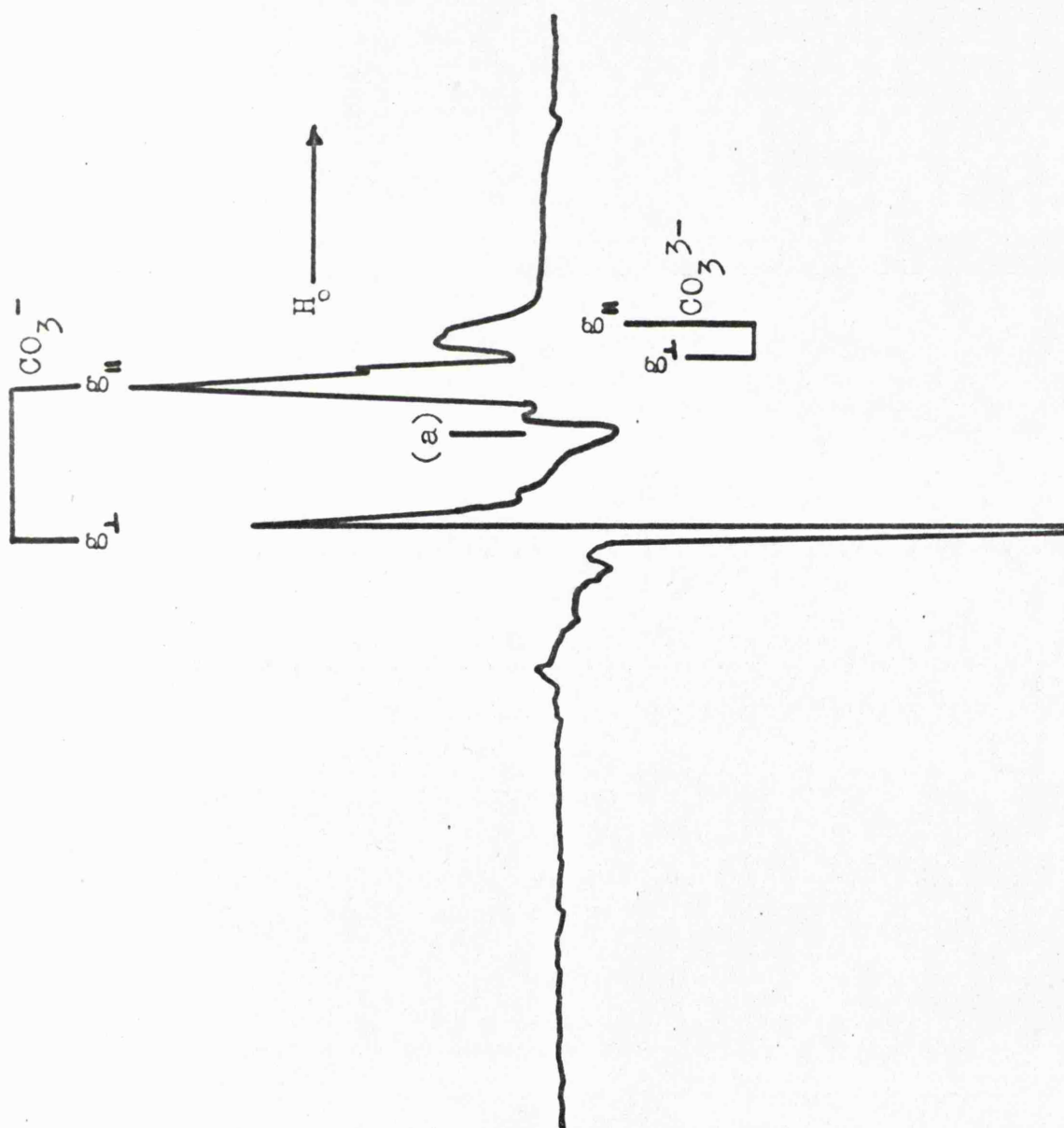


Figure IV.8. ESR spectrum of the radicals  $\text{CO}_3^{3-}$  and  $\text{CO}_3^{3-}$  in irradiated, nitrate-doped calcite measured at 77°K.

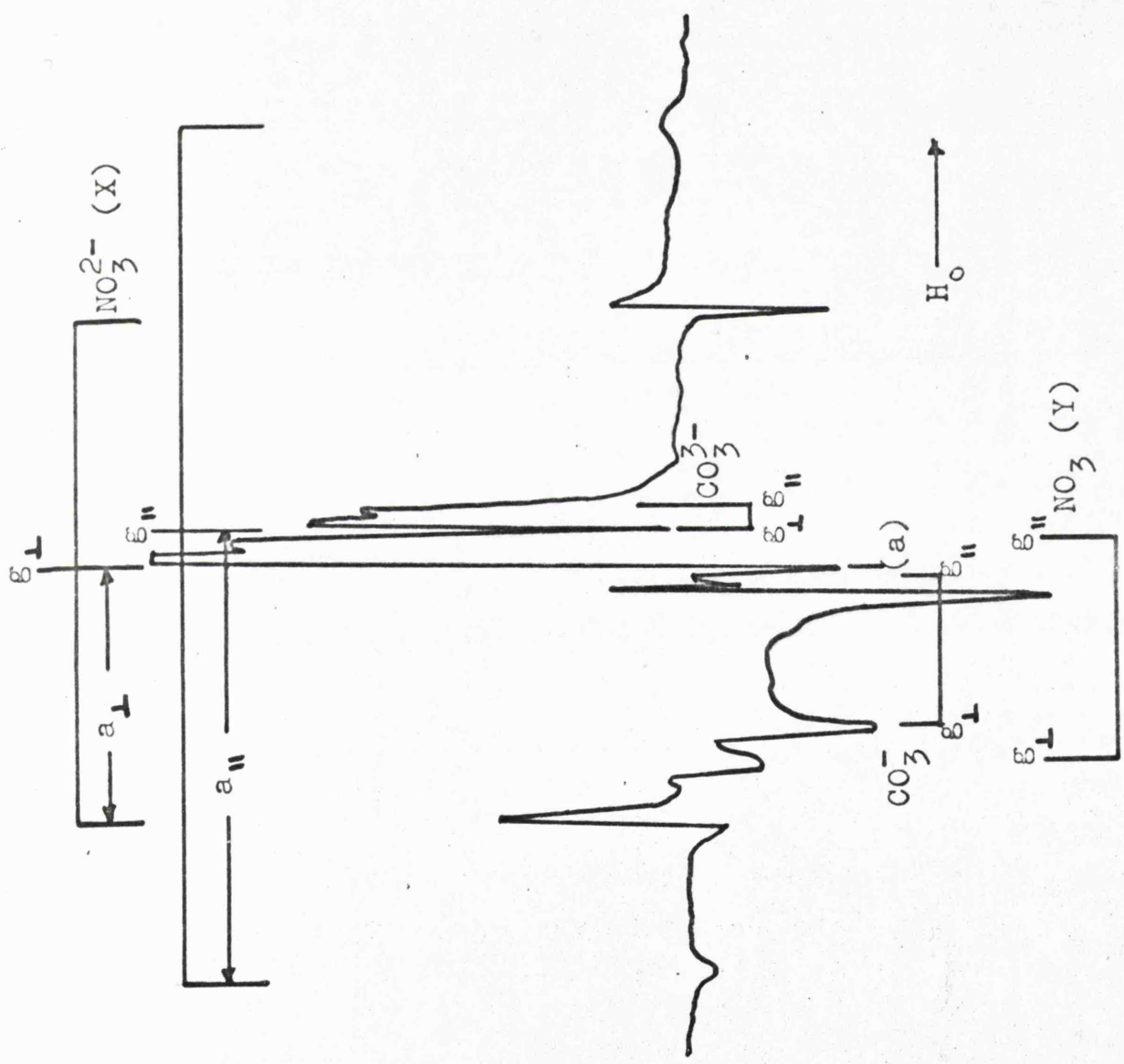


Figure IV.9. ESR spectrum of irradiated, nitrate-doped calcite measured at 120°K.

species, (b) in Figure IV.12 remained. Radical (b) decayed rapidly at 330°K whilst X was stable for more than 48 hours at 420°K. Irradiation of the doped carbonate at room temperature gave X and (b) directly, whilst (b) and the  $\text{CO}_2^-$  radical-anion<sup>37</sup> were the radiation damage products of pure calcite at this temperature. Therefore, the presence of nitrate ions in the calcite lattice suppressed the formation of the  $\text{CO}_2^-$  ion.

## DISCUSSION

### 1. The Identification of Radical X

For the following reasons radical X is almost certainly  $\text{NO}_3^{2-}$ :

a) The ESR spectrum of X could best be interpreted in terms of a species possessing axially symmetric g- and A-tensors and containing a single magnetic nucleus of spin  $I = 1$ . We have assumed this nucleus to be  $^{14}\text{N}$  ( $I = 1$ , 99.64% isotopic abundance) and have completed a spin-population analysis of the nitrogen 2s- and 2p-orbitals accordingly. Values of 0.082 for the 2s-orbital and 0.64 for the 2p-orbital were obtained if we assumed that the components of the nitrogen hyperfine tensor had the same signs. These values correspond to a 2p/2s ratio of 7.8. The alternative sign-combination has

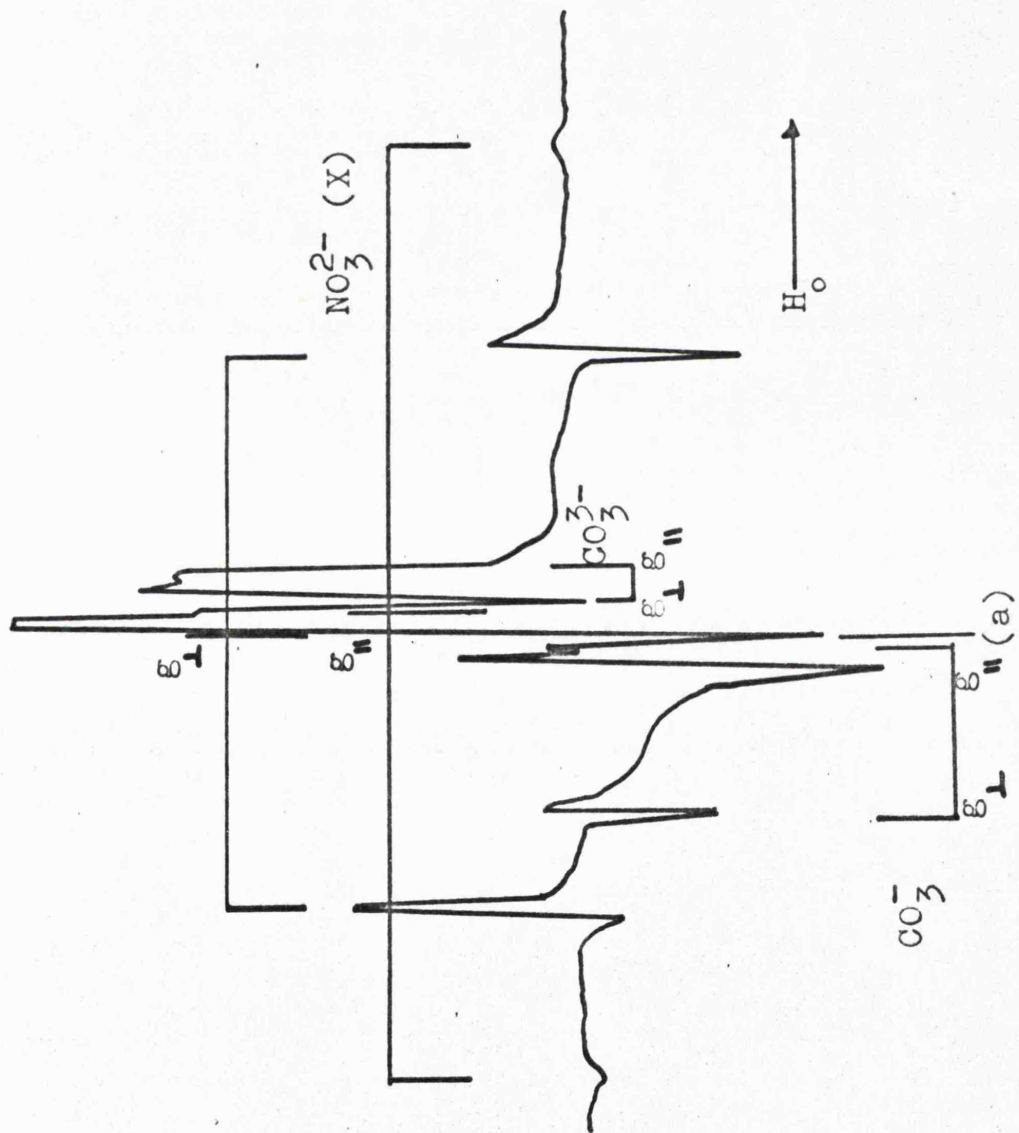


Figure IV.10. ESR spectrum of irradiated, nitrate-doped calcite measured at 150°K.

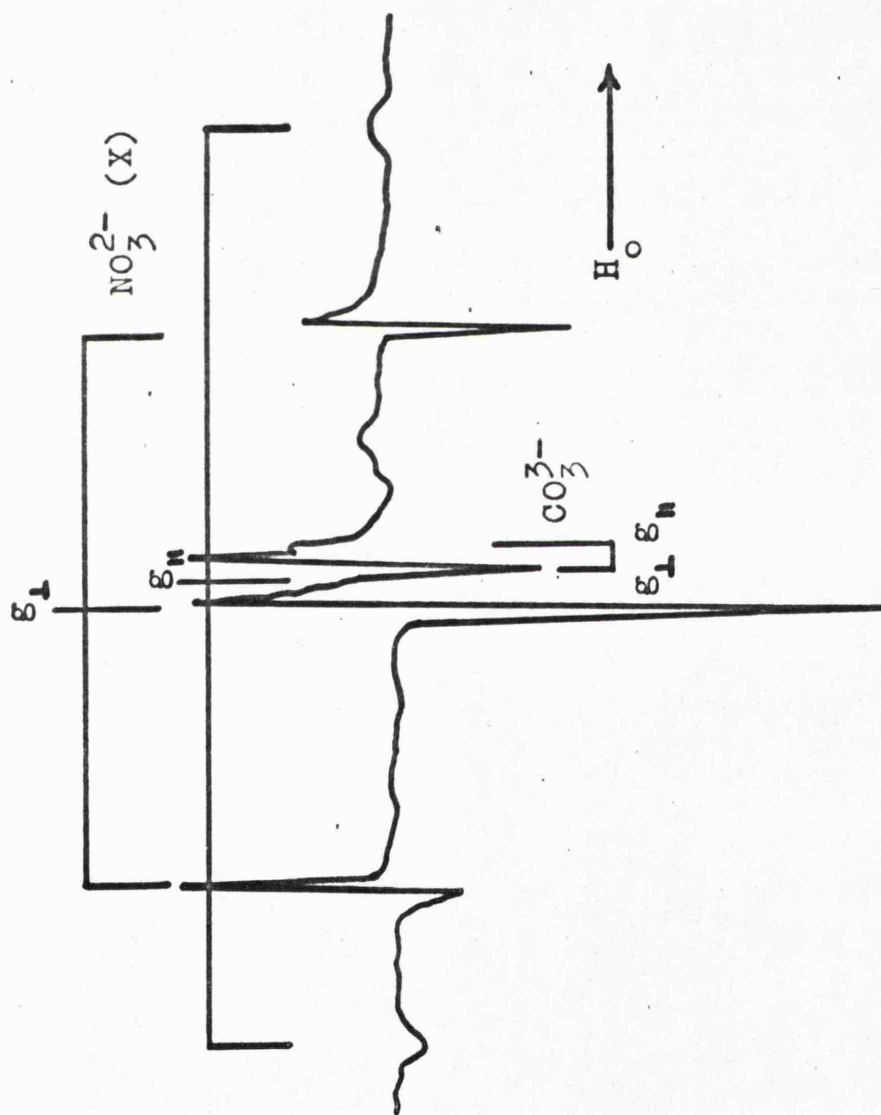


Figure IV.11. ESR spectrum of irradiated, nitrate-doped calcite measured at 200°K.

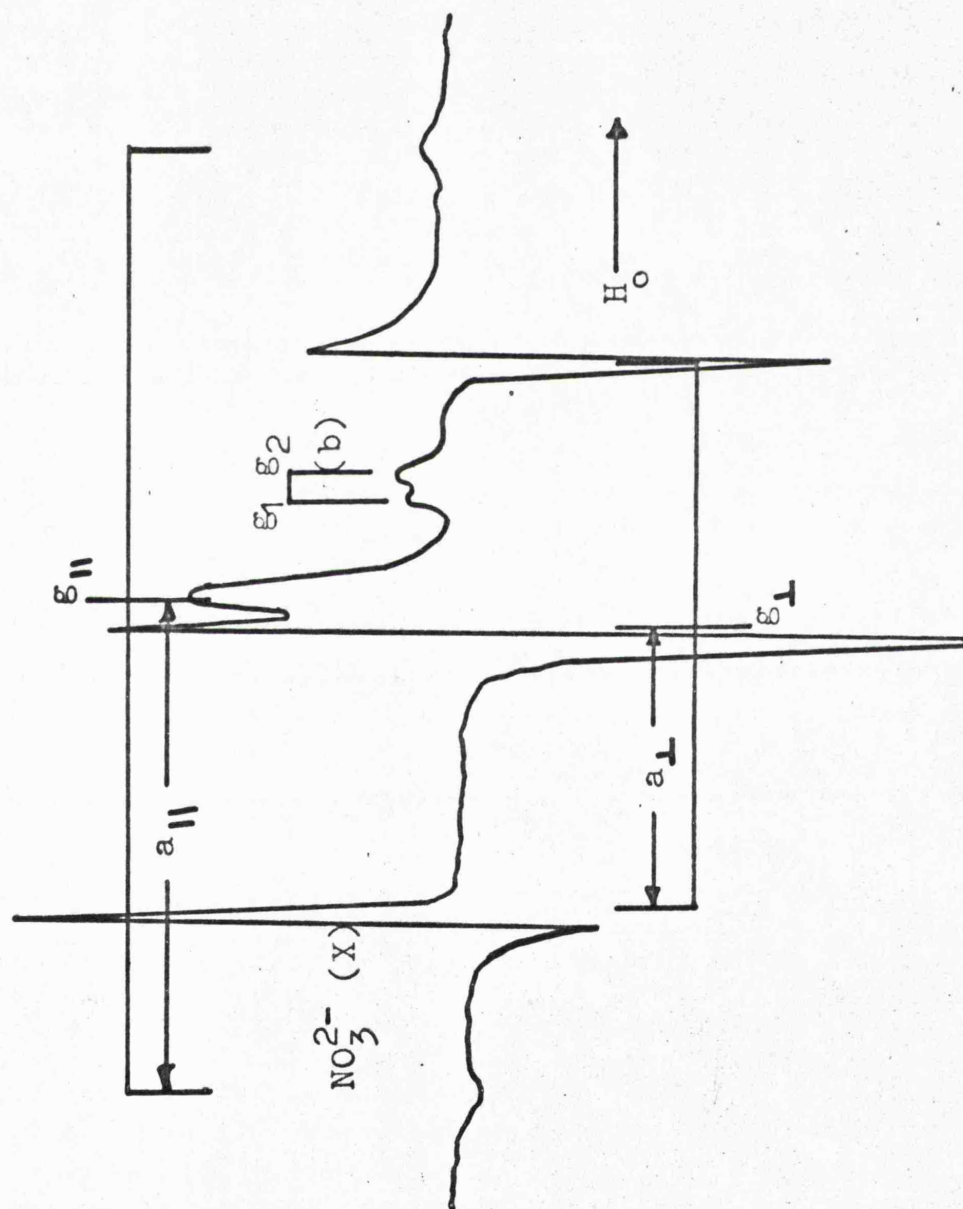


Figure IV.12. ESR spectrum of irradiated, nitrate-doped calcite measured at 300°K.

been rejected as this leads to a 2p-orbital population much greater than unity.

b) The high thermal stability of this radical in  $\text{CaCO}_3$  supports our assignment, for the  $\text{NO}_3^{2-}$  radical no longer requires charge compensation within the lattice.

c) There was a parallel increase in intensity of ESR features from X as the  $\text{CO}_3^{3-}$  electron-excess centre decayed. This would seem to indicate that X is formed as a direct consequence of electron capture by a nitrate ion, lending further support to our assignment.

## 2. The Identification of Radical Y

Radical Y is most probably the unstable nitrogen trioxide molecule. However, we were unable to detect hyperfine interactions involving  $^{14}\text{N}$  in the ESR spectrum of this centre and consequently this must be regarded as a tentative identification. We base our assignment on the following factors:

a) The experimental g-tensor for Y is remarkably similar to that reported for the  $\text{NO}_3$  radical trapped in single crystals of potassium nitrate<sup>41</sup> (see Table IV.4). The principal values of the reported A-tensor are small so that the  $^{14}\text{N}$  hyperfine structure, for

TABLE IV.4. The Electron Spin Resonance Data for the Radicals  $\text{NO}_3^{2-}$ ,  $\text{NO}_3$ ,  $\text{CO}_3^{2-}$  and  $\text{CO}_3^-$  in Calcium Carbonate.

Species	Medium	g-tensor			Hyperfine coupling constants in gauss			Reference
		$g_{\parallel}$	$g_{\perp}$	$g_{av}$	$B_{\parallel}$	$B_{\perp}$	$A_{iso}$	
$\text{NO}_3^{2-}$	$\text{CaCO}_3$ (X)	2.0027	2.0066	2.0053	21.7	-10.9	45.1	a
	$\text{KNO}_3$	2.002	2.006	2.005	19.3	-9.7	41.7	47
	KCl	2.0020	2.0068	2.0052	20.7	-10.3	40.8	50
$\text{NO}_3$	$\text{CaCO}_3$ (Y)	2.0039	2.0225	2.0162	-	-	-	a
	$\text{KNO}_3$	2.0031	2.0232	2.0165	-0.57	0.28	-3.74	41
$\text{CO}_3^{2-}$	$\text{CaCO}_3$	2.0016	2.0032	2.0027	-	-	-	a
	$\text{CaCO}_3$	2.0013	2.0031	2.0025	40	-20	131.3	36
	$\text{CaCO}_3$	2.0051	2.0162	2.0125	-	-	-	a
$\text{CO}_3^-$	$\text{CaCO}_3$	2.0051	2.0165	2.0127	-2.5	1.2	-11.9	36
	$\text{KHCO}_3$	2.0086	2.0184	2.0151	-2.0	1.0	-11.0	39
	Radical (a) $\text{CaCO}_3$	$g = 2.0088$ (single line)						a
Radical (b) $\text{CaCO}_3$	$g_1 = 1.9955$ $g_2 = 1.9929$						a	

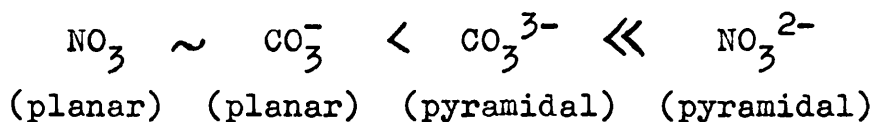
a. This work.

$\text{NO}_3$  in  $\text{CaCO}_3$ , could well be hidden within the line-width of the g-features ( $\Delta H_{\text{ms}} \cong 5$  gauss).

b) The appearance of spin-resonance features from Y occurred with the simultaneous loss of signals from the  $\text{CO}_3^-$  centre. This hole-transfer process occurred when the irradiated sample was annealed above  $220^\circ\text{K}$ .

### 3. The Relative Stabilities of the $\text{NO}_3^{2-}$ , $\text{NO}_3$ , $\text{CO}_3^-$ and $\text{CO}_3^{3-}$ Radicals in Calcium Carbonate

From the annealing experiments, the observed order of stability for the four identified centres was:



The energy barrier to electron-hole transmission is a minimum when the required change in geometry of the participant ions is small.<sup>47</sup> Electron transfer from neighbouring carbonate ions will therefore, readily annihilate  $\text{NO}_3 | \text{CO}_3^{2-} |$  centres. The resulting planar  $\text{CO}_3^-$  ions will have a greater mobility, and therefore a lower thermal stability than the corresponding pyramidal  $\text{CO}_3^{3-} | \text{CO}_3^{2-} |$  electron-excess centres. These in turn will be far less stable than the  $\text{NO}_3^{2-} | \text{CO}_3^{2-} |$  centres because of their excess charge and mobility by electron transfer.

#### 4. The Structures of the $\text{NO}_3^{2-}$ and $\text{CO}_3^{3-}$ Radicals

Figure IV.7 is the Walsh orbital-correlation diagram<sup>40</sup> for  $\text{AB}_3$  molecules from which we conclude that, in the 25 valence-electron radicals  $\text{NO}_3^{2-}$  and  $\text{CO}_3^{3-}$ , the unpaired electron occupies an antibonding molecular orbital of  $a_1$ -symmetry. This orbital is constructed from the 2s- and  $2p_z$ -atomic orbitals of the central atom and the oxygen 2s- and 2p-orbitals, where the z-axis is the molecular  $C_3$ -symmetry axis.

If we assume that Coulson's orthogonality<sup>20</sup> relationships between the hybridisation ratio  $\lambda$  (where  $\lambda^2 = 2p/2s$  ratio) and the BAB angle ( $\theta$ ) hold for these  $\text{AB}_3$  systems, then we can estimate the bond angles in  $\text{NO}_3^{2-}$  and  $\text{CO}_3^{3-}$  from the equation:<sup>20</sup>

$$\cos \theta = \frac{1}{2} \left[ \frac{3}{2\lambda^2 + 3} - 1 \right] \dots\dots (5)$$

From the spin-resonance data included in Table IV.4 we estimate the hybridisation ratios to be 7.8 ( $\text{NO}_3^{2-}$ ) and 5.25 ( $\text{CO}_3^{3-}$ ), corresponding to bond angles of  $115^\circ$  and  $113^\circ$  respectively. These angles are almost midway between those of planar radicals ( $120^\circ$ ) and the strongly pyramidal isoelectronic species such as  $\text{PO}_3^{2-}$  ( $\sim 110^\circ$ ).<sup>48</sup>

Plots of the total spin-density ( $a_s^2 + a_p^2$ ) on the central atom versus  $\Delta\chi$  (where  $\Delta\chi$  is the difference in electronegativity between the ligand and central atoms)

for a variety of  $\text{AO}_3$  and  $\text{AO}_2$  oxy-radicals are reasonably linear, and show a marked increase in antibonding spin-density on A as  $\Delta\chi$  increases.<sup>11</sup> Figure IV.13 shows such a plot for 25 valence-electron  $\text{AO}_3$  radicals from which it is clear that, whereas the points corresponding to the second and third row isostructural species fall on a straight line,  $\text{NO}_3^{2-}$  and  $\text{CO}_3^{3-}$  are well removed. There is also very little change in the unpaired electron distribution on going from nitrogen to carbon, although  $\Delta\chi$  increases significantly. It seems as though there is a greater tendency for radicals of the first row elements to be planar (possibly for steric reasons) and it is those radicals with intermediate bond angles that are particularly sensitive to changes in electronegativity. There is a steady decrease in the  $2p/2s$  ratio on going from  $\text{NO}_3^{2-}$  (7.8) to  $\text{CO}_3^{3-}$  (5.25) and to the isoelectronic  $\text{CF}_3$  ( $\sim 3$ ) as the spin-density on the central atom rises. This increase in  $2s$ -character on the central atom is equivalent to an increase in its electronegativity and hence to a fall in the antibonding unpaired electron density thereon. The  $\text{CF}_3$  radical has a hybridisation ratio close to three and should therefore, have the same shape as the second and third row radicals.

We conclude that, in a series of radicals having

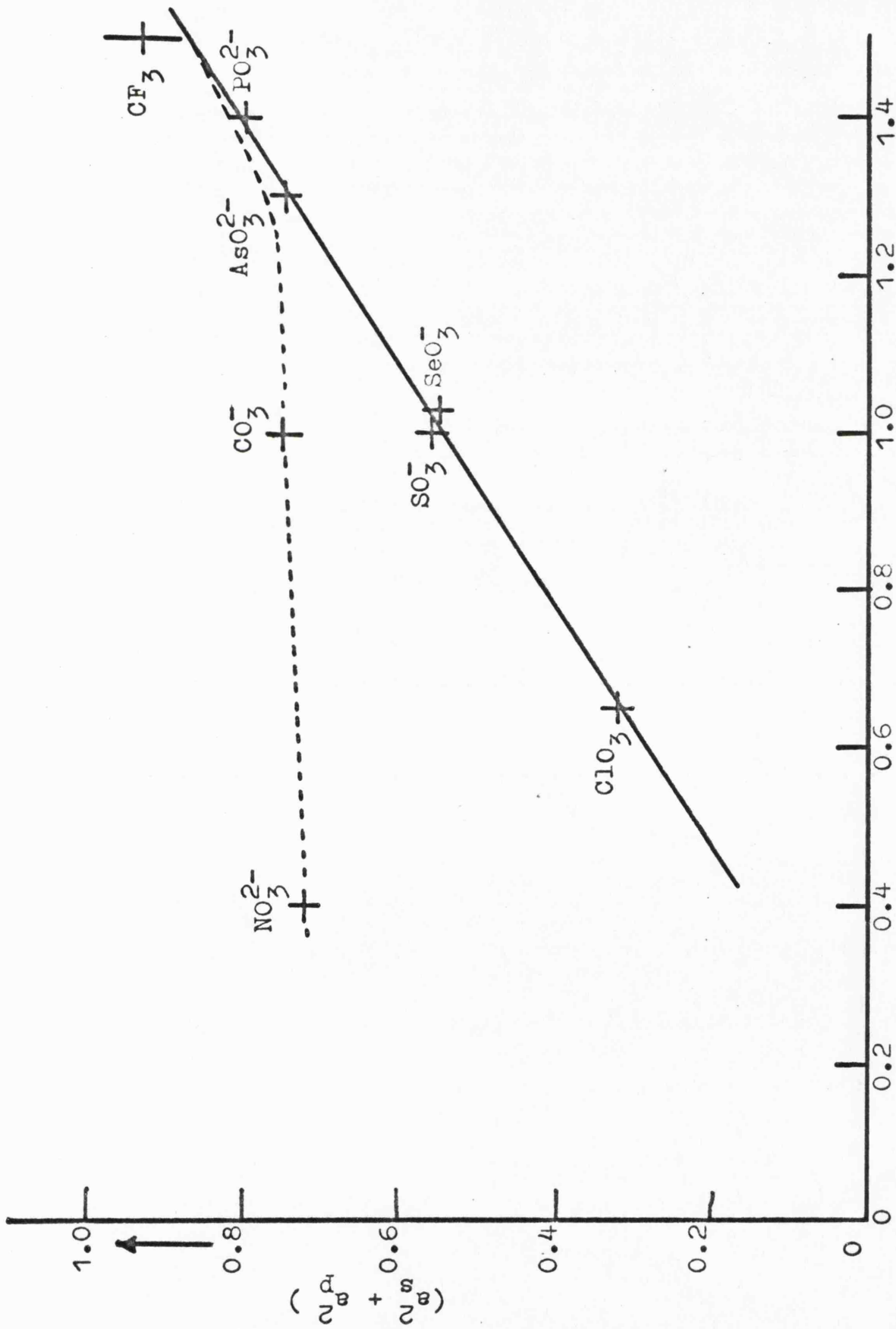


Figure IV.13. The variation of the total antibonding electron density on the central atom ( $n_a^p + n_a^w$ ) in  $\text{AO}_3$  radicals with  $\Delta\chi$ .

shapes which are intermediate between normal extremes, an increase in the electronegativity difference between the outer and central atoms will lead to an increased bending and to a decrease in the normal growth of spin-density on the central atom.

#### MECHANISM OF RADIATION DAMAGE IN NITRATE-DOPED CALCITE

The primary radiation damage process in calcite is expected to be inner-electron ejection from a carbonate ion, resulting in the formation of the  $\text{CO}_3^- | \text{CO}_3^{2-} |$  and  $\text{CO}_3^{3-} | \text{CO}_3^{2-} |$  centres. These radicals were unstable at room temperature and decomposed regenerating secondary electrons. In the absence of impurity ions the parent hole centres underwent dissociative electron capture, resulting in the formation of  $\text{CO}_2^-$  radical-anions. During this process the carbonate emitted an intense blue luminescence.

When nitrate ion impurities were present in the lattice the regenerated secondary electrons were preferentially trapped at  $\text{NO}_3^-$  ion sites, and consequently the formation of the  $\text{CO}_2^-$  radical-anion was suppressed.

#### SECTION C

#### THE 27 VALENCE-ELECTRON SPECIES $\text{ClO}_3^{2-}$

#### EXPERIMENTAL RESULTS

The presence of impurity ions in precipitated samples

of calcium carbonate was confirmed by infrared spectroscopy.

Calcium carbonate doped with chlorate ions gave only the  $\text{CO}_3^{3-}$  and  $\text{CO}_3^-$  radicals when irradiated at  $77^\circ\text{K}$ .<sup>36</sup> When the powder was subsequently annealed to  $220^\circ\text{K}$  there was a marked reduction in the intensity of ESR features arising from the  $\text{CO}_3^-|\text{CO}_3^{2-}|$  centre, as a consequence of which features from a third paramagnetic species, N in Figure IV.14 were observed. At room temperature the  $\text{CO}_3^{3-}|\text{CO}_3^{2-}|$  centre decayed rapidly, with the subsequent appearance of spin-resonance signals from a further two paramagnetic centres, labelled O and P in Figure IV.14.

Radical N was a chlorine containing species whose weak ESR spectrum was difficult to identify at  $300^\circ\text{K}$  and 10 mW microwave power. However, at  $77^\circ\text{K}$  and 100 mW signals from O and P were completely saturated and only the spectrum of N was detectable (Figure IV.15). Under these conditions it was possible to complete the analysis of the ESR spectrum of the latter centre. Radical N was extremely stable in the calcite lattice and signals from this centre were observed even after the powder had been annealed at  $500^\circ\text{K}$  for several days, when both radicals O and P had decomposed.

Radical O was also formed when pure calcite was irradiated at room temperature and it has been previously

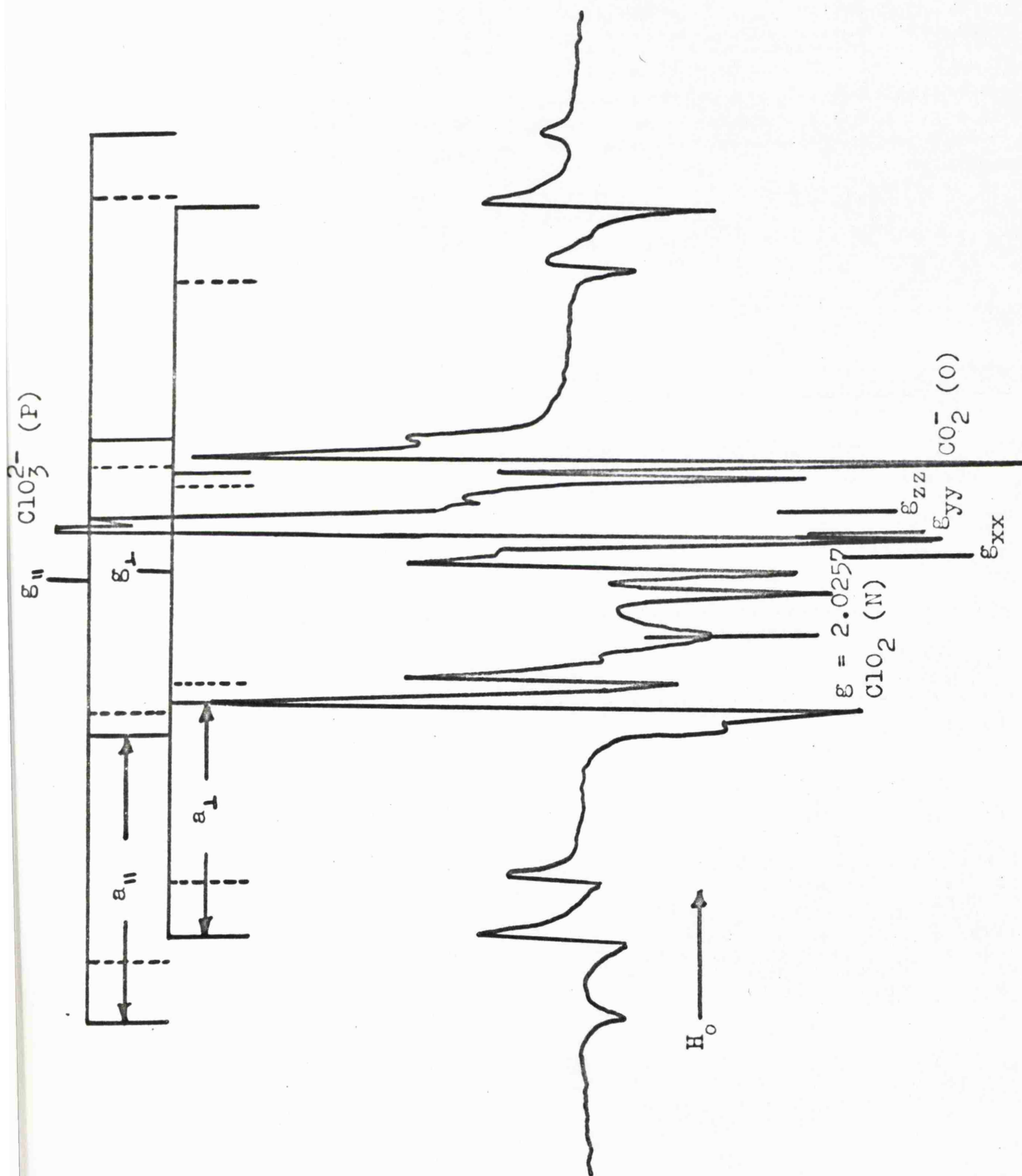


**Figure IV.14.** ESR spectrum of irradiated, chlorate-doped calcite measured at 300°K and 10 mW.

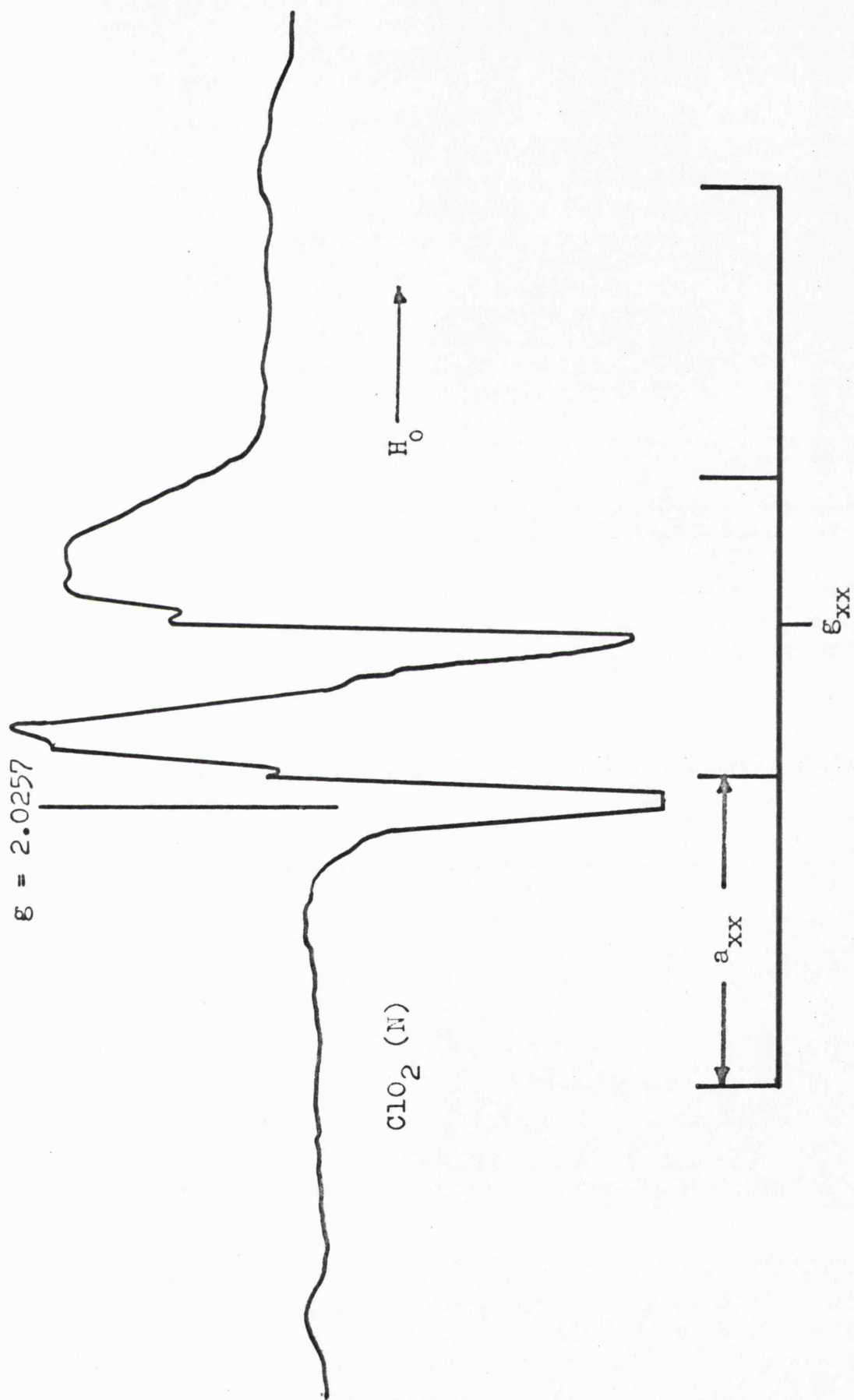


Figure IV.15. ESR spectrum of irradiated, chlorate-doped calcite measured at  $77^\circ\text{K}$  and 100 mW.

identified as the  $\text{CO}_2^-$  radical-anion.<sup>37</sup>

Radical P also appeared to contain a single chlorine atom, for it was possible to detect features corresponding to the two abundant chlorine nuclei,  $^{35}\text{Cl}$  and  $^{37}\text{Cl}$ , in the ESR spectrum of this species. This centre was stable at  $300^\circ\text{K}$  for several months, but decomposed with a half-life of 16 hours at  $420^\circ\text{K}$ . Its decomposition did not result in the formation of further paramagnetic species.

Irradiation of chlorate-doped powder samples of calcite at  $300^\circ\text{K}$  led to the formation of the radicals N, P, and  $\text{CO}_2^-$  directly. When a sample of calcite doped with both nitrate and chlorate was exposed to high energy radiation, only the electron-excess  $\text{NO}_3^{2-}|\text{CO}_3^{2-}|$  centre<sup>38</sup> and radical N were formed. The formation of  $\text{CO}_2^-$  and P was inhibited by the presence of the deeper  $\text{NO}_3^-|\text{CO}_3^{2-}|$  electron trap in the carbonate lattice.

## DISCUSSION

### 1. The Identification of Radical N

Radical N is almost certainly chlorine dioxide, which has been studied extensively in the solid, liquid and gas phases.<sup>51,52,53</sup> ESR powder spectra of  $\text{ClO}_2$  in a variety of matrices including frozen aqueous sulphuric acid,<sup>54</sup> carbon tetrachloride,<sup>54</sup> ethanol, and potassium perchlorate<sup>51</sup>

are characterised by a common intense feature at  $g \approx 2.026$ . Radical N exhibited a similarly intense absorption at this position and the ESR spectrum of this centre, measured at high microwave power and  $77^\circ\text{K}$ , was identical to that of chlorine dioxide in, for example, vitreous sulphuric acid. (Compare Figure IV.15 with Figure VII.9 of Chapter VII). Under high resolution it was also possible to detect four sets of hyperfine features for N (corresponding to  $a_{xx}$  of  $\text{ClO}_2$ ) centred upon  $g_{xx} = 2.0015$ . These facts substantiate our identification of this centre as chlorine dioxide.

The dioxide is known to be a decomposition product of a variety of unstable chlorine oxides and oxyanions (see Chapters VI and VII).

## 2. The Identification of Radical P

For the following reasons Radical P is thought to be the electron-excess species  $\text{ClO}_3^{2-}$ :

- a) The ESR spectrum of C was characteristic of a radical having axially symmetric  $g$ - and  $A$ -tensors. It must also contain a single chlorine atom, for it was possible to detect ESR features corresponding to the two abundant magnetic isotopes of this nucleus ( $^{35}\text{Cl}$ ,  $I = 3/2$ , 75.4% abundance; and  $^{37}\text{Cl}$ ,  $I = 3/2$ , 24.6% abundance).

The spin populations of the chlorine 3s- and 3p-orbitals were derived from the theoretical values for spin populations of unity. When we assumed that both the perpendicular and parallel hyperfine coupling constants had the same sign we obtained values of 0.067 for the 3s-orbital and 0.14 for the 3p-orbital, corresponding to a 3p/3s ratio of 2.0.

The alternative sign combination for the coupling constants resulted in a 3p-orbital occupancy greater than unity, and was therefore rejected. Tables IV.5 and 6 include the spin-resonance and molecular parameters for P obtained from this analysis.

b) The most probable alternative structure for P, derived from an isolated  $\text{ClO}_3^-$  anion, is  $\text{ClO}_3$ . However, the derived hybridisation ratio of 2.0 is considerably smaller than that reported for chlorine trioxide trapped in a number of irradiated perchlorates. Furthermore, the total chlorine spin-density in P is only 0.21 compared to 0.42 reported for  $\text{ClO}_3$  (see Table IV.6). Of course radical P could be a  $\text{ClO}_3$  radical whose ESR parameters have been considerably modified by the carbonate lattice, but in our experience trapped radicals are not usually so sensitive to the nature of their environment.

TABLE IV.5. Electron Spin Resonance Data for  $\text{ClO}_3^{2-}$  and  $\text{ClO}_2$  in Calcite, and Related Species.

Radical Matrix	g-tensor <sup>a</sup>			<sup>35</sup> Cl Hyperfine <sup>a</sup> tensor in gauss			Reference
	$g_{\parallel}$	$g_{\perp}$	$g_{av}$	$B_{\parallel}$	$B_{\perp}$	$A_{iso}$	
$\text{ClO}_3^{2-}$	2.0121	2.0105	2.0110	14	-7.0	113	b
$\text{CaCO}_3$ (P)							
$\text{ClO}_2$		$g_{xx} = 2.0015$			$a_{xx} = 74.2$		b
$\text{CaCO}_3$ (N)							
$\text{ClO}_3$	2.007	2.008	2.008	25	-13	128	57
$\text{NH}_4\text{ClO}_4$							
$\text{ClO}_3$	2.0066	2.0132	2.0110	29	-15	122	54
$\text{KClO}_4$							
$\text{ClO}_3$	2.0069	2.0103	2.0092	33	-17	133	54
$\text{Mg}(\text{ClO}_4)_2$							

a. Corrected to 2nd-order by application of the Breit-Rabi <sup>58</sup> equation.

b. This work.

TABLE IV.6.      The Molecular Parameters of  $\text{ClO}_3^{2-}$  and  $\text{ClO}_3$ .

Radical	Matrix	$a_s^2$ (Chlorine 3s)	$a_p^2$ (Chlorine 3p)	$a_p^2/a_s^2$	$a_s^2+a_p^2$	Ref.
$\text{ClO}_3^{2-}$	$\text{CaCO}_3$	0.067	0.140	2.0	0.207	a
$\text{ClO}_3$	$\text{NH}_4\text{ClO}_4$	0.080	0.290	3.63	0.370	57
$\text{ClO}_3$	$\text{KClO}_4$	0.076	0.340	4.47	0.416	54
$\text{ClO}_3$	$\text{Mg}(\text{ClO}_4)_2$	0.083	0.390	4.70	0.473	54

a. This work.

We are therefore, inclined to rule out the possibility that P is  $\text{ClO}_3$ .

- c) Radical P is an electron-excess centre. Nitrate ions have been found to be most effective electron scavengers. When these ions were concurrently coprecipitated with chlorate by calcium carbonate, radiation-generated electrons from the matrix anions were preferentially trapped at  $\text{NO}_3^- | \text{CO}_3^{2-} |$  centres. This inhibited the formation of P, whilst the production of N ( $\text{ClO}_2$ ) was unaffected.
- d) The appearance of ESR signals from P concurrent with the loss of features from the electron-excess  $\text{CO}_3^{3-}$  anion, would suggest that radical P was formed by thermally initiated electron transfer from  $\text{CO}_3^{3-} | \text{CO}_3^{2-} |$  centres to chlorate impurity ion sites.
- e) The high thermal stability of P is in accord with this radical having an  $\text{XO}_3^{2-}$  structure.

### 3. The Electronic Structure and Stereochemistry of the $\text{ClO}_3^{2-}$ Radical Anion

From the Walsh orbital-correlation diagram for  $\text{AB}_3$  molecules<sup>40</sup> (Figure IV.7) we predict that the unpaired electron of the  $\text{ClO}_3^{2-}$  anion occupies an antibonding molecular orbital of  $a_1'$ -symmetry. This orbital is constructed from the  $3s$ - and  $3p_z$ -atomic orbitals of chlorine

overlapping with the 2p-orbitals of oxygen lying along the Cl-O bonds. The z-axis is the molecular  $C_3$ -symmetry axis.

The observed significant 3s-orbital contribution from chlorine, coupled with a hybridisation ratio less than three, suggests that  $ClO_3^{2-}$  is a species whose stereochemistry deviates little from planarity. It is surprising, however, that there is such a large delocalisation of spin-density onto oxygen (see Table IV.6) when one considers the predicted high antibonding character of the molecular orbital containing the unpaired electron.

We would also predict an axially symmetric g-tensor for this species.  $g_{||}$  is expected to be much greater than the free-spin value, the deviation arising through the magnetic coupling of the  $a_1'$ -level and the close, but lower-lying  $a_2'$ -orbital. Similarly, the in-plane  $g_{\perp}$ -factor will be greater than 2.0023, but the deviation will be somewhat smaller than that predicted for  $g_{||}$ . This positive g-shift must arise through the magnetic coupling of the  $a_1'$ - and the lower lying  $e''$ -levels.

It is encouraging that the experimental parameters are very similar to those we have predicted, but this simple picture of a slightly pyramidal tetra-atomic radical is open to criticism.  $ClO_3^{2-}$  is one electron

short of  $\text{ClF}_3$ <sup>55</sup> whose structure is shown in Figure IV.16. We might expect, therefore, that  $\text{ClO}_3^{2-}$  has a stereochemistry midway between tetrahedral (as in  $\text{ClO}_3^-$ ) and trigonal bipyramidal (as in  $\text{ClF}_3$ ). There is also the possibility that this centre is undergoing a dynamic Jahn-Teller distortion similar to that proposed for  $\text{PF}_4$  in  $\gamma$ -irradiated  $\text{KPF}_6$  powder.<sup>56</sup> However, we feel that this is unlikely, since the ESR parameters of this centre were insensitive to drastic changes in temperature.

#### MECHANISM OF RADIATION DAMAGE

When the doped calcite was irradiated at 77°K and subsequently annealed to room temperature, it was possible to follow the consecutive decomposition of the matrix defect centres. At 220°K, the  $\text{CO}_3^- | \text{CO}_3^{2-} |$  centre decayed, and although we could not detect signals attributable to  $\text{ClO}_3$  radicals at this temperature, a weak ESR absorption from  $\text{ClO}_2$  was observed. We conclude that chlorine dioxide was formed from the decomposition of transient  $\text{ClO}_3$  radicals, produced by hole transfer from the carbonate electron-deficient centres to  $\text{ClO}_3^-$  impurity ions.

At 300°K, the  $\text{CO}_3^{3-} | \text{CO}_3^{2-} |$  centre decayed with the subsequent formation, by electron transfer, of the electron-excess  $\text{ClO}_3^{2-}$  radical.

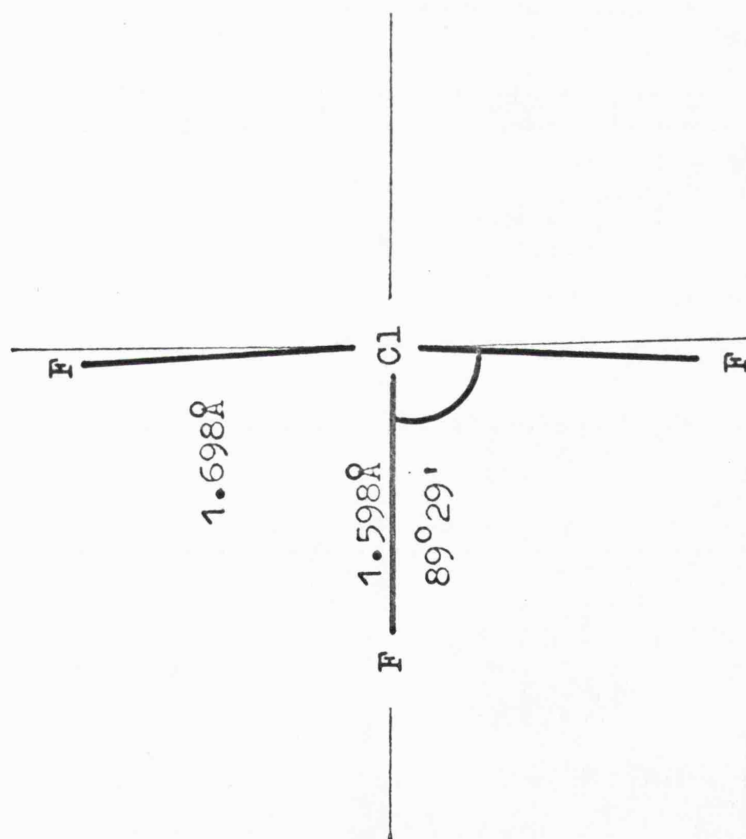


Figure IV.16. The configuration of the ClF<sub>3</sub> molecule.

CHAPTER V

THE 33 VALENCE-ELECTRON  $\text{ClO}_4^{2-}$  ANION AND  
RELATED SPECIES

THE 33 VALENCE-ELECTRON  $\text{ClO}_4^{2-}$  ANION AND RELATED SPECIES

Morton has detected two paramagnetic centres in  $\text{KClO}_4$  crystals  $\gamma$ -irradiated at  $77^\circ\text{K}$  which he suggested might be  $\text{ClO}_4$  radicals trapped in magnetically distinct sites.<sup>59</sup> The spin-resonance parameters reported for the two centres are not similar (see Table V.1) and radical (II) is less stable than radical (I).

The theoretical justification for his assignment is unconvincing and we feel that whilst (I) may be the peroxy-chlorine compound  $\begin{array}{c} \text{O} \\ \diagup \\ \text{Cl} - \text{O} - \text{O} \\ \diagdown \\ \text{O} \end{array}$  (see Chapter VII) (II) is probably the electron-excess species  $\text{ClO}_4^{2-}$ . In view of our previous success in specifically preparing such electron-excess species by doping the parent ion into a suitable host crystal,<sup>38,60</sup> we attempted to form the  $\text{ClO}_4^{2-}$  radical by irradiating barium sulphate containing a trace of perchlorate impurity. In this chapter we compare and contrast the spin-resonance and molecular parameters obtained for this centre in the sulphate matrix with those of Morton's radical (II) and the recently reported iso-structural species  $\text{AsO}_4^{4-}$  (or  $\text{As}(\text{OH})_4$ ),<sup>61</sup>  $\text{PF}_4$ ,<sup>56</sup>  $\text{PCl}_4$ <sup>62</sup> and  $\text{SF}_4^+$ <sup>63</sup>

EXPERIMENTAL PROCEDURE

All reagents used were AnalaR grade purified further by recrystallisation. Samples of barium sulphate doped

with perchlorate ions were prepared by precipitation from aqueous solutions of barium chloride containing approximately 10% of  $\text{KClO}_4$ . The samples were allowed to digest at  $340^\circ\text{K}$  overnight and dried under vacuum for several days prior to their irradiation. If the powders were dried at temperatures above approximately  $450^\circ\text{K}$  some decomposition of the coprecipitated  $\text{ClO}_4^-$  ions occurred. Powdered samples of the doped sulphate were exposed to  $\gamma$ -radiation doses ranging from 2 to 30 Mrads at both  $77^\circ\text{K}$  and room temperature.

#### EXPERIMENTAL RESULTS

The spectrum of a polycrystalline sample of perchlorate-doped  $\text{BaSO}_4$ , irradiated and examined at  $77^\circ\text{K}$ , is shown in Figure V.1. Both radicals A and B exhibited hyperfine interactions characteristic of species containing a single chlorine atom. It was possible to detect features in the ESR spectra of both A and B corresponding to the two abundant isotopes  $^{35}\text{Cl}$  and  $^{37}\text{Cl}$ , whose relative intensities were in accord with the natural abundance ratio of 3.07 and whose separation was consistent with their magnetic moment ratio of 1.202. Radical C contained no detectable interacting nucleus.

When the sulphate was annealed to  $300^\circ\text{K}$  the spectrum changed markedly. Whilst A was stable at this temperature

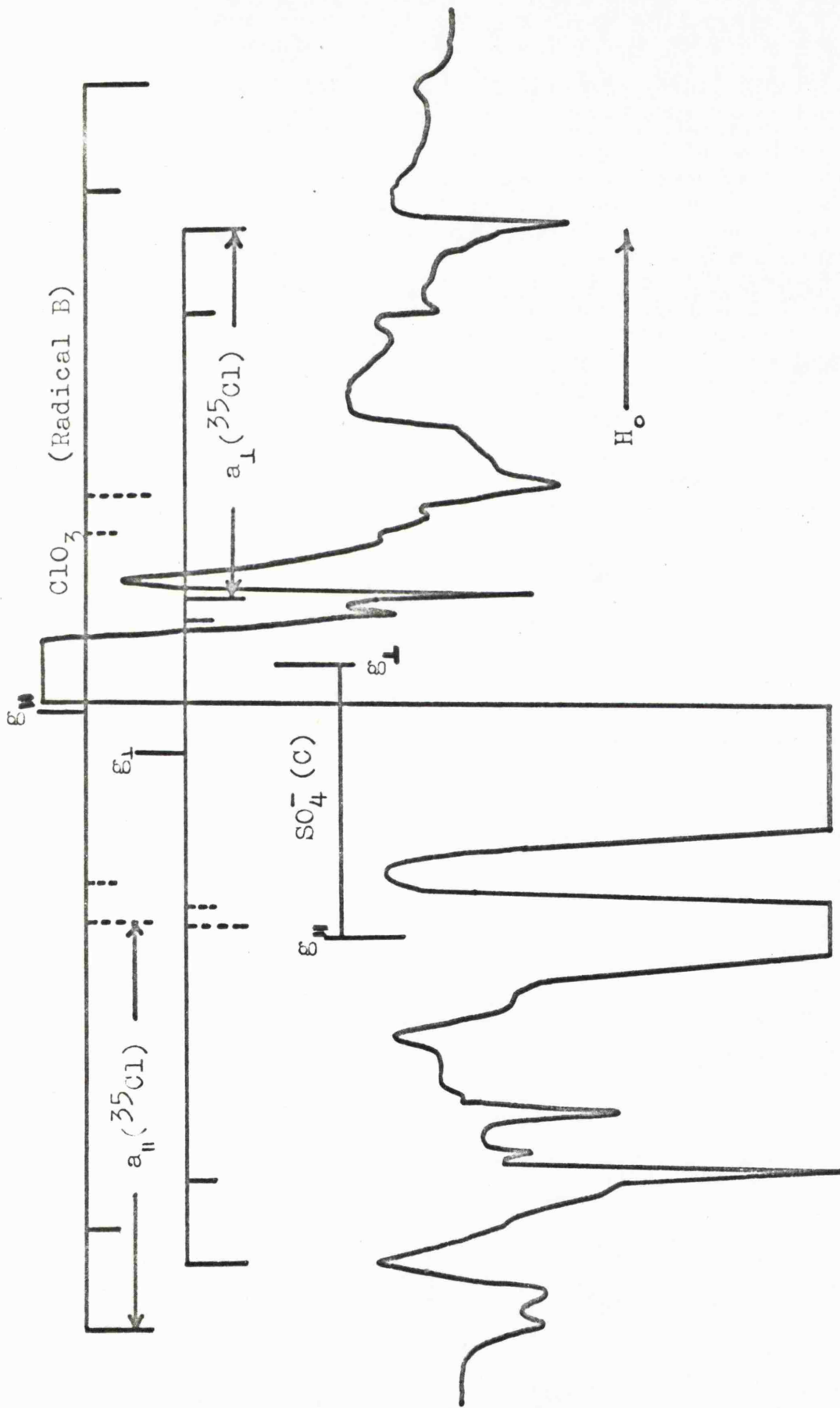


Figure V.1. An ESR spectrum of irradiated, perchlorate-doped BaSO<sub>4</sub> measured at 77°K and 10 mW.

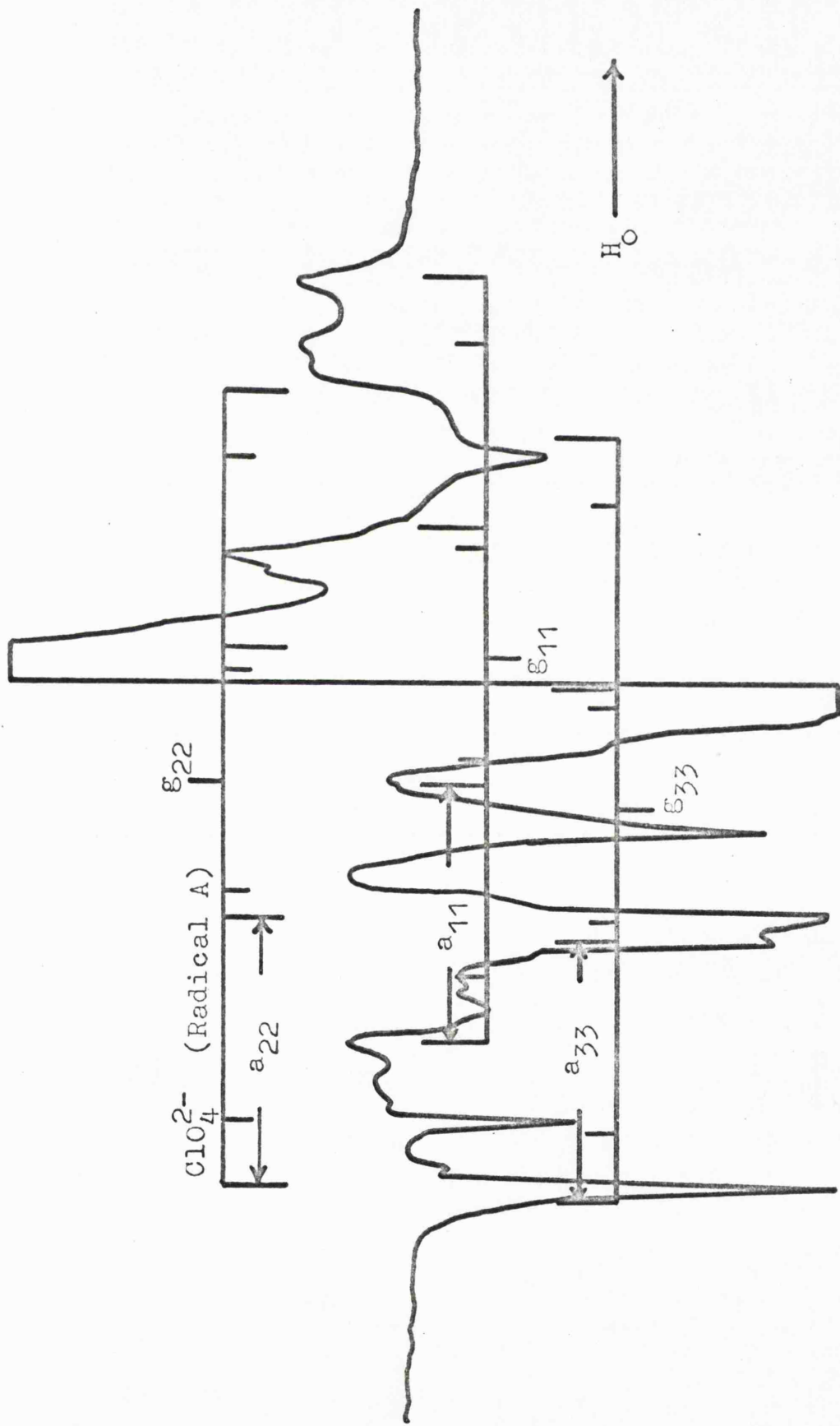


Figure V.2. An ESR spectrum of irradiated, perchlorate-doped  $\text{BaSO}_4$  measured at  $300^\circ\text{K}$  and 10 mW.

both radicals B and C had decayed, the decomposition of C giving rise to a new paramagnetic species D (Figure V.3). Irradiation of the doped sulphate at room temperature gave A and D directly, though only radical D was formed when pure barium sulphate was irradiated at 300°K.

When nitrate was concurrently coprecipitated with perchlorate by barium sulphate, exposure of the powder to ionising radiation at 77°K led to the formation of radicals B and C and the well-characterised  $\text{NO}_3^{2-} | \text{SO}_4^{2-} |$  centre.<sup>38</sup> When annealed to 300°K radicals B and C again decayed, with the formation of D, whilst the nitrate centre was stable at this temperature.

To facilitate the interpretation of the complex X-band ESR spectrum of the irradiated doped powder, further spectra were measured at both Q- and S-band frequencies.

## DISCUSSION

### 1. The Identification of Radical A

The ESR spectrum of this centre was interpreted in terms of the spin-Hamiltonian:

$$\mathcal{H} = \beta (g_{11} H_1 S_1 + g_{22} H_2 S_2 + g_{33} H_3 S_3) + A_{11} I_1 S_1 + A_{22} I_2 S_2 + A_{33} I_3 S_3$$

where  $S = \frac{1}{2}$  and  $I = \frac{3}{2}$

For the following reasons we are tempted to assign the resulting parameters (Table V.1) to the  $\text{ClO}_4^{2-} | \text{SO}_4^{2-} |$

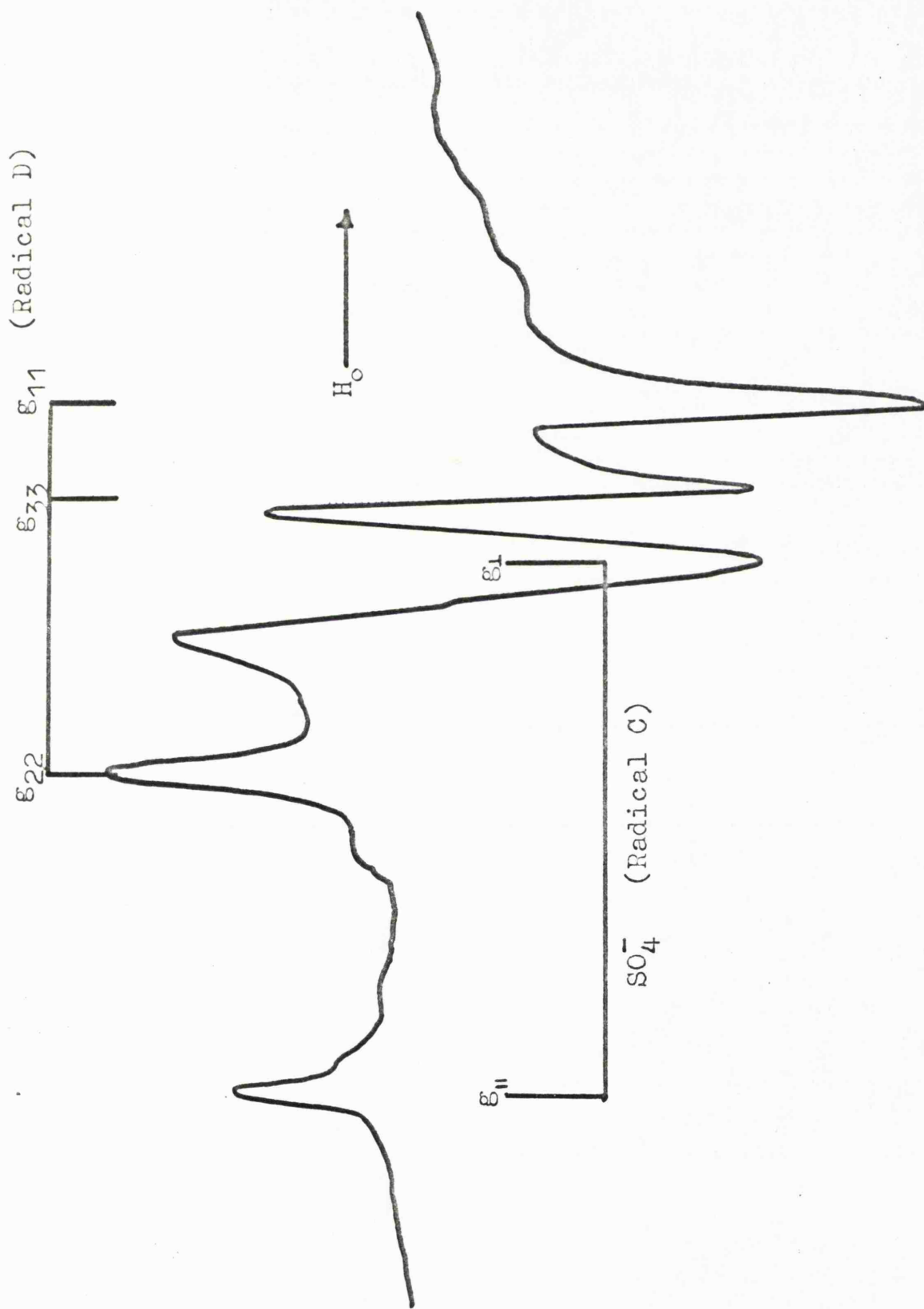


Figure V.3. The central region of the ESR spectrum of irradiated, perchlorate-doped BaSO<sub>4</sub> at 250°K showing signals arising from SO<sub>4</sub><sup>-</sup> (Radical C) and SO<sub>2</sub><sup>-</sup> (Radical D).

TABLE V.1. Electron Spin Resonance Data for the  $\text{ClO}_4^{2-}$  and  $\text{ClO}_3$  Radicals in  $\text{BaSO}_4$ , and Related Radicals.

Radical	Matrix	g-tensor (a)					Hyperfine tensor in Gauss (a)				Ref.
		$g_{11}$	$g_{22}$	$g_{33}$	$g_{av}$	$B_{11}$	$B_{22}$	$B_{33}$	$A_{iso}$		
$^1\text{ClO}_4$ (I)	$\text{KClO}_4$ 77°K	2.0024	2.0548	2.0553	2.0375	0	0	0	57.2	59	
$^1\text{ClO}_4$ (II)		2.0050	2.0360	2.0380	2.0260	-5.3	-3.3	8.7	74.3	59	
$\text{ClO}_4^{2-}$ (A)	$\text{BaSO}_4$ 77°K	2.0021	2.0249	2.0325	2.0198	0	3.3	-3.3	76.8	b	
	$\text{BaSO}_4$ 300°K	2.0020	2.0255	2.0325	2.0200	0	2.9	-2.9	74.6	b	
$\text{ClO}_3$ (B)	$\text{BaSO}_4$ 77°K	2.0068	2.0147	2.0147	2.0121	35.4	-16.7	-16.7	129.8	b	
$\text{ClO}_3$	$\text{KClO}_3$ 77°K	2.0030	2.0083	2.0083	2.0065	36	-18	-18	140	60	
$\text{ClO}_3$	$\text{KClO}_4$ 300°K	2.0066	2.0132	2.0132	2.0110	29	-15	-15	122	54	

a. Corrected to 2nd-order by application of the Breit-Rabi equation. 58

b. This work.

centre:

- a) The presence of  $\text{NO}_3^- | \text{SO}_4^{2-} |$  electron trapping centres in the sulphate lattice inhibited the formation of radical A, suggesting that this centre was formed as a direct result of electron trapping at a perchlorate ion site.
- b) The observed high thermal stability of this centre is in accord with our suggestion that A has the structure  $\text{XO}_4^{2-}$ .
- c) In Table V.2 the spin-resonance data for the well-characterised radicals  $\text{ClO}$ ,  $\text{ClO}_2$ ,  $\text{ClO}_3$ , and  $\text{ClO}_3^{2-}$  are collated for comparison with those of radical A. Also included are data for  $\text{Cl}_2^-$  which is isoelectronic with  $\text{ClO}^{2-}$ .

None of the listed radicals possesses the combination of a significant chlorine isotropic coupling, a very small anisotropic coupling, and positive g-value variations, characteristic of A. The choice of structure for this centre lies therefore, between the species  $\text{ClO}_2^{2-}$ ,  $\text{ClO}_4$ , and  $\text{ClO}_4^{2-}$  whose formation from a perchlorate ion seems most likely.  $\text{ClO}_2^{2-}$  would be a 21 valence-electron  $\text{AB}_2$  species and from the appropriate Walsh orbital-correlation diagram<sup>64</sup> (Figure VI.18) we would predict that it is probably

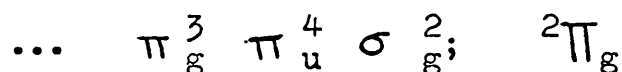
TABLE V.2. Electron Spin Resonance and Molecular Parameters for a  
Number of Well-Characterised Chlorine Radicals

Radical		Direction	$a_s^2(\text{Cl})$	$a_p^2(\text{Cl})$	$a_s^2 + a_p^2$	Ref.
(A) $\text{ClO}_4^{2-}$	$\epsilon$	11 22 33 2.0020 2.0255 2.0325				
	$a(^{35}\text{Cl})^*$	74.6 77.5 71.7	0.045	0.03-0.06	0.1	a'
$\text{ClO}$	$\epsilon$	2.0100 1.9965 2.0035				
	$a(^{35}\text{Cl})^*$	18.7 -4.6 -2.0	0.002	0.14	0.14	71
$\text{ClO}_2$	$\epsilon$	2.0025 2.017 2.011				
	$a(^{35}\text{Cl})^*$	72.7 -9.6 -10.0	0.56	0.01	0.57	51
$\text{ClO}_3$	$\epsilon$	2.0030 2.0083 2.0083				
	$a(^{35}\text{Cl})^*$	176 122 122	0.083	0.36	0.443	60
$\text{ClO}_3^{2-}$	$\epsilon$	2.0121 2.0105 2.0105				
	$a(^{35}\text{Cl})^*$	127 106 106	0.067	0.14	0.207	60
$\text{Cl}_2^-$	$\epsilon$	2.0012 2.0426 2.0426				
	$a(^{35}\text{Cl})^*$	91.1 9.3 9.3	0.024	0.582	0.606	72

\* All hyperfine couplings are quoted in gauss.

a) This work.

linear with a  ${}^2\Sigma_g$  ground state. The  $g_{\perp}$ -factor for this radical is expected to be very close to the free-spin value since the configuration:



would be highly excited. The significant positive g-shifts observed for A seem to rule out this possibility. The observed isotropic hyperfine coupling of 74.6 gauss is considerably larger than that we would expect for  $\text{ClO}_4$  by analogy to isoelectronic species, such as  $\text{PO}_4^{2-}$ .<sup>65</sup>

We consider therefore, that the foregoing arguments virtually eliminate all possibilities except  $\text{ClO}_4^{2-}$  for the structure of radical A.

## 2. The Identification of Radical B

A comparison of the spin-resonance parameters of radical B with those reported for the  $\text{ClO}_3$  radical trapped in a variety of matrices (Table V.1) leaves little doubt that this species is chlorine trioxide.

## 3. The Identification of Radicals C and D

The identification of the two radicals formed on irradiation of both perchlorate-doped and fused  $\text{BaSO}_4$  is based upon a comparison of their spectral parameters, given in Table V.3, with those of already well-substantiated species. On this basis alone it is concluded that

TABLE V.3. Electron Spin Resonance Data for Various Sulphur Oxyanions

Radical	Matrix	$g_{11}$	$g_{22}$	$g_{33}$	$g_{av}$	Ref.
$SO_4^-$ (C)	$BaSO_4$ 77°K	2.0307	2.0076	2.0076	2.0153	a
$SO_4^-$	$K_2SO_4$	2.0486	2.0082	2.0037	2.0202	66
$SO_4^-$	$K_2S_2O_8$	2.0310	2.0082	2.0064	2.0152	67
$SO_2^-$ (D)	$BaSO_4$ 300°K	2.0010	2.0168	2.0045	2.0074	a
$SO_2^-$	$K_2S_2O_5$	2.0018	2.0103	2.0055	2.0058	68
$SO_3^-$	$K_2CH_2(SO_3)_2$	2.0036	2.0036	2.0036	2.0036	69
$SO_3^-$	$K_2SO_4$	2.0033	2.0033	2.0023	2.0030	66

a. This work.

C and D are most probably  $\text{SO}_4^-$  and  $\text{SO}_2^-$  respectively.

Although the g-tensor of radical C is axially symmetric, the principal values are very similar to those reported for the  $\text{SO}_4^-$  radical trapped in X-irradiated  $\text{K}_2\text{SO}_4$ <sup>66</sup> and photolysed alkali metal persulphates.<sup>67</sup>

The radical  $\text{SO}_2^-$ , in which the unpaired electron occupies a  $2b_1$ -antibonding molecular orbital, has been detected as a radiolysis product of  $\text{K}_2\text{S}_2\text{O}_5$ <sup>68</sup> and  $\text{K}_2\text{CH}_2(\text{SO}_3)_2$ .<sup>69</sup> Since the radical possesses  $C_{2v}$ -symmetry it is characterised by a completely anisotropic g-tensor. There is little doubt that D is  $\text{SO}_2^-$ , for the alternative structure  $\text{SO}_3^-$  is well-known and has an almost isotropic g-tensor whose principal values deviate little from free-spin.

However, we were unable to detect hyperfine interactions involving  $^{33}\text{S}$  for these centres ( $^{33}\text{S}$ ;  $I = 3/2$ , 0.74% isotopic abundance) and therefore, could not confirm these tentative assignments.

#### 4. The Structure of $\text{ClO}_4^{2-}$

The energy level scheme for tetrahedral  $\text{XO}_4$  molecules is shown in Figure V.4.  $\text{ClO}_4^{2-}$  is a 33 valence-electron species and will have its unpaired electron in either the  $2\bar{a}_1$  or  $3\bar{t}_2$ -orbital\* in the undistorted anion, whichever is

\*The asterisk in  $\pi^*$  or the bar in  $\bar{a}_1$  denote antibonding character.

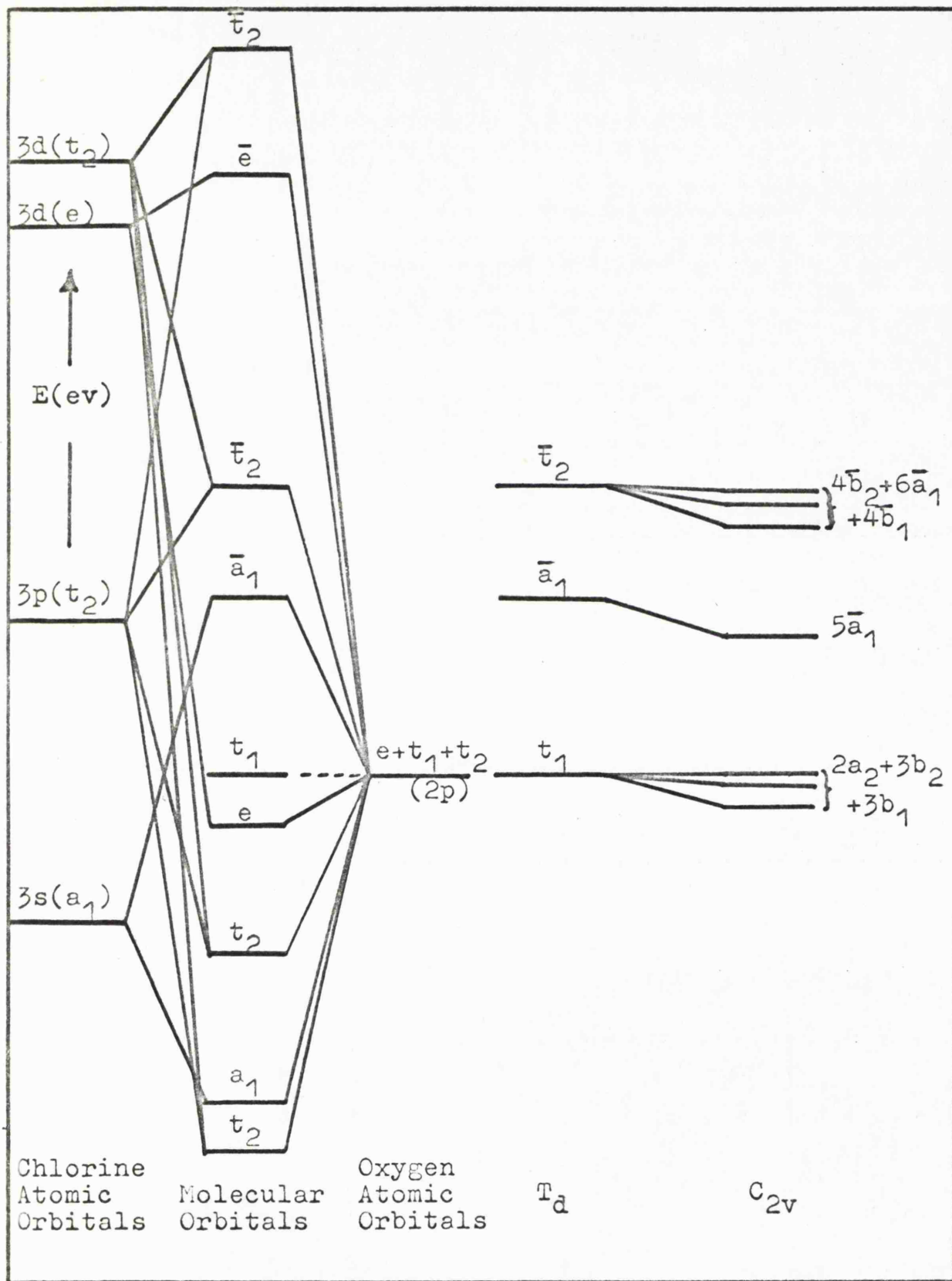


Figure V.4. The molecular orbital diagram for tetrahedral  $XO_4$  molecules.

the lower in energy. Figure V.5 illustrates the variation in orbital energies for tetrahedral  $XO_4$  molecules as the electronegativity of the central atom changes and for  $ClO_4$ , where  $\chi_O \cong \chi_{Cl}$ , the  $2\bar{a}_1$ -level has been calculated to be approximately 2.5 eV lower than  $3\bar{t}_2$ .<sup>33</sup> We therefore expect, and indeed find, that a spin-population analysis of the hyperfine tensor for this radical (Table V.1) indicates that the unpaired electron occupies a molecular orbital which has significant s-character on the central atom. The observed anisotropic chlorine coupling, albeit small, is then a measure of the distortion of this anion from a purely tetrahedral structure, for it reflects the presence of p-character in the molecular orbital. One would not expect any intrinsic Jahn-Teller distortion for a radical having a  ${}^2A_1$ -ground state and therefore, the destruction of tetrahedral symmetry may be environmentally induced, perhaps through a non-spherical distribution of adjacent cations. If this is so it is not surprising that there is some discrepancy, however small, between the anisotropic parameters obtained for  $ClO_4^{2-}$  in barium sulphate and those reported by Morton for centre (II) in  $KClO_4$ ,<sup>59</sup> if indeed the latter centre is  $ClO_4^{2-} | ClO_4^- |$ . The observed spectral parameters can best be accommodated if we assume that this induced distortion of the tetroxy-

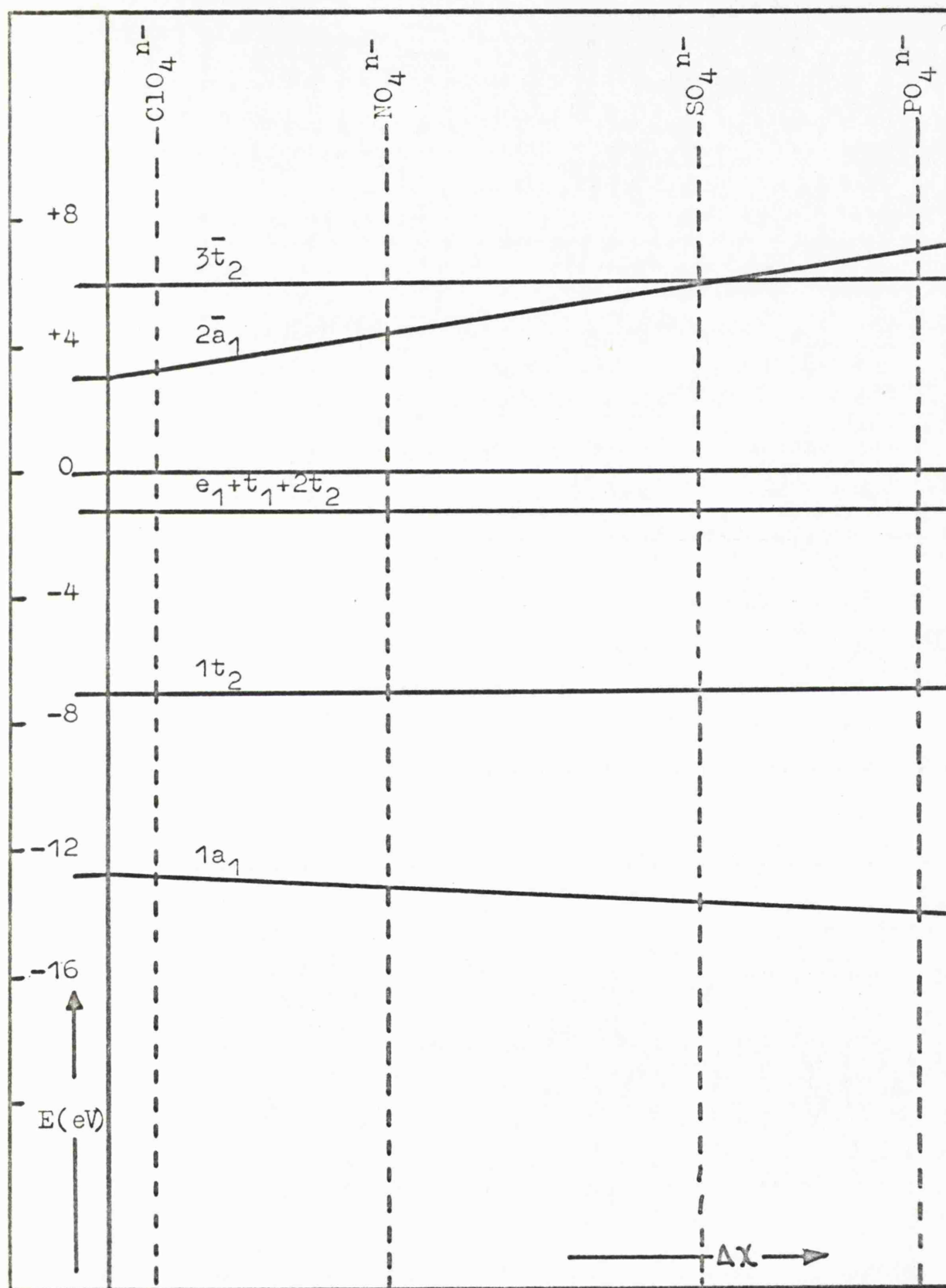


Figure V.5. The variation of the orbital energies for tetrahedral  $XO_4$  molecules with  $\Delta\chi$

anion reduces its symmetry to  $C_{2v}$ . Then the deviations of the anisotropic g-factors from the free-spin value must arise through the following excitations:

$$\Delta g_{11}: \dots (a_2)(b_1)^2(b_2)^2(\bar{a}_1)^2; {}^2A_2 \leftarrow \dots (a_2)^2(b_1)^2(b_2)^2(\bar{a}_1); {}^2A_1$$

$$\Delta g_{22}: \dots (a)^2(b_1)(b_2)^2(\bar{a}_1)^2; {}^2B_1 \leftarrow \dots (a_2)^2(b_1)^2(b_2)^2(\bar{a}_1); {}^2A_1$$

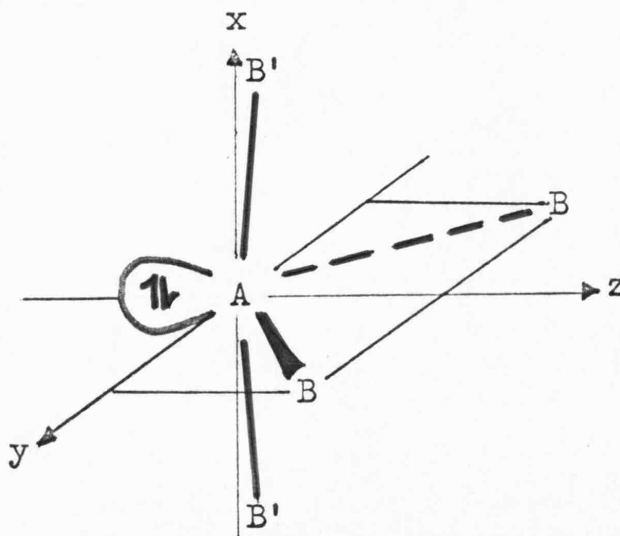
$$\Delta g_{33}: \dots (a_2)^2(b_1)^2(b_2)(\bar{a}_1)^2; {}^2B_2 \leftarrow \dots (a_2)^2(b_1)^2(b_2)^2(\bar{a}_1); {}^2A_1$$

Since  $g_{11} \ll g_{22} < g_{33}$  we conclude that, when the distortion of the tetrahedral anion to  $C_{2v}$ -symmetry splits the non-bonding  $t_1$ -level into  $a_2$ -,  $b_1$ - and  $b_2$ -orbitals, the  $a_2$ -level is lowest in energy. Although the ESR experiment indicates that a distortion of the anion has certainly occurred, the exact configuration adopted is not easily predicted from "Molecular Orbital Theory".

At room temperature the isoelectronic molecule  $PF_4$ , made by exposing  $KPF_6$  or  $NH_4PF_6$  to ionising radiation, gives a purely isotropic spectrum in which all four fluorine atoms appear to be magnetically equivalent.<sup>56</sup>

When the irradiated samples are cooled, the spectrum broadens markedly before giving a very complex and, as yet, uninterpreted powder spectrum. This broadening is considered to arise from an inversion process of an unsymmetrical  $PF_4$  unit, such that two inequivalent pairs

of fluorine atoms are interconverted.<sup>56</sup> This proposal is supported by the observation that  $\text{PF}_4$  in an  $\text{SF}_6$  matrix at low temperatures gives an isotropic spectrum characterised by two pairs of inequivalent fluorine atoms.<sup>63</sup> The analogous chlorine species,  $\text{PCl}_4$ , prepared by the UV-photolysis of phosphorus trichloride, is also reported to possess two pairs of non-equivalent ligand atoms, and a trigonal bipyramidal structure has been proposed for this radical (Figure V.6 ).<sup>62</sup> In contrast the isoelectronic radical  $\text{SF}_4^+$  in solid  $\text{SF}_6$  is reported to have four magnetically equivalent fluorine atoms even at  $96^\circ\text{K}$ .<sup>63</sup> We can satisfactorily account for the structures of these radicals and, indeed, predict the most probable configuration for the  $\text{ClO}_4^{2-}$  anion, using simple arguments based upon the "Valence-Shell Electron-Pair Repulsion Theory." The configuration of maximum probability for an  $\text{AB}_4$  molecule having 5 electron pairs is:



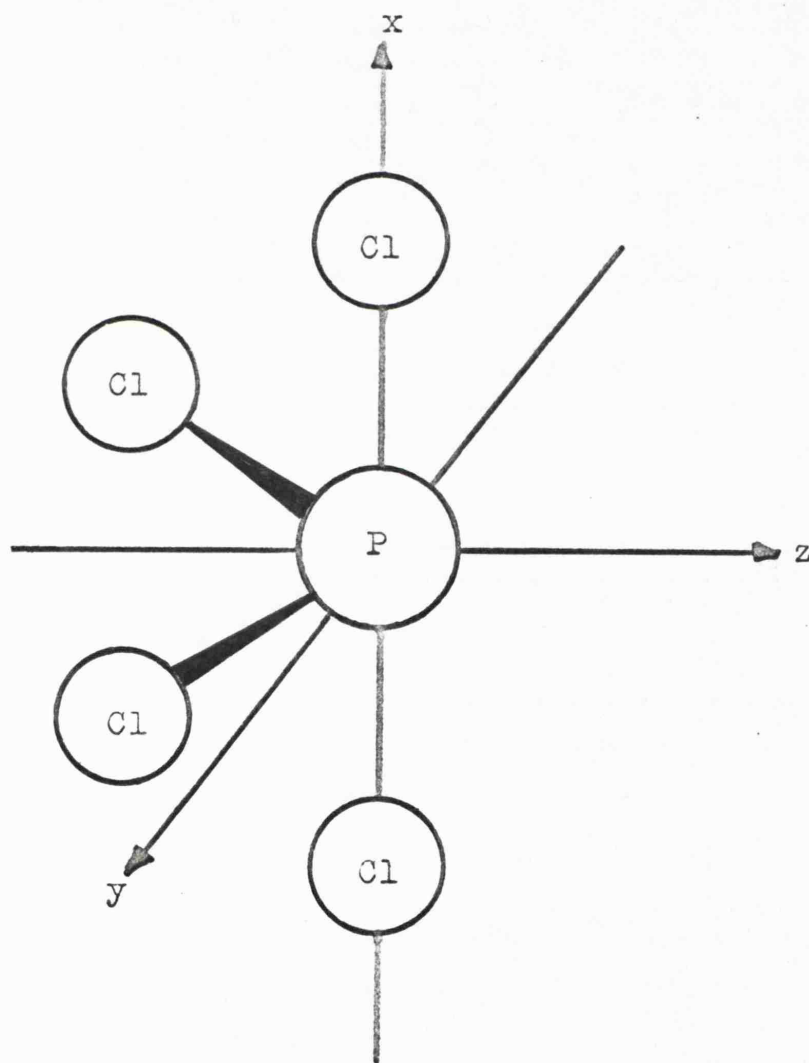
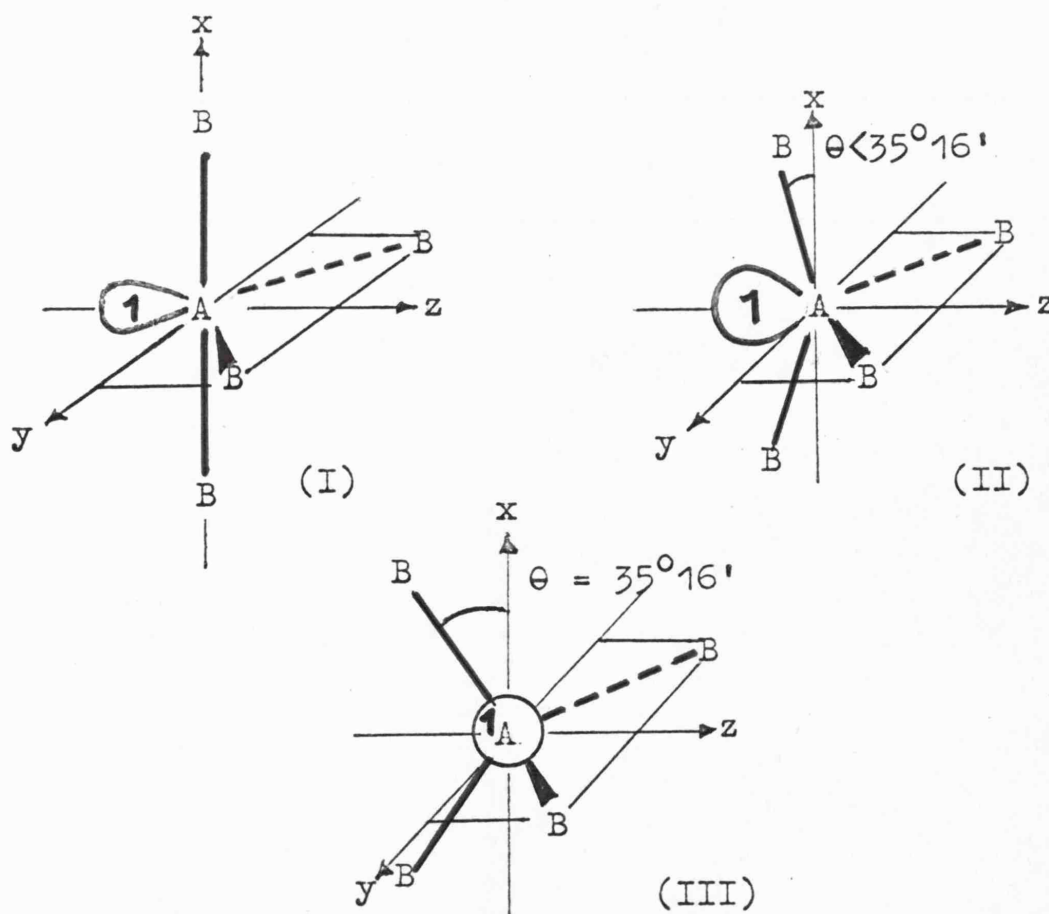


Figure V.6. The proposed structure for the radical  $\text{PCl}_4$  in a  $\text{PCl}_3$  matrix.

For example, the 34 valence-electron  $\text{SF}_4$  molecule is known to have this structure, where the axial S-F' bonds are longer and weaker than the equatorial S-F bonds and the sulphur non-bonding electrons are accommodated in an equatorial  $\text{sp}^2$ -lone pair orbital. In contrast, the 32 valence-electron perchlorate anion  $\text{ClO}_4^-$  is tetrahedral. The radicals  $\text{PF}_4$ ,  $\text{PCl}_4$ ,  $\text{SF}_4^+$  and  $\text{ClO}_4^{2-}$  have 33 valence-electrons, so that we expect them to adopt configurations between these two extremes and the three most probable alternative structures for these species are



The total antibonding electron density ( $a_s^2 + a_p^2$ ) on the central atom in a variety of paramagnetic molecules and ions has been shown to decrease as  $\Delta\chi$  falls (where  $\Delta\chi = \chi_{\text{ligand}} - \chi_{\text{central atom}}$ ). For the series of radicals  $\text{PF}_4$ ,  $\text{PCl}_4$  and  $\text{SF}_4^+$   $\Delta\chi$  is large, so that the unpaired electrons are expected to be confined largely on the central atoms. Consequently, structure (I) is the configuration of maximum probability for these radicals, where the electrostatic interactions between the electron-pairs will be a minimum. The anisotropic spin-resonance data for these species have not been obtained, but if they have this trigonal bipyramidal configuration in which the unpaired electron occupies an essentially  $sp^2$ -lone pair orbital on phosphorus or sulphur, then the observed isotropic spin-densities ( $a_s^2$ ) of about 0.3 correspond to unit occupancy of these central-atom orbitals. For the isoelectronic tetroxide  $(\text{AsO}_4)^{4-}$ , prepared by the action of  $\gamma$ -rays upon  $\text{KH}_2\text{AsO}_4$  at  $77^\circ\text{K}$ ,  $\Delta\chi$  is again large and  $a_s^2$  on the central atom is close to 0.3.<sup>61</sup> However, the detection of hyperfine coupling to four equivalent protons for certain orientations of this radical would suggest that it is best considered as  $\text{As}(\text{OH})_4$ , where the  $\text{AsO}_4^{4-}$  unit is rigidly held close to the tetrahedral configuration (III) through hydrogen-bonding to the protons

of adjacent units in the  $\text{KH}_2\text{AsO}_4$  crystal. Hence, the unpaired electron of  $\text{AsO}_4^{4-}$  in  $\text{KH}_2\text{AsO}_4$  must be located in an orbital which is constructed principally from the arsenic 4s-level.

In contrast,  $\Delta\chi$  for  $\text{ClO}_4^{2-}$  is small and probably negative, so that the unpaired electron is principally confined to the ligand oxygen atoms. Because of this loss of spin-density from the region between the axial Cl—O' bonds, this radical is expected to adopt the slightly distorted tetrahedral structure (II) in which the unpaired electron occupies a molecular orbital having significant 3s-character on chlorine. This structure is in accord with the molecular and spin-resonance parameters of  $\text{ClO}_4^{2-}$  included in Tables V.1 and V.4.

We conclude therefore, that whilst the radicals  $\text{PF}_4$ ,  $\text{PCl}_4$  and  $\text{SF}_4^+$  may well have trigonal bipyramidal structures, the species  $\text{ClO}_4^{2-}$  in  $\text{BaSO}_4$  and  $(\text{AsO}_4)^{4-}$  in  $\text{KH}_2\text{AsO}_4$  are distorted only slightly from the tetrahedral configuration.

#### MECHANISM OF FORMATION

Exposure of perchlorate doped barium sulphate to  $\gamma$ -rays at 77°K gives the radicals  $\text{SO}_4^-$ ,  $\text{ClO}_4^{2-}$  and  $\text{ClO}_3$ .

Chlorine trioxide is probably formed when the perchlorate hole-centre  $\text{ClO}_4$ , unstable in this lattice at

TABLE V.4. Molecular Parameters for the  $\text{ClO}_4^{2-}$  and  $\text{ClO}_3^-$

Radicals in  $\text{BaSO}_4$

Radical	$a_s^2$	$a_p^2$	$a_s^2 + a_p^2$	$a_p^2/a_s^2$
$\text{ClO}_4^{2-}$	0.04	0.03 -0.06	0.07 -0.10	1.5
$\text{ClO}_3^-$	0.074	0.354	0.428	4.78

77°K, undergoes homolytic bond fission. However, we cannot rule out the possibility that this molecule is derived from chlorate ion impurities concurrently coprecipitated with perchlorate by the sulphate. On annealing, the  $\text{SO}_4^- | \text{SO}_4^{2-} |$  and  $\text{ClO}_3 | \text{SO}_4^{2-} |$  centres decay, the former giving rise to the  $\text{SO}_2^-$  radical, and the latter decomposes into products that are not detectable by ESR spectroscopy. This is unusual, for  $\text{ClO}_3$  is known to undergo thermally initiated decomposition into the relatively stable paramagnetic dioxide in chlorate and perchlorate matrices, where the process has been monitored spectroscopically.<sup>70</sup> Both the  $\text{SO}_2^-$  host radical and  $\text{ClO}_4^{2-}$  are extremely stable in  $\text{BaSO}_4$ .

PART II

SPECTROSCOPIC INVESTIGATIONS OF RADIATION

DAMAGE IN  $\text{KClO}_3$  AND  $\text{KClO}_4$

CHAPTER VI

RADIATION DAMAGE IN POTASSIUM CHLORATE

### RADIATION DAMAGE IN POTASSIUM CHLORATE

Alkali metal chlorates are particularly susceptible to high-energy radiation, and high yields of paramagnetic products can often be obtained with comparatively small radiation doses (of the order of  $10^{-2}$  Mrads). This property, coupled with the fact that a variety of defect centres are often formed, has stimulated widespread interest in these systems and the literature abounds with conflicting identifications for the radiation-produced species.

The ESR and electronic spectra of irradiated potassium chlorate are particularly complex, and consequently a complete analysis of the radiation damage products has yet to be accomplished. In  $\gamma$ -irradiated  $\text{KClO}_3$  at  $295^\circ\text{K}$ , Hastey et.al.<sup>73</sup> claimed to have identified the superoxide anion  $\text{O}_2^-$  and a 'two-chlorine' centre  $(\text{OCl}-\text{ClO}_3)^-$ , in which the 'monoxide' interacts weakly with the chlorate ion. Because the spin-resonance parameters of the 'ClO-fragment' were not consistent with those predicted for this radical Atkins et.al.<sup>54</sup> preferred to reassign this centre to a  $(\text{Cl}-\text{ClO}_3)^-$  species containing a considerably flattened chlorate ion. Furthermore, the strong line centred close to  $g = 2.01$  at  $295^\circ\text{K}$ , which was ascribed by Hastey and coworkers<sup>73</sup> to  $\text{O}_2^-$ , exhibited considerable

g-anisotropy at 77°K. Atkins et.al.<sup>54</sup> noted that the observed parameters for this centre were close to those expected for the ozonide anion  $O_3^-$ , the central g-value being identical with that reported for sodium ozonide.<sup>74</sup> A subsequent ESR investigation by Fayet and Thieblemont,<sup>75</sup> whose results appeared in the literature when the present investigation was complete, identified the products of radiation-damage in  $KClO_3$  as  $O_3^-$  a 'two-chlorine' centre designated (Cl-ClX), and a third radical,  $ClO_2$ .

From a detailed spectroscopic investigation of the radiation-colouring of  $KClO_3$  single crystals at 295°K, Ramasastry and Sastry<sup>78</sup> concluded that the stable products were  $ClO^-$ ,  $ClO_2^-$ ,  $ClO_2$  and  $O_3^-$ . These species were characterised by absorption bands at 260 (38,500), 310 (32,200), 360 (27,800), and 450 nm ( $22,200\text{ cm}^{-1}$ ) respectively.

We have attempted to resolve some of the ambiguities outlined above and to reconcile the identified products with an appropriate mechanism for the radiolysis of potassium chlorate.

### EXPERIMENTAL PROCEDURE

#### 1. The Crystal Structure of Potassium Chlorate

$KClO_3$  is monoclinic and the dimensions of the unit cell, which contains two molecules, are  $a = 4.65\text{Å}$ ,  $b = 5.59\text{Å}$ ,  $c = 7.09\text{Å}$  and  $\beta = 109^\circ 38'$ . It belongs to the

space group  $C_{2h}^2$  and has characteristic cleavage planes parallel to the (001) and (100) faces. The 'plate-like' crystals are tabular parallel to the (001) face and they are frequently twinned with (001) as the twinning-plane.<sup>77</sup>

Figure VI.1 is a projection of the atomic positions of K, Cl and O in the ac-plane for a single unit cell of  $KClO_3$ . The positions of the atoms along the b-axis are indicated as fractions of the length of side b relative to the ac-plane.

## 2. Sample Preparation

Single crystals of  $KClO_3$  of suitable dimensions for ESR experiments (0.3 x 0.4 x 0.3 cms) were grown by the slow evaporation of saturated aqueous solutions of the AnalaR grade salt. A polarising microscope was used both to eliminate twinned crystals and, coupled with crystal morphology, to determine the unit cell directions.

Powder samples of  $KClO_3$  were obtained by milling single crystals whose dimensions were unsuitable for single-crystal investigations.

Samples of potassium chlorate were exposed to  $\gamma$ -radiation doses ranging from 0.02 to 3.5 Mrads at both 77°K and room temperature.

## 3. Electron Spin Resonance Spectra

In single-crystal investigations, crystals were

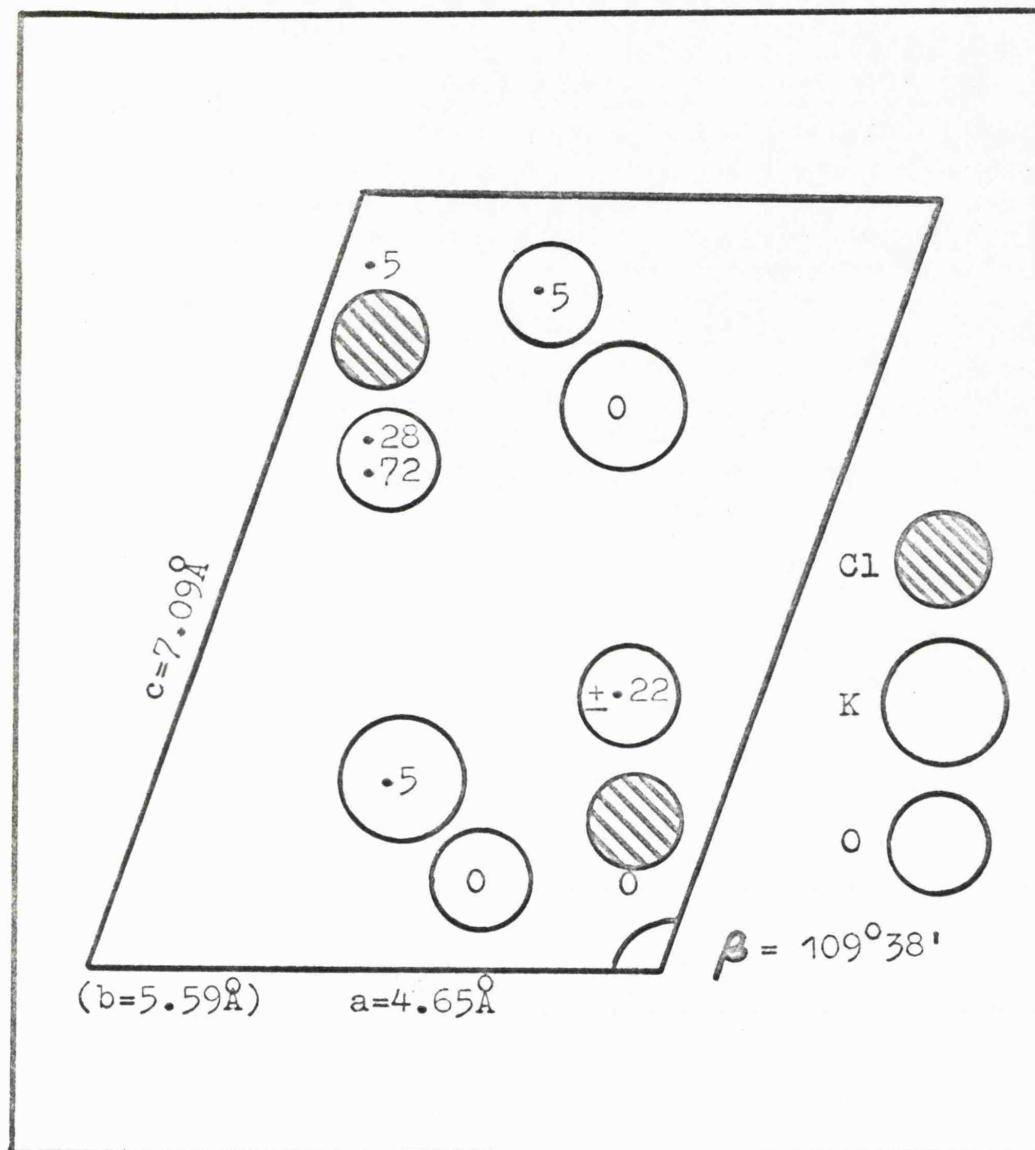


Figure VI.1. The atomic positions of K, Cl and O in the  $ac$ -plane of the  $\text{KClO}_3$  unit cell.

mounted with silicone grease onto the end of a Perspex rod with an accuracy of  $\pm 2^\circ$ . The rod fitted snugly into the ESR spectrometer cavity and a protractor of large radius attached to the end of this rod enabled accurate orientations ( $\pm 0.25^\circ$ ) of the crystal to be made. The characteristic angular variations of ESR features arising from the radiation-produced radicals were monitored as the crystal was rotated in turn about three orthogonal directions perpendicular to the applied magnetic field ( $H_0$ ). The crystallographic a, b and c' axes were chosen for convenience. The c' axis is perpendicular to both a and b, and therefore, to the (001) face, and makes an angle  $19^\circ 38'$  to c. Individual spectra were measured every  $5^\circ$ , except in certain orientations when it was necessary to reduce this interval to  $2.5^\circ$ .

Variable-temperature measurements were carried out on powder samples irradiated at  $77^\circ\text{K}$  and carefully warmed, at 5 deg. K intervals, to room temperature.

The interpretation of the often complex ESR spectra was facilitated by supplementary measurements at Q-band frequency.

#### 4. Electronic Spectra

The electronic spectrum of a thin 'plate-like' single crystal of irradiated  $\text{KClO}_3$  was measured at room

temperature in the region 220-270 nm (45,000 - 37,000  $\text{cm}^{-1}$ ). The subsequent photolysis of the centres produced by irradiation was accomplished using a high-pressure mercury-arc lamp, emitting principally  $3650\text{\AA}$  radiation.

### EXPERIMENTAL RESULTS

#### 1. The Interpretation of the ESR Spectra of Chlorine Containing Radicals

There are two magnetic isotopes of chlorine,  $^{35}\text{Cl}$  and  $^{37}\text{Cl}$ , each having a nuclear spin  $I = 3/2$  and the ratio of their natural abundances is 3.07 : 1. In a single crystal therefore, each chlorine isotope will give rise to a set of four hyperfine lines, the intensity of the set arising from the  $^{35}\text{Cl}$  nucleus being 3.07 times that of the set from  $^{37}\text{Cl}$ . Furthermore, the ratio of the hyperfine splittings arising from the two nuclei will be approximately equal to their magnetic moment ratio ( $\gamma^{35}\text{Cl}/\gamma^{37}\text{Cl}$ ) of 1.202.

Since chlorine has a nuclear spin  $I = 3/2$ , it possesses a quadrupole moment,  $Q$  (for  $^{35}\text{Cl}$  the electric quadrupole moment  $eQ = -0.079 \times 10^{-24} \text{ cm}^2$ ). The quadrupole moment, effectively an asymmetric distribution of charge within the nucleus, interacts with the electric field set up by both the valence electrons of the atom and by the crystalline environment, which, in the absence of an

applied magnetic field ( $H_0$ ), determines the axis of quantisation of the nuclear spins. When  $H_0$  is parallel to the crystal-field symmetry axis, the nuclear hyperfine levels are first-order shifted by an amount which depends on  $M_I$  but is independent of  $M_S$ , so that the frequencies of the allowed transitions ( $\Delta M_I = 0$ ) are unaffected (see Figure IV.2). However, when  $H_0$  is applied at an angle  $\theta$  to the symmetry axis of the crystal-field, second-order effects must be taken into account. The equations representing the second-order shifts in the nuclear hyperfine levels have been shown to contain terms in  $\theta$ ,  $M_I$ ,  $M_S$  and  $Q'$ , where  $Q'$  represents the interaction of  $Q$  with the electric field gradient  $\left| \frac{\partial^2 V}{\partial Z^2} \right|$  at the nucleus:

$$Q' = \frac{3eQ}{4I(2I-1)} \left| \frac{\partial^2 V}{\partial Z^2} \right| \dots\dots(6)$$

This means that the shift is different for each level and consequently the nuclear hyperfine lines are unequally spaced. The quadrupole interaction results in maximum separation either at the ends or in the middle of a group of hyperfine features, depending on the sign of  $Q$ , rather than a progressive increase or decrease with  $H_0$ . Furthermore, the quadrupole interaction tries to align the nucleus along the symmetry axis, whereas the

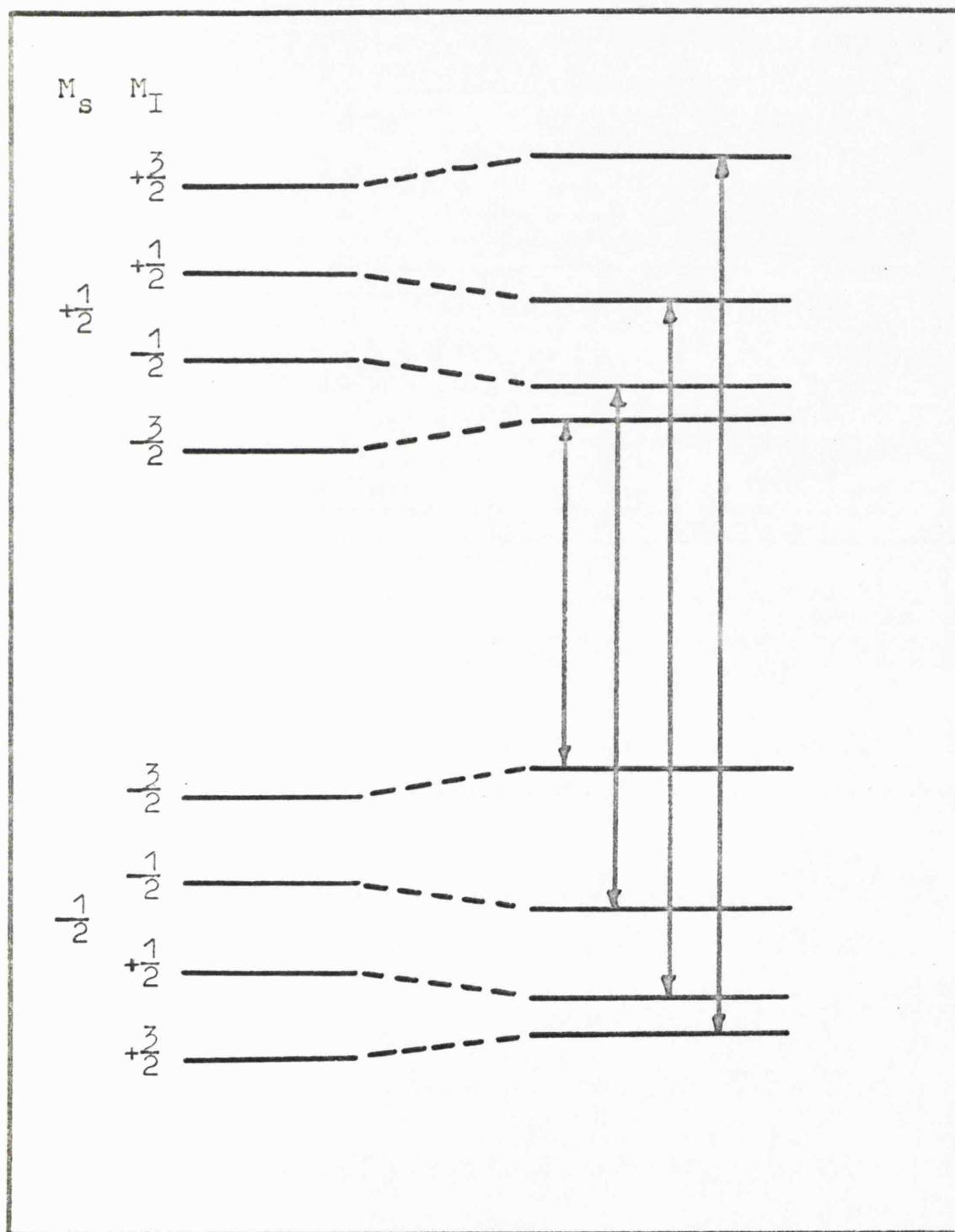


Figure VI.2.

The energy levels for a system with electron spin  $S = \frac{1}{2}$  and  $I = \frac{3}{2}$  showing the effect of the nuclear quadrupole moment when  $H_0$  is parallel to the crystal-field symmetry axis.

magnetic field established by the electrons tries to align the nucleus along the resultant magnetic field direction. The result of this competition between the electrostatic and magnetic interactions is a scrambling of the nuclear energy levels so that the  $2I + 1$  levels, usually represented by  $|M_I\rangle$ , may become admixed with the  $|M_I \pm 1\rangle$  states to an extent  $\alpha$ . The normal selection rule  $\Delta M_I = 0$  now breaks down and transitions with  $\Delta M_I = \pm 1$  or  $\pm 2$  become allowed (see Figure IV.3). The intensity of these 'forbidden' transitions is proportional to  $\alpha$ , which becomes progressively larger as the angle ( $\theta$ ) between  $H_0$  and the symmetry axis of the quadrupole interaction increases to  $90^\circ$ . These 'forbidden' lines appear quite strongly in certain orientations in single crystals and almost certainly confuse the interpretation of powder spectra. However, powder spectra at Q-band become simpler to interpret because the three-fold increase in the magnetic field strength, compared to X-band, tends to align the nucleus parallel to  $H_0$  and consequently  $\alpha$  approaches zero. The problem of unambiguously analysing the ESR spectra of chlorine containing radicals, often complicated by the superposition of features corresponding to the 'allowed' ( $\Delta M_I = 0$ ) and 'forbidden' ( $\Delta M_I = \pm 1, \pm 2$ ) transitions,

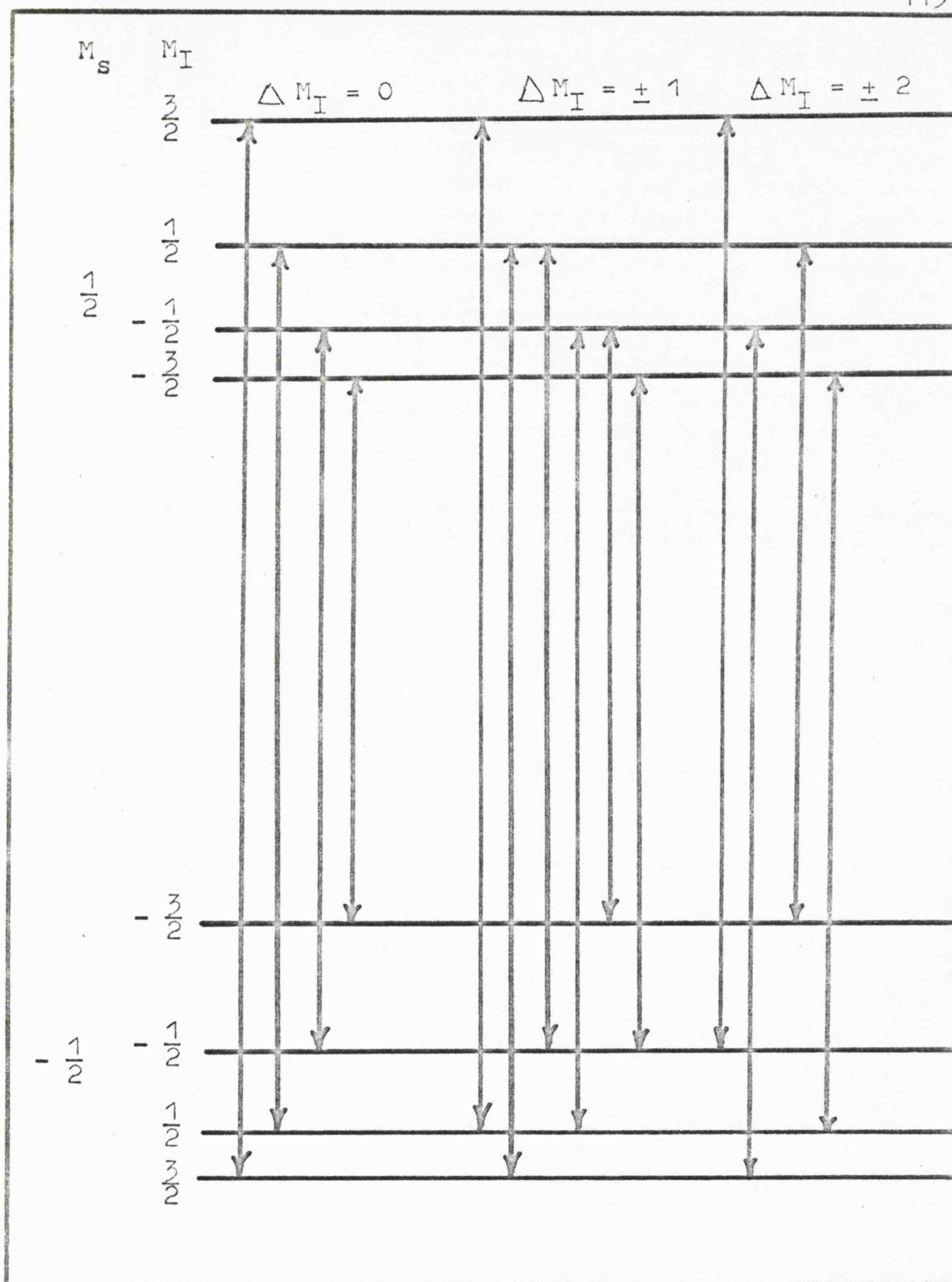


Figure VI.3. The 'allowed' and 'forbidden' transitions for a system with  $S = \frac{1}{2}$  and  $I = \frac{3}{2}$  when  $H_0$  makes an angle  $\theta$  to the crystal-field symmetry axis.

is also simplified by the fact that the sets of hyperfine lines corresponding to the  $^{35}\text{Cl}$  and  $^{37}\text{Cl}$  nuclei have the characteristic intensity and separation ratio's mentioned previously.

The effect of the quadrupole interaction upon the ESR spectra of these radicals is accounted for by the addition of the term:

$$H_Q = Q' \left( I_z^2 - \frac{1}{3} I(I+1) \right) \dots\dots(7)$$

to the spin-Hamiltonian described in Chapter I. We have not undertaken a complete analysis of these quadrupole interactions in the compounds studied and no quadrupole coupling constants are included in the Tables. Despite this limitation the principal values obtained after a rigorous treatment of these quadrupole terms show little difference from those obtained by the normal analysis of powder spectra for the chlorine oxides.

## 2. Electron Spin Resonance Spectra of $\text{KClO}_3$

### a) $\gamma$ -irradiated at $295^\circ\text{K}$

#### i) Single-crystal Spectra

The exposure of potassium chlorate to  $\gamma$ -rays at room temperature resulted in the formation of three distinct defect centres. Figure VI.4 shows the ESR spectrum,

Radical B



Radical A



Radical C

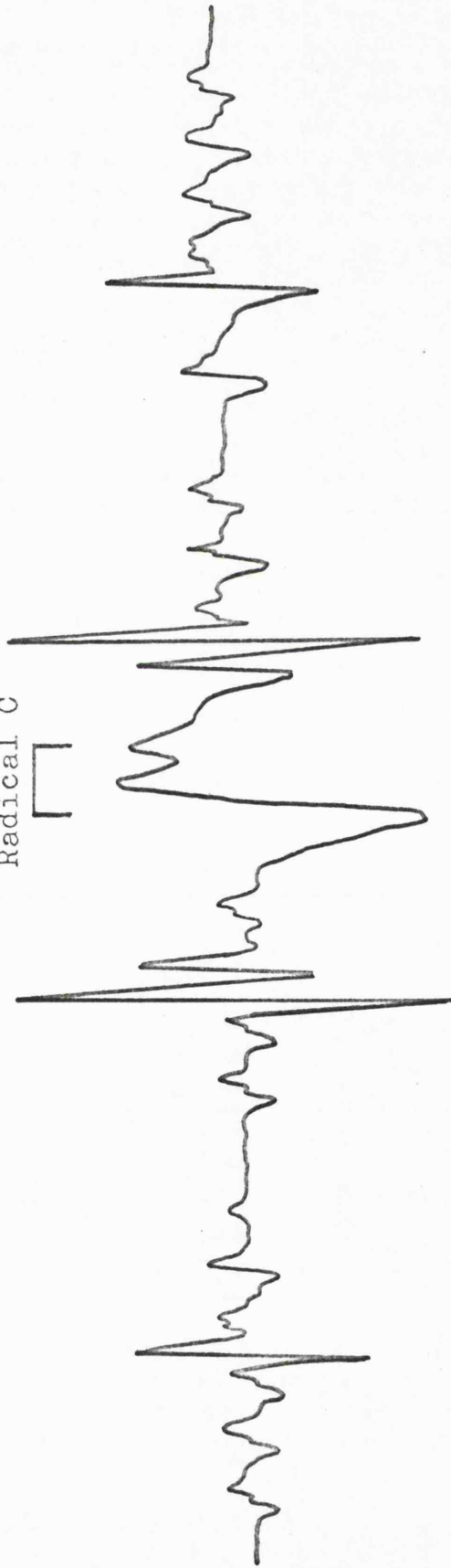


Figure VI.4. The ESR spectrum, measured at 9.3 Gc/s, of an irradiated single crystal of  $\text{KClO}_3$  with  $H_0$  parallel to the  $a$ -axis. 117

measured at 295°K, of a single crystal of  $\text{KClO}_3$  oriented with the applied magnetic field ( $H_0$ ) parallel to the crystal a-axis. The origins of the hyperfine lines are marked on the diagram. Both radicals A and B contained chlorine and occupied single, magnetically distinct sites in the chlorate lattice, whilst C appeared to contain no interacting magnetic nuclei.

Radical A was responsible for a quartet of features arising from the interaction of the unpaired electron with a single chlorine nucleus, for it was possible to detect features corresponding to both the  $^{35}\text{Cl}$  and  $^{37}\text{Cl}$  isotopes in this orientation.

Radical B appeared to contain two chlorine atoms, since in certain orientations of the crystal it was possible to detect hyperfine lines corresponding to the isotopic combinations  $^{35}\text{Cl}\text{—}^{35}\text{Cl}$ ,  $^{35}\text{Cl}\text{—}^{37}\text{Cl}$ ,  $^{37}\text{Cl}\text{—}^{35}\text{Cl}$ , and even  $^{37}\text{Cl}\text{—}^{37}\text{Cl}$ . In poorly resolved spectra however, it was only possible to discern features attributable to the  $^{35}\text{Cl}\text{—}^{35}\text{Cl}$  pair, giving the impression that B was characterised by a simple quartet of quartets.

Radical C gave rise to a very broad resonance that often obscured features from A and B, particularly in the regions of minimum hyperfine splitting.

Figures VI.5 to 7 are plots of the angular variations

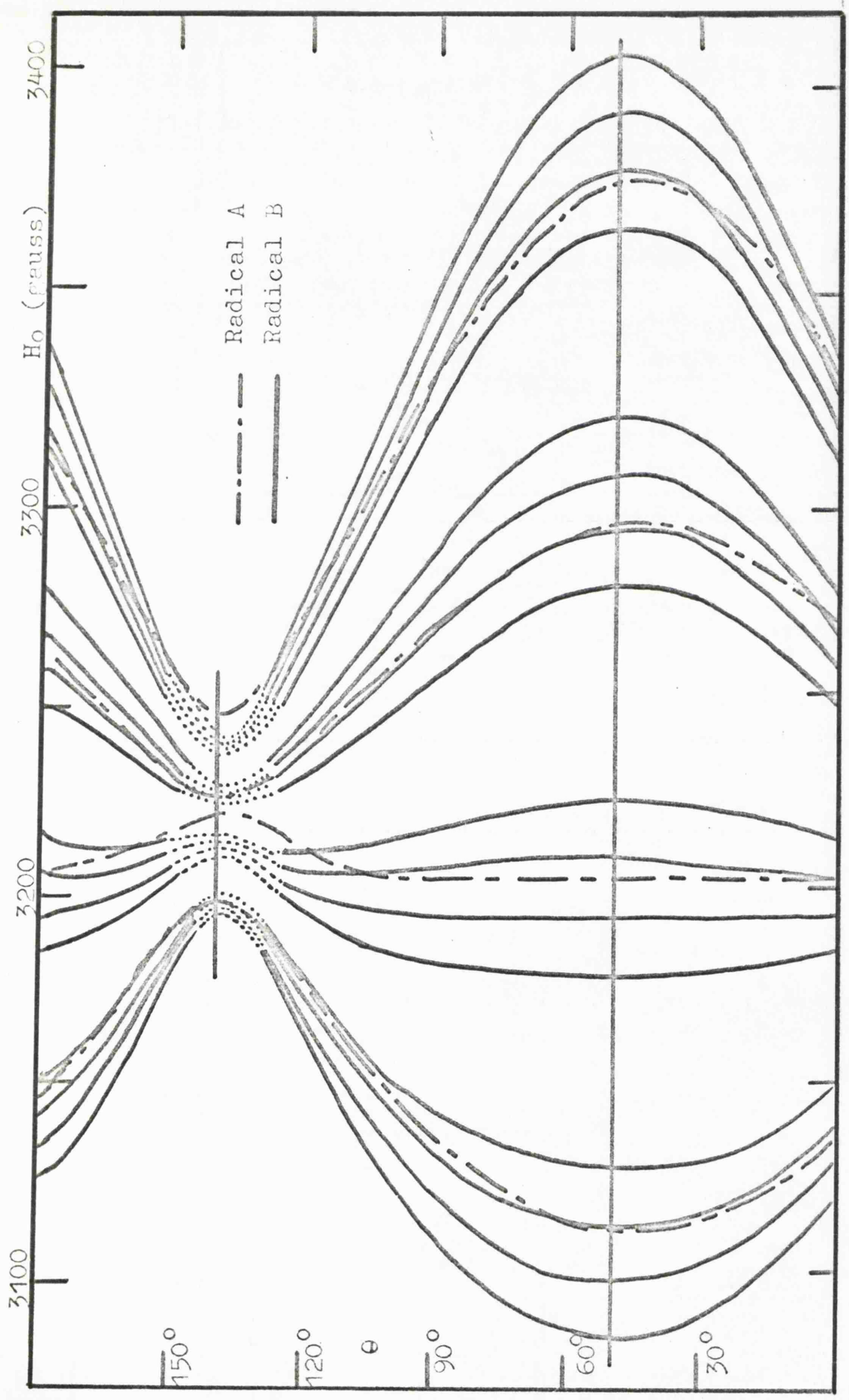


Figure VI.5. The angular variation of the hyperfine features from radicals A and B as  $H_0$  explores the ab-plane.  $\theta$  is the angle between  $H_0$  and the  $a$ -axis.

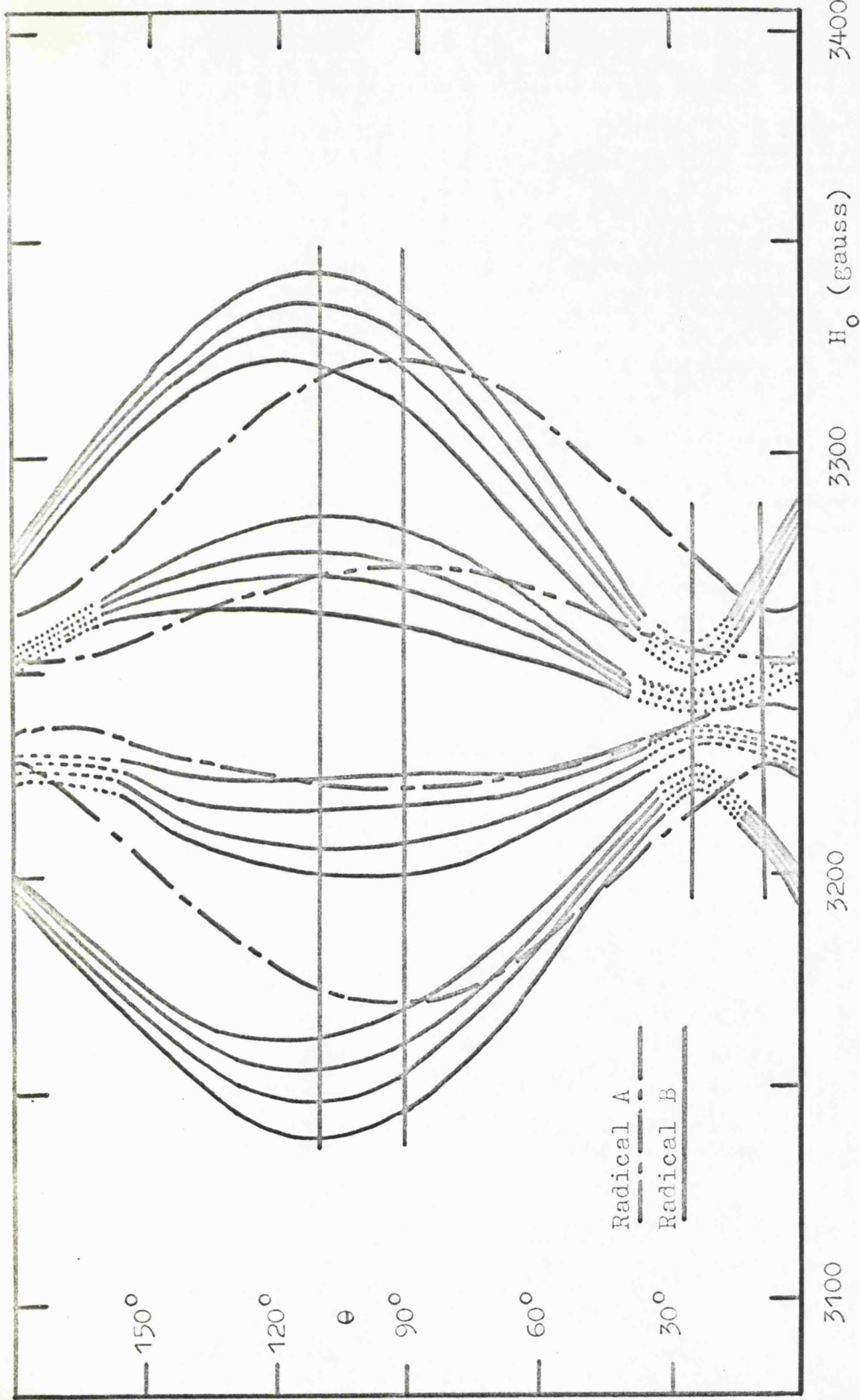


Figure VI.6. The angular variation of the hyperfine features from radicals A and B as  $H_0$  explores the  $ac'$ -plane.  $\theta$  is the angle between  $H_0$  and the  $c'$ -axis.

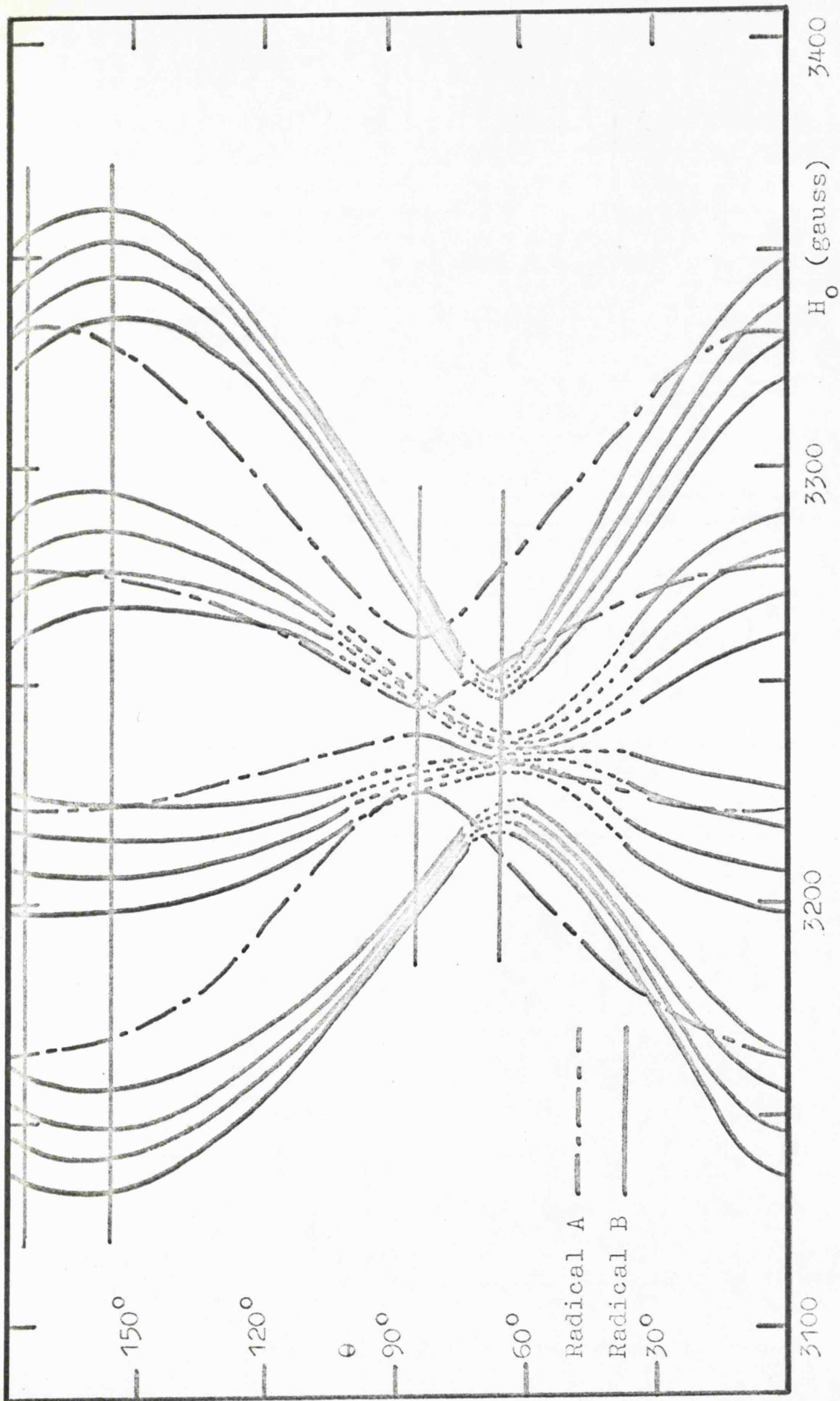


Figure VI.7. The angular variation of the hyperfine features from radicals A and B as  $H_0$  explores the  $bc'$ -plane.  $\theta$  is the angle between  $H_0$  and the  $b$ -axis.

of hyperfine features corresponding to radicals A and B as  $H_0$  explored the crystal ab, ac' and bc' planes in turn. The ESR spectra of these centres were fitted to the spin-Hamiltonian:

$$\mathcal{H} = H \cdot g \cdot S + I \cdot A \cdot S \quad \dots\dots(8)$$

$$\text{where } S = \frac{1}{2} \text{ and } I = \frac{3}{2}$$

and the principal values and direction cosines of the g- and A-tensors (see Table VI.1) were evaluated using Schonland's<sup>15</sup> method.

The spectra of radical A were analysed unambiguously in the three planes. However, for B, the values of  $a_{xx}$  and  $g_{xx}$  were more precisely determined than the remaining parameters, for at the position of minimum hyperfine splitting the spectra were particularly complex. The 32 features corresponding to the  $\Delta M_I = 0$  transitions for the various isotopic combinations of B overlapped with the 8 allowed transitions of A and with broad resonance of C, together with the 'forbidden' transitions of both A and B (whose intensity is a maximum in this region), in a very narrow region of the spectrum ( $\sim 50$  gauss). These regions are therefore dotted in Figures VI.5 to 7. The spin-resonance features arising from radical C exhibited a very small angular dependence, consequently they have

TABLE VI.1. Electron Spin Resonance Data for the Radicals  $\text{ClO}_2$  and  $(\text{ClO}_2\text{-Cl})^-$  in a Single Crystal of  $\text{KClO}_3$ .

Radical and Identification	g-tensor			Direction Cosines			Experimental	Anisotropic	Isotropic	Direction Cosines $a'$		
	$g_{xx}$	$g_{yy}$	$g_{zz}$	a	b	c'				a	b	c'
A ( $\text{ClO}_2$ )	2.0018	2.0167	2.0111	+0.99	+0.05	+0.16	$a_{xx}=+79.9$ $a_{yy}=-13.4$ $a_{zz}=-12.5$	$B_{xx}=+61.9$ $B_{yy}=-31.4$ $B_{zz}=-30.5$	18.0	+0.97	-0.03	+0.23
	$(g_{av}=2.0101)$											
B ( $\begin{matrix} a\text{ClO}_2 \\   \\ b\text{Cl} \end{matrix}$ )	2.0022	2.022	2.014	+1.00	+0.02	+0.02	$a_{xx}=+86.6$ $a_{yy}=-12$ $a_{zz}=-9$	$B_{xx}=+64.6$ $B_{yy}=-34$ $B_{zz}=-31$	22.0	+0.97	-0.01	+0.24
	$(g_{av}=2.0127)$											
							$b_{Cl}^-$					
							$a_{xx}=13.8$ $a_{yy}=1$ $a_{zz}=1$	$B_{xx}=+8.5$ $B_{yy}=-4.3$ $B_{zz}=-4.3$	5.3	+0.73	+0.26	+0.62

$a'$ .  $\text{KClO}_3$  is monoclinic with  $\beta = 109^\circ 38'$  so that the angle between  $c'$  and the crystallographic  $c$  axis is  $19^\circ 38'$ .

\* These directions have no significance.

been omitted from these plots for clarity. The ESR parameters of this centre, included in Table VI.2 were obtained from a powder spectrum measured at  $77^{\circ}\text{K}$ .

Initially, radicals A and B were produced in approximately equal abundance, however, when the crystal was annealed to  $313^{\circ}\text{K}$  a decrease in the intensity of features from A was accompanied by a parallel increase in those from B. We conclude therefore, that at least some of A was converted to B as a result of the annealing process. At this temperature radical A decayed, by a first-order process with respect to A, with a half-life of approximately 5 minutes and Figure VI.8 is the thermal decay curve for this process. After 40 minutes at this temperature the ESR spectrum was remarkably similar to that reported by Hasty et.al.<sup>73</sup> for X-irradiated  $\text{KClO}_3$  at room temperature. Radical B annealed rapidly when the crystal was heated to  $345^{\circ}\text{K}$ , whereas no perceptible decay of C occurred even when the crystal was heated to  $400^{\circ}\text{K}$ .

When an irradiated single crystal of  $\text{KClO}_3$  was photo-bleached with  $3650\text{\AA}$  radiation, ESR signals from a fourth centre (D) appeared at the expense of both A and B. Radical C was apparently unaffected by the photolysis but was sensitive to radiation in the visible region and was bleached slowly when left exposed in the laboratory.

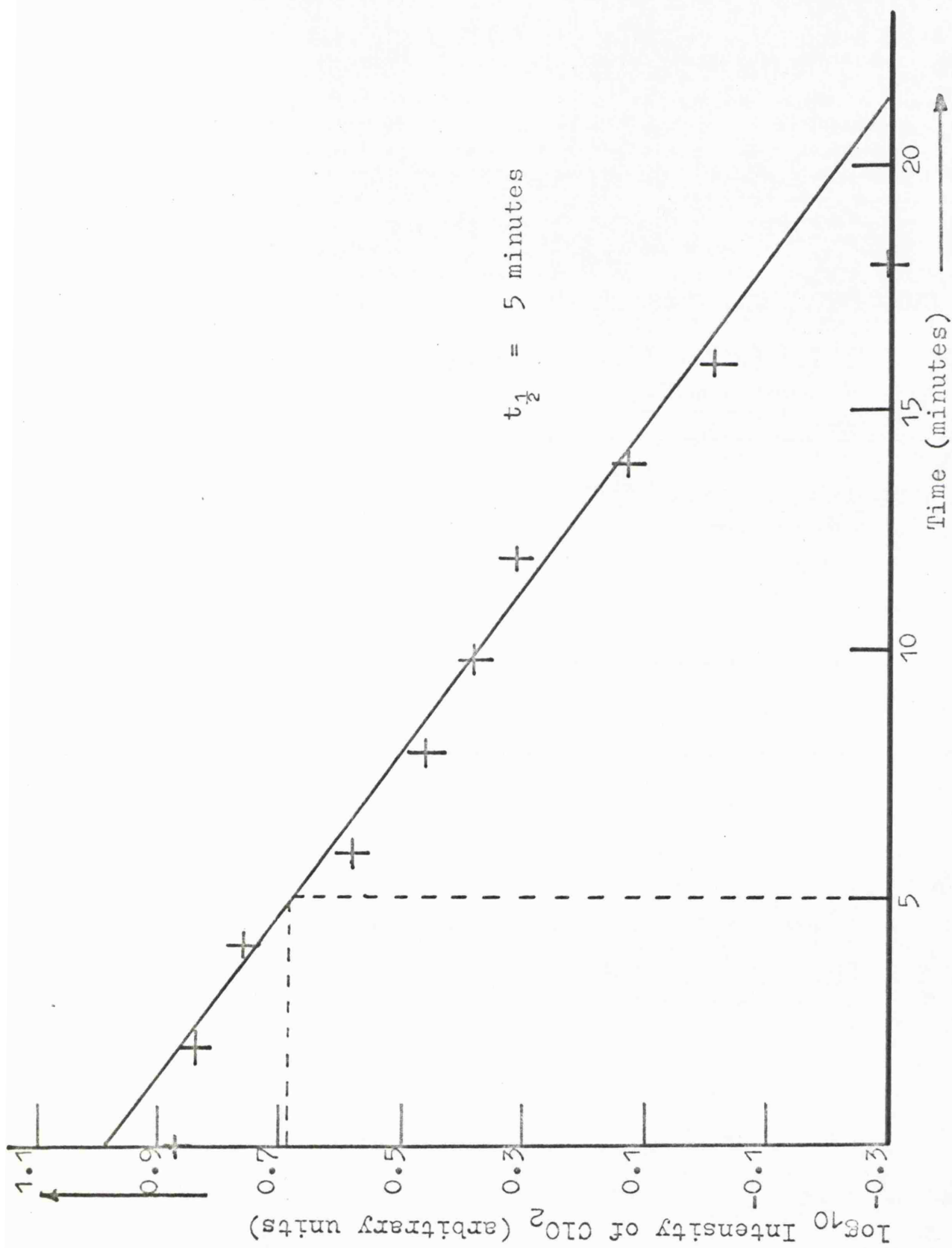


Figure VI.8. Thermal decay curve for radical A in a  $\text{KClO}_3$  matrix.

Figure VI.9 is a Q-band spectrum of D in a single crystal of  $\text{KClO}_3$  measured with  $H_0$  parallel to the crystal a-axis. The spectrum consists basically of a septet of lines with the intensity distribution 1:2:3:4:3:2:1. Figure VI.10 is a plot of the angular variation of the hyperfine lines from D as  $H_0$  explores the ab-plane. Radical D was thermally stable in the chlorate lattice up to  $420^\circ\text{K}$ .

ii) Powder Spectra

Figure VI.11 is an ESR spectrum, measured at  $295^\circ\text{K}$ , of irradiated  $\text{KClO}_3$  powder and again the origins of the hyperfine lines are marked on the diagram. Only the parameters  $a_{xx}$  and  $g_{xx}$  for radicals A and B could be derived from this spectrum. Radical A was also characterised by an intense absorption centred at  $g = 2.026 - 2.027$  in the powder spectrum. When the powder was cooled, the broad central resonance from C narrowed markedly and Figure VI.12 shows the three well-resolved g-features of this radical at  $77^\circ\text{K}$ . The spectra of radicals A and B were also better resolved at this temperature, but this did not lead to any additional information. In variable-temperature experiments, the parameters  $a_{xx}$  and  $g_{xx}$  of A and B showed a significant temperature sensitivity, reaching maximum values when the powder was cooled to  $4.2^\circ\text{K}$ .

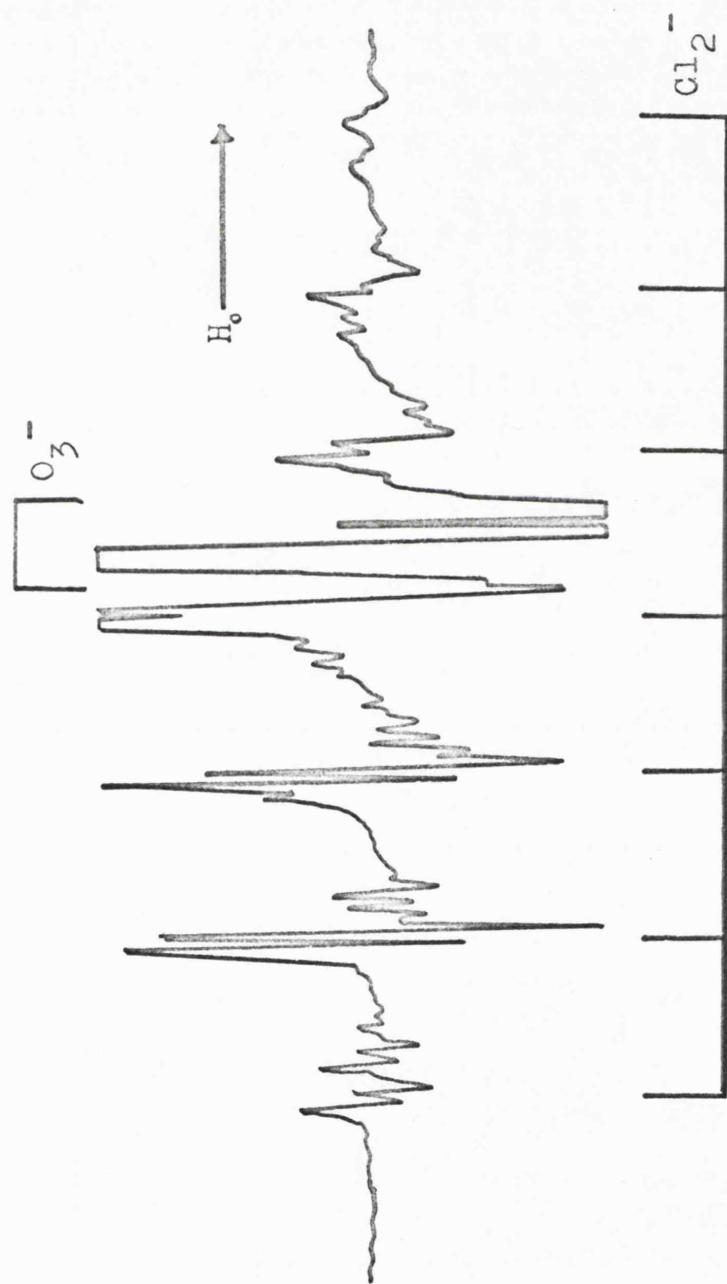


Figure VI.9. The ESR spectrum of radical D in a single crystal of  $\text{KClO}_3$  measured at 34 Gc/s with  $H_0$  parallel to the a-axis.

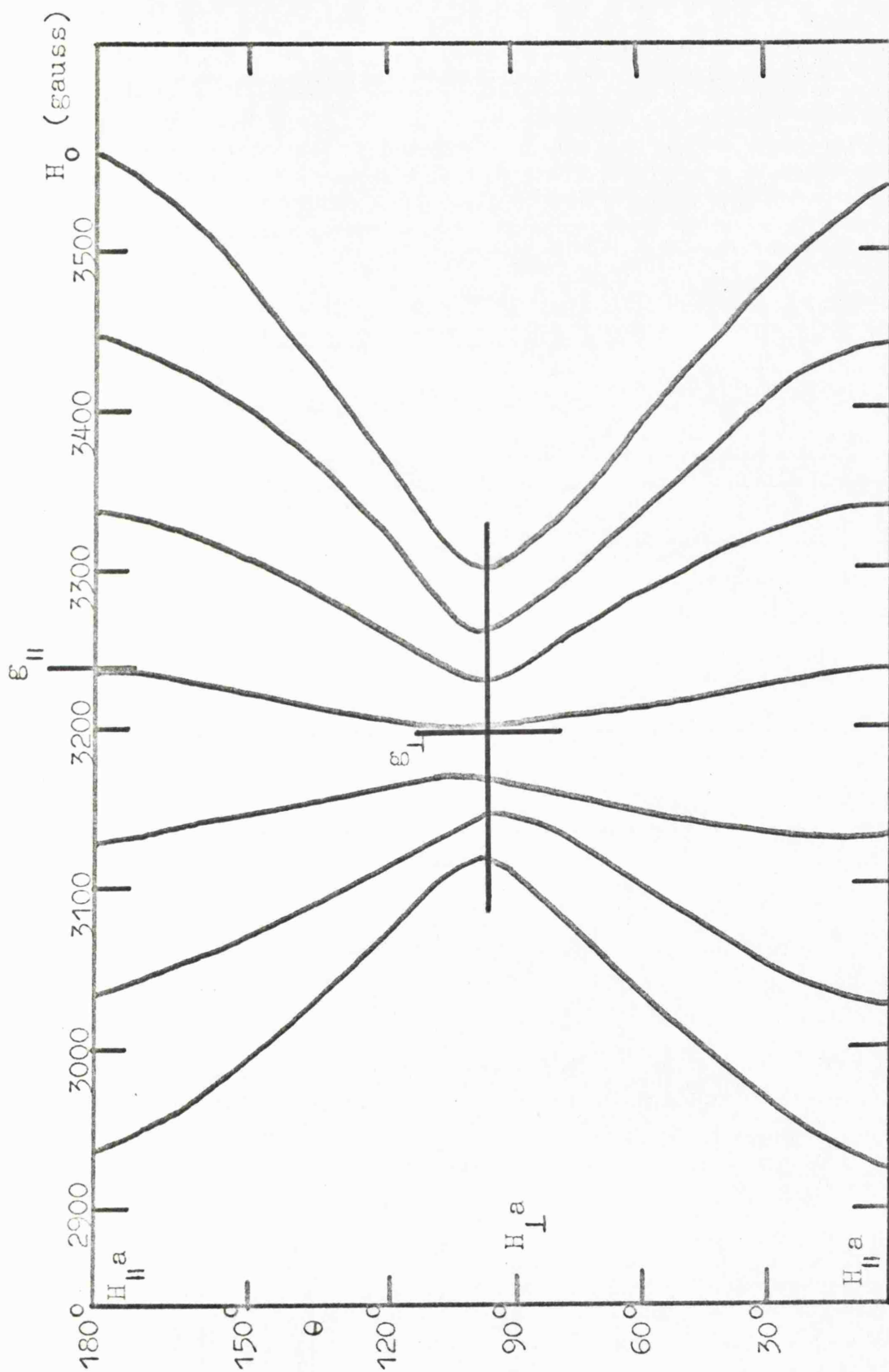


Figure VI.10. The angular variation of the hyperfine features from radical D as  $H_0$  explores the ab-plane.

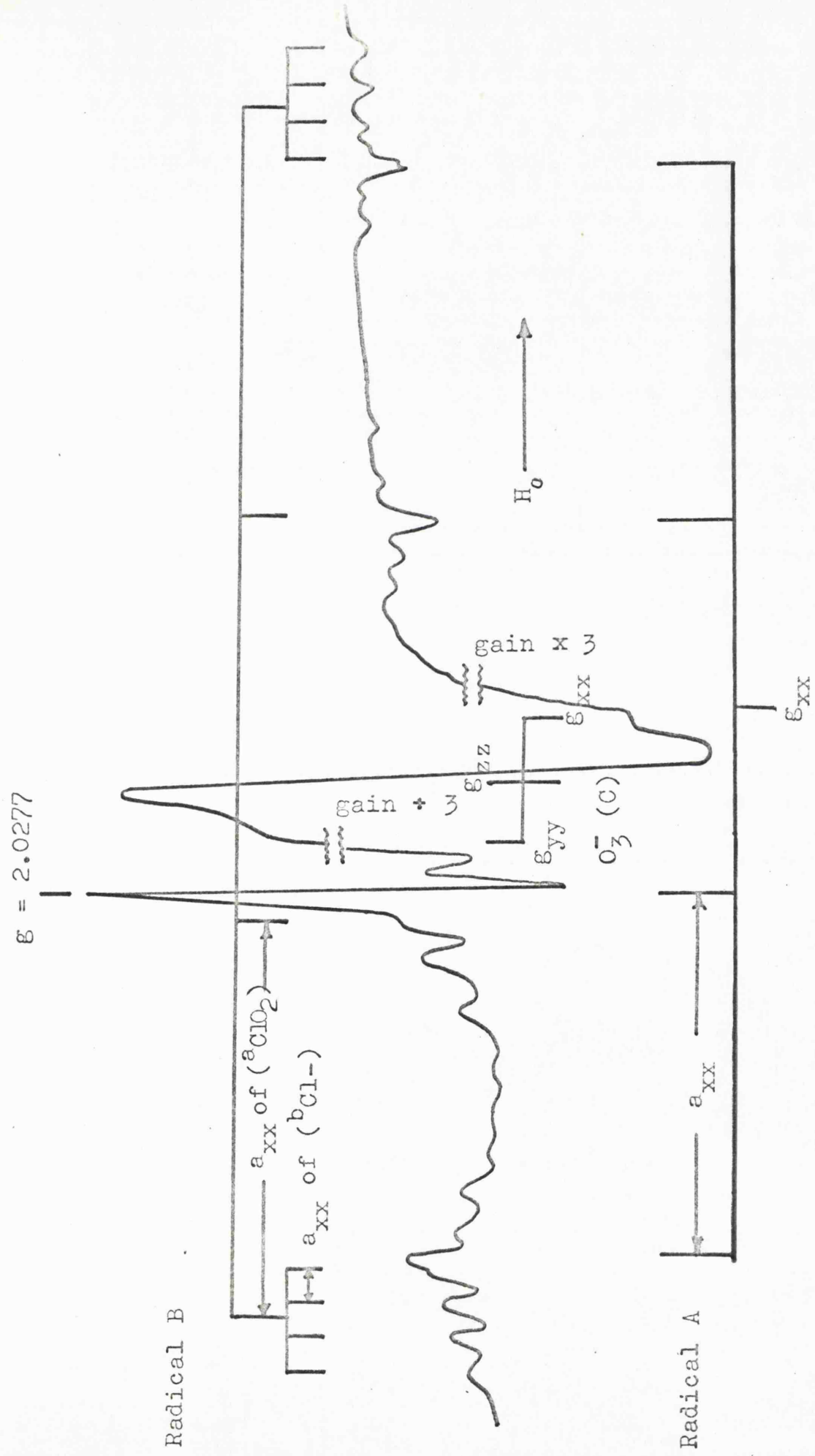


Figure VI.11. Powder ESR spectrum of  $\text{KClO}_3$  measured at  $295^\circ\text{K}$ .

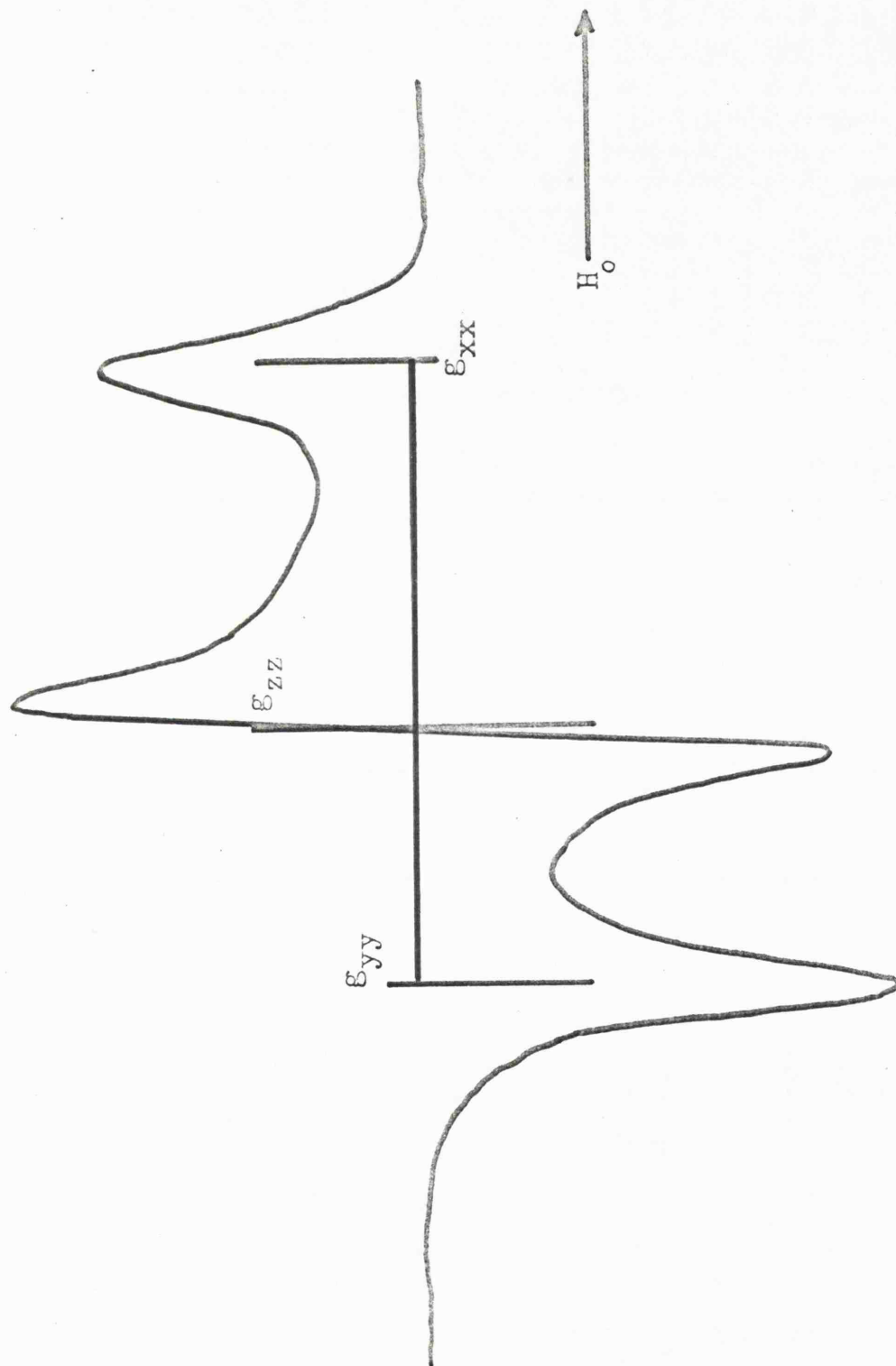


Figure VI.12. The ESR spectrum of Radical C in a  $\text{KClO}_3$  powder measured at  $77^\circ\text{K}$ .

The spin-resonance parameters obtained from these powder spectra are shown in Table VI.2 for comparison with those derived from the single-crystal study.

b)  $\gamma$ -irradiated at 77°K

A complete single-crystal investigation of the low temperature, radiation damage of  $\text{KClO}_3$  has yet to be accomplished. However, we have attempted a partial analysis of the extremely complex powder spectrum of  $\text{KClO}_3$  irradiated and measured at 77°K.

The exposure of potassium chlorate powder to  $\gamma$ -rays at 77°K resulted in the formation of several paramagnetic defect centres. After 20 minutes irradiation two distinct species could be identified from the complex ESR spectrum. These are labelled E and F in Figure VI.13. It was also clear that radical A was formed at this temperature, since the characteristically intense feature at  $g \cong 2.027$  was dominant in this spectrum, whilst signals from radicals B and C were absent. The ESR spectra of radicals E and F were interpreted in terms of axially symmetric species possessing both  $g$ - and  $A$ -anisotropy, and the spin-resonance data obtained from this analysis are included in Table VI.4.

Figure VI.14 is the ESR spectrum of the irradiated powder after it had been annealed at 90°K for approxi-

TABLE VI.2. Electron Spin Resonance Data for the Radicals  $\text{ClO}_2$ ,  $(\text{ClO}_2\text{-Cl})^-$   
and  $\text{O}_3^-$  derived from  $\gamma$ -irradiated  $\text{KClO}_3$  Powder.

Radical	$g_{xx}$	$g_{yy}$	$g_{zz}$	$g_{av}$	$a_{xx}$ ( $^{35}\text{Cl}$ ) in Gauss	Temp. $^{\circ}\text{K}$	Ref.
A. $(\text{ClO}_2)$	2.0028				79.65 83.10 85.80	295 77 4.2	b
B. $(^a\text{ClO}_2\text{-}^b\text{Cl})^-$	2.0022				$(^a\text{Cl})$ 85.84 $(^b\text{Cl})$ 14.0	295	b
C. $(\text{O}_3)^-$	2.0026	2.0180	2.0116	2.0107		77	b
$\text{NaO}_3$ a.				2.012			74

a. Included for comparison with C.

b. This work.

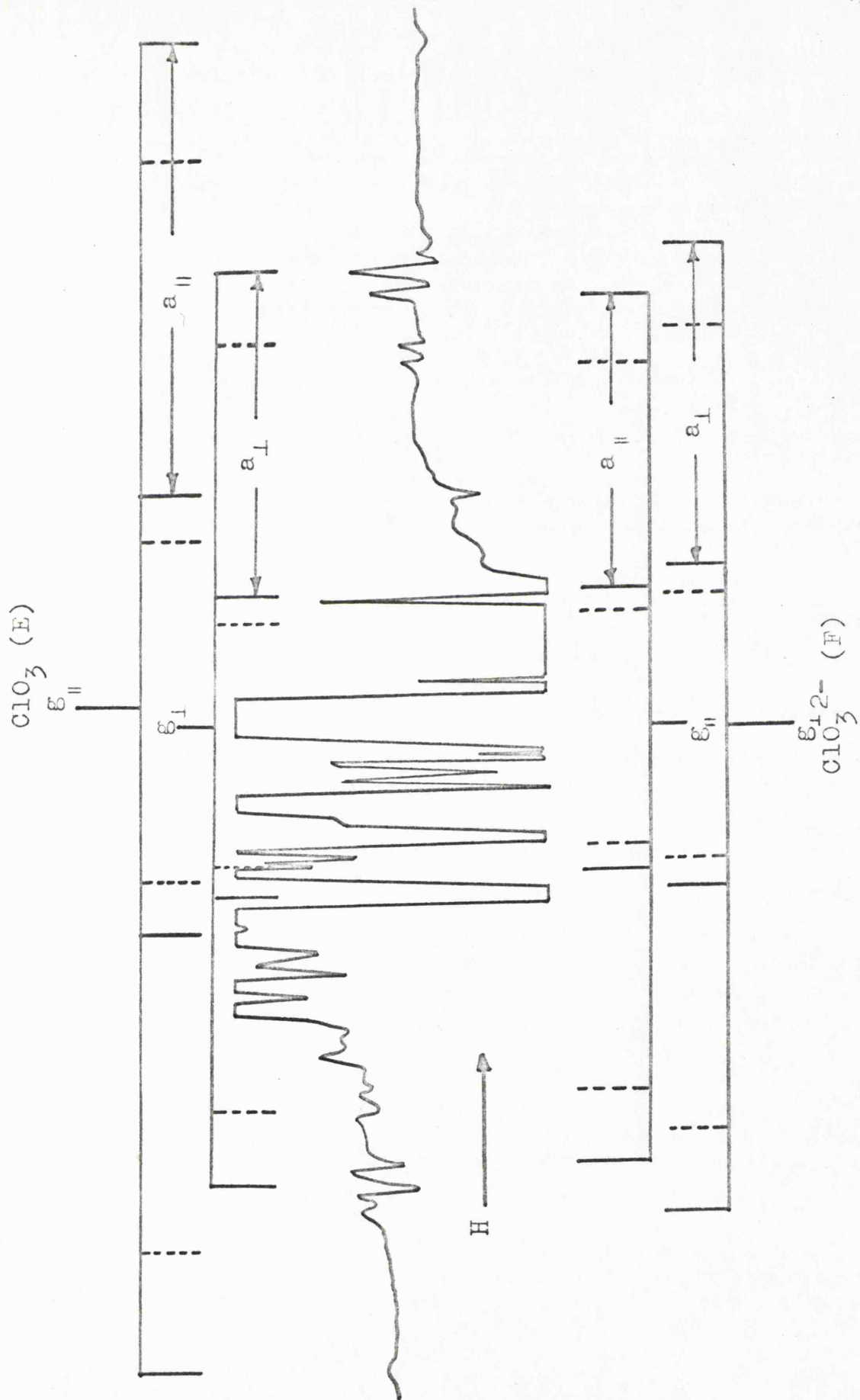


Figure VI.13. The powder ESR spectrum of  $\text{KClO}_3$  irradiated and measured at  $77^\circ\text{K}$ .

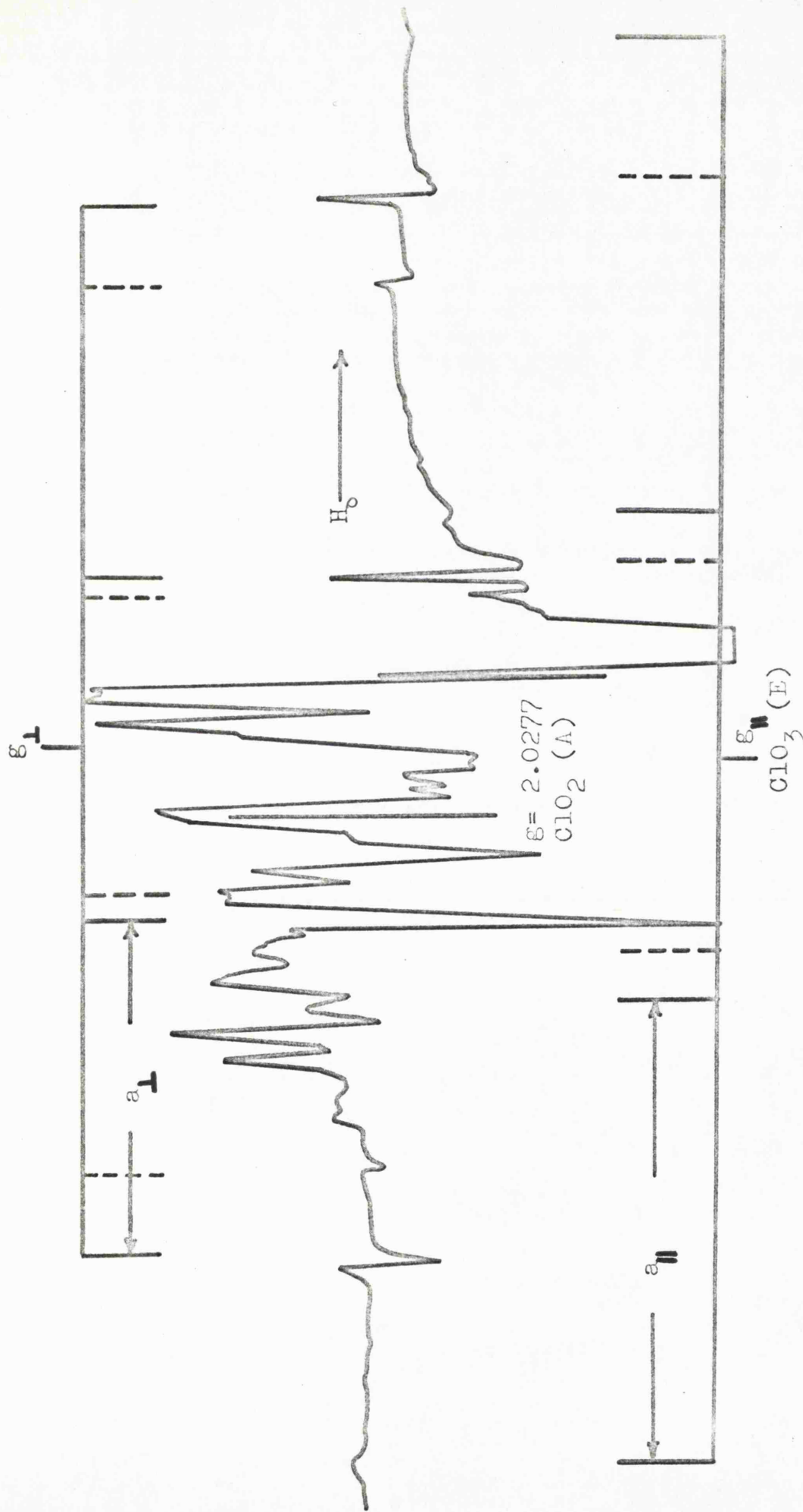


Figure VI.14. The powder ESR spectrum of  $KClO_3$  irradiated at  $77^{\circ}K$  and measured at  $90^{\circ}K$ .

ately 10 minutes. At this temperature radical F rapidly decayed. When the sample was heated to 120°K, only the spectrum of radical A was observed and this can be seen in Figure VI.15. Finally, annealing to 295°K resulted in the simultaneous formation of radicals B and C and in an increased yield of A.

### 3. The Electronic Spectrum of Irradiated KClO<sub>3</sub>

Figure VI.16 shows the optical absorption spectrum of a thin 'plate-like' single crystal of KClO<sub>3</sub> which had been exposed to a  $\gamma$ -radiation dose of approximately 0.5 Mrads at 295°K. The crystal was mounted in the UV spectrometer with the tabular (001) face perpendicular to the incident radiation. This spectrum has been previously analysed in terms of the overlap of several individual absorptions with maxima at 216 (46,400), 240 (41,700), 305 (32,800), 360 (27,800), and 445 nm (22,500 cm<sup>-1</sup>).<sup>78</sup> (This analysis is marked on the diagram).

When the irradiated crystal was photobleached with 3650Å radiation, a weak band, with a maximum intensity at 380 nm (26,300 cm<sup>-1</sup>), developed at the expense of the 360 nm (27,800 cm<sup>-1</sup>) absorption. (see Figure VI.17). This absorption is assigned to radical D, whilst A or B was responsible for the band at 360 nm (27,800 cm<sup>-1</sup>).

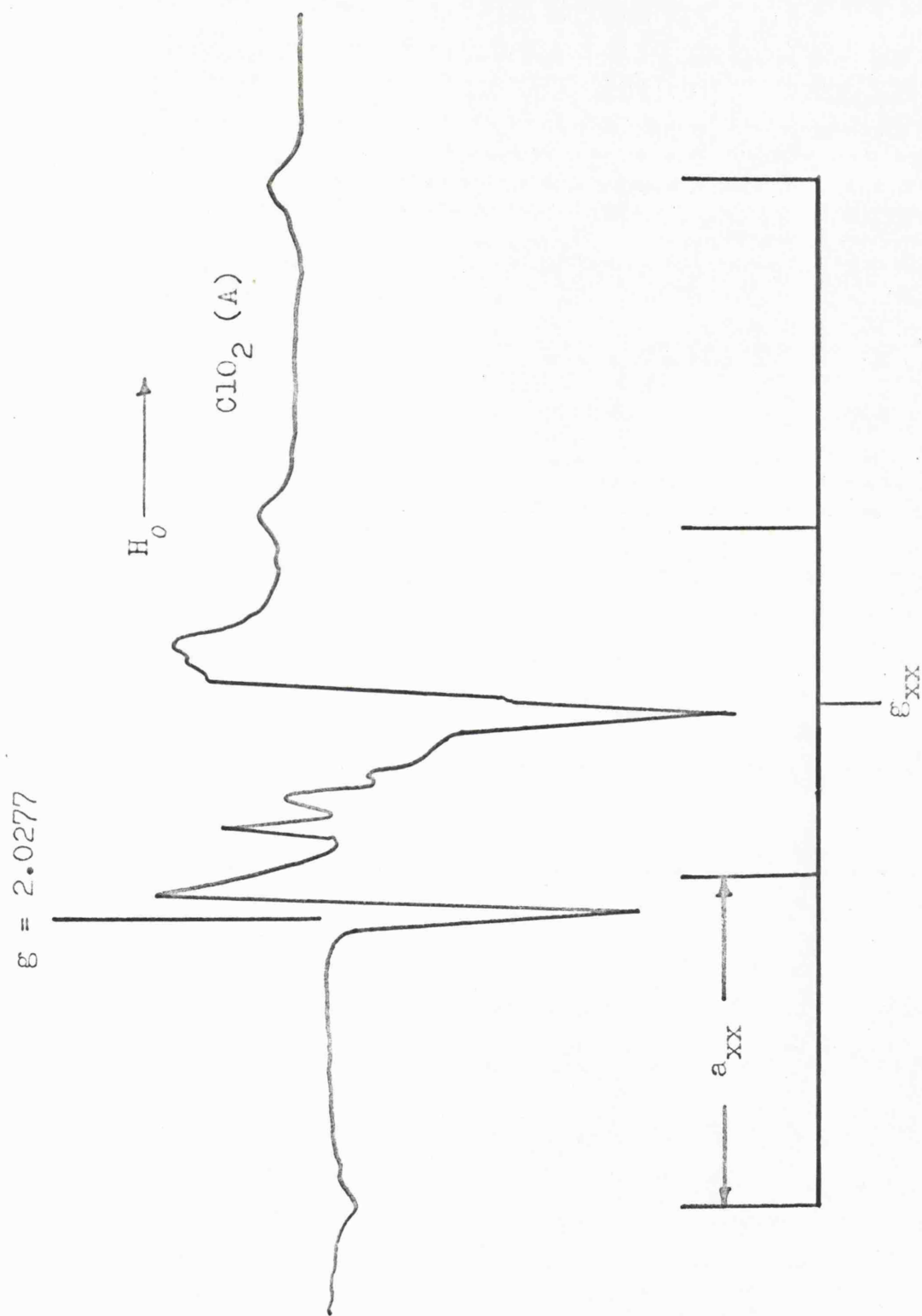


Figure VI.15. The powder ESR spectrum of  $\text{KClO}_3$  irradiated at  $77^\circ\text{K}$  and measured at  $120^\circ\text{K}$ .

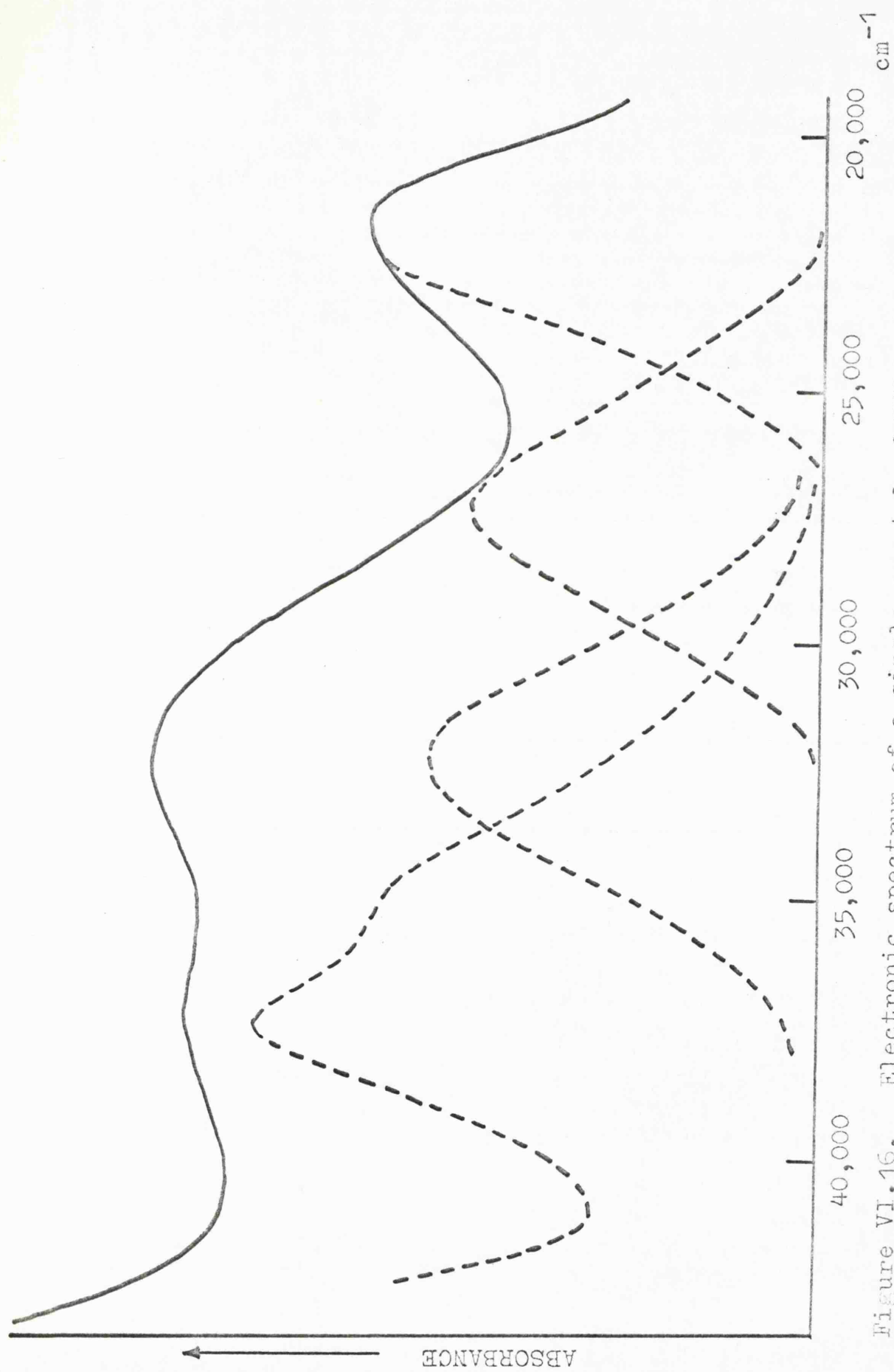
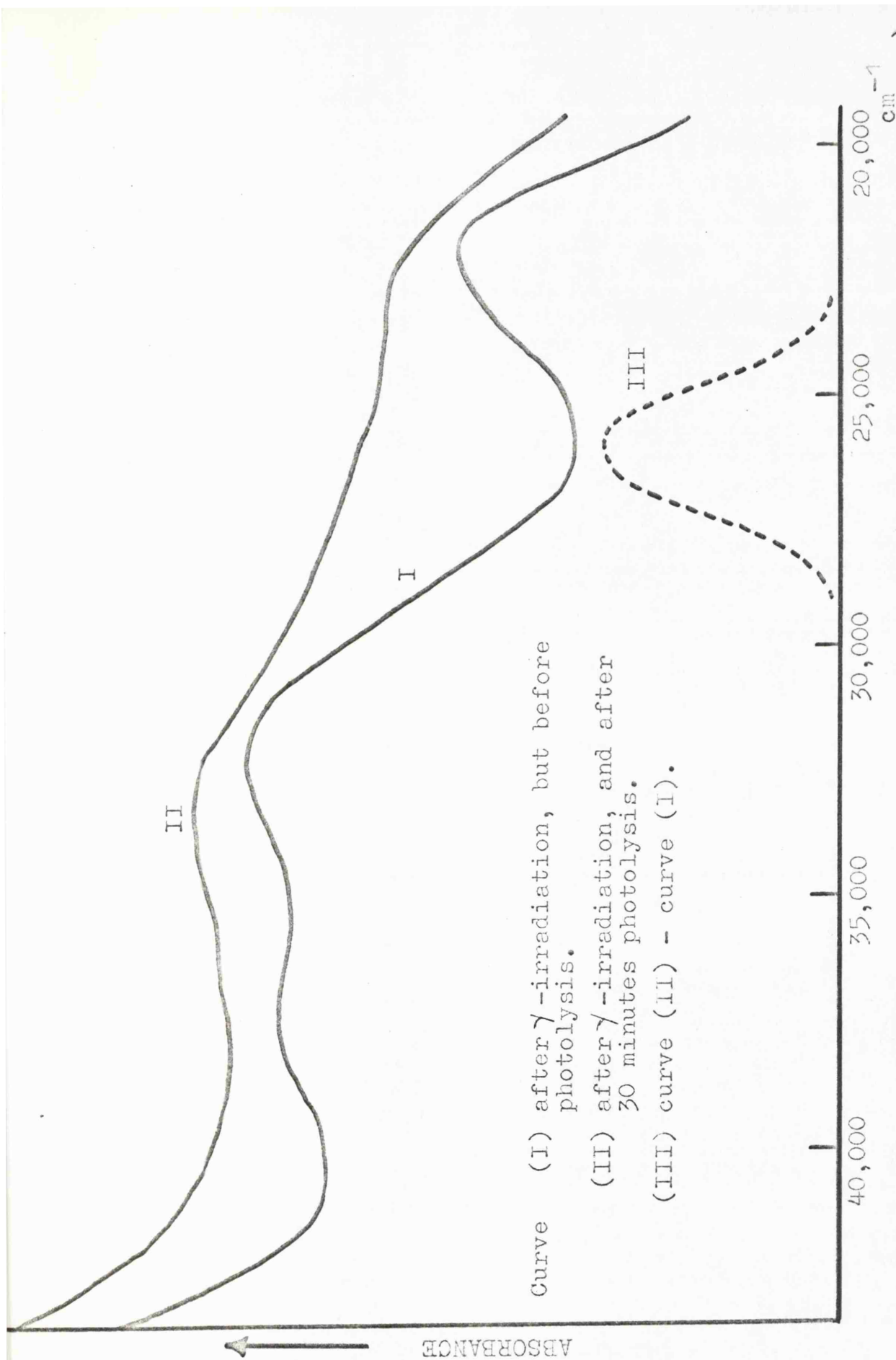


Figure VI.16. Electronic spectrum of a single crystal of  $\text{KClO}_3$  irradiated and measured at  $295^\circ\text{K}$ .



Curve (I) after  $\gamma$ -irradiation, but before photolysis.  
 (II) after  $\gamma$ -irradiation, and after 30 minutes photolysis.  
 (III) curve (II) - curve (I).

Figure VI.17. Effect of 3650Å radiation on the radical-products of  $\gamma$ -irradiation in a  $KClO_3$  single crystal.

## DISCUSSION

### 1. The Identification of the Radiation Damage Centres in $\text{KClO}_3$

#### a) Radical A

For the following reasons this species is almost certainly chlorine dioxide:

i) The observed spin-resonance parameters of radical A (Table VI.1) are very similar to those previously reported for  $\text{ClO}_2$  trapped in a variety of matrices.

ii) Powder spectra of the dioxide invariably exhibit an intense absorption centred upon  $g = 2.026 - 2.027$ . Radical A has a similarly intense feature at  $g = 2.0277$  in the chlorate matrix.

iii) The optical absorption band with a maximum intensity at 360 nm ( $27,800 \text{ cm}^{-1}$ ) almost certainly arises from the  ${}^2A_2 \leftarrow {}^2B_1$  transition of  $\text{ClO}_2$ . This transition occurs at 355 nm ( $28,200 \text{ cm}^{-1}$ ) for the dioxide dissolved in  $\text{CH}_3\text{OH}$  or  $\text{CCl}_4$ ,<sup>68</sup> and at 365 nm ( $27,400 \text{ cm}^{-1}$ ) in the gas phase.<sup>79</sup>

#### b) Radical B

This radical contains two inequivalent chlorine

atoms. Figures VI.5 to 7 illustrate the splitting of the four widely spaced lines originating from this centre into subsets of four. We have labelled the nucleus responsible for the major hyperfine splitting  $^a\text{Cl}$  and that responsible for the subsidiary interaction  $^b\text{Cl}$ . We have discounted the possibility that this minor splitting arises from superhyperfine interactions with a  $\text{K}^+$  ion ( $^{39}\text{K}$ ,  $I = 3/2$ , 93.08% isotopic abundance) for two reasons. Firstly, one would expect the coupling to an alkali metal ion to be almost isotropic, by analogy to the  $\text{Na}^+ - \text{CO}_2^-$  centre in irradiated sodium formate,<sup>80</sup> whereas the subsidiary interaction in  $\text{KClO}_3$  is highly anisotropic. Secondly, it was possible, in certain orientations, to identify features corresponding to the chlorine isotopic combinations  $^a(^{35}\text{Cl}) - ^b(^{35}\text{Cl})$ ,  $^a(^{35}\text{Cl}) - ^b(^{37}\text{Cl})$ ,  $^a(^{37}\text{Cl}) - ^b(^{35}\text{Cl})$  and  $^a(^{37}\text{Cl}) - ^b(^{37}\text{Cl})$ .

For the following reasons we conclude that this centre is probably  $(^b\text{Cl} - ^a\text{ClO}_2)^-$ :

- i) Figure VI.5 shows the angular variation of the ESR spectra of radicals A and B as  $H_0$  explores the ab-plane. There is a striking similarity between the symmetry properties of the hyperfine features of these radicals in this plane; a similarity which is also reflected in the ac'-and bc'-planes.

ii) It is clear, from Table VI.1 that the form of the A-tensor in  $\text{ClO}_2$  (radical A) is very similar to that ascribed to  $^{35}\text{Cl}$  in radical B.

iii) Although the g-tensor in B is more anisotropic than in  $\text{ClO}_2$ , the average g-values are similar.

iv) The  $^{35}\text{Cl}$ -hyperfine tensor is axially symmetric, as expected for a 'chloride-like' anion.

v) The relative and absolute magnitudes of the isotropic and anisotropic coupling tensors for  $^{35}\text{Cl}$  are very similar to those reported for the  $\text{Cl}^-$  fragments of the H-centre  $(\text{Cl}_4)^{3-}$ .<sup>81</sup>

vi) The chloride ion is known to be one of the stable radiolysis products of  $\text{KClO}_3$ .<sup>76</sup>

c) Radical C

Radical C contains no detectable magnetic nuclei and was originally identified, by Hasty et.al.,<sup>73</sup> as the superoxide ion. However,  $\text{O}_2^-$  is a  $^2\Pi_{3/2}$  species and as such is expected to possess an axially symmetric g-tensor with principal values that deviate markedly from the free-spin value. Extensive investigations by Känzig and coworkers<sup>82</sup> have shown that this radical trapped in a variety of alkali halide lattices is characterised by a g-tensor of the form:  $g_{\parallel} \approx 2.3$  and  $g_{\perp} \approx 1.94$ . The

g-tensor of radical C, obtained from a powder spectrum measured at 77°K, is shown in Table VI.2. It is clear that these values are close to those expected for the 19 valence-electron  $O_3^-$  ion, isoelectronic with  $ClO_2$ , where the central value ( $g_{zz}$ ) is identical with that observed for solid  $NaO_3$ .<sup>74</sup> We therefore identify radical C as the ozonide anion.

The small angular variation of features from C in a crystal of  $KClO_3$ , coupled with the fact that the single-crystal spectrum of this centre resembled the broad anisotropic resonance expected from a powder, seems to indicate that  $O_3^-$  ions occupy a large number of magnetically distinct sites in the chlorate lattice. The diffuse reflectance spectrum of solid  $NaO_3$  exhibits an intense absorption with a maximum intensity at 440 nm (22,700  $cm^{-1}$ ).<sup>74</sup> We are, therefore, tempted to assign the 445 nm (22,500  $cm^{-1}$ ) band in irradiated  $KClO_3$  to the  ${}^2A_2 \leftarrow {}^2B_1$  transition of the ozonide anion.

#### d) Radical D

Radical D, produced by the photolysis of  $\gamma$ -irradiated  $KClO_3$ , is undoubtedly the  $V_K$ -centre  $Cl_2^-$ . Fayet and Thieblemont<sup>75</sup> have concluded that the principal values of the g- and A-tensors of this centre lie in the crystallographic ab-plane. Therefore, a complete single-

crystal study of this centre was unnecessary, for the principal values  $g_{\parallel}$ ,  $g_{\perp}$ ,  $a_{\parallel}$  and  $a_{\perp}$  could be obtained by measuring spectra in the ab-plane alone. These values are very similar to those reported by Schoemaker for  $\text{Cl}_2^-$  trapped in KCl and included in Table VI.3 for comparison.<sup>83</sup>

The spin-resonance features from this centre in  $\text{KClO}_3$  were curiously split into doublets. This splitting may have arisen from a weak coupling to a neighbouring proton trapped in the chlorate lattice, or because the photolytically generated  $\text{Cl}_2^-$  ions occupied two magnetically distinct crystal sites differing only slightly in their relative orientations. We consider the latter explanation more probable because  $\text{Cl}_2^-$  ions generated in  $\text{KClO}_3$  crystals grown from 99.8%  $\text{D}_2\text{O}$  still exhibited this doublet splitting and because of a marked increase in this splitting when the spectrum was measured at Q-band frequency.

e) Radical E

Radical E is thought to be chlorine trioxide. The spin resonance data for this centre were obtained from a spectrum, measured at  $100^\circ\text{K}$ , of  $\text{KClO}_3$  powder which had been irradiated for approximately 20 minutes at  $77^\circ\text{K}$ . The data were derived from this spectrum by the applica-

TABLE VI.3. Electron Spin Resonance Data for the  $V_k$ -Centre  $Cl_2^-$  and Related Species.

Matrix	g-tensor	$^{35}Cl$ Hyperfine tensor in gauss										Ref.		
		Direction Cosines			Anisotropic			Iso-tropic			Direction Cosines			
		a	b	c'	$B_{xx}$	$B_{yy}$	$B_{zz}$	a	b	c'	a		b	c'
$KClO_3$ at 295°K (Radical D)	$g_{xx}$ = 2.0436	*	*	*	$B_{xx}$ = -31			*	*	*	*	a'		
	$g_{yy}$ = 2.0436	*	*	*	$B_{yy}$ = -31			*	*	*	*			
	$g_{zz}$ = 2.0029	1	0	0	$B_{zz}$ = +62			1	0	0	0			
	$g_{av}$ = 2.030													
KCl at 20°K	$g_{xx}$ = 2.0428				$B_{xx}$ = -25.8			43.6				83		
	$g_{yy}$ = 2.0447				$B_{yy}$ = -25.8									
	$g_{zz}$ = 2.004				$B_{zz}$ = +51.7									
	$g_{av}$ = 2.0262													
$Cl_4^{3-}$ in NaCl at 295°K	$g_{xx}$ = 2.0256				$yCl$			36				81		
	$g_{yy}$ = 2.0256				$B_{xx}$ = -36.5									
	$g_{zz}$ = 1.9962				$B_{yy}$ = -36.5									
	$g_{av}$ = 2.0158				$B_{zz}$ = +73									
				$xCl$				8.8						
				$B_{xx}$ = -4.4										
				$B_{yy}$ = -4.4										
				$B_{zz}$ = +9.8										

144

a. In the H-centre  $Cl_4^{3-}$ ,  $yCl$  refers to the hyperfine tensor for the middle two equivalent chlorine nuclei, and  $xCl$  refers to that for the outer two equivalent chlorine nuclei, i.e. ( $xCl \dots yCl - Cl^y \dots xCl$ ).

\* These directions have no significance. a'. This work.

tion of the Breit-Rabi equation<sup>58</sup> to the outermost ( $M_I = \pm \frac{3}{2}$ ) perpendicular and parallel transitions, since the central region of the spectrum was extremely complex owing to the superposition of the 'allowed' ( $\Delta M_I = 0$ ) and 'forbidden' ( $\Delta M_I = \pm 1, \pm 2$ ) transitions of a number of chlorine-containing radicals. These data, included in Table VI.4, are remarkably similar to those reported for chlorine trioxide trapped in a variety of perchlorate matrices, and it is on this basis that we identify E as  $\text{ClO}_3$ .

f) Radical F

A comparison of the spin-resonance data obtained for F and those of the  $\text{ClO}_3^{2-} | \text{CO}_3^{2-} |$  centre in chlorate-doped calcite (Table VI.4) leaves little doubt that they relate to the same radical. Again the tabulated parameters for  $\text{ClO}_3^{2-}$  in  $\text{KClO}_3$  were obtained by the application of the Breit-Rabi<sup>58</sup> equation to the outer-most hyperfine features which correspond to transitions for the nuclear spin states  $M_I = \pm \frac{3}{2}$ .

The fact that both radical F and  $\text{ClO}_3$  were formed in the low temperature radiolysis of  $\text{KClO}_3$  completely rules out the possibility, mentioned in Chapter IV that the stable chlorine centre in chlorate-doped  $\text{CaCO}_3$  was  $\text{ClO}_3$  whose molecular and spin-resonance parameters

TABLE VI.4. Electron Spin Resonance Data for the  $\text{ClO}_3^-$  and  $\text{ClO}_3^{2-}$  Radicals.

Radical Matrix	g-tensor			$^{35}\text{Cl}$ hyperfine tensor in gauss		
	$g_{\parallel}$	$g_{\perp}$	$g_{av}$	$B_{\parallel}$	$B_{\perp}$	$A_{iso}$
$\text{ClO}_3^{2-}$ (F) $\text{KClO}_3$	2.0110	2.0083	2.0092	8.6	- 4.3	118.7
$\text{ClO}_3^{2-}$ $\text{CaCO}_3$	2.0121	2.0105	2.0110	14	- 7.0	113
$\text{ClO}_3^-$ (E) $\text{KClO}_3$	2.0030	2.0083	2.0065	36	-18	140
$\text{ClO}_3^-$ $\text{KClO}_4$ <sup>a</sup>	2.0066	2.0132	2.0110	29	-15	122

a. Reference 54

were seriously modified by the carbonate environment.

## 2. The Electronic and Molecular Structures of the Radicals Trapped in Irradiated $\text{KClO}_3$

### a) The $\text{ClO}_2$ Centre

Chlorine dioxide has 19 valence-electrons and, therefore, from the Walsh orbital-correlation diagram<sup>64</sup> for  $\text{AB}_2$  molecules (Figure VI.18), the unpaired electron is expected to occupy an antibonding  $2b_1$ -orbital which is constructed from the  $3p_x$ -orbital of chlorine and the  $2p_x$ -orbitals of the ligand oxygen atoms. The x-axis is perpendicular to the molecular plane, whereas the y-axis lies along the O-O direction and the z-axis is the molecular  $\text{C}_2$ -symmetry axis.

The deviations of the experimental g-factors from the free-spin value arise from the following excitations:

$$\Delta g_{xx}: \dots (1a_2)(3b_2)^2(4a_1)^2(2b_1)^2; {}^2A_2 \leftarrow \dots (1a_2)^2(3b_2)^2(4a_1)^2(2b_1); {}^2B_1$$

$$\Delta g_{yy}: \dots (1a_2)^2(3b_2)^2(4a_1)(2b_1)^2; {}^2A_1 \leftarrow \dots (1a_2)^2(3b_2)^2(4a_1)^2(2b_1); {}^2B_1$$

$$\Delta g_{zz}: \dots (1a_2)^2(3b_2)(4a_1)^2(2b_1)^2; {}^2B_2 \leftarrow \dots (1a_2)^2(3b_2)^2(4a_1)^2(2b_1); {}^2B_1$$

We therefore expect, and indeed find, that

$g_{yy} \rangle g_{zz} \rangle g_{xx} \cong 2.0023$ . The experimental  $g_{xx}$  value of 2.0022 implies that there is a negligible contribution from chlorine 3d-orbitals to the molecular orbitals

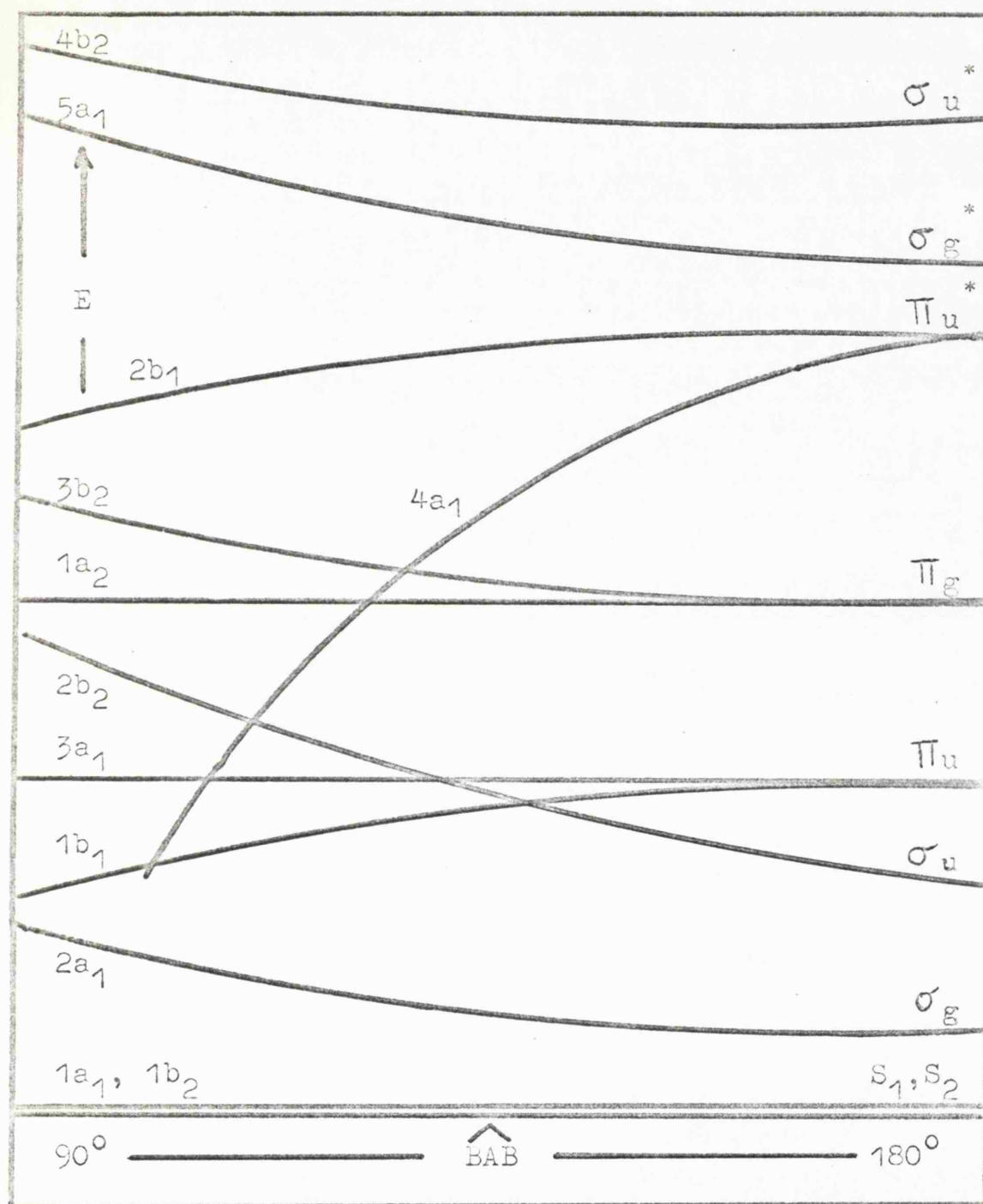


Figure VI.18. The Walsh orbital-correlation diagram for  $AB_2$  molecules and ions.

of  $\text{ClO}_2$ , for significant d-orbital contributions would lead to a negative value for  $\Delta g_{xx}$ .

There is no ambiguity about the signs of the experimental hyperfine coupling constants, since  $A_{\text{iso}}$  for  $^{35}\text{ClO}_2$  is known to be approximately +16 gauss.<sup>54</sup> The tensor  $A_1$ , representing the dipolar coupling of the electron with the  $^{35}\text{Cl}$  nucleus, is not axially symmetric and can be resolved into two component tensors of the form  $(2B, -B, -B)$  and  $(-B', -B', +2B')$ .

viz:

$$\begin{array}{c} \left| \begin{array}{ccc} +61.9 & & \\ & -31.4 & \\ & & -30.5 \end{array} \right| = \left| \begin{array}{ccc} +62.2 & & \\ & -31.1 & \\ & & -31.1 \end{array} \right| + \left| \begin{array}{ccc} -0.3 & & \\ & -0.3 & \\ & & +0.6 \end{array} \right| \text{ gauss} \\ A_1 \qquad \qquad \qquad A'_1 \qquad \qquad \qquad A''_1 \end{array}$$

The major component  $A'_1$  is cylindrically symmetric about the x-axis and corresponds to the electron in the  $2b_1$ -level of the dioxide. From this tensor we estimate the chlorine  $3p_x$ -orbital population ( $a_{p_x}^2$ ) to be 0.62. The subsidiary tensor  $A''_1$  and  $A_{\text{iso}}$  arise from spin-polarisation and correspond to unpaired electron density in the  $4a_1$ -molecular orbital which is constructed from the chlorine  $3p_z$ - and  $3s$ -atomic orbitals. We estimate the  $3p_z$ - and  $3s$ -orbital spin-populations to be 0.006 and

0.01 respectively.

The results in Table VI.2 clearly show that the experimental g- and A-tensors of  $\text{ClO}_2$  in  $\text{KClO}_3$  have a marked temperature sensitivity. The values of  $a_{xx}$  for  $^{35}\text{ClO}_2$  were 79.9, 83.1 and 85.8 gauss at  $295^\circ$ ,  $77^\circ$  and  $4.2^\circ\text{K}$  respectively. The  $a_{xx}$ -value of 85.8 gauss at  $4.2^\circ\text{K}$  can be compared with the value  $80 \pm 5$  gauss for  $^{35}\text{ClO}_2$  in  $\text{KClO}_4$ , estimated from an extrapolation of the results of Byberg and coworkers<sup>51</sup> to this temperature, and also with Curl's<sup>53</sup> gas-phase value of 74 gauss. This discrepancy between the values obtained for  $\text{ClO}_2$  in ionic lattices at  $4.2^\circ\text{K}$  and the gas-phase value is hard to explain. At low temperatures one would expect the librational motion of radicals trapped in crystalline matrices to be a minimum, consequently the observed A-factors should approach those obtained in the gas phase. The steadily increasing value of  $a_{xx}$ , as the temperature was lowered, may have been a consequence of the increasing influence of neighbouring  $\text{K}^+$  ions on trapped  $\text{ClO}_2$  molecules as the lattice contracted. If the approaching potassium ions perturbed the ligand atoms of  $\text{ClO}_2$  to such an extent that they effected a slight increase in the electronegativity of the interacting oxygens, then this would lead to an increased antibonding electron

density on the central chlorine atom and a concomitant overall increase in the principal values of the chlorine A-tensor.

From the principal directions (x, y and z) of the g-tensor (see Table VI.1) we can estimate the orientation of the  $\text{ClO}_2$  radical relative to the unit cell of  $\text{KClO}_3$ . The y-axis is parallel to the O-O bond direction and lies along the crystallographic b-direction, the x-axis is perpendicular to the molecular plane and is parallel to a, and the z-axis lies along the molecular  $\text{C}_2$ -symmetry axis which is necessarily parallel to c'. One  $\text{ClO}_2$  molecule is formed either from Cl (0), O (+0.22) and O (-0.22), or from Cl (0.50), O (+0.72) and O (+0.28) in the  $a_1b_1c_1$  unit cell (see Figure VI.20), the sites being magnetically indistinguishable.

b) The 'Two-Chlorine' Centre ( ${}^b\text{Cl}-{}^a\text{ClO}_2$ )<sup>-</sup>

For the purpose of this discussion the 'two-chlorine' centre is treated as an isolated  ${}^a\text{ClO}_2$  molecule which is slightly perturbed by a neighbouring  ${}^b\text{Cl}^-$  ion. The close similarity between the spin-resonance parameters of the ' ${}^a\text{ClO}_2$ -like' moiety and  $\text{ClO}_2$  (radical A) is taken as adequate justification for this assumption. From the data in Table VI.1 it is clear that the x-axis of the  ${}^a\text{ClO}_2$  fragment in the 'two-chlorine' centre, like that of  $\text{ClO}_2$ , is

parallel to the crystallographic a-axis, whereas, the y- and z-principal directions are shifted by approximately  $16 \pm 5^\circ$  in the bc'-plane with respect to the corresponding values in  $\text{ClO}_2$ . Whilst  $g_{xx}$  has retained its free-spin value in  $({}^b\text{Cl}-{}^a\text{ClO}_2)^-$ , the chloride ion perturbation of the  $\text{ClO}_2$ -fragment has resulted in increased values for both  $g_{yy}$  and  $g_{zz}$ . It appears that this weak interaction between  ${}^b\text{Cl}^-$  and  ${}^a\text{ClO}_2$  has resulted in a lowering in energy of the antibonding  $2b_1$ -orbital and a concomitant increase in the magnetic coupling to the lower lying  $4a_1$ - and  $3b_2$ -levels, which is reflected in the increased values of  $\Delta g_{yy}$  and  $\Delta g_{zz}$ .

For the analysis of the major hyperfine tensor corresponding to  ${}^a\text{ClO}_2$ , we have assumed that the signs of the hyperfine coupling constants are identical to those of  $\text{ClO}_2$  in this lattice. We obtained an isotropic coupling of 22 gauss and as before (see  $\text{ClO}_2$ ) the anisotropic tensor could be resolved into two axially symmetric components of the form  $(2B, -B, -B)$  and  $(-B', -B', +2B')$  where  $2B = 65.6$  gauss and  $2B' = 2$  gauss. A spin-population analysis based on these values indicates that the total spin-density on the central chlorine atom is approximately 0.66, an increase of 5.5% compared to the chlorine spin-density in  $\text{ClO}_2(\text{A})$ . If the spin-density

on  ${}^b\text{Cl}$  were acquired by direct electron transfer one would have expected a reduction in the total electron density on  ${}^a\text{Cl}$ , in contrast to the observed increase. This increase can be accounted for if a spin-polarisation mechanism is operative, giving rise to a small negative spin-density on  ${}^b\text{Cl}$  with a subsequent increase in the positive spin-density on  ${}^a\text{Cl}$ . The  ${}^a\text{ClO}_2$ -fragment is thus an electron-excess centre and the  ${}^b\text{Cl}^-$  becomes 'hole-like' in character, the radical being electronically similar to the well-known  $V_K$ -centre.<sup>83</sup>

We are unable to determine the signs of the components of the  ${}^b\text{Cl}$  experimental A-tensor. However,  $A_{\text{iso}}({}^b\text{Cl})$  and  $2B({}^b\text{Cl})$  are expected to be negative, for the reason outlined above, and consequently there are only three sign-combinations to be considered. We cannot determine which is the correct combination to use, but fortunately both  $2B$  and  $A_{\text{iso}}$  vary little between the three alternatives. We can therefore, make approximate estimates for the  ${}^b\text{Cl}$   $3p_z$ - and  $3s$ -orbital spin-populations, which are 0.096 and 0.003 respectively. The corresponding  $3p/3s$  ratio of about 30 is characteristic of a species in which the unpaired electron is confined to a molecular orbital principally constructed from a  $3p$ -atomic orbital on chlorine. We have not neglected

the possibility, proposed by Hasty et.al.<sup>73</sup> and supported by Atkins and coworkers,<sup>54</sup> that the secondary chlorine splitting is caused by a 'ClO<sub>3</sub>-like' fragment. The main objection to this is that the observed 3p/3s-ratio of 30 is far larger than that expected, even for a considerably flattened chlorate ion. Mechanistically, it is also easier to envisage the formation of the V<sub>K</sub>-centre Cl<sub>2</sub><sup>-</sup> from the photolytically induced decomposition of (Cl-ClO<sub>2</sub>)<sup>-</sup> rather than from (O<sub>3</sub>Cl-ClO<sub>2</sub>)<sup>-</sup>.

Each chlorate ion in KClO<sub>3</sub> has one near-neighbour in the unit cell diagonally above it, at a distance of 3.65Å. Figure VI.20 shows two unit cells in which the dashed line joins two such neighbouring anions. It seems very probable that the chlorine atoms of the (Cl-ClO<sub>2</sub>)<sup>-</sup> centre arise from such a pair of ions, and we have estimated the positions of the constituent atoms in this centre from the principal directions of the g- and A-tensors. For <sup>b</sup>Cl, the x<sub>b</sub>-axis lies approximately along the C<sub>3</sub>-symmetry axis of the parent ClO<sub>3</sub><sup>-</sup> ion making an angle of 27° ± 5° with the x<sub>a</sub>-axis of <sup>a</sup>ClO<sub>2</sub>, both principal directions lying in the ac-plane. For <sup>a</sup>Cl, the z<sub>a</sub>-axis lies approximately 16° ± 5° out of the ac-plane, and consequently the y<sub>a</sub>-axis makes an angle of 16 ± 5° to the crystallographic b-axis (see Figure VI.19).

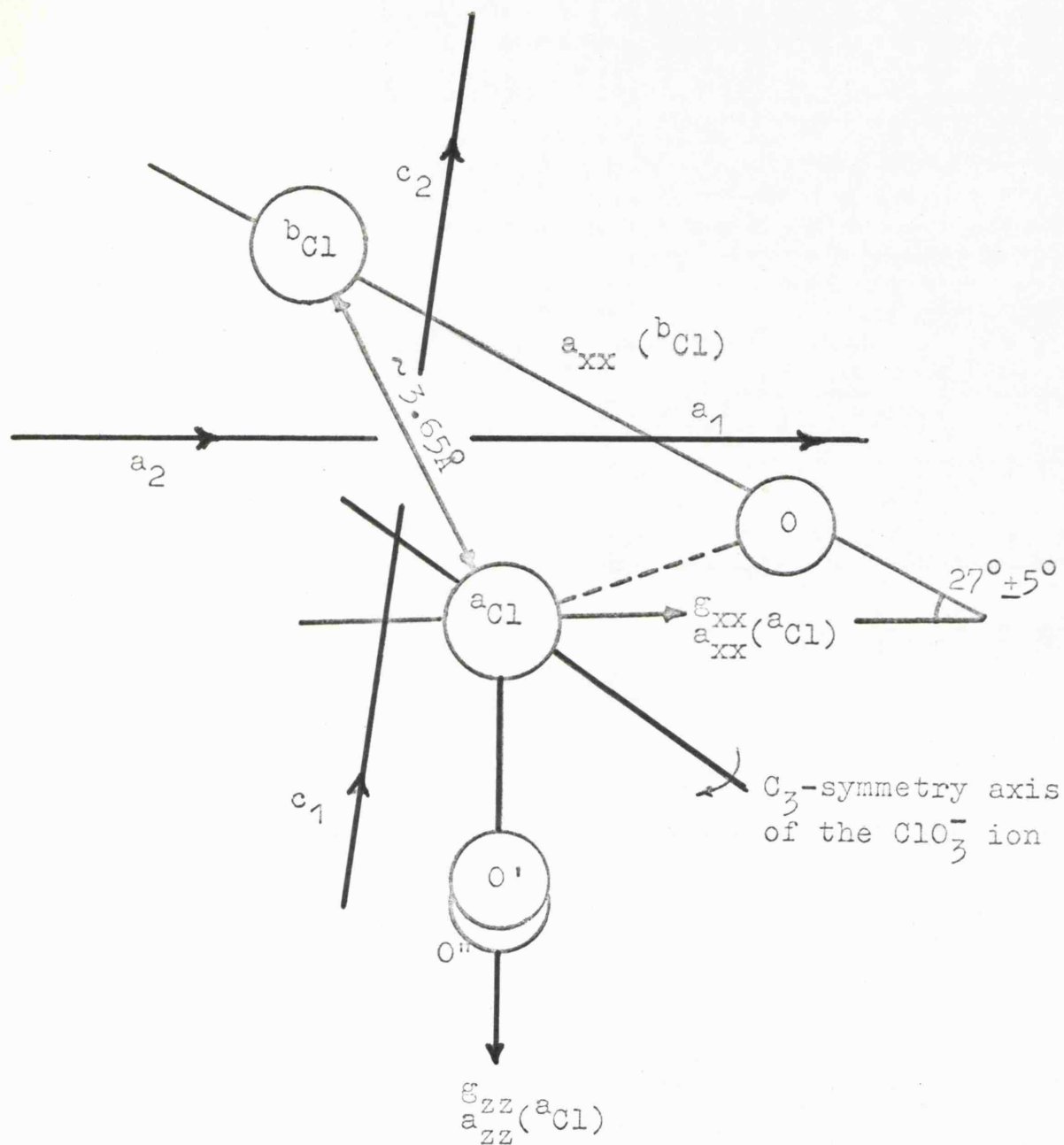
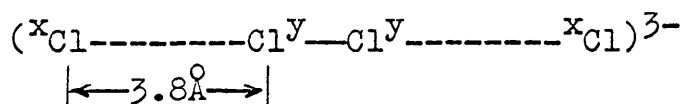


Figure VI.19. The orientation of the  $(b_{Cl}-a_{Cl}O_2)^-$  centre in  $KClO_3$  with respect to the crystallographic  $a$ ,  $b$  and  $c$  axes.

Finally, it is interesting to compare the distribution of unpaired electron density in the  $(\text{Cl}-\text{ClO}_2)^-$  centre with that in the recently reported H-centre:



formed in X-irradiated alkali metal chlorides at  $20^\circ\text{K}$ .<sup>81</sup> (see Table VI.3). A spin-population analysis of the hyperfine parameters reported for this centre suggests that approximately 0.73 of the unpaired electron is distributed between the central  $^{\text{y}}\text{Cl}$  atoms of the  $\text{Cl}_2^-$  ion, whilst about 10% is delocalised onto the axial  $^{\text{x}}\text{Cl}^-$  ions. The resultant 3p/3s-ratio on  $^{\text{x}}\text{Cl}$  is 49, the 3p-character being 0.098 and the 3s-character being 0.002. These data and the corresponding values for the  $(\text{Cl}-\text{ClO}_2)^-$  centre are included in Table VI.5, and we believe that the close similarity of these results further substantiates our identification of  $^{\text{b}}\text{Cl}$  as a 'Cl<sup>-</sup>-like' fragment.

c) The Ozonide Anion  $\text{O}_3^-$

This radical appears to occupy a large number of magnetically distinct sites in the chlorate lattice and consequently we were unable to obtain the direction cosines of the g-tensor. Therefore, we cannot determine

TABLE VI.5. The Molecular Parameters of the  $\text{ClO}_2$ ,  $(\text{ClO}_2\text{-Cl})^-$ ,  $\text{ClO}_3^{2-}$ ,  $\text{ClO}_3^-$  and  $\text{Cl}_2^-$  centres in  $\text{KClO}_3$ .

Radical	Temp. °K	$a_{p_x}^2$	$a_{p_z}^2$	$a_s^2$	$a_p^2/a_s^2$	Bond Angle	$a_s^2+a_p^2$	
$\text{ClO}_2$	295	0.62	0.006	0.01	62	-	0.63	
$\left[ \begin{array}{c} \text{aClO}_2^- \\   \\ \text{bCl} \end{array} \right]$	295	0.66	0.02	0.013	51	-	0.67	
		0.085	-	0.003	28	-	0.09	
$\text{ClO}_3^{2-}$	77	-	0.086	0.071	1.2	-	0.16	
$\text{ClO}_3^-$	77	-	0.36	0.083	4.34	112°	0.44	
$\text{Cl}_2^-$	295	-	0.62	0.024	26	-	-	
$\text{Cl}_4^{3-}$ in NaCl	20	$^y\text{Cl}$	-	0.72	0.02	36	-	0.74
		$^x\text{Cl}$	-	0.098	0.002	49	-	0.01

the relative orientations of the radicals in these sites.

The g-tensor of this radical has the form  $g_{yy} \gg g_{zz} > g_{xx} \approx 2.0023$ , which is typical of a 19 valence-electron dioxide having a  ${}^2B_1$ -ground state (see  $ClO_2$ ).

d) The  $V_K$ -centre  $Cl_2^-$

For the analysis of the hyperfine tensor shown in Table VI.3 we have assumed that sign combination for the components of the A-tensor which gives a total unpaired electron density closest to unity. The unpaired electron occupies a  $\sigma^*$ -molecular orbital constructed from the halogen  $3p_z$ -atomic orbitals so that the observed isotropic coupling, which corresponds to a  $3s$ -orbital occupancy of 0.024, must arise through a spin-polarisation mechanism.

From the direction cosines of the g- and A-tensors, we concur with Fayet and Thieblemont's<sup>75</sup> conclusion that the Cl-Cl internuclear axis of the  $Cl_2^-$ -centre (the z-direction) is parallel to the crystallographic a-axis of  $KClO_3$ .

The  $Cl_2^-$  centre was remarkably stable in the chlorate lattice, annealing only when the crystal was heated above  $420^\circ K$  for several hours. This is unusual, for the  $V_K$ -centres in alkali halide lattices are very unstable and often decay rapidly, even at  $77^\circ K$ . This increased

stability in  $\text{KClO}_3$  is probably due to the inability of  $\text{Cl}_2^-$  to migrate from site to site in this lattice, in contrast to its behaviour in the alkali halides.

e) The  $\text{ClO}_3$  Centre

Chlorine trioxide is a 25 valence-electron species in which the unpaired electron is expected to occupy a molecular orbital of  $a_1$ -symmetry constructed from the chlorine  $3s$ - and  $3p_z$ -orbitals and the oxygen  $2p$ -orbitals. The  $z$ -axis is the molecular  $C_3$ -symmetry axis. From the axially symmetric  $A$ -tensor of this radical which is included in Table VI.4 we have estimated the spin-populations of the chlorine  $3p_z$ - and  $3s$ -orbitals to be 0.36 and 0.083 respectively. The corresponding  $3p/3s$  ratio of 4.34 was inserted into equation (5) to calculate an approximate  $\widehat{\text{OClO}}$  bond angle of  $112^\circ$  for this radical.

The  $g$ -tensor of the trioxide is characteristic of a 25 valence-electron species, having a  ${}^2A_1$ -ground state, where  $g_\perp > g_{\parallel} > 2.0023$ . The deviations of the experimental  $g$ -factors from the free-spin value arise from the following excitations:

$$\begin{aligned} \Delta g_\perp : & \dots (2e)^3(3e)^4(a_2)^2(6a_1)^2; {}^2E \leftarrow \dots (2e)^4(3e)^4(a_2)^2(6a_1); {}^2A_1 \\ & \text{and } (2e)^4(3e)^3(a_2)^2(6a_1)^2; {}^2E \leftarrow \dots (2e)^4(3e)^4(a_2)^2(6a_1); {}^2A_1 \\ \Delta g_{\parallel} : & \dots (2e)^4(3e)^4(a_2)(6a_1)^2; {}^2A_2 \leftarrow \dots (2e)^4(3e)^4(a_2)^2(6a_1); {}^2A_1 \end{aligned}$$

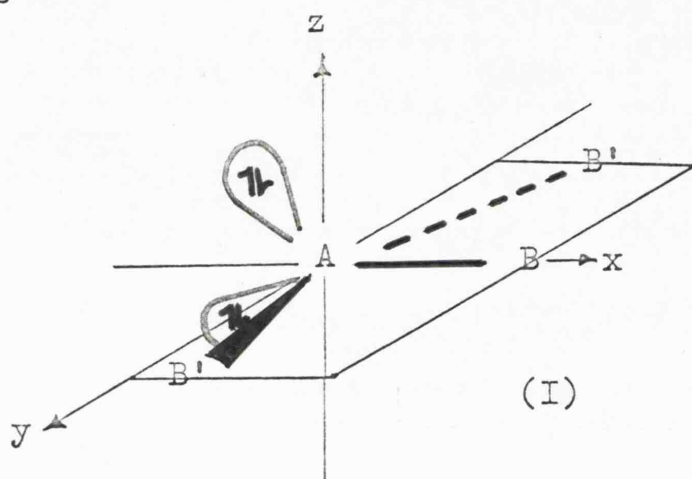
Since the  $1a_2$ -orbital is closer to the  $6a_1$ -level than either the  $2e$ - or  $3e$ -orbitals, one might predict  $\Delta g_{\parallel}$  to be larger than  $\Delta g_{\perp}$ . However, the  $1a_2$ -orbital is confined entirely to the ligands whilst the  $6a_1$ -orbital is expected to have considerable central atom character. Consequently there is little mutual overlap. In this case therefore, the energy difference is not the overriding consideration and we find that  $\epsilon_{\perp} > \epsilon_{\parallel} > 2.0023$ .

f) The  $\text{ClO}_3^{2-}$  Centre

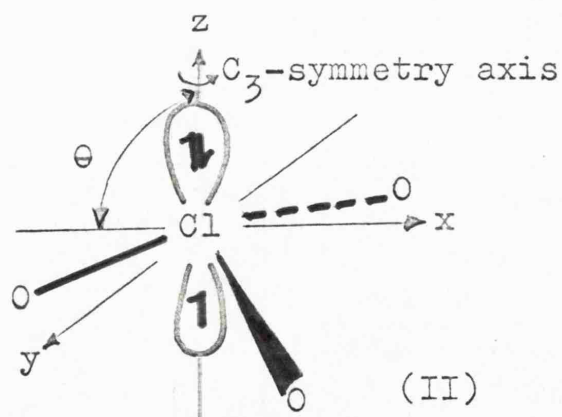
In Chapter IV.C we predicted that the unpaired electron of  $\text{ClO}_3^{2-}$  would occupy an antibonding  $a_1'$ -orbital constructed from the chlorine  $3s$ - and  $3p_z$ -atomic orbitals and the  $2p$ -orbitals of oxygen lying along the Cl-O bonds. The spin-populations of the chlorine  $3p_z$ - and  $3s$ -orbitals have been calculated from the data in Table VI.4 to be 0.086 and 0.071 respectively, corresponding to a  $3p/3s$  ratio of 1.2. The spin-resonance data of  $\text{ClO}_3^{2-}$  in calcite are also included in this Table for comparison.

We can establish the most stable structure for the  $\text{ClO}_3^{2-}$  radical-ion from simple arguments based upon the "Valence-Shell Electron-Pair Repulsion Theory." The most probable configuration for an  $\text{AB}_3$  molecule or ion having

five electron pairs on the central atom, two of which are non-bonding, is



For example, the 28 valence-electron species  $\text{ClF}_3$  is known to have a trigonal bipyramidal structure, the four atoms forming a distorted 'T'-shape, with  $\widehat{\text{FClF}} = 87^\circ 29'.55$ . In contrast, the  $\text{ClO}_3^-$ , having two fewer non-bonding electrons, is pyramidal. Consequently, we might expect the  $\text{ClO}_3^{2-}$  ion, having 27 valence-electrons, to adopt a configuration midway between these two extremes. Indeed, the configuration of maximum probability, in which the electrostatic repulsion between the electron pairs is a minimum, for this radical is



Brown and Peel<sup>84</sup> have recently concluded that chlorine 3d-orbitals play a marginal role in bonding in  $\text{ClF}_3$ , and that the structure of this molecule can be satisfactorily accounted for using molecular orbitals constructed from a basis set of chlorine 3s, 3p<sub>x</sub>, 3p<sub>y</sub> and 3p<sub>z</sub>-atomic orbitals and the fluorine 2p $\sigma$ -levels. By analogy, we are tempted to reject the possibility of 3d-orbital involvement in bonding in  $\text{ClO}_3^{2-}$ , so that the Cl-O bonding  $\sigma$ -levels must be constructed from chlorine 3s- and 3p-orbitals and the oxygen 2p $\sigma$ -levels. As a consequence of this significant chlorine 3s-orbital contribution to the bonding orbitals the effective difference in electronegativity between the ligands and the central atom,  $\Delta\chi$ , is expected to be small and negative. Hence, a considerable fraction of the antibonding unpaired electron will be delocalised onto the oxygen atoms, resulting in the angle  $\theta$  in structure (II) being greater than  $90^\circ$ .

This is just the structure we predicted in Chapter IV for  $\text{ClO}_3^{2-}$  from the Walsh orbital-correlation scheme for  $\text{AB}_3$  molecules,<sup>40</sup> and is in accord with the experimental spin-resonance and molecular parameters of this ion, included in Tables VI.4 and VI.5. The axially symmetric g- and A-tensors reflect the  $\text{C}_{3v}$ -symmetry of the ion, and

the unpaired electron is considerably delocalised onto the oxygen ligand atoms.

#### MECHANISM OF RADIATION DAMAGE IN $\text{KClO}_3$

Figure VI.20 shows a projection of the atomic positions of the Cl and O atoms in adjacent unit cells of  $\text{KClO}_3$ . One unit cell labelled  $a_1c_1$  and a second  $a_2c_2$ , which is diagonally below and joined to it at a corner, have been projected along b. The positions of the constituent atoms along the b-axis are indicated as fractions of the length of side b relative to the  $a_1c_1$ -plane. Each chlorate ion lies  $3.65\text{\AA}$  away from its nearest neighbour (joined to it by a broken line in the figure) and is separated by more than  $5\text{\AA}$  from the next nearest chlorate ion. The primary irradiation process is probably the ejection from an isolated anion of an inner-electron which may then be trapped at an adjacent  $\text{ClO}_3^-$  ion, or transmitted through the lattice as a conduction electron and subsequently trapped at a distant anion site. This would result in the formation of several inequivalent defect centres:

- i)  $\text{ClO}_3-\text{ClO}_3^{2-}$ ; the pair of radicals being separated by  $3.65\text{\AA}$
- ii)  $\text{ClO}_3-\text{ClO}_3^{2-}$ ; with a separation of more than  $5\text{\AA}$

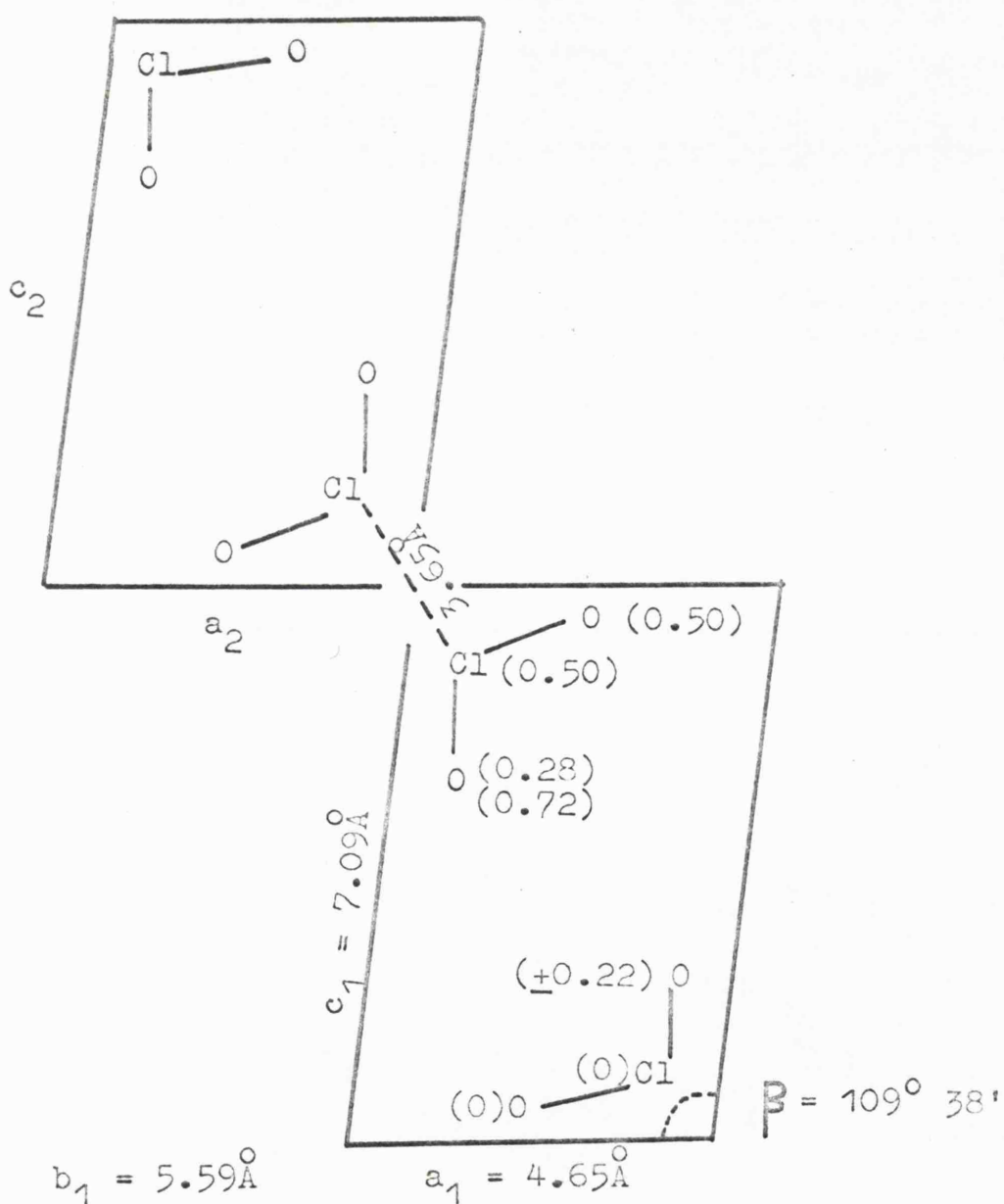


Figure VI.20. A projection along the  $b$ -axis of the atomic positions of the Cl and O atoms in two adjacent unit cells of  $\text{KClO}_3$ .

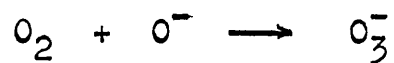
iii) isolated  $\text{ClO}_3$  and  $\text{ClO}_3^{2-}$  ions.

Chlorine trioxide is known to decompose to the more stable  $\text{ClO}_2$  in the gas phase<sup>85</sup> and in ionic lattices such as  $\text{KClO}_4$  (see Chapter VIII), and it is reasonable to assume that this is one process that gives rise to chlorine dioxide in potassium chlorate. Therefore, we only have to postulate that chloride and ozonide anions result from the decomposition of  $\text{ClO}_3^{2-} | \text{ClO}_3^- |$  centres to explain the formation of all the detected paramagnetic species in irradiated  $\text{KClO}_3$ . Centre (i) would result in the production of the 'two-chlorine' centre  $(\text{Cl}-\text{ClO}_2)^-$  and ozonide ions, whilst the decay of centres (ii) and (iii) would lead to isolated  $\text{ClO}_2$ ,  $\text{Cl}^-$  and  $\text{O}_3^-$  species.

In view of the high electron affinity of  $\text{ClO}_3$  ( $E_A = 3.96 \text{ eV}$ )<sup>86</sup> the dissociative recombination of radiation-ejected electrons with their parent ions is likely to occur, resulting in the formation of a variety of molecules and ions, including the species  $\text{ClO}^-$ ,  $\text{ClO}_2^-$ ,  $\text{O}_2$ ,  $\text{Cl}^-$ ,  $\text{ClO}_2$  and  $\text{O}_2^-$  which have been detected both by spectroscopy<sup>78</sup> and chemical analysis.<sup>76</sup>

A surprising result of this investigation is that  $\text{O}_3^-$  ions appear to occupy a multitude of distinct sites in the chlorate lattice, whilst the isostructural  $\text{ClO}_2$  molecule is restricted to a single, magnetically distinct

position. This probably indicates that ozonide anions are produced by several different reaction pathways, including diffusion-controlled processes of the form:



CHAPTER VII

RADIATION DAMAGE IN POTASSIUM PERCHLORATE

### RADIATION DAMAGE IN POTASSIUM PERCHLORATE

Electron spin resonance studies of radiation damage in potassium perchlorate have been reported by several workers. Cole<sup>87</sup> has tentatively assigned the spectrum of one stable defect centre to the trapped  $\text{ClO}_2$  molecule by a comparison of the observed spectral parameters with those previously reported for this dioxide. His conclusion was later supported by Symons and coworkers<sup>54</sup> who also identified the less stable species  $\text{ClO}_3$  trapped in this lattice. Byberg et.al.<sup>51</sup> have recently reinvestigated the earlier results of Cole, undertaking a more rigorous analysis of the  $\text{ClO}_2$  spin-resonance parameters by taking into account the significant quadrupole interaction terms in the spin-Hamiltonian for this centre. In essence however, their conclusions differ little from those of the latter author.

Morton<sup>59</sup> claims to have prepared the species  $\text{ClO}_4$  by the exposure of  $\text{KClO}_4$  crystals to  $\gamma$ -rays at  $77^\circ\text{K}$ . He suggested that this radical was formed in two magnetically distinct sites in the lattice, which he labelled (I) and (II), and proposed that these inequivalent sites seriously modified the stability and structure of the tetroxide. The spin-resonance parameters reported for these centres in irradiated  $\text{KClO}_4$  are listed in Table VII.1.

TABLE VII.1. Electron Spin Resonance Parameters for a Variety of  
Chlorine Oxides in Potassium Perchlorate

Radical	g-tensor		<sup>35</sup> Cl Hyperfine tensor in gauss					Ref.	
	$g_{xx}$	$g_{yy}$	$g_{xx}$	$g_{av}$	$B_{xx}$	$B_{yy}$	$B_{zz}$		$A_{iso}$
ClO <sub>2</sub>	2.0036	2.0183	2.0088	2.0102	57.6	-30.8	-26.8	15.4	54
ClO <sub>2</sub>	2.0025	2.0161	2.0115	2.0100	51.0	-24.0	-26.9	18.0	51
ClO <sub>3</sub>	2.0066	2.0132	2.0132	2.0110	-15.0	-15.0	29.0	122	54
ClO <sub>4</sub> (I)	2.0024	2.0548	2.0553	2.0375	0	0	0	57.2	59
ClO <sub>4</sub> (II)	2.0050	2.0360	2.0380	2.0260	-5.3	-3.3	8.7	74.3	59

Optical absorption studies of the ultraviolet photolysis of chlorine dioxide were first reported by Norman and Porter in 1955.<sup>88</sup> They photolysed ClO<sub>2</sub> trapped in a glassy hydrocarbon matrix at 77°K and monitored the increasing intensity of a new absorption at approximately 260 nm (38,500 cm<sup>-1</sup>) as the characteristic ClO<sub>2</sub> band at 360 nm (27,800 cm<sup>-1</sup>) decayed. They attributed the new absorption to chlorine monoxide.\* Symons and coworkers<sup>54</sup> subsequently repeated the experiment in frozen sulphuric and phosphoric acid matrices, following the photolytically induced decomposition of the dioxide by ESR spectroscopy. They noted that the original spectrum of ClO<sub>2</sub> was almost completely replaced by a second spectrum which they naturally ascribed to the monoxide. However, the molecular and spin-resonance parameters they deduced from the poorly resolved ESR spectra were not in good agreement with those expected for this  $2\Pi_{3/2}$  radical.<sup>54</sup>

Rochkind and Pimentel,<sup>89</sup> and Arkell and Schwager<sup>90</sup> have examined the photolysis of matrix-isolated ClO<sub>2</sub> by IR spectroscopy. Both groups of workers detected two new infrared bands which they tentatively assigned to the 'peroxy-chlorine' species ClOO. This radical has also

\*By chlorine monoxide we shall denote ClO, although the material Cl<sub>2</sub>O is also known by this name.

been postulated as an intermediate necessary to the understanding of the kinetics of the photolytically induced gas-phase reaction between chlorine and oxygen. Porter and Wright<sup>91</sup> have proposed the following pathway for the reaction:



In this chapter we describe the results of a comprehensive reinvestigation by both magnetic resonance and optical spectroscopy, of the photolytically induced decomposition of chlorine dioxide trapped in single crystals of  $\text{KClO}_4$  and a variety of glassy matrices. We conclude with some comments on the mechanism of radiation damage in  $\text{KClO}_4$  and propose some tentative structures for the radiolysis products.

#### EXPERIMENTAL PROCEDURE

##### 1. The Crystal Structure of $\text{KClO}_4$

Potassium perchlorate crystals are orthorhombic with four molecules per unit cell. The unit cell has dimensions  $a = 8.834\text{\AA}$ ,  $b = 5.650\text{\AA}$  and  $c = 7.240\text{\AA}$ , and belongs

to the space group  $V_n^{1692}$ .

Figure VIII.1 is a projection of the atomic positions of the K, Cl and O atoms onto the ac-plane for one unit cell of  $KClO_4$ . The  $ClO_4^-$  ion is almost tetrahedral with the chlorine atom and two oxygen atoms of each ion located in a mirror plane. The remaining oxygen atoms and the chlorine atom define a plane perpendicular to ac.

## 2. Sample Preparation

### a) Single crystals and powders of $KClO_4$

Single crystals of  $KClO_4$  were grown by the slow evaporation of saturated aqueous solutions of the AnalaR grade salt. The crystal axes of specimens having suitable dimensions for single-crystal investigations (0.3 x 0.3 x 0.5 cms) were identified by the use of a polarising microscope in conjunction with crystal morphology. Large single crystals were carefully polished down to dimensions suitable for optical measurements (0.8 x 0.5 x 0.1 cms) prior to irradiation.

Powder samples for diffuse reflectance, IR, and ESR measurements were obtained by milling-down small or aggregated crystals.

Samples of the crystals and powders were exposed to  $\gamma$ -radiation doses of approximately 3 Mrads at 77°, 195° and 295°K.

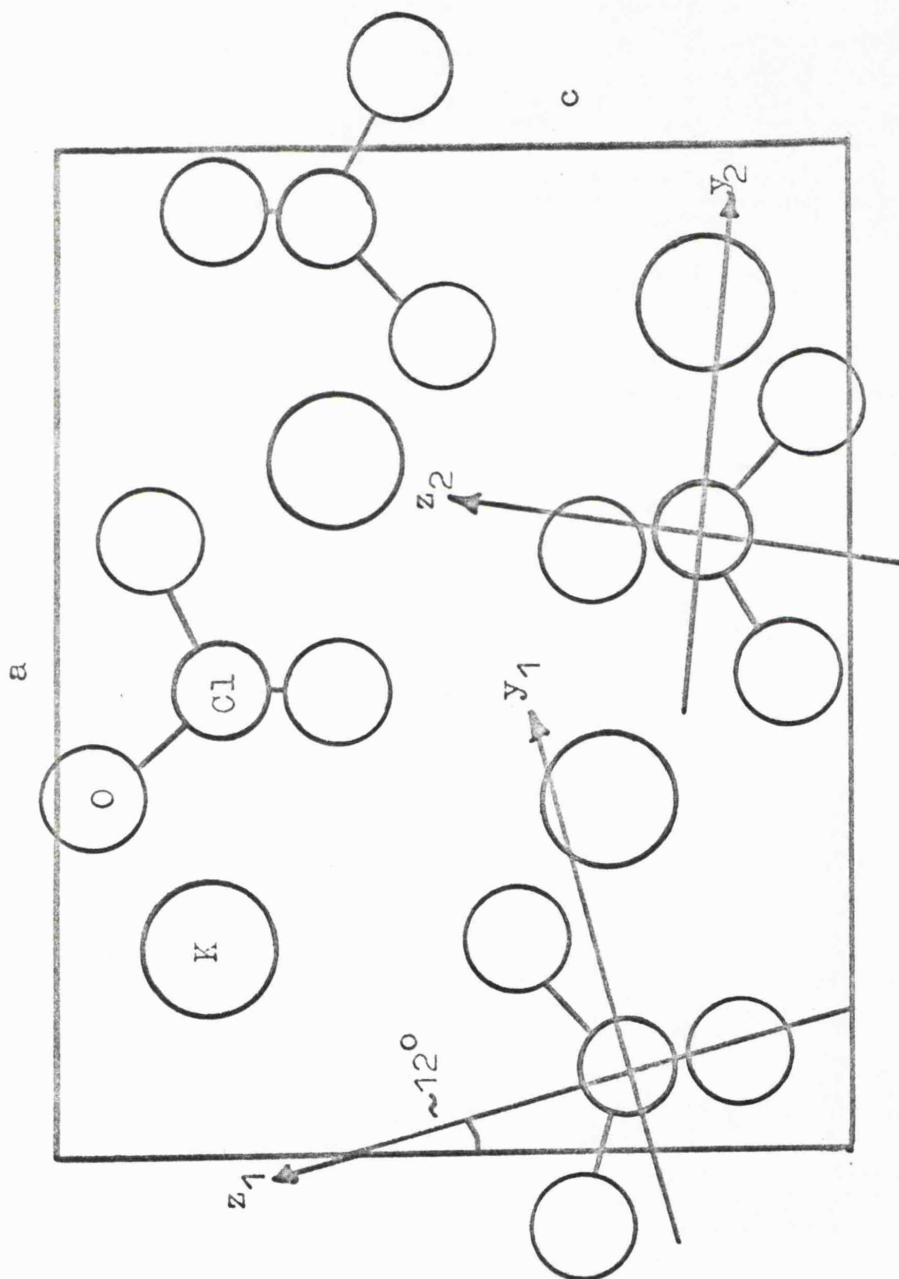
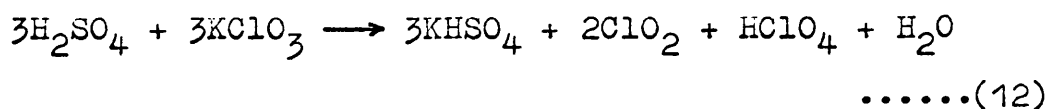


Figure VII.1. A projection of the atomic positions of K, Cl and O onto the ac-plane of the  $\text{KClO}_4$  unit cell showing the two magnetically non-equivalent sites for  $\text{ClO}_2$ . (reference 51).

b) Glasses containing chlorine dioxide

Chlorine dioxide was chemically generated at 295°K by the addition of KClO<sub>3</sub> powder to 90% aqueous H<sub>2</sub>SO<sub>4</sub>. The chlorate disproportionates to chlorine dioxide and perchloric acid in this medium, according to the equation:



The dioxide was then displaced from solution by a stream of dry nitrogen gas and redissolved in a variety of solvents including cold aqueous solutions of sulphuric, phosphoric and hydrochloric acids, carbon tetrachloride and isopentane. Suitable solvents combined good optical transparency in the vitreous state with a degree of chemical inertness towards the highly reactive ClO<sub>2</sub>. (It was necessary to use solvents that vitrified on cooling for the ESR measurements, since solvents which did not glassify tended to aggregate the solute in clusters. Consequently the ESR spectra of paramagnetic solutes were poorly resolved because of spin-spin broadening).

3. Electron Spin Resonance Spectra

Single crystals of  $\gamma$ -irradiated KClO<sub>4</sub> were photo-bleached with 3650Å radiation at 295°K for approximately

20 minutes prior to the measurement of spectra. The characteristic angular variations of ESR features arising from the photolysis products were then monitored as the crystal was rotated in turn about the crystallographic a, b, and c axes. The interpretation of the single-crystal results was facilitated by supplementary measurements of powder spectra at X- and Q-band frequencies.

Samples of chlorine dioxide trapped in glassy matrices were photolysed with  $3650\text{\AA}$  radiation at temperatures close to  $77^\circ\text{K}$ . The photolysis process was progressively monitored by ESR spectroscopy.

#### 4. Electronic Spectra

The electronic spectrum of an irradiated crystal of  $\text{KClO}_4$  was measured at intervals as the radiolysis products were progressively photobleached with  $3650\text{\AA}$  radiation at  $300^\circ\text{K}$ . Similarly, the optical absorption spectrum of a sample of  $\text{ClO}_2$  in vitreous 90% aqueous  $\text{H}_2\text{SO}_4$  was measured as the dioxide was irradiated with  $3650\text{\AA}$  light.

#### 5. Infrared Spectra

A small quantity of  $\gamma$ -irradiated  $\text{KClO}_4$  crystals, which had subsequently been photolysed, was powdered, mixed with dried KBr, and pressed into a disc of about 1 cm diameter and 0.5 mm thickness. This disc was fitted

into the low temperature attachment of the infrared spectrometer (see Chapter I ) and spectra were measured at both 77°K and room temperature. The spectra obtained were poorly resolved and obscured by the intense background absorption of the  $\text{ClO}_4^-$  ion. Better results were obtained by measuring the IR spectrum at 77°K of a photolysed solution of  $\text{ClO}_2$  in rigid carbon tetrachloride.

#### EXPERIMENTAL RESULTS

##### 1. Electron Spin Resonance Investigations of the Photolysis of Chlorine Dioxide

###### a) In single crystals of $\text{KClO}_4$

When potassium perchlorate was  $\gamma$ -irradiated at 195°K and subsequently annealed at room temperature for several days, the stable radicals  $\text{ClO}_2$  and  $\text{O}_3^-$  were formed.<sup>51</sup> When the irradiated crystal was then bleached with 3650Å radiation the  $\text{ClO}_2$  centre decayed giving rise to a third paramagnetic species G. Figure VII.2 shows the ESR spectrum, measured at 77°K, of G and  $\text{O}_3^-$  in a single crystal of  $\text{KClO}_4$  with the applied magnetic field ( $H_0$ ) in the ac-plane. The spectrum was characterised by two sets of quartets (corresponding to hyperfine interactions with  $^{35}\text{Cl}$  nuclei), originating from a single chlorine-containing radical (G) occupying two magnetically distinct sites.

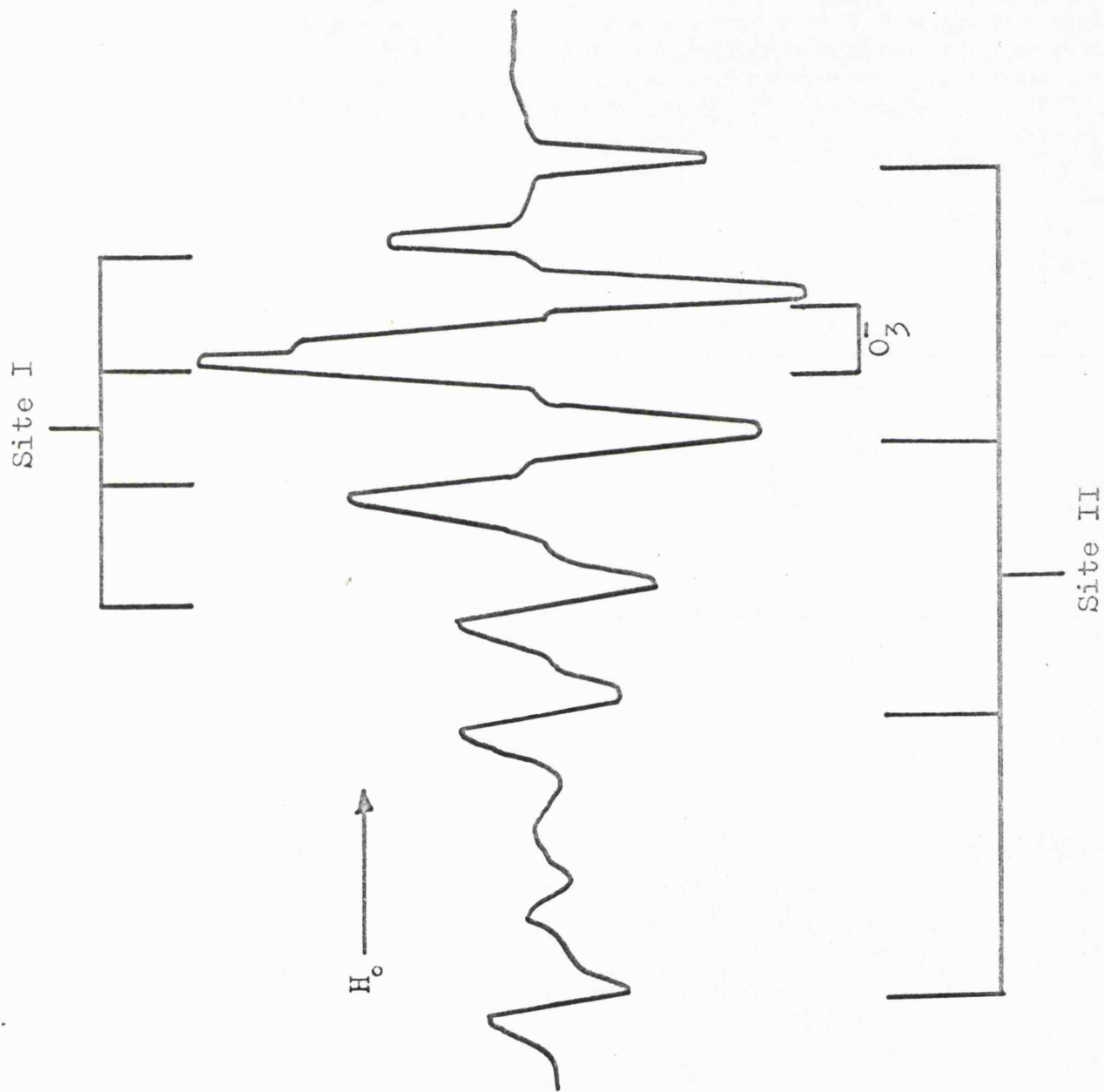


Figure VII.2. ESR spectrum of radical G and  $O_3^-$ , measured at 9.3 Gc/s, in a single crystal of  $KClO_4$  with  $H_0$  making an angle of  $20^\circ$  to the a-axis.

These quartets are superimposed on the broad central resonance of the  $O_3^-$  ion.

Figures VII.3 to 5 are plots of the angular variations of the hyperfine features which corresponded to the 'allowed' transitions of radical G as the magnetic field explored in turn the ac-, bc-, and ab-plane of the irradiated crystal. It was noted that within each set of hyperfine features the spacing was not always equal and that in certain orientations 'forbidden' transitions occurred. The intensity of these latter transitions was often about equal to that of features arising from the  $\Delta M_I = 0$  transitions of both G and unphotolysed  $ClO_2$  remaining in the crystal. For this reason it was decided not to undertake a complete analysis of these 'forbidden' lines and therefore, no quadrupole terms were included in the spin-Hamiltonian used to describe G. The principal values of the g- and A-tensors of radical G, evaluated using Schonland's method,<sup>15</sup> are summarised in Table VII.2.

The principal values  $g_{33}$  and  $a_{33}$  occurred twice in the ac-plane at  $\pm 55^\circ$  from the c-axis, two values arising because G occupied two distinct sites in this lattice. Since  $g_{11}$  and  $a_{11}$  also lay in this plane,  $g_{22}$  and  $a_{22}$  were necessarily parallel to the b-axis. Figures VII.6 to 8 show the angular variations of the g- and A-tensors of

TABLE VII.2. Electron Spin Resonance Parameters of ClO<sub>2</sub> and

Radical	Matrix	Nucleus	Related Species				Hyperfine tensor in gauss			Ref	
			g <sub>11</sub>	g <sub>22</sub>	g <sub>33</sub>	g <sub>av</sub>	a <sub>11</sub>	a <sub>22</sub>	a <sub>33</sub>		A <sub>iso</sub>
ClO <sub>2</sub> (G)	KClO <sub>4</sub>	<sup>35</sup> Cl	1.9983	2.0017	2.0130	2.0043	5.3	7.2	14.9	a	
	(single-crystal)										
	KClO <sub>4</sub>	<sup>35</sup> Cl	b	2.0019	2.0127	b	b	6.8	15.2	a	
	(powder at 34 Gc/s)										
	H <sub>2</sub> SO <sub>4</sub>	<sup>35</sup> Cl	b	b	2.0115	b	b	b	15.3	a	
'ClO'	H <sub>2</sub> SO <sub>4</sub>	<sup>35</sup> Cl	1.9909	1.9909	2.0098	1.9972	0	0	-17.1	-5.7	54
	KClO <sub>4</sub>	<sup>35</sup> Cl	1.9965	2.0035	2.0100	2.0033	-4.6	-2.0	18.7	4.0	93
	(single-crystal)										
FOO	Argon	<sup>19</sup> F	2.0008	2.0022	2.0080	2.0037	±50	±14	±103	±13	101

a) This work.

b) These parameters could not be derived from the spectra.

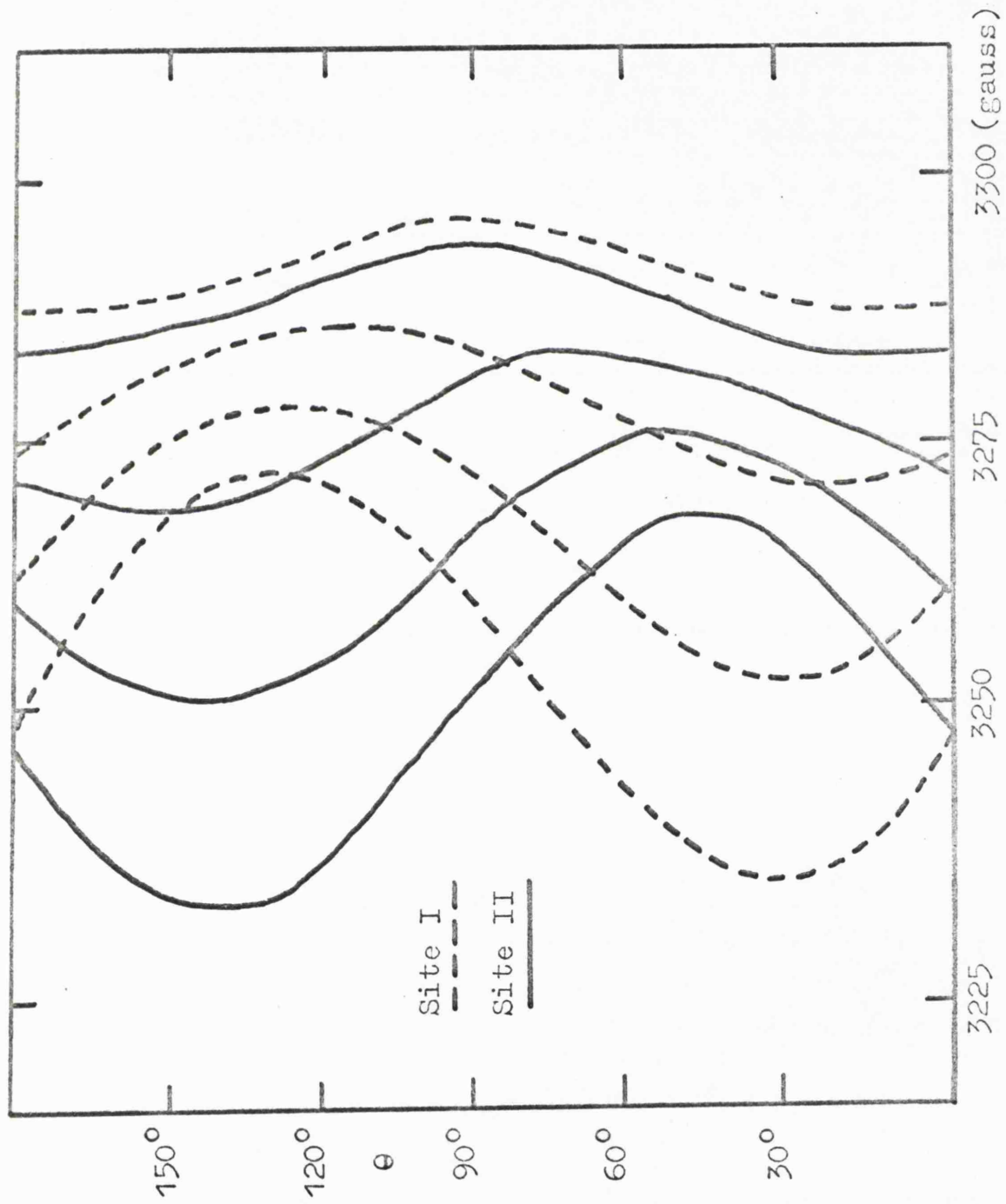


Figure VII.3. Angular variation of the hyperfine features of radical G in  $KClO_4$  as  $H_0$  explores the ac-plane.  $\theta$  is the angle between  $H_0$  and the a-axis.

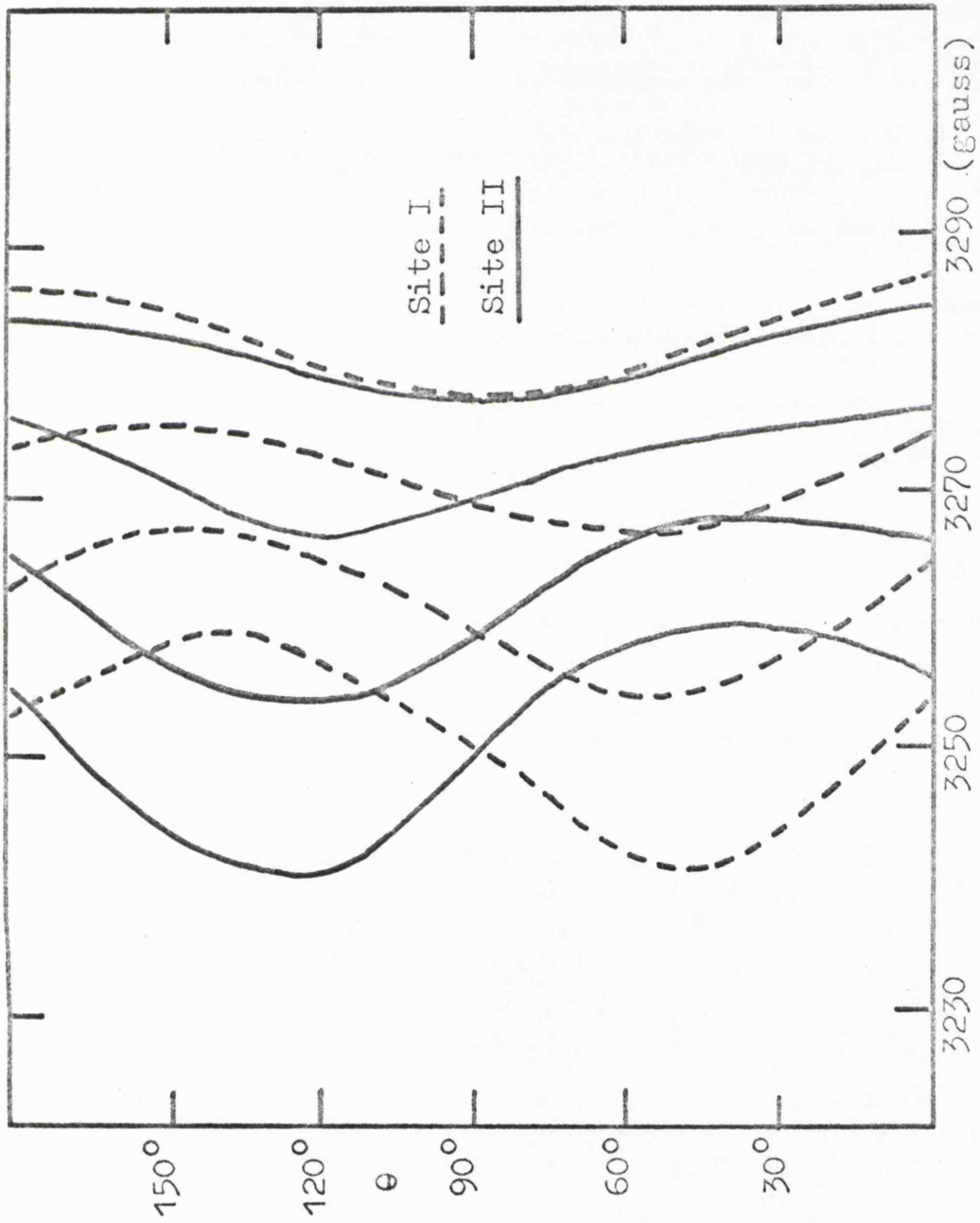


Figure VII.4. Angular variation of the hyperfine features of radical G in  $\text{KClO}_4$  as  $H_0$  explores the bc-plane.  $\theta$  is the angle between  $H_0$  and the b-axis.

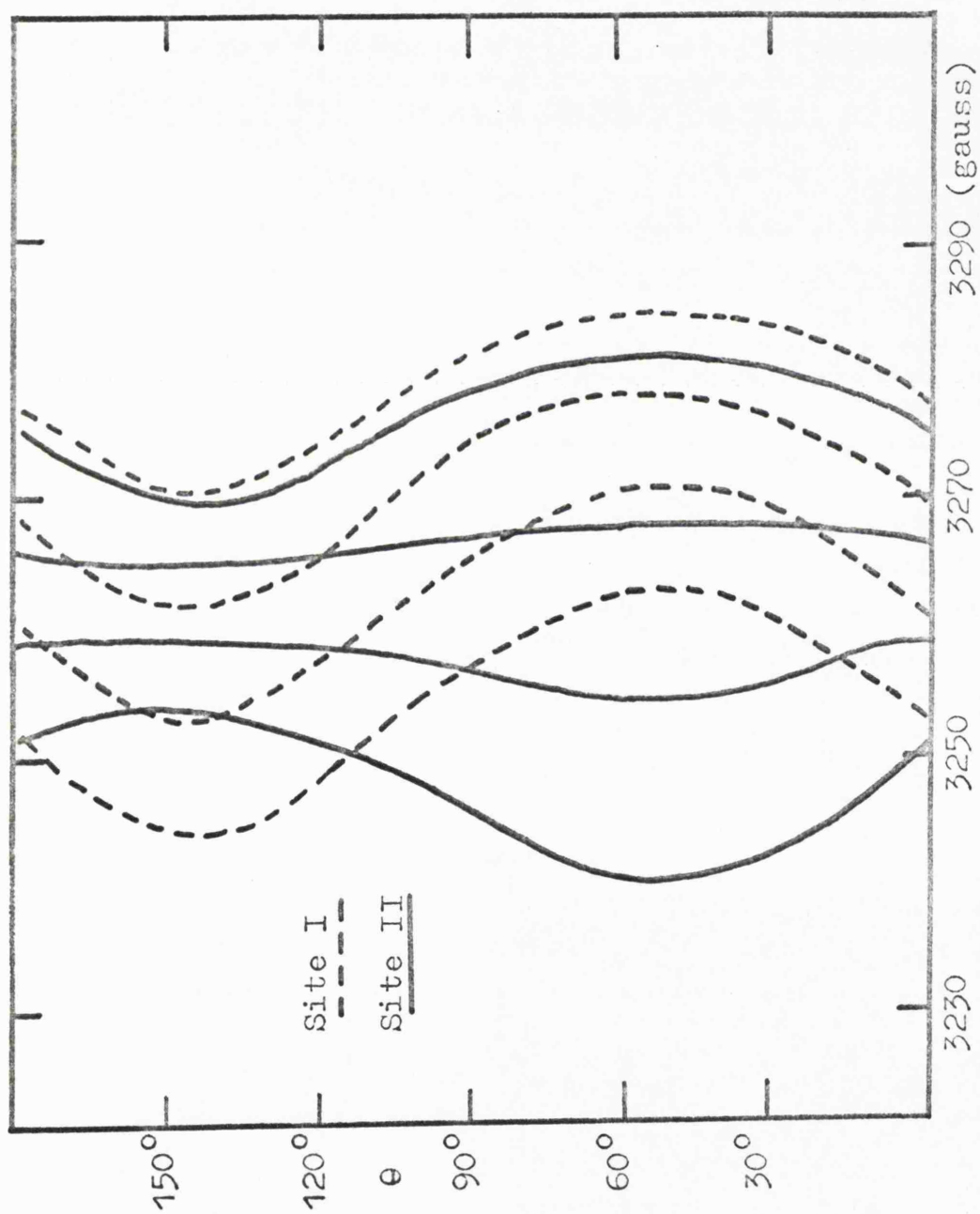


Figure VII.5. Angular variation of the hyperfine features of radical G in  $\text{KClO}_4$  as  $\text{H}_2\text{O}$  explores the ab-plane.  $\theta$  is the angle between  $\text{H}_2\text{O}$  and the b-axis.

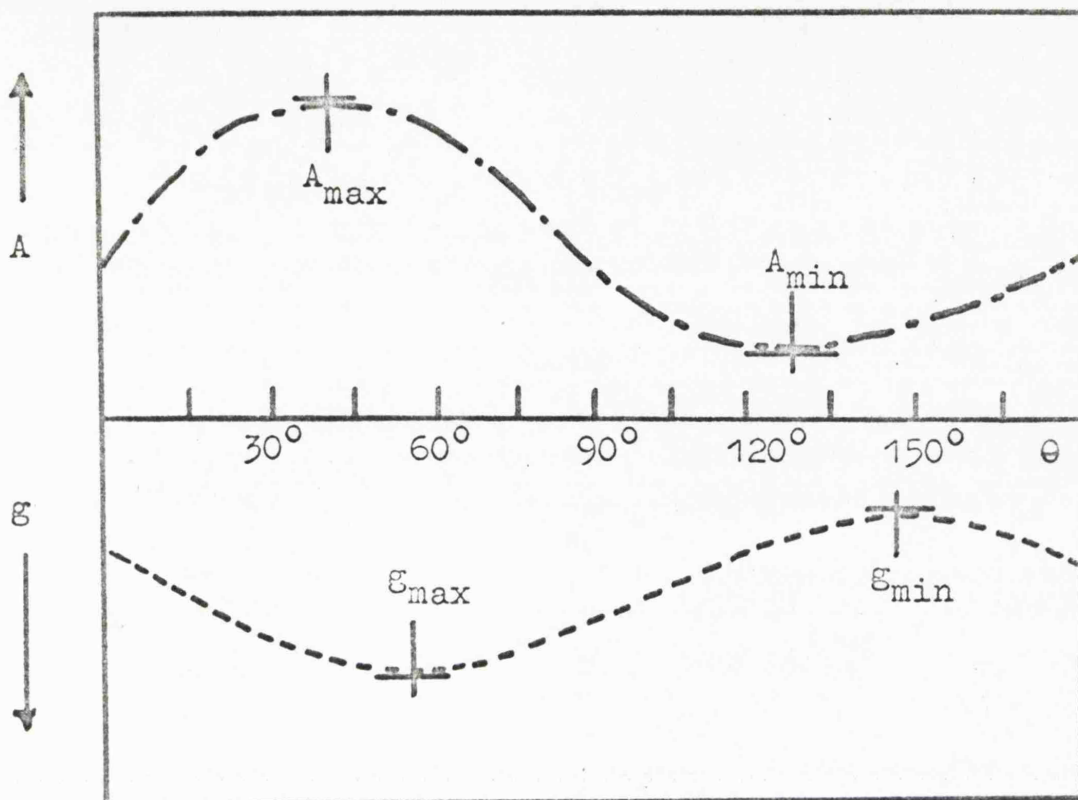


Figure VII.6. Angular variations of the g- and A-factors of radical G in  $\text{KClO}_4$  as  $\text{H}_0$  explores the ac-plane.

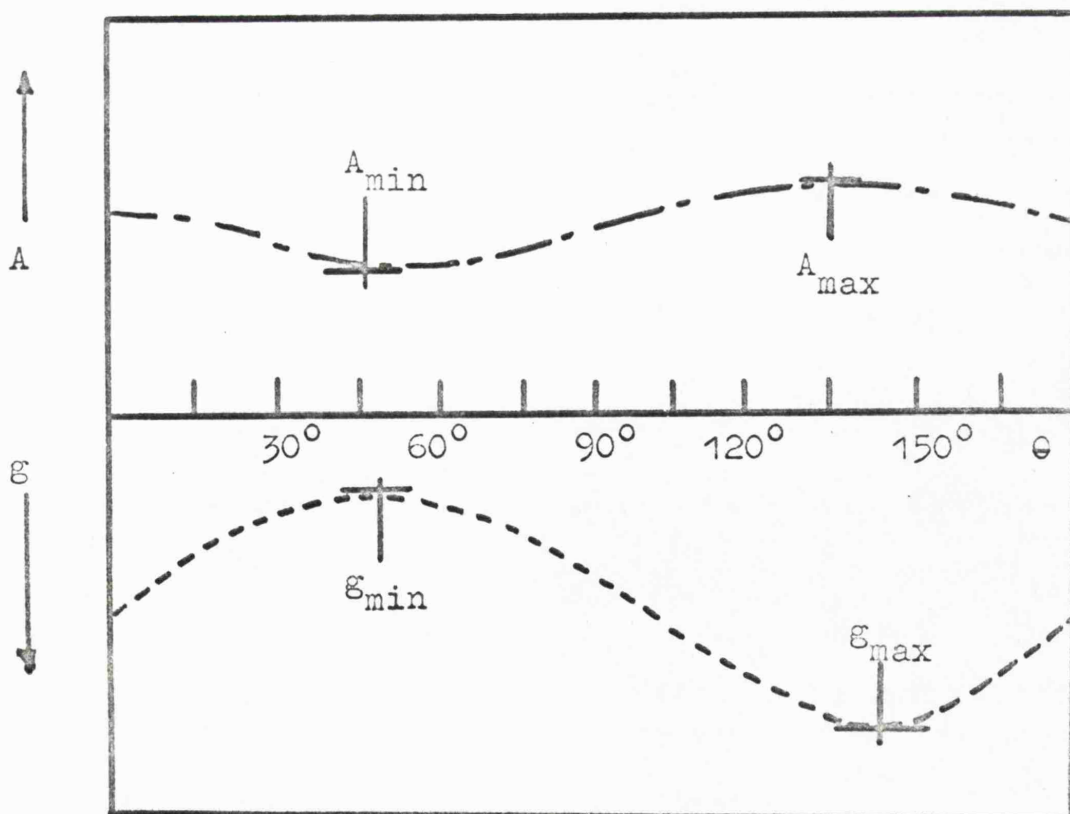


Figure VII.7. Angular variations of the g- and A-factors of radical G in  $\text{KClO}_4$  as  $\text{H}_0$  explores the bc-plane.

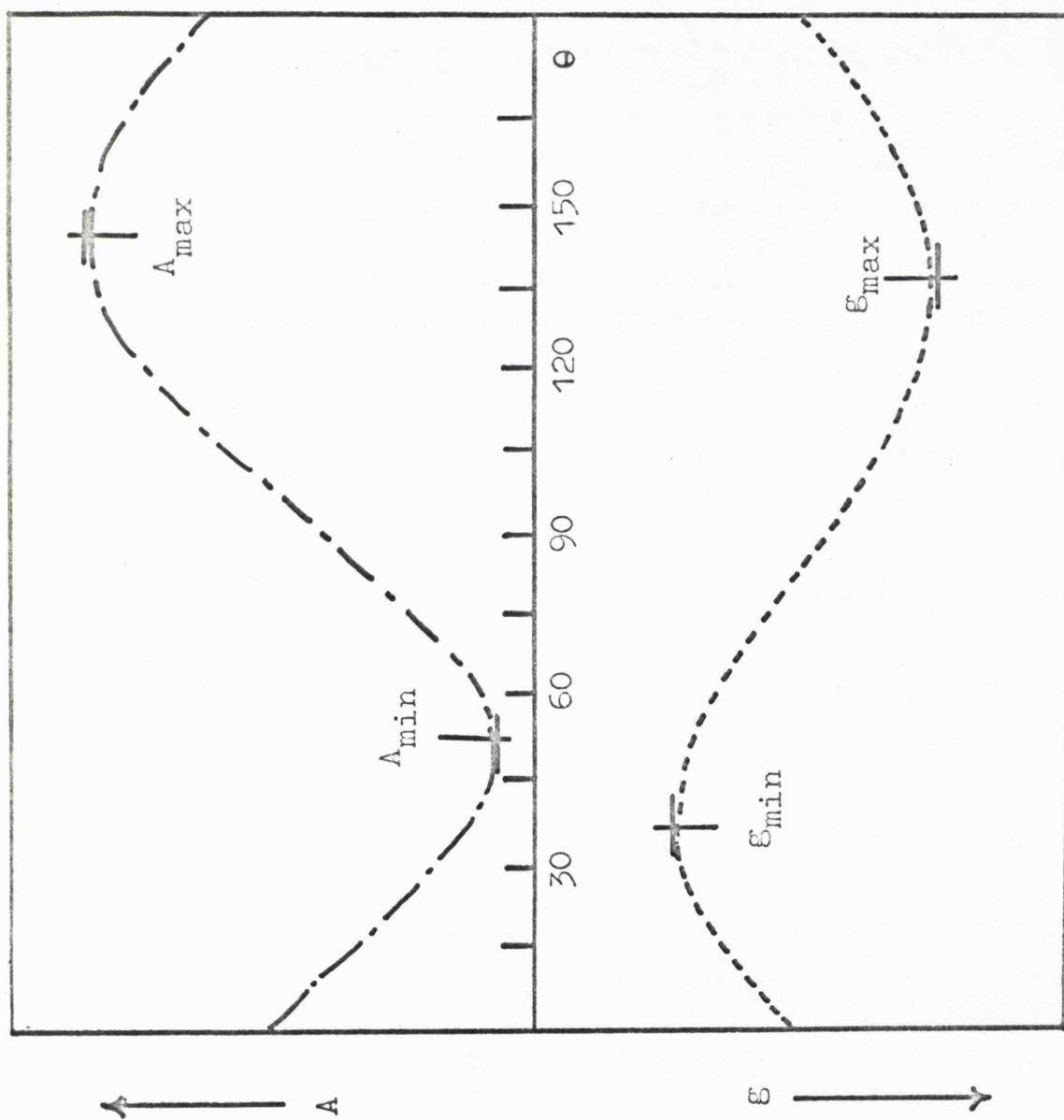


Figure VII.8. Angular variations of the  $g$ - and  $A$ -factors of radical G as  $H_2O$  explores the ab-plane.

radical G in the ac-, bc-, and ab-planes. It is quite clear from these plots that the principal axes of these tensors were not spacially coincident and that the values  $g_{11}$ ,  $a_{11}$ ,  $g_{33}$  and  $a_{33}$  were insensitive to small changes in  $\theta$ . Consequently we could not determine their relative positions to a greater accuracy than  $\pm 10^\circ$ . For this reason we have not included direction cosines in Table VII.2 although we believe an upper limit of  $15-20^\circ$  can be set for the angle between the corresponding axes of  $g_{11}$  and  $a_{11}$ , and between  $g_{33}$  and  $a_{33}$ .

These results are in good agreement with those of Byberg<sup>93</sup> (see Table VII.2) reported soon after the present investigation was complete. However, as we shall see later, we do not agree with his conclusions about the structure of radical G.

Considerable broadening of the ESR spectrum of radical G occurred when the crystal was warmed above  $140^\circ\text{K}$ . However, even after heating to  $295^\circ\text{K}$  the spectrum remeasured at  $77^\circ\text{K}$  was identical to that before the heat treatment. This line-broadening at high temperature has been associated with a spin-rotational interaction<sup>71</sup> similar to that discussed for  $\text{ClO}_2$ .<sup>94</sup>

Radical G decayed with a half-life of approximately 12 hours at  $295^\circ\text{K}$  resulting in a concomitant increase in

the concentration of  $\text{ClO}_2$ . At  $323^\circ\text{K}$  G was completely converted to the dioxide in less than 4 hours. At this stage it was possible to repeat the whole cycle and photolytically regenerate G. The concentrations of both  $\text{ClO}_2$  and G decreased slightly after each cycle indicating that the interconversions were not quite quantitative.

b) In powders and glasses

The X-band spectrum of chlorine dioxide in frozen 90% aqueous  $\text{H}_2\text{SO}_4$ , shown in Figure VII.9 was surprisingly complex and consequently, from this spectrum Symons and coworkers<sup>54</sup> could only derive the parameters  $a_{xx}$  and  $g_{xx}$ . This complexity arises through the superposition of a number of 'allowed' and 'forbidden' transitions in the central region of the spectrum. The Q-band spectrum of this system (Figure VII.10) was simplified by a marked reduction in the intensity of features corresponding to the transitions  $\Delta M_I = \pm 1, \pm 2$  (see Chapter VI). An analysis of this spectrum yielded all the diagonal components of the g- and A-tensors listed in Table VII.3.

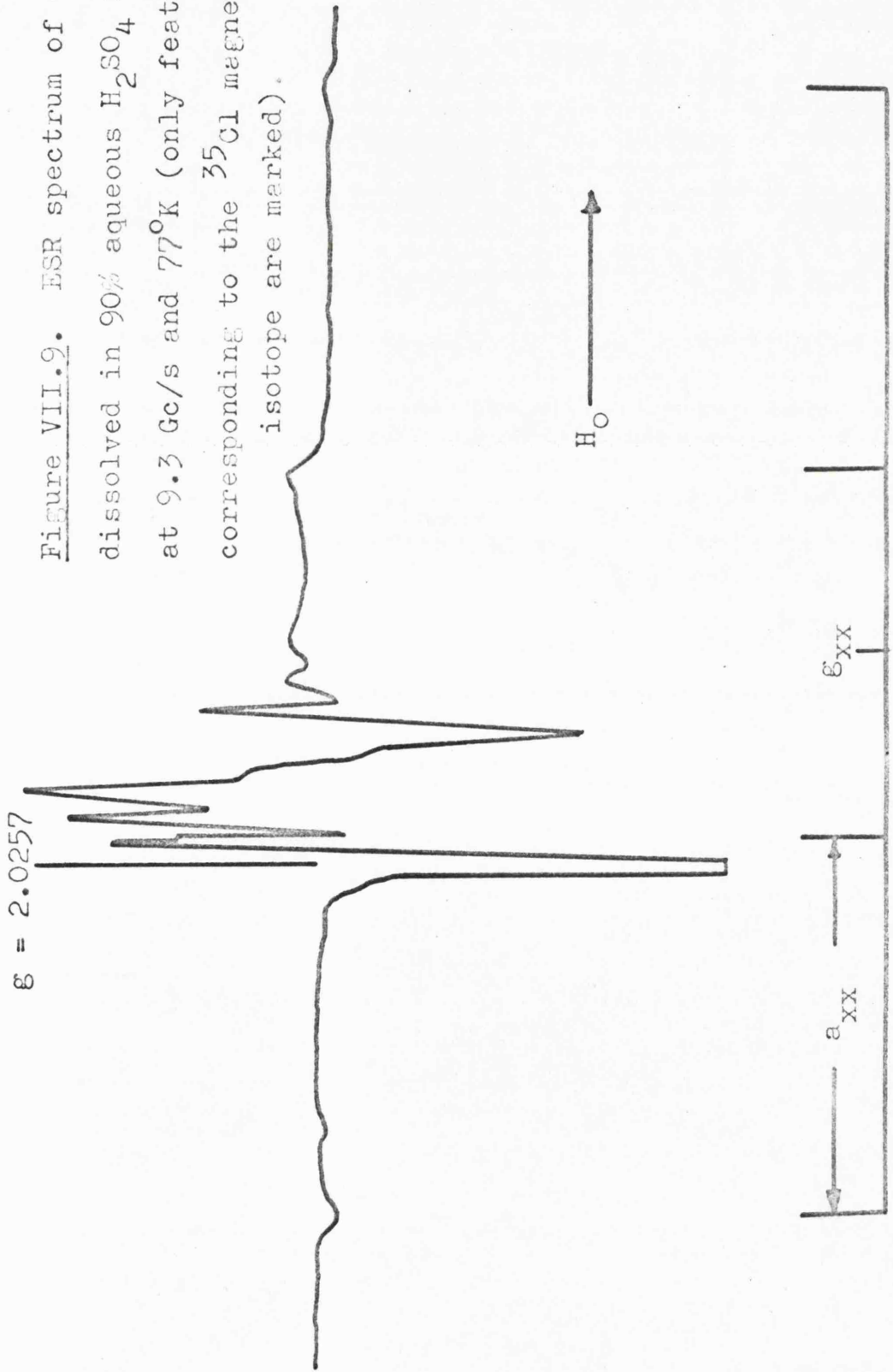
When a sample of  $\text{ClO}_2$  in vitrified  $\text{H}_2\text{SO}_4$  was photolysed at  $77^\circ\text{K}$  for approximately 30 minutes, the strong ESR absorption of the dioxide was almost completely replaced by new features associated with radical G. The loss of  $\text{ClO}_2$  during photolysis was most conveniently

TABLE VII.3. Electron Spin Resonance Parameters of Chlorine Dioxide  
in Aqueous H<sub>2</sub>SO<sub>4</sub>

Temperature	Measurement Frequency	g-tensor		<sup>35</sup> Cl Hyperfine tensor in gauss					
		g <sub>xx</sub>	g <sub>yy</sub>	g <sub>zz</sub>	g <sub>av</sub>	a <sub>xx</sub>	a <sub>yy</sub>	a <sub>zz</sub>	A <sub>iso</sub>
295°K	9.3 Gc/s				2.0098				+16.5
77°K	9.3 Gc/s	2.0015	a	a	a	70.5	a	a	a
77°K	34 Gc/s	2.0025	2.0170	2.0110	2.0102	73.7	-9.6	-10.0	+18.0

a) These parameters could not be derived in this matrix

Figure VII.9. ESR spectrum of  $\text{ClO}_2$  dissolved in 90% aqueous  $\text{H}_2\text{SO}_4$  measured at 9.3 Gc/s and 77°K (only features corresponding to the  $^{35}\text{Cl}$  magnetic isotope are marked).



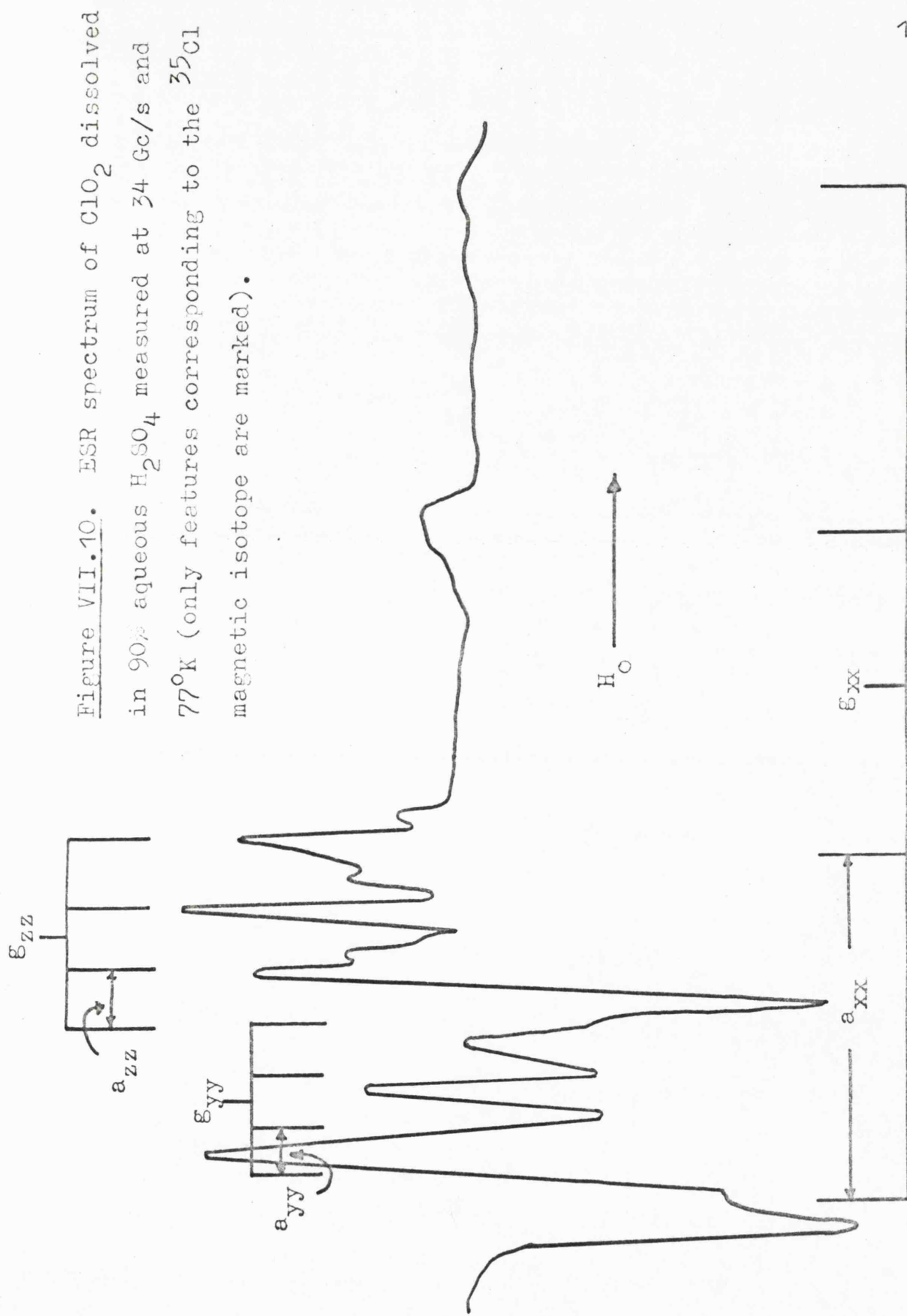


Figure VII.10. ESR spectrum of  $\text{ClO}_2$  dissolved in 90% aqueous  $\text{H}_2\text{SO}_4$  measured at 34 Gc/s and 77°K (only features corresponding to the  $^{35}\text{Cl}$  magnetic isotope are marked).

followed by the observation of the characteristic intense absorption at  $g = 2.0257$ , which arose from the overlap of several 'allowed' and 'forbidden' transitions. At the same time the appearance of G was monitored by the increasing intensity of a strong feature at  $g = 1.999$ . Figure VII.11 shows ESR spectra, measured at  $77^\circ\text{K}$ , of  $\text{ClO}_2$  in  $\text{H}_2\text{SO}_4$  as the system was progressively photolysed. A similar spectrum to VII.11d has been shown by Symons and coworkers (Figure 3 of reference 54) in which they assign a peak 'd' to radical G. However, an examination of Figure VII.11 suggests that this peak ( $g = 2.0257$ ) results from residual unphotolysed  $\text{ClO}_2$  and that the shoulder on the high field side of this absorption arises from G. Because the small hyperfine coupling constants were coupled with linewidths close to 4 gauss, only the values  $g_{33}$  and  $a_{33}$  for G in this matrix could be extracted from the spectra measured at both X- and Q-band frequencies.

Figures VII.12 and 13 show powder spectra of G in  $\text{KClO}_4$  at X- and Q-band frequencies; partial analyses have been included on the diagrams. At 8 mm wavelength features corresponding to  $g_{33}$  and  $a_{33}$  were well-resolved, but the remaining parameters were less readily obtained because of the overlap of spin-resonance features from G with the very intense absorption of the  $\text{O}_3^-$  ion in the free-

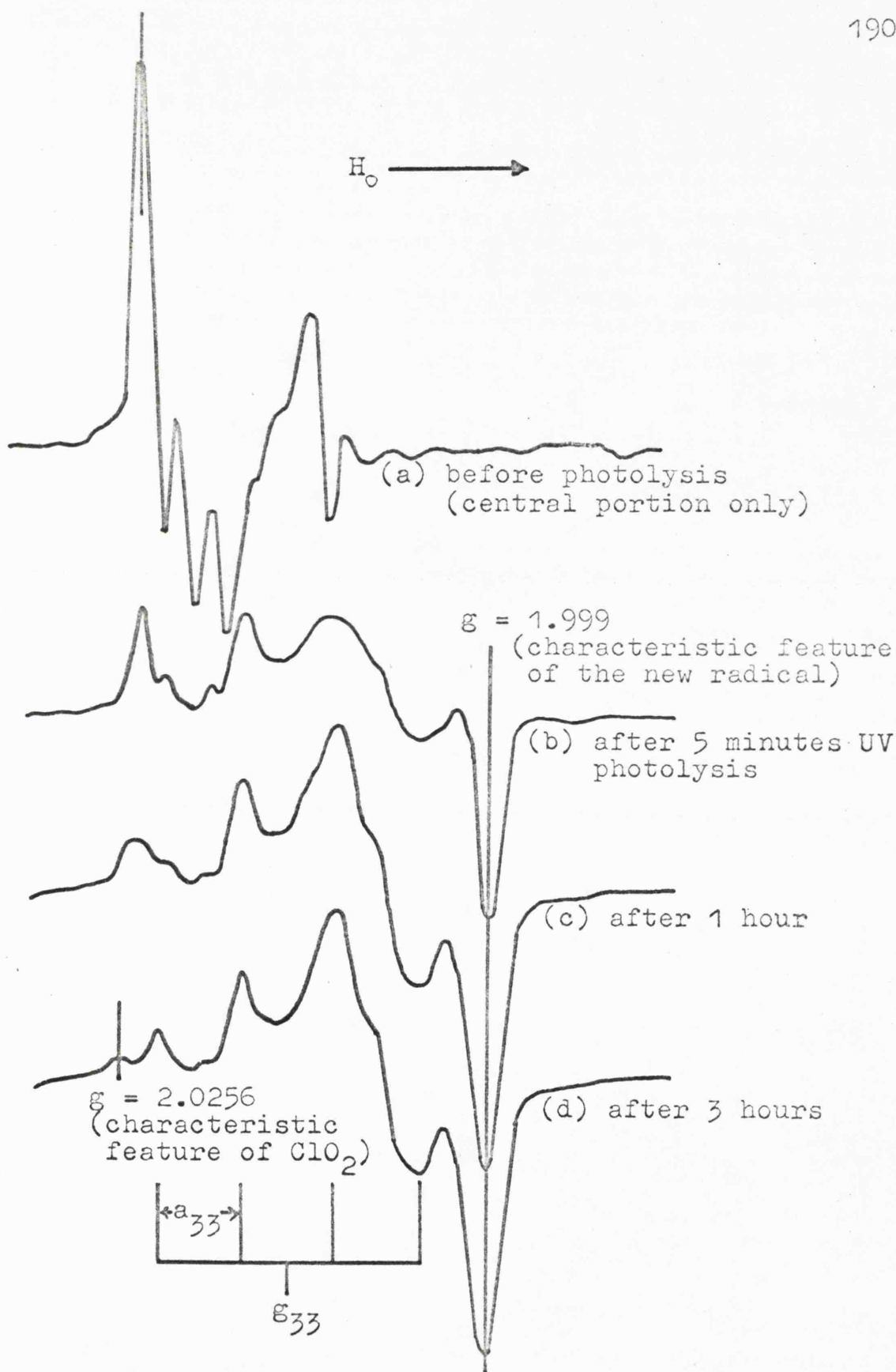


Figure VII.11. ESR spectra, measured at  $77^\circ K$  and  $9.3 \text{ Gc/s}$ , of  $ClO_2$  in 90% aqueous  $H_2SO_4$  as the system was progressively photolysed with  $3650\text{\AA}$  radiation.

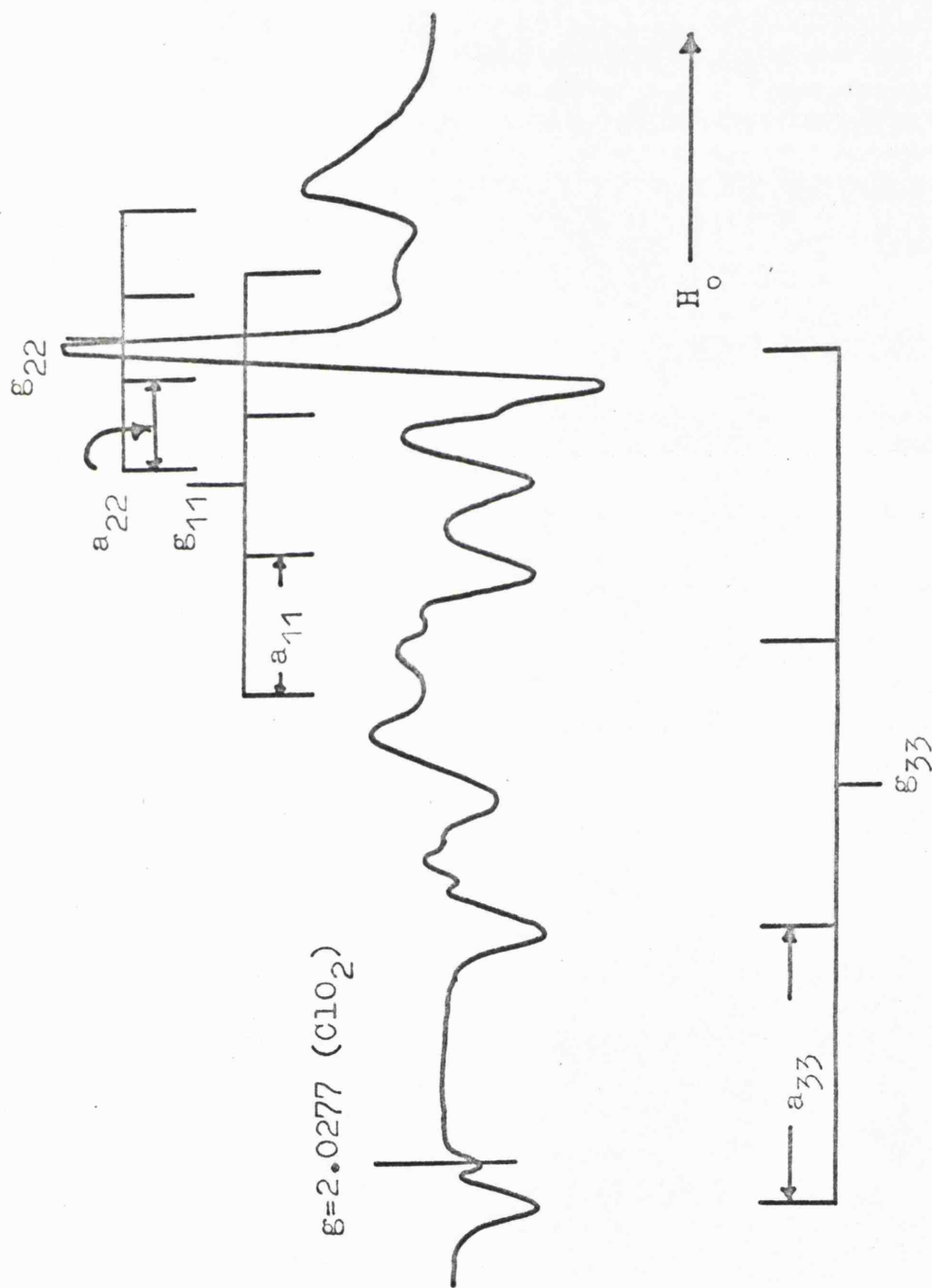


Figure VII.12. The ESR spectrum of radical G in  $\text{KClO}_4$  powder measured at  $77^\circ\text{K}$  and  $9.3 \text{ Gc/s}$  (only hyperfine features corresponding to  $^{35}\text{Cl}$  are marked).

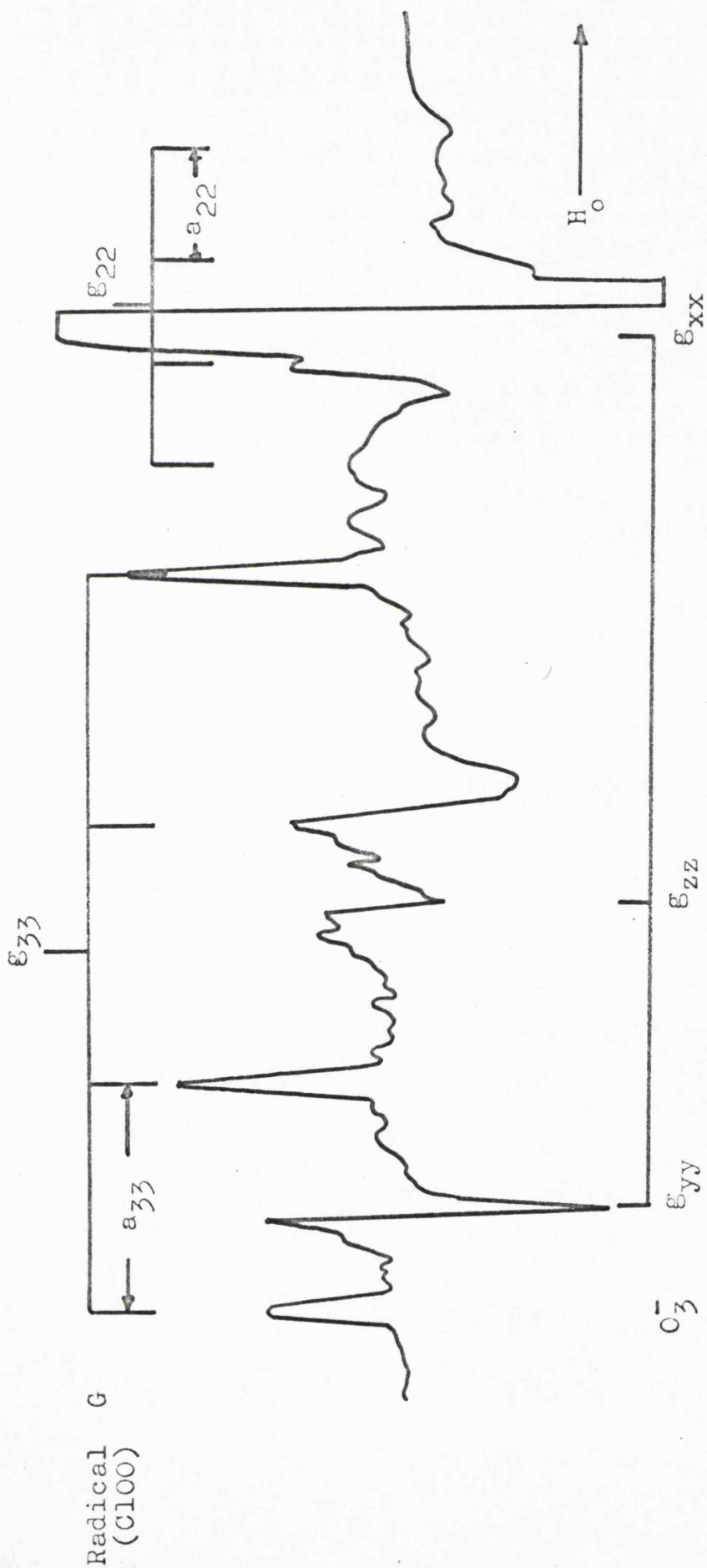


Figure VII.13. The ESR spectrum of radical G in  $KClO_4$  powder measured at  $77^\circ K$  and 34 Gc/s (only hyperfine features corresponding to  $^{35}Cl$  are marked).

spin region. The data derived for G in vitreous sulphuric acid and powdered  $\text{KClO}_4$  are included in Table VII.2.

## 2. Electronic and Infrared Investigations of the Photolysis of Chlorine Dioxide

Chlorine dioxide has a characteristic absorption band with a maximum intensity at 365 nm ( $27,400 \text{ cm}^{-1}$ ) in aqueous sulphuric acid.<sup>80</sup> On photolysis at  $77^\circ\text{K}$  this band rapidly decayed with a parallel increase in intensity of a strong peak at 260 nm ( $38,500 \text{ cm}^{-1}$ ). The intensity of the original absorption was approximately half that of the 260 nm ( $38,500 \text{ cm}^{-1}$ ) peak after four hours photolysis. Figure VII.14 shows optical spectra of  $\text{ClO}_2$  in vitreous sulphuric acid as the sample was progressively photolysed with  $3650\text{\AA}$  radiation.

The ultraviolet spectrum of a single crystal of  $\gamma$ -irradiated  $\text{KClO}_4$  exhibited two intense absorptions at 370 nm ( $27,000 \text{ cm}^{-1}$ ) and 430 nm ( $23,200 \text{ cm}^{-1}$ ) corresponding to the radicals  $\text{ClO}_2$  and  $\text{O}_3^-$ . The effect of  $3650\text{\AA}$  radiation on these centres is shown in Figure VII.15. A rapid diminution in intensity of the 370 nm ( $27,000 \text{ cm}^{-1}$ ) absorption was accompanied by a corresponding increase in intensity of a broad band around 280 nm ( $35,700 \text{ cm}^{-1}$ ).

Attempts have also been made to measure the IR

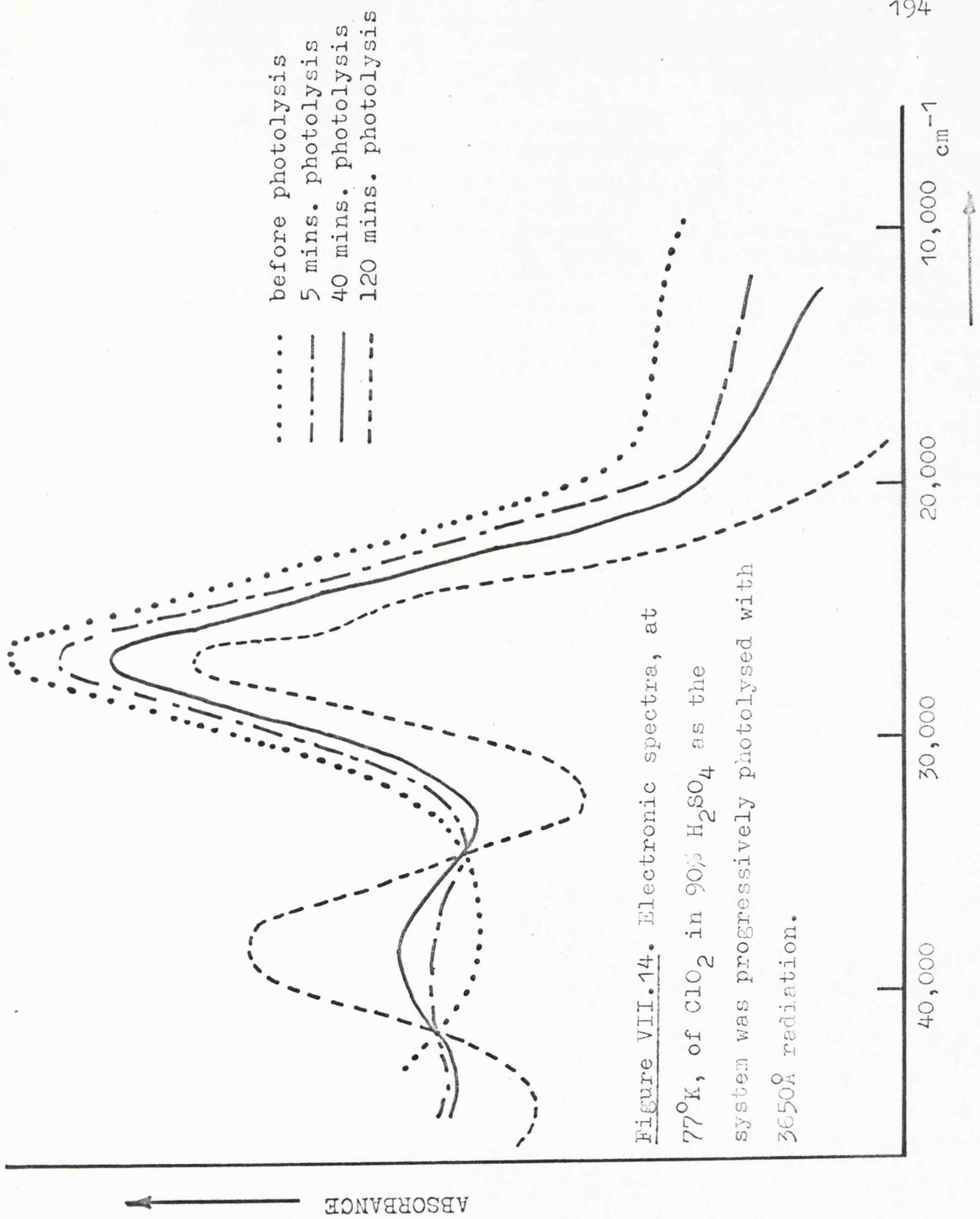


Figure VII.14. Electronic spectra, at 77°K, of ClO<sub>2</sub> in 90% H<sub>2</sub>SO<sub>4</sub> as the system was progressively photolysed with 3650Å radiation.

Curve (I) after irradiation, but before photolysis.

(II) after irradiation, and after 30 minutes photolysis.

(III) curve (II) - curve (I).

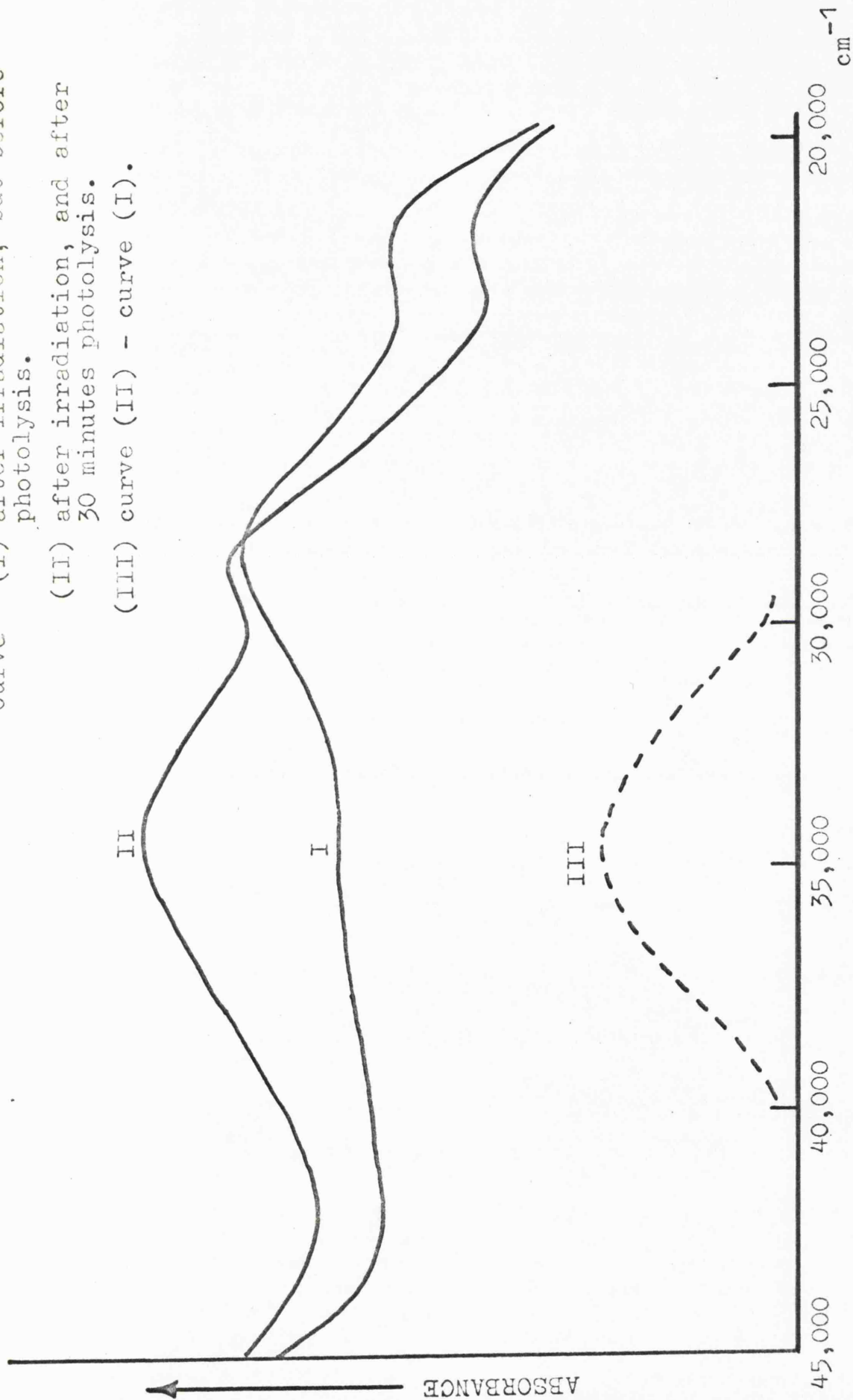


Figure VII.15. The electronic spectrum of an irradiated single crystal of  $\text{KClO}_4$  and the effect of  $3650\text{\AA}$  radiation on the radical-products.

spectrum of radical G, but experiments using  $\text{KClO}_4$  and  $\text{H}_2\text{SO}_4$  matrices were unsuccessful. However,  $\text{ClO}_2$  in rigid  $\text{CCl}_4$  was photolysed to produce G, and the IR spectrum obtained at  $77^\circ\text{K}$ , although poorly resolved, showed two new bands at approximately  $1430$  and  $1440\text{ cm}^{-1}$ .

## DISCUSSION

### 1. The Identification of Radical G

Symons<sup>95</sup> has recently suggested that the photolytic product of  $\text{ClO}_2$  in rigid media (radical G) is in fact the 'peroxy-chlorine' species  $\text{ClOO}$  and, for the following reasons, we have reaffirmed this conclusion:<sup>96</sup>

- a)  $\text{ClO}_2$  and G are readily interconverted in a variety of host matrices. This would appear to suggest that G is isomeric with  $\text{ClO}_2$ .
- b) The g-tensor of G is very similar to those of  $\text{FOO}$ ,  $\text{ClO}_2$ ,  $\text{NO}_2^{2-}$  and  $\text{O}_3^-$ , all of which are isostructural with  $\text{ClOO}$ . The parameters for  $\text{FOO}$  are included in Table VII.2. for comparison.
- c) Rochkind and Pimentel,<sup>89</sup> and also Arkel and Schwager,<sup>90</sup> have produced a species thought to be  $\text{ClOO}$  by photolysis of  $\text{ClO}_2$  in solid nitrogen ( $20^\circ\text{K}$ ) and argon ( $4.2^\circ\text{K}$ ). Their principal evidence for this identification was the detection of an IR absorption at  $1440\text{ cm}^{-1}$  which was assigned to an

O-O stretch. The equivalent vibration appears at  $1500\text{ cm}^{-1}$  in FOO, at  $1390\text{ cm}^{-1}$  in HOO, and at  $1556\text{ cm}^{-1}$  in  $\text{O}_2$  (Raman). Our IR results are in accord with these findings.

d) Morris and Johnston<sup>97</sup> have recently reported the detection of both ClO and ClOO in the gas-phase photolysis of chlorine dioxide by an ingenious molecular modulation technique. Fortunately, the absorption maxima of both ClO and ClOO coincided almost exactly [ $257.7\text{ nm}$  ( $38,800\text{ cm}^{-1}$ ) and  $247.5\text{ nm}$  ( $40,400\text{ cm}^{-1}$ ) respectively], but by varying the frequency of the incident radiation it was possible to observe the spectra of ClO and ClOO independently. Radical G is characterised by a strong absorption at  $260\text{ nm}$  ( $38,500\text{ cm}^{-1}$ ) in vitreous  $\text{H}_2\text{SO}_4$  and at  $280\text{ nm}$  ( $35,700\text{ cm}^{-1}$ ) in  $\text{KClO}_4$ .

e) The most likely alternative structure for G is ClO, a  $^2\Pi_{3/2}$  diatomic radical. In order to accommodate the observed spin-resonance results for G in terms of this species, it is necessary to postulate that a very large 'crystal field' interaction has lifted the degeneracy of the  $\Pi_{2p}^*$ -molecular orbitals. It is difficult to see why

such an interaction should occur to the same extent in two very different environments; namely vitreous aqueous sulphuric acid and potassium perchlorate. The results of Symons and coworkers, Byberg and the present investigation indicate a maximum chlorine spin-density of approximately 20% in G. For ClO one would have expected the anti-bonding unpaired-electron to be more closely associated with chlorine than with oxygen, since oxygen is slightly the more electronegative atom. Indeed, recent gas-phase electron resonance and rotational spectroscopic studies of ClO have shown that the chlorine spin-density in this diatomic is close to 0.50.<sup>98,99</sup>

## 2. The Electronic and Molecular Structures of Radical G

The O-O stretching frequency in the series of AOO radicals FOO, ClOO and HOO is peculiarly insensitive to the nature of A. This fact has prompted Spratley and Pimentel<sup>100</sup> to describe these species in terms of molecules having bond angles close to 90° with a weak  $\sigma$ -interaction between A and what is virtually a slightly perturbed oxygen molecule. Their proposed molecular orbital scheme is shown in Figure VII.16 for FOO. The  $\pi_y^*$ -antibonding orbital of the oxygen molecule overlaps with the  $2p_y$ -

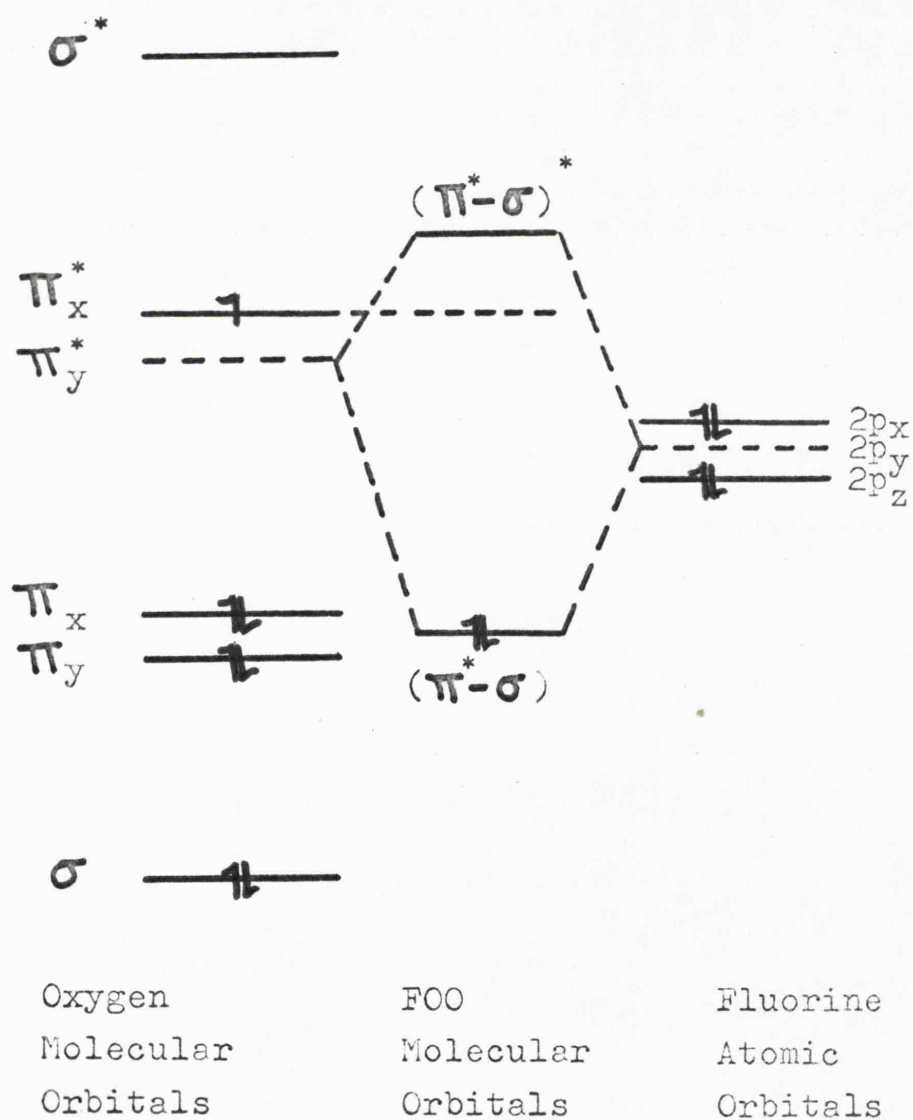


Figure VII.16. The molecular orbital scheme for FOO proposed by Spratley and Pimentel (reference 100).

orbital of fluorine to form a weak  $\sigma - \pi^*$  bond, consequently the unpaired electron would be accommodated in the unperturbed oxygen  $\pi_x^*$ -level. However, we see no compelling reason to assume that the bond angle in ClOO should be close to  $90^\circ$  and we prefer not to abandon the more conventional Mulliken-Walsh description which has so satisfactorily accounted for the bonding in a wide range of inorganic radicals. Therefore, since ClOO is a 19 valence-electron  $\pi$ -radical, one would expect the  $\widehat{\text{ClOO}}$  bond angle to be in the region  $110-120^\circ$ , by analogy with the isoelectronic species  $\text{ClO}_2$  ( $118.5^\circ$ ) and  $\text{NO}_2^{2-}$  ( $115^\circ$ ). Arkel and Schwager<sup>90</sup> have proposed a  $\widehat{\text{ClOO}}$  angle of approximately  $110^\circ$  from the results of their IR studies.

Since the electronegativities of chlorine and oxygen are approximately equal, we expect that the spin-density distribution in ClOO will resemble that in  $\text{ClO}_2$  and  $\text{O}_3^-$ ; approximately 0.64 on the central atom and 0.18 delocalised onto the ligands. For such an electron distribution in ClOO we predict the following contributions to the chlorine hyperfine tensor:

- a) A small isotropic coupling arising from the polarisation of the  $\sigma$ -bonding orbitals. This coupling is expected to be small and negative,

through the cancellation of a positive term from spin directly on chlorine by a negative contribution from spin-density on the central oxygen atom.

b) There will be two major contributions to the anisotropic hyperfine tensor. The first, resulting from spin-density in a chlorine 3p-orbital, will have the form  $(-B, +2B, -B)$  where the major component is perpendicular to the ClOO molecular plane (axis 2). The second, smaller in magnitude than the first, will have the form  $(+B', +B', -2B')$  and results from negative spin-density polarised into the Cl-O  $\sigma$ -bonding level. Its major component will be parallel to the Cl-O bond direction (axis 3). Since  $|2B|$  is expected to be larger than  $|2B'|$ , a combination of these components will result in an experimental tensor having a large positive value perpendicular to the molecular plane, a negative value along the Cl-O bond which will be somewhat smaller in magnitude, and a small negative term orthogonal to these. The form of the expected experimental hyperfine tensor and its relationship to the molecular structure of ClOO is shown in Figure VII.17.

c) Calculations using a point-dipole approximation

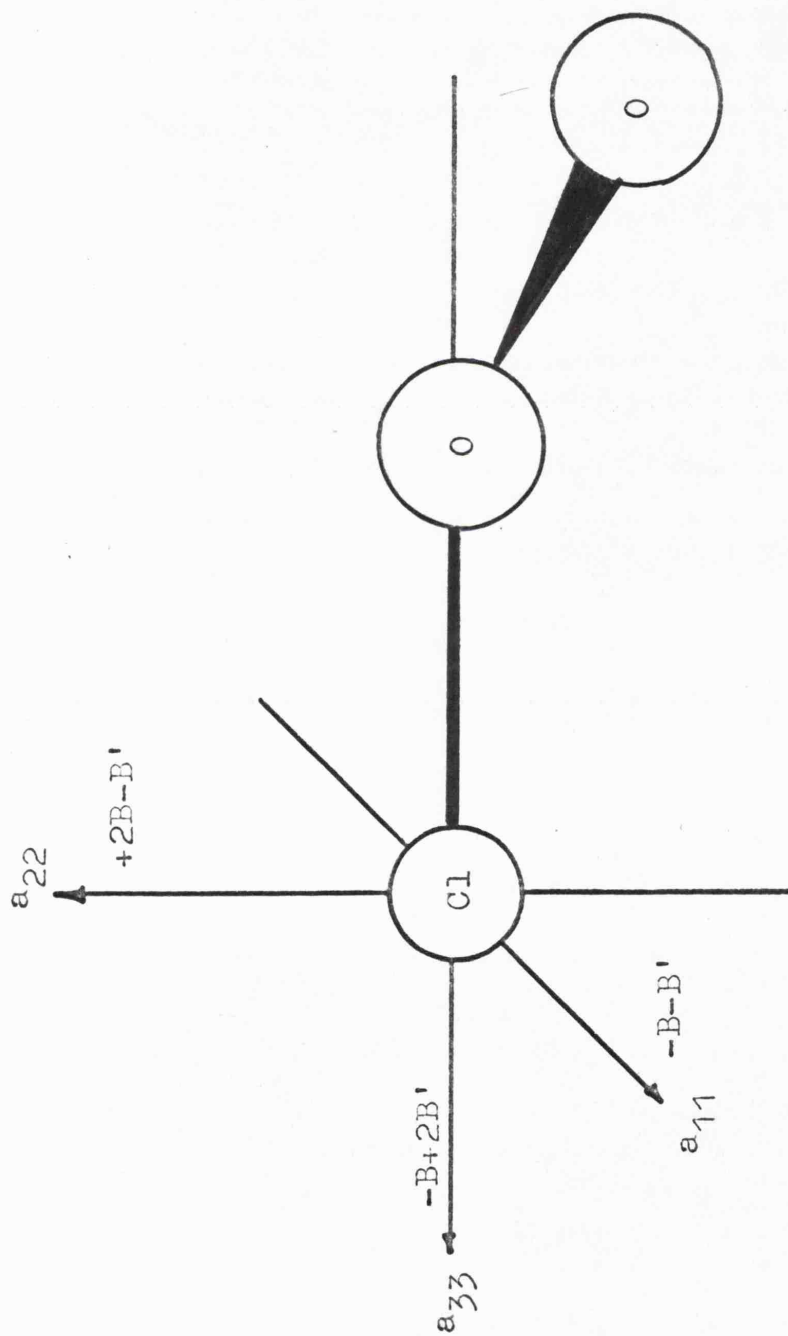


Figure VII.17. The relationship of the predicted A-tensor of ClOO to the configuration of the radical.

show that the indirect dipolar coupling of the chlorine nucleus to spin-density on the central oxygen atom will give a contribution of  $<1$  gauss to the experimental A-tensor and therefore, can be neglected.

In Table VII.4 the eight possible forms of the hyperfine tensor, assuming all the possible sign permutations for the components, have been listed. In this Table the B tensor represents the total anisotropic coupling. Only combination (vi) fulfills all the criteria listed above. This has a negative isotropic coupling and an anisotropic tensor which can be resolved into two axially symmetric components of the form  $(-4.2, +8.4, -4.2)$  gauss and  $(+3.2, +3.2, -6.4)$  gauss. The former tensor corresponds to a chlorine 3p-orbital population of 0.084, whilst the latter arises from spin-polarisation of the Cl-O  $\sigma$ -bonding electrons. The molecular parameters derived from this analysis of the experimental A-tensor are given in Table VII.5. It should be noted however, that the large number of uncertainties, particularly the unknown contributions from quadrupole interactions, make these conclusions rather tentative. Nevertheless they are consistent with the proposed structure.

The form of the g-tensor in ClO is expected to be

TABLE VII.4.

Possible Forms of the Hyperfine Tensor for ClOO,  
Together with the Breakdown into Isotropic and

Anisotropic Contributions

	(i)	(ii)	(iii)	(iv)	(v)	(vi)	(vii)	(viii)
$a_{11}$	+5.3	-5.3	-5.3	+5.3	+5.3	-5.3	-5.3	+5.3
$a_{22}$	+7.2	-7.2	+7.2	-7.2	-7.2	+7.2	-7.2	+7.2
$a_{33}$	+14.9	-14.9	+14.9	-14.9	+14.9	-14.9	+14.9	-14.9
$A_{iso}$	+9.1	-9.1	+5.6	-5.6	+4.3	-4.3	+0.8	-0.8
$B_{11}$	-3.8	+3.8	-10.9	+10.9	+1.0	-1.0	-6.1	+6.1
$B_{22}$	-1.9	+1.9	+1.6	-1.6	-11.5	+11.5	-8.0	+8.0
$B_{33}$	+5.8	-5.8	+9.3	-9.3	+10.6	-10.6	+14.1	-14.1

TABLE VII.5. The Molecular Parameters of ClO<sub>2</sub>  
and ClOO

Radical	Matrix	$a_{p_x}^2$	$a_{p_y}^2$	$a_{p_z}^2$	$a_s^2$	$b_o^2$
ClO <sub>2</sub>	H <sub>2</sub> SO <sub>4</sub>	0.59	-	0.040	0.009	0.40
	KClO <sub>4</sub>	0.51	-	0.018	0.011	0.48
		$a_{p(11)}^2$	$a_{p(22)}^2$	$a_{p(33)}^2$		
ClOO (G)	KClO <sub>4</sub>	-	0.084	0.064	0.002	0.850

similar to that in  $\text{ClO}_2$  and  $\text{O}_3^-$ . In these isoelectronic  $\text{AO}_2$  radicals the g-factor that deviates the least from the free-spin value is oriented perpendicular to the molecular plane, whereas the maximum g-factor lies in the molecular plane parallel to the ligand O-O direction. Whilst we also expect  $g_{22}$  (2.0017) of  $\text{ClOO}$  to be perpendicular to the molecular plane and spatially coincident with  $a_{22}$ , the large spin-orbit coupling with chlorine ( $\lambda_{\text{Cl}} = 586 \text{ cm}^{-1}$  whilst  $\lambda_{\text{O}} = 151 \text{ cm}^{-1}$ ) will try to align the maximum g-value ( $g_{33}$ ) along the chlorine-central oxygen atom direction. Consequently,  $g_{33}$  will tend to lie somewhere between the Cl-O bond direction and the direction defined by the chlorine and outer oxygen atoms, and will make an angle  $\theta$  (estimated previously to be  $10-15^\circ$ ) with the  $a_{33}$  direction. The Third g-factor ( $g_{11}$ ) will be orthogonal to  $g_{22}$  and  $g_{33}$  making an angle  $\theta$  to  $a_{11}$  and should have a value intermediate between  $g_{33}$  and  $g_{22}$ . However, it is clear from Table VII.2 that  $g_{11}$  has a significant negative deviation from the free-spin value which might arise from undetectable chlorine 3d-orbital contributions to the molecular orbitals of the 'peroxy-chlorine' radical or through the magnetic coupling of the electron with suitable higher lying unoccupied orbitals (for example  $6a'$  in  $\text{C}_s$ -symmetry).

### 3. The Geometry of the ClOO Centre in KClO<sub>4</sub>

It is reasonable to assume that the ClOO molecule occupies an identical site to that of its isomeric precursor ClO<sub>2</sub>. Consequently, as the experimental data outlined in Section VII.1 suggest, the ClOO molecule lies in the ac-plane of the unit cell of KClO<sub>4</sub>. However, the Cl-O direction (axis a<sub>33</sub>) in ClOO is not coincident with either of the two Cl-O bonds in ClO<sub>2</sub>. Figure VII.18 shows the suggested orientation of a single ClOO molecule, with respect to the parent ClO<sub>2</sub> (shown dashed in the figure) in the KClO<sub>4</sub> lattice. The second magnetically distinct site is obtained by the rotation of the b-axis by  $\pm 55^\circ$ .

### 4. The Electronic Spectrum of ClOO

Morris and Johnston<sup>97</sup> have recently detected both ClO and ClOO in flash-photolysed chlorine-oxygen mixtures. The absorption maxima of ClO and ClOO occurred at 257.7 nm (38,800 cm<sup>-1</sup>) and 247.5 nm (40,400 cm<sup>-1</sup>) respectively. Therefore, the intense absorptions with maxima around 270 nm (37,000 cm<sup>-1</sup>) arising from the photolysis of ClO<sub>2</sub> in both KClO<sub>4</sub> and vitreous H<sub>2</sub>SO<sub>4</sub> may be superpositions of the optical absorptions of both ClO and ClOO. However, we have been unable to detect the former diatomic radical by ESR spectroscopy, even at temperatures as low as

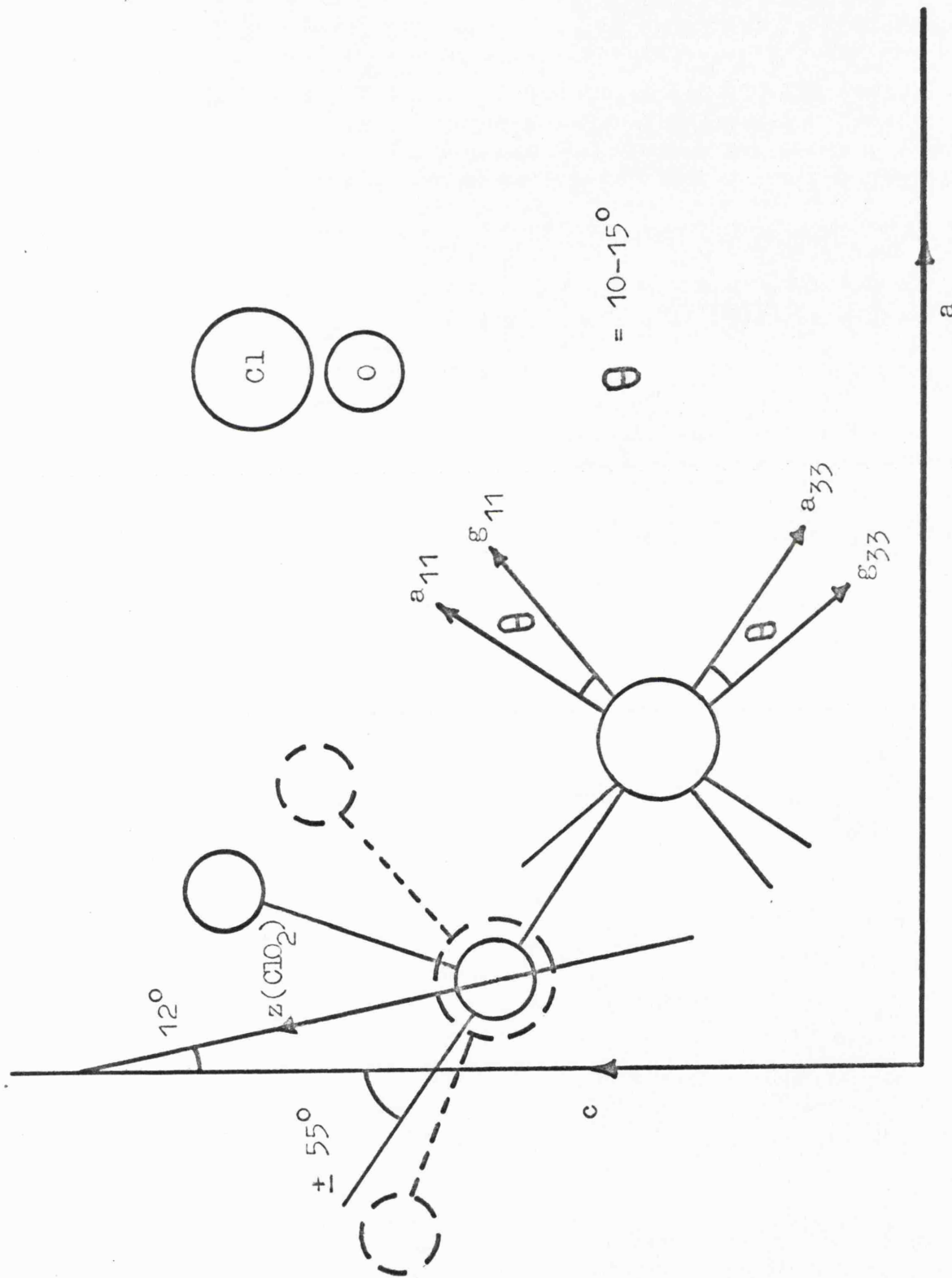


Figure VII.18. The relative orientations of ClO and the parent ClO<sub>2</sub> molecule (shown dashed) in the KClO<sub>4</sub> unit cell.

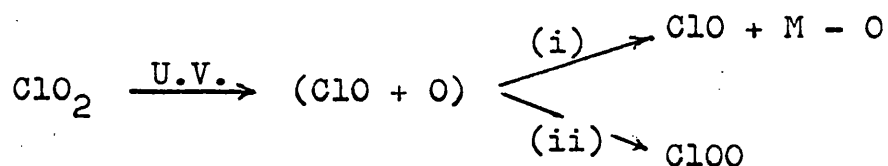
approximately 1.3°K, in either the acid or perchlorate matrices.

The  ${}^2A_2 \leftarrow {}^2B_1$  transitions of the radicals  $ClO_2$  and  $O_3^-$  occur at 370 nm ( $27,000\text{ cm}^{-1}$ ) and 430 nm ( $23,300\text{ cm}^{-1}$ ) respectively in  $KClO_4$ . We are tempted to suggest that the  $ClOO$  absorption at 280 nm ( $35,700\text{ cm}^{-1}$ ) in this matrix is the corresponding  ${}^2A'' \leftarrow {}^2A'$  transition in  $C_s$ -symmetry.

##### 5. The Isomerisation of Chlorine Dioxide

$ClO_2$  was photolytically converted to  $ClOO$  in vitreous sulphuric acid and approximately 50% of the original dioxide was regenerated when the matrix was melted. In  $KClO_4$  the isomerisation of chlorine dioxide resulted in an almost quantitative conversion to  $ClOO$ , whereas in  $KClO_3$  (see Chapter VI) photolysis resulted in the destruction of  $ClO_2$  with no apparent formation of  $ClOO$ . Thus, the photolytic decomposition products of  $ClO_2$  depend upon the environment, being different in  $KClO_3$ ,  $KClO_4$  and rigid sulphuric acid.

We propose the following mechanism for the process:



where (ClO + O) represents the initial products trapped in a cage in the matrix, (i) represents the interaction of the ejected oxygen atom with the matrix anion M, and (ii) is the intramolecular isomerisation to ClOO.

In sulphuric acid approximately 50% of the reaction proceeds via (i), M - O being the diamagnetic monoper-sulphuric acid, and the products are ClO and ClOO in roughly equal proportions. In KClO<sub>4</sub> (ii) is the principal reaction pathway, presumably because a reaction through step (i) would lead to the formation of unstable ClO<sub>5</sub><sup>-</sup> ions, which will not be favoured.

In contrast, the reaction



is expected to be favoured in KClO<sub>3</sub> so that the ejected oxygen atom is extracted from the cage before ClOO formation can take place. The ClO<sub>4</sub><sup>-</sup> ion has been detected previously as a stable radiolysis product of KClO<sub>3</sub>.<sup>76</sup>

#### ASPECTS OF RADIATION DAMAGE IN KClO<sub>4</sub>

The exposure of KClO<sub>4</sub> crystals to γ-rays at 77°K results in the formation of two inequivalent chlorine-containing centres. Morton<sup>59</sup> has ascribed these centres to trapped ClO<sub>4</sub> radicals, denoted by (I) and (II) in Table VII.1, which occupy two magnetically distinct sites

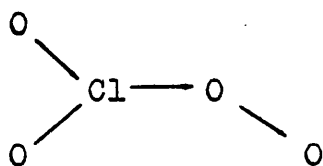
in the perchlorate lattice. The g- and A-tensors of radicals (I) and (II) are not similar and radical (II) was less stable than (I), decomposing when the matrix was annealed to 100°K. Whilst it is possible that the two radicals are ClO<sub>4</sub> occupying different lattice sites, experience suggests that the effect of the host lattice is not usually so pronounced as this. For example, the g- and A-tensors of ClO<sub>2</sub> in sulphuric acid, KClO<sub>3</sub> and KClO<sub>4</sub> are all very similar. Also, by analogy to the isoelectronic species PO<sub>4</sub><sup>2-</sup> and SO<sub>4</sub><sup>-</sup>, the observed spin-resonance parameters are rather surprising for a 31 valence-electron tetroxide. The magnetic properties of radicals (I) and (II) are given, together with those of PO<sub>4</sub><sup>2-</sup> and SO<sub>4</sub><sup>-</sup>, in Table VII.6. It can be seen that both the total 3s-character ( $a_s^2$ ) and the chlorine 3p/3s ratio of (I) and (II) are unexpectedly large, and that the g-tensors of these species are quite different from those of the other radicals. It was stated in Chapter V that the magnetic properties of radical (II) were remarkably similar to those we have previously assigned to ClO<sub>4</sub><sup>2-</sup>. The identity of radical (I) still poses a problem, since most of the 'normal' mono-chlorine species are known. One alternative that has recently been proposed is the peroxy-species: <sup>47</sup>

TABLE VII.6A. Electron Spin Parameters for Some XO<sub>4</sub> Radicals

Radical	Medium	Nucleus	g-tensor			Hyperfine tensor in gauss				Ref.	
			$g_{xx}$	$g_{yy}$	$g_{zz}$	$g_{av}$	$B_{xx}$	$B_{yy}$	$B_{zz}$		$A_{iso}$
PO <sub>4</sub> <sup>2-</sup>	Calcite	<sup>31</sup> P	2.0072	2.0033	2.0122	2.0076	-0.34	0.96	-0.49	19.1	65
SO <sub>4</sub> <sup>-</sup>	K <sub>2</sub> S <sub>2</sub> O <sub>8</sub>	<sup>33</sup> S	2.0047	2.0034	2.0142	2.0074	-	-	-	4	66
ClO <sub>4</sub> <sup>2-</sup>	BaSO <sub>4</sub>	<sup>35</sup> Cl	2.0020	2.0255	2.0325	2.0200	0	2.9	-2.9	74.6	102
ClO <sub>4</sub> (I)	KClO <sub>4</sub>	<sup>35</sup> Cl	2.0024	2.0548	2.0553	2.0375	0	0	0	57.2	59
ClO <sub>4</sub> (II)		<sup>35</sup> Cl	2.0050	2.0360	2.0380	2.0260	-5.3	-3.3	8.7	74.3	59

TABLE VII.6B. Molecular Parameters for Some XO<sub>4</sub> Radicals

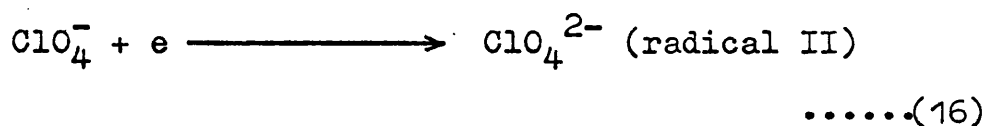
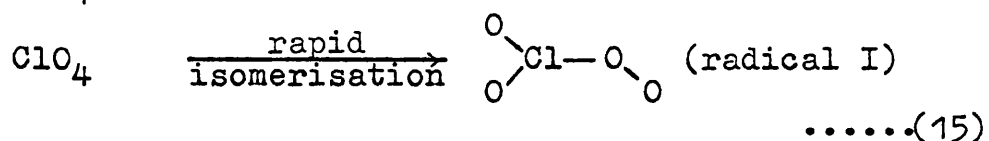
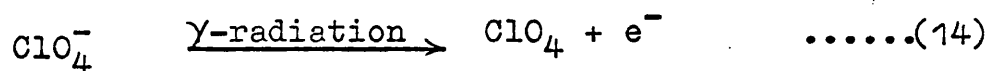
	$a_s^2$	$a_p^2$	$(a_p^2 + a_s^2)$	$a_p^2/a_s^2$
PO <sub>4</sub> <sup>2-</sup>	0.0053	0.004	0.009	0.76
SO <sub>4</sub> <sup>-</sup>	0.004	-	0.004	-
ClO <sub>4</sub> <sup>2-</sup>	0.04	0.03	0.07	1.5
		-0.06	-0.10	
ClO <sub>4</sub> (I)	0.034	-	0.034	-
ClO <sub>4</sub> (II)	0.044	0.09	0.134	2.0

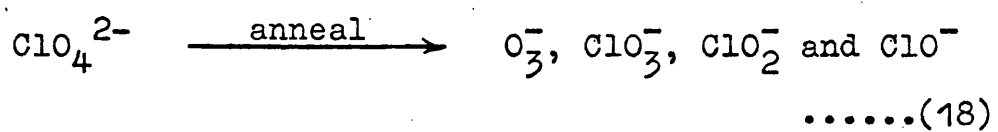
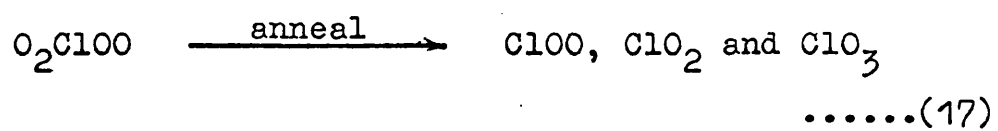


The orbital of the unpaired electron would be considerably delocalised onto the 'peroxy-oxygens', consequently the observed magnetic parameters would bear considerable resemblance to those of the  $\sigma$ -radical  $\text{ClO}_3$ .

$\gamma$ -irradiation of  $\text{KClO}_4$  at  $77^\circ\text{K}$  followed by careful annealing to room temperature showed that the subsequent decomposition products of (I) and (II) were  $\text{ClOO}$ ,  $\text{O}_3^-$  and  $\text{ClO}_3$ . At  $295^\circ\text{K}$  both  $\text{ClOO}$  and  $\text{ClO}_3$  decomposed to the relatively stable  $\text{ClO}_2$ . We conclude that  $\text{ClO}_2$  is not a precursor of  $\text{ClOO}$  in the radiolysis process, but, rather surprisingly, that the reverse is the case.

It is now possible to propose a tentative mechanism for the radiation damage of  $\text{KClO}_4$  based on these observations:





The stable products  $\text{ClO}_3^-$ ,  $\text{ClO}_2^-$ ,  $\text{ClO}^-$  and  $\text{O}_2$  have been detected by spectroscopic and chemical analyses.<sup>76</sup>

PART III

TRAPPED SILVER AND CADMIUM RADICALS IN GLASSY MATRICES

CHAPTER VIII

SECTION ATHE MATRIX ISOLATION OF SILVER AND CADMIUM SPECIES IN UNUSUAL VALENCY STATES

Trapped silver atoms have recently been identified in irradiated glasses containing silver ions.<sup>103</sup> This observation is of potential importance to both the radiation chemist and the glass technologist, and also suggests one important approach to probing environmental interactions. Silver atoms trapped in polar and non-polar media by the simultaneous condensation of silver and solvent vapour have magnetic properties which are very similar to those reported for the free atom.<sup>104</sup> In contrast, silver atoms formed by the irradiation of rigid solutions containing argentous ions have considerably modified properties. In general, the silver hyperfine coupling is reduced from the free atom value and there is a significant negative g-shift.<sup>103</sup> This difference has been explained in terms of the following model.<sup>105</sup> Silver atoms trapped from the gas phase simply occupy holes in the rigid solvent lattice. A small increase in the silver hyperfine coupling can then be attributed to the effects of Pauli exclusion forces upon the wavefunctions of the trapped atom (see Chapter III). On the other hand, a decrease in this hyperfine coupling must arise from the overriding

influence of van der Waals (dispersion) forces.<sup>31</sup> In solution silver ions strongly co-ordinate the solvent molecules which are expected to be held in place when the argentous solutions are frozen. The addition of an electron will not displace them to any great extent, so that the unpaired electron acts as a probe of the environment of the parent cation.

In this section evidence is presented for the formation of a number of paramagnetic silver species in  $\gamma$ -irradiated rigid solvents, particularly aqueous sulphuric acid. Where possible, their magnetic properties and structures are compared and contrasted with those of their isoelectronic cadmium-containing analogues.

#### EXPERIMENTAL PROCEDURE

##### 1. Sample Preparation

The silver and cadmium salts and the sulphuric acid were AnalaR grade and were used without further purification. Water was triply distilled from alkaline potassium permanganate and all organic solvents were dried over metallic sodium prior to their vacuum distillation.

Samples of  $^{109}\text{AgClO}_4$  were obtained by the evaporation of a solution of  $^{109}\text{Ag}$  foil (98%) in a 50/50 mixture of 100 vol.  $\text{H}_2\text{O}_2$  and concentrated  $\text{HClO}_4$ . Before irradiation all the solutions were degassed by pumping on the samples at

77°K, thawing, agitating and refreezing; this cycle being repeated at least four times. Samples for ESR measurements were prepared by freezing drops of these solutions to beads in liquid nitrogen. These beads were transferred at 77°K to suitable containers which were sealed and then exposed to  $\gamma$ -radiation doses ranging from 0.02 to 32 Mrads at this temperature. Samples suitable for ESR measurement at 8 mm wavelength were prepared by directly irradiating 0.2 ml aliquots of the frozen solutions in 5 cm quartz ESR tubes which had an approximate internal diameter of 0.15 cms. Optical absorption spectra were measured on  $\gamma$ -irradiated, degassed solutions in quartz cells with a (0.1 x 1.5 cm) cross-section.

## 2. Electron Spin Resonance Spectra

After irradiation the beads were either transferred, under liquid nitrogen and in the dark, to a sample tube which could be placed into a prepared ESR variable-temperature accessory, or into a quartz Dewar of liquid nitrogen which could be directly inserted into the spectrometer cavity. In variable-temperature experiments, ESR spectra were measured at 2 deg. K intervals as the samples were warmed to room temperature.

## 3. Electronic Spectra

The irradiated quartz sample cells were transferred,

in the dark and under liquid nitrogen, to a cell holder which in turn was inserted into the cooled compartment of the variable-temperature accessory described in detail in Chapter I. Considerable fracturing of the vitreous media often occurred when the samples were carefully warmed, resulting in a loss of optical transparency. To overcome this, samples were maintained at any one fixed temperature for at least 20 minutes before the measurement of spectra.

## EXPERIMENTAL RESULTS

### 1. Electron Spin Resonance Studies of Radiation Damage

#### a) Aqueous sulphuric acid

The exposure of frozen aqueous sulphuric acid to  $\gamma$ -rays at 77°K resulted in the formation of two detectable paramagnetic species (Figure VIII.1). The more abundant radical was characterised by a broad anisotropic absorption centred upon  $g = 2.0134$ , whilst the second radical was responsible for an isotropic doublet of 506 gauss centred close to the free-spin  $g$ -value. The polymeric nature of sulphuric acid glasses has prompted Russell<sup>106</sup> to identify the former radical as a hole-defect trapped at an acid polymer end-group and having the structure  $-(SO_3)_nOSO_2$ . (For convenience, we shall denote this matrix hole-centre by ' $SO_4^-$ ' in both Sections A and B of this Chapter).

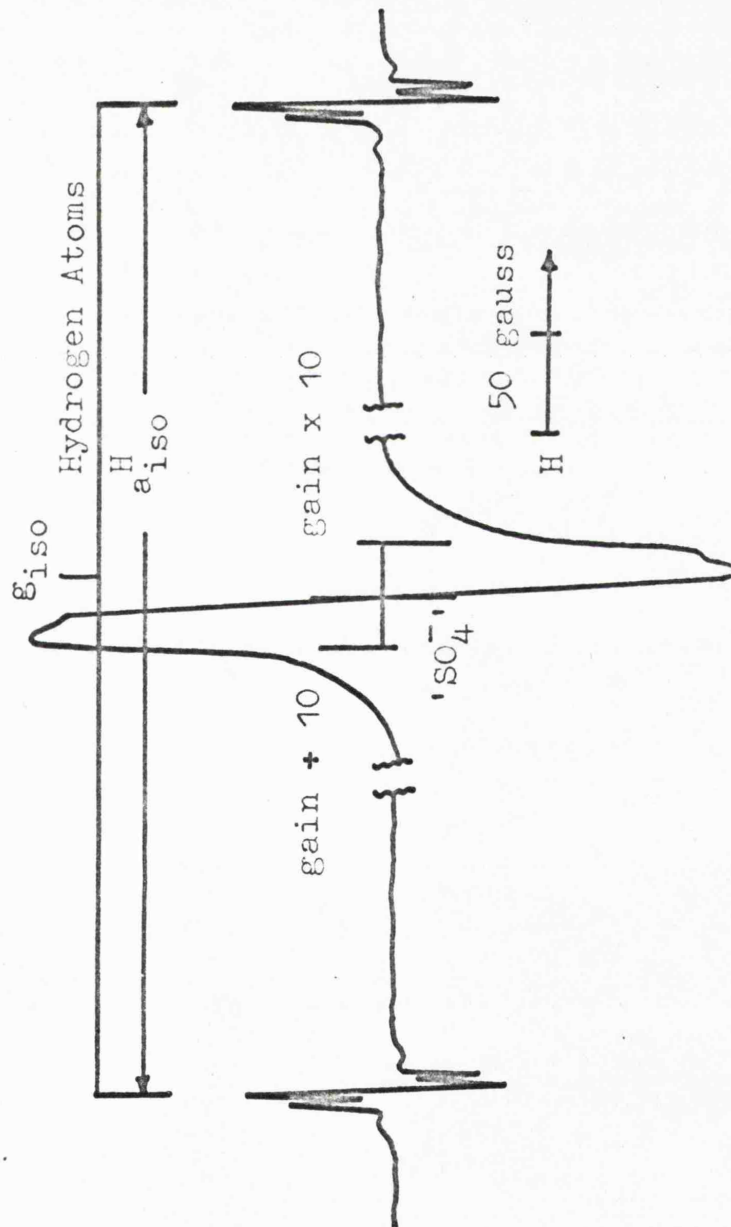


Figure VIII.1. ESR spectrum, measured at 77°K, of  $\gamma$ -irradiated frozen aqueous sulphuric acid.

Furthermore, Livingston et.al. have described the second centre as a hydrogen atom trapped in the glassy matrix.<sup>107</sup>

It is clear from Figure VIII.1 that each of the atomic hydrogen hyperfine lines was accompanied by a pair of satellite features, separated by approximately 12 gauss. The intensity of these satellites varied with respect to the main line as the inverse square of the applied magnetic field strength. As the microwave power was increased the main lines broadened, whereas both the intensity and resolution of the satellites increased. At approximately 50 mW a further set of satellite lines, separated by about 24 gauss, could be detected. (Figure VIII.2). These satellite features have been previously attributed to the concurrent spin-inversion of the electron and one or more protons at a distance of approximately  $1.8\text{\AA}$ .<sup>107,108</sup>

Low concentrations of ferrous ions ( $<0.05\text{ M}$ ) in the diluted acid suppressed the formation of the ' $\text{SO}_4^-$ ' hole-centre, whereas the yield of atomic hydrogen was apparently unaffected.

b)  $\text{Ag}_2\text{SO}_4$  in aqueous sulphuric acid

Figure VIII.3 shows ESR spectra, measured at  $77^\circ\text{K}$ , of  $\gamma$ -irradiated 5.0M aqueous  $\text{H}_2\text{SO}_4$  containing varying concentrations of  $\text{Ag}_2\text{SO}_4$ . Whilst the formation of the

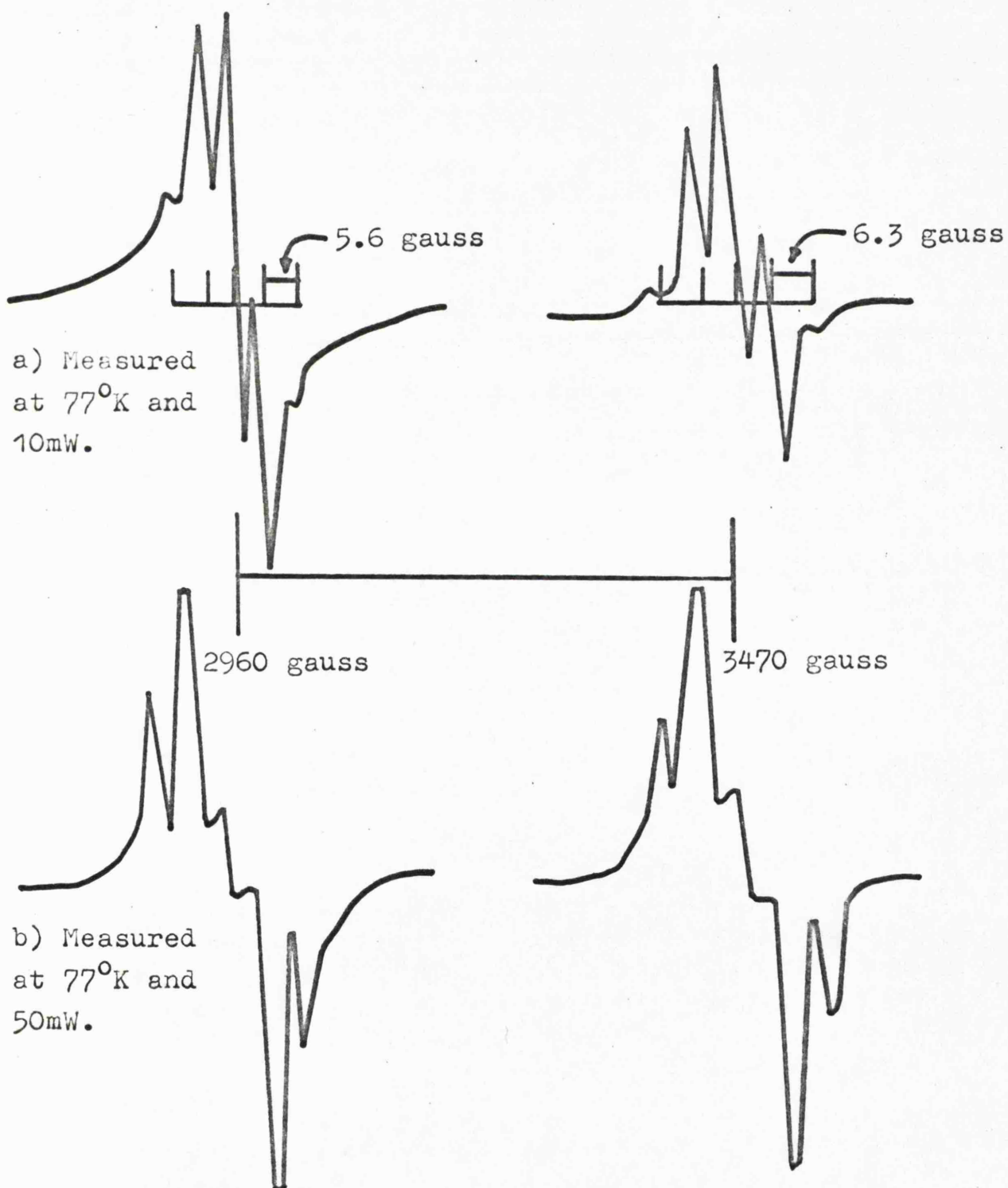


Figure VIII.2. The low-field and high-field features of hydrogen atoms trapped in frozen aqueous  $\text{H}_2\text{SO}_4$ .

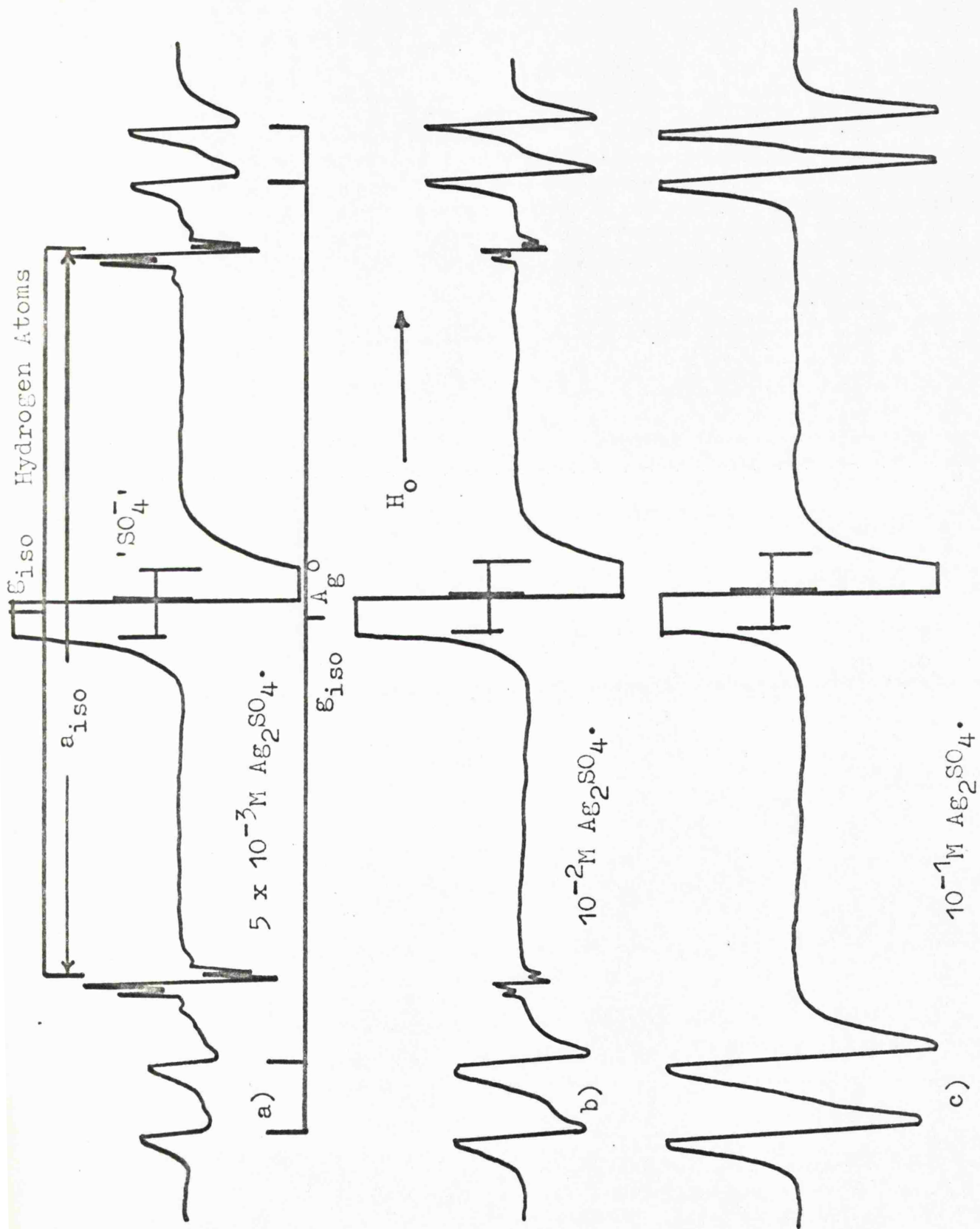


Figure VIII.3. ESR spectra, measured at 77°K, of irradiated 5.0 M aqueous  $\text{H}_2\text{SO}_4$  containing various concentrations of  $\text{Ag}_2\text{SO}_4$ .

sulphate hole-centre was unaffected by the increasing  $\text{Ag}^+$  ion concentration, the yield of trapped hydrogen atoms was suppressed by the presence of the transition metal ions in the glass.

The spectra consisted of a pair of broad doublets separated by approximately 680 gauss and these are thought to arise from aquated silver atoms.<sup>103</sup> (Naturally occurring silver has two magnetic isotopes:  $^{109}\text{Ag}$ ,  $I = \frac{1}{2}$ ,  $\gamma_N = -1.422 \times 10^{-4}$ , 48.1% abundance, and  $^{107}\text{Ag}$ ,  $I = \frac{1}{2}$ ,  $\gamma_N = -1.237 \times 10^{-4}$ , 51.9% abundance). These features were superimposed upon signals attributable to trapped hydrogen atoms and the ' $\text{SO}_4^-$ ' centre.

The ESR spectrum of a glassy sample of  $\gamma$ -irradiated 7.5 M aqueous  $\text{H}_2\text{SO}_4$  containing 0.1 M  $\text{Ag}_2\text{SO}_4$  is shown in Figure VIII.4. The increased acid concentration of the vitreous matrix clearly resulted in the formation of two new silver-containing centres at the expense of aquated silver atoms. The more abundant radical, labelled A in the Figure, gave rise to a pair of broad anisotropic doublets with a major splitting of 302 gauss and a subsidiary coupling of about 120 gauss. Superimposed upon the broad resonance from A were numerous, poorly resolved superhyperfine splittings. When the sulphuric acid concentration of the matrix was increased further, there was a

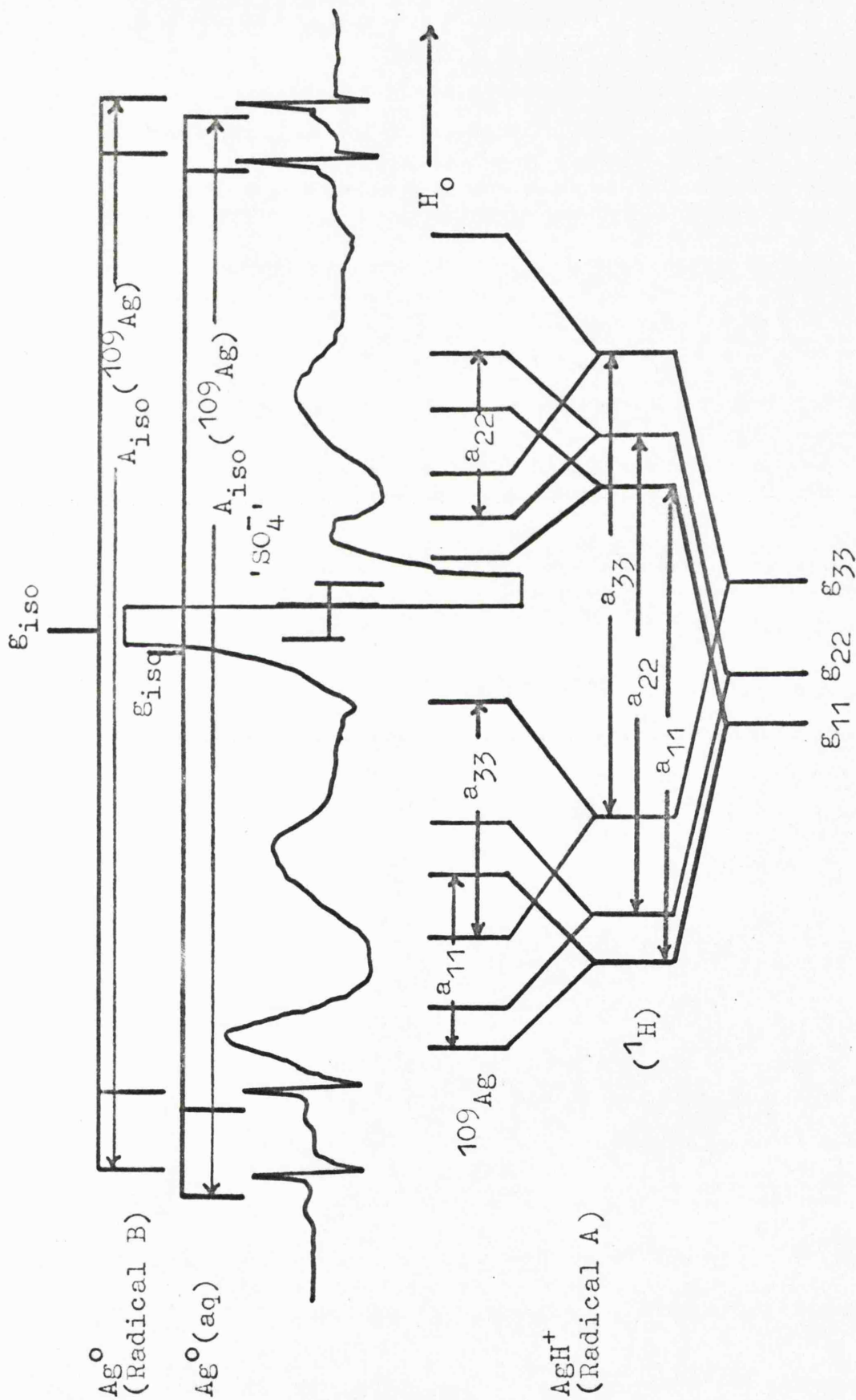


Figure VIII.4. ESR spectrum, measured at 77°K, of irradiated 0.1M  $Ag_2SO_4$  in 7.5M aqueous  $H_2SO_4$ .

concomitant increase in the concentration of A. However, in acid environments greater than 8.0 M no superhyperfine features could be detected in the ESR spectrum of this centre.

The second radical, B, was responsible for a remarkably narrow-lined doublet at both low-field and high-field separated by approximately 650 gauss. Each of the spin-resonance features from this centre was accompanied by a weak pair of satellite lines whose separation varied with the applied magnetic field and whose intensity, with respect to the main lines, increased as the microwave power increased (see Figure VIII.5) ESR signals from B could not be detected in environments having acid concentrations greater than 8.0 M or less than 7.0 M. Warming the irradiated sample to 100°K resulted in a loss of signals from B and an increase in the concentration of aquated silver atoms. There was also a marked reduction in the ESR linewidth of A and an increase in the resolution of the superhyperfine splittings associated with this centre. (Figure VIII.6.

When the experiment was repeated using 0.1 M  $\text{Ag}_2\text{SO}_4$  dissolved in 7.5 M  $\text{D}_2\text{SO}_4$  in  $\text{D}_2\text{O}$ , there was a noticeable linewidth reduction in the ESR spectra of both aquated silver atoms and radical B. In this matrix the broad

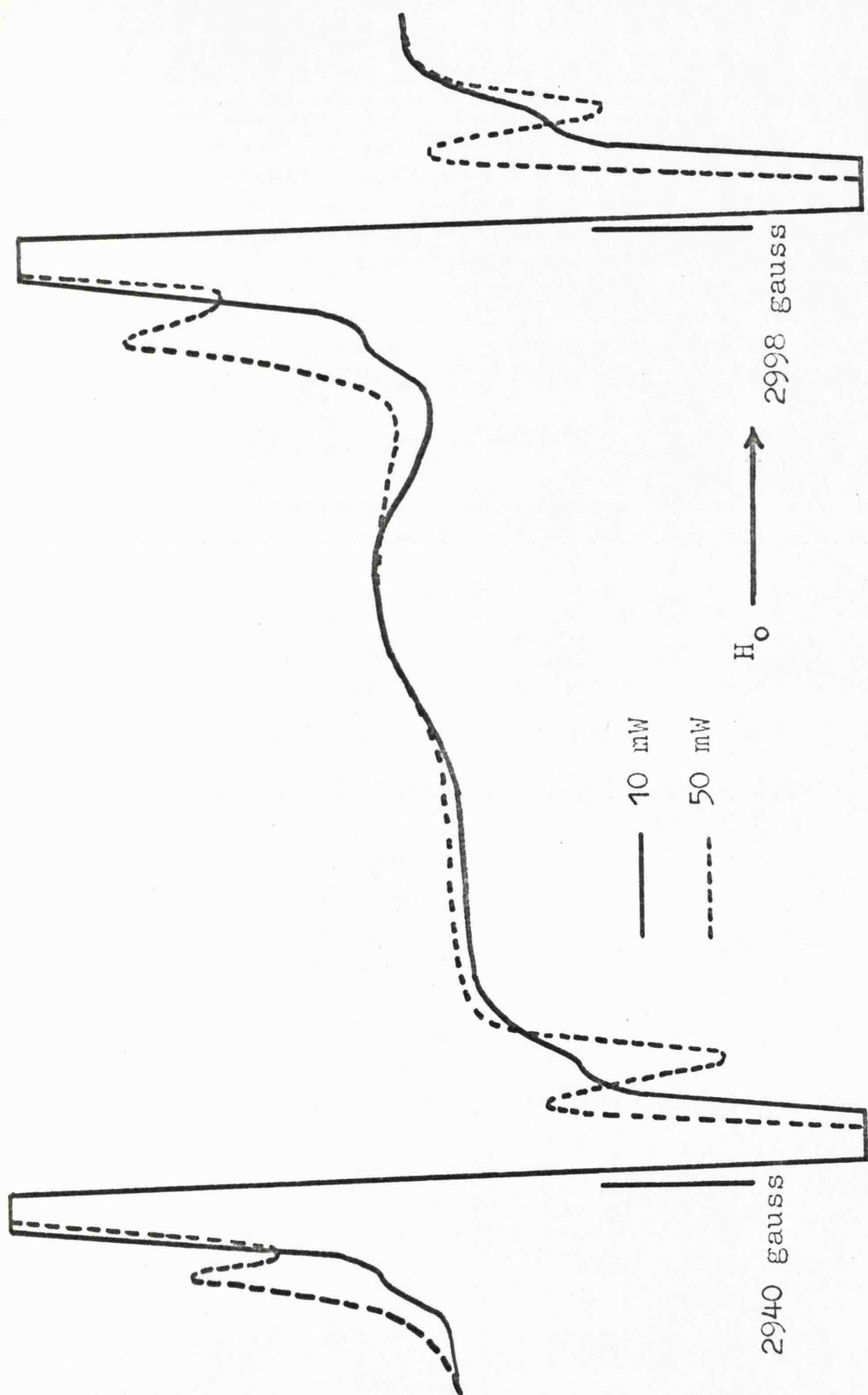


Figure VIII.5. The effect of increasing microwave power on the satellite lines accompanying the  $\Delta M_I = 0$  transitions of trapped silver atoms (Radical B) in 7.5 M aqueous  $H_2SO_4$ .

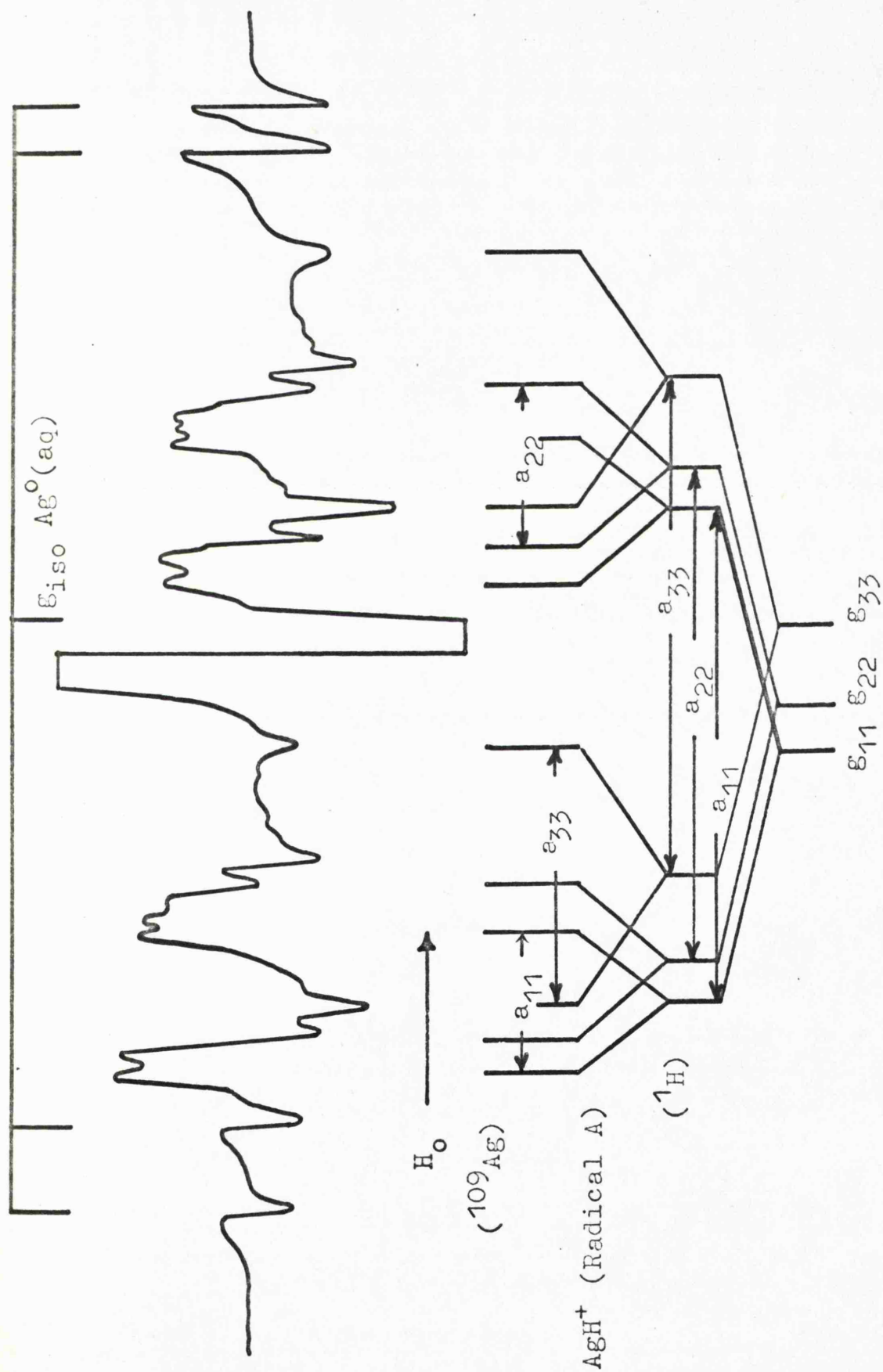


Figure VIII.6. ESR spectrum, measured at 100°K, of irradiated 0.1 M  $\text{Ag}_2\text{SO}_4$  in 7.5 M aqueous  $\text{H}_2\text{SO}_4$ .

quartet of features associated with A collapsed to give what appeared to be a pair of triplets spread over approximately 220 gauss. However, considerable overlapping between features from A and the broad resonance arising from the 'sulphate' hole-centre occurred in the central region of the spectrum, making an unambiguous analysis impossible.

To facilitate the analysis of the complex X-band ESR spectra, supplementary measurements were made at Q- and S-band frequencies, and the experiments were repeated using silver salts enriched with the  $^{109}\text{Ag}$  isotope.

c)  $\text{CdSO}_4$  in aqueous  $\text{H}_2\text{SO}_4$

The ESR spectra of  $\gamma$ -irradiated frozen  $\text{CdSO}_4$  solutions in aqueous  $\text{H}_2\text{SO}_4$  were characterised by an intense axially symmetric resonance centred upon  $g \cong 1.99$  and a corresponding broader and weaker feature close to  $H_0 = 5100$  gauss. These features were superimposed upon signals from the matrix hole-centre and trapped hydrogen atoms. The cadmium-containing radical giving rise to these features is labelled C in Figure VIII.7. Again the presence of impurity metal ions in the vitreous aqueous acid did not inhibit the formation of the ' $\text{SO}_4^-$ ' centre, although the yield of hydrogen atoms was significantly reduced. Radical C was the only paramagnetic cadmium species

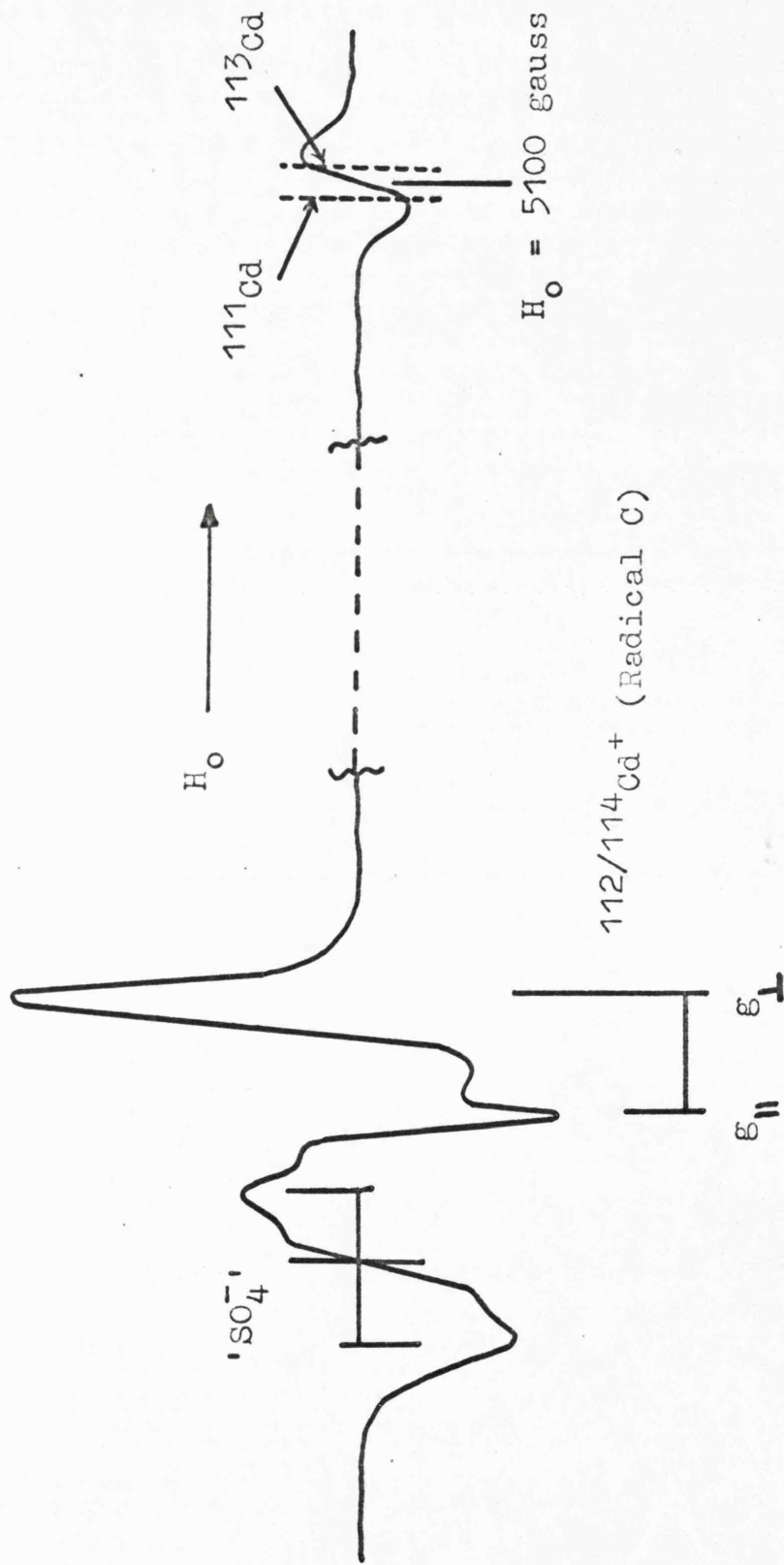


Figure VIII.7. ESR spectrum, measured at 77°K, of irradiated 0.1 M CdSO<sub>4</sub> in aqueous H<sub>2</sub>SO<sub>4</sub>.

detected in acid environments ranging from 4.5 M to 18 M. When  $\text{Cd}^{2+}$  ions were introduced into the aqueous acid as  $\text{Cd}(\text{NO}_3)_2$ ,  $\gamma$ -irradiation yielded the ' $\text{SO}_4^-$ ',  $\text{NO}_3$  and  $\text{NO}_2$  radicals. The presence of nitrate in the matrix inhibited the formation of radical C.

d)  $\text{AgClO}_4$  in  $\text{CH}_3\text{OH}$  and  $\text{CH}_3\text{CH}_2\text{OH}$

When a frozen solution of silver perchlorate in methanol was exposed to  $\gamma$ -rays the paramagnetic products of radiation damage, stabilised at  $77^\circ\text{K}$ , were solvated silver atoms<sup>103</sup> and the  $\text{CH}_2\text{OH}$  and  $\text{CHO}$  matrix radicals<sup>109</sup> (Figure VIII.8). Warming the sample to  $100^\circ\text{K}$  resulted in a marked reduction in the intensity of features from the  $\text{CH}_2\text{OH}$  radical with the simultaneous formation of a new paramagnetic species, D. Radical D was characterised by a broad intense doublet ( $\Delta H_{\text{MS}} \cong 30$  gauss) of approximately 120 gauss (Figure VIII.9a). When the experiment was repeated using  $\text{CD}_3\text{OD}$ , the ESR spectrum at  $100^\circ\text{K}$  was essentially identical to that in methanol, except that there was a small linewidth reduction.

A species, E, giving rise to an axially symmetric doublet centred close to the free-spin g-value, was formed when a solution of  $\text{AgClO}_4$  in ethanol was irradiated at  $77^\circ\text{K}$  and subsequently annealed to  $100^\circ\text{K}$ . (Figure VIII.9b).

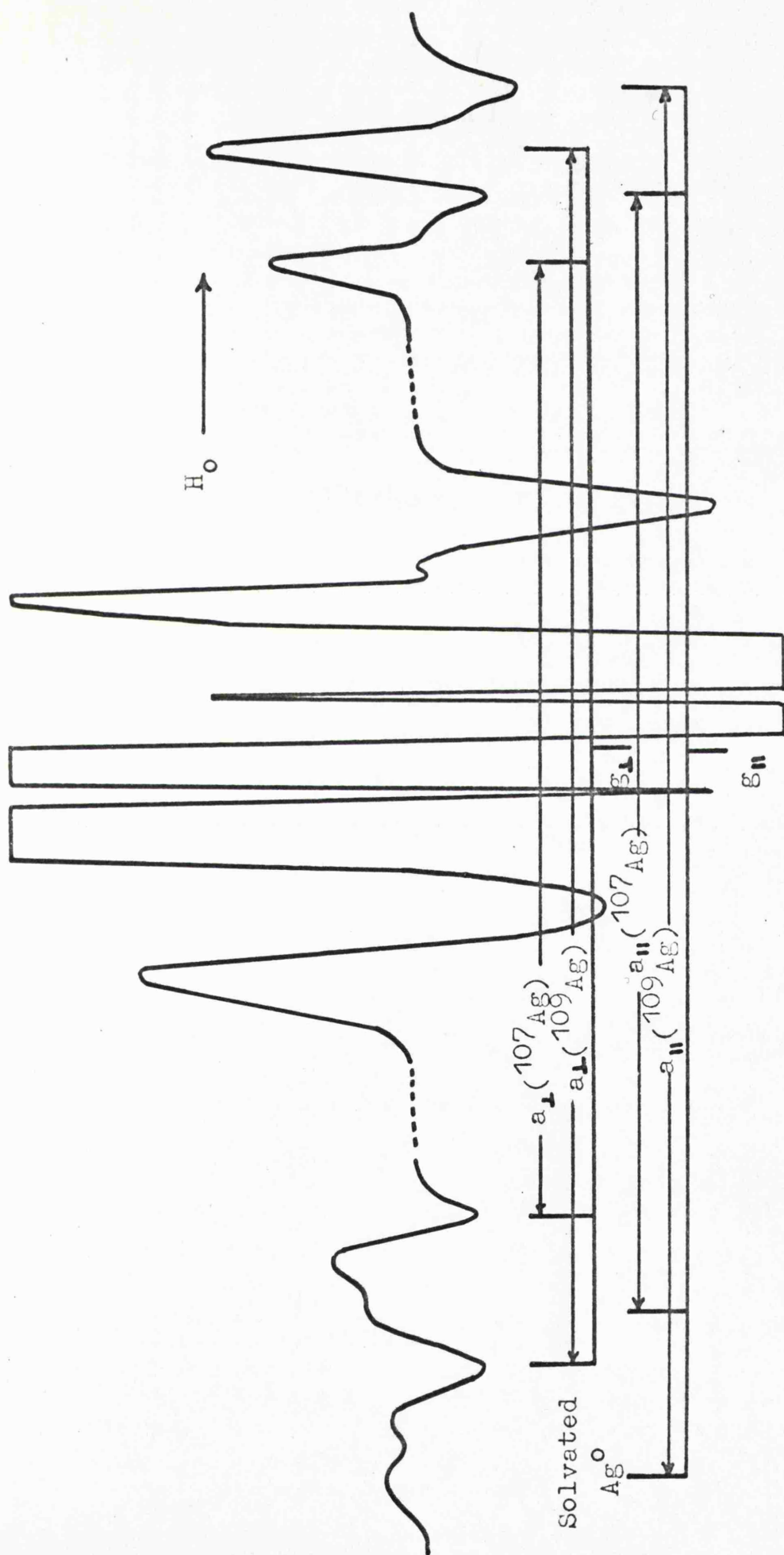


Figure VIII.8. ESR spectrum, measured at  $77^\circ \text{K}$ , of irradiated  $0.1 \text{ M AgClO}_4$  in methanol.

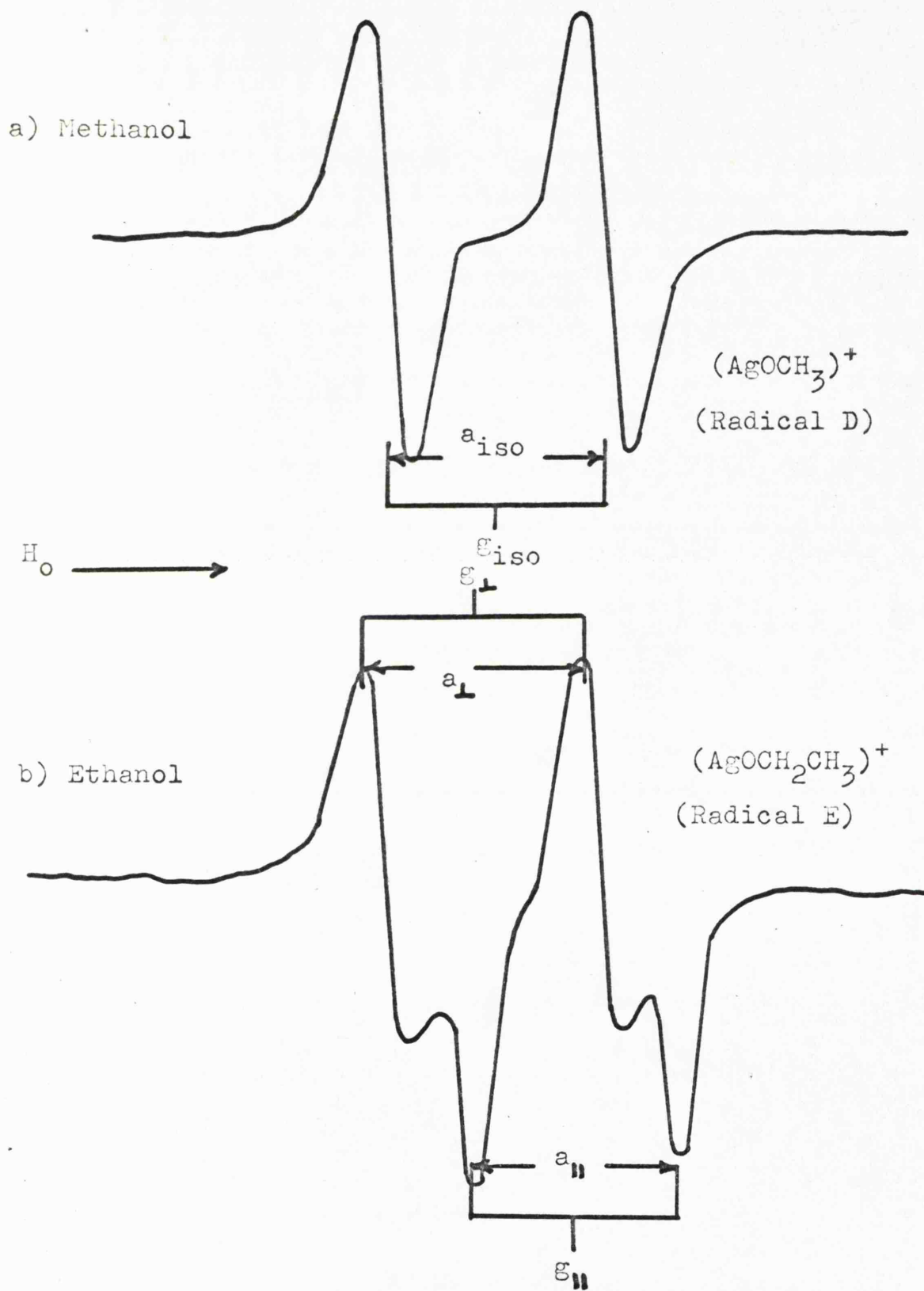


Figure VIII.9. ESR spectra, measured at 100°K, of AgClO<sub>4</sub> in alcoholic matrices.

e) Cd(ClO<sub>4</sub>)<sub>2</sub> in CH<sub>3</sub>OH and CH<sub>3</sub>CH<sub>2</sub>OH

Figure VIII.10 shows the ESR spectra of  $\gamma$ -irradiated frozen solutions of cadmium perchlorate in methanol and ethanol. The paramagnetic products of radiation damage were CH<sub>2</sub>OH and CHO from methanol, <sup>109</sup>CH<sub>3</sub>CHOH from ethanol, and a species, F, which was present in both matrices and whose spin-resonance parameters closely resemble those of C in aqueous H<sub>2</sub>SO<sub>4</sub>. (A relatively narrow absorption centred on  $g \approx 1.99$  and a corresponding broader and weaker feature at approximately  $H_0 = 5100$  gauss). Annealing the alcoholic matrices to 100°K did not generate cadmium species corresponding to the silver-containing radicals D and E. 110

## 2. Electronic Spectra of the Products of Radiation

### Damage

#### a) Aqueous sulphuric acid

The optical absorption spectrum, measured at 77°K of a de-aerated and  $\gamma$ -irradiated H<sub>2</sub>SO<sub>4</sub> glass is shown in Figure VIII.11. The very weak absorption at  $\sim 600$  nm (17,000 cm<sup>-1</sup>), characteristic of irradiated quartz, dominated the spectrum of an empty cell which had been exposed to  $\gamma$ -rays at 77°K. The absorption with a maximum intensity at 444 nm (22,500 cm<sup>-1</sup>) has been previously assigned to the 'sulphate' hole-centre ( $\epsilon = 3000 \pm 400$ ).<sup>111</sup>

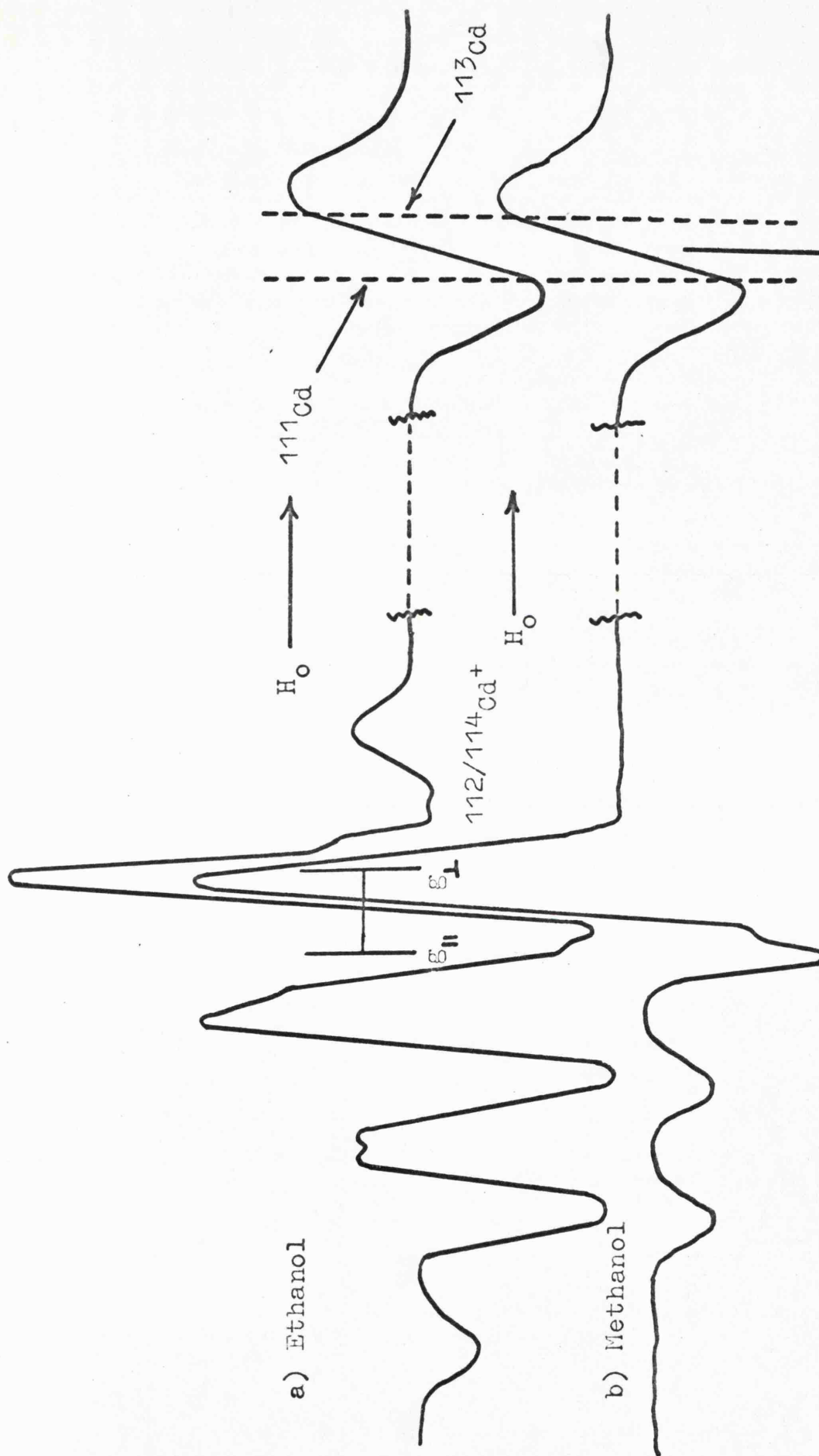


Figure VIII.10. ESR spectra, measured at  $77^\circ\text{K}$ , of irradiated  $0.1\text{ M Cd}(\text{ClO}_4)_2$  in alcoholic matrices.  $H_0 = 5100\text{ Gauss}$

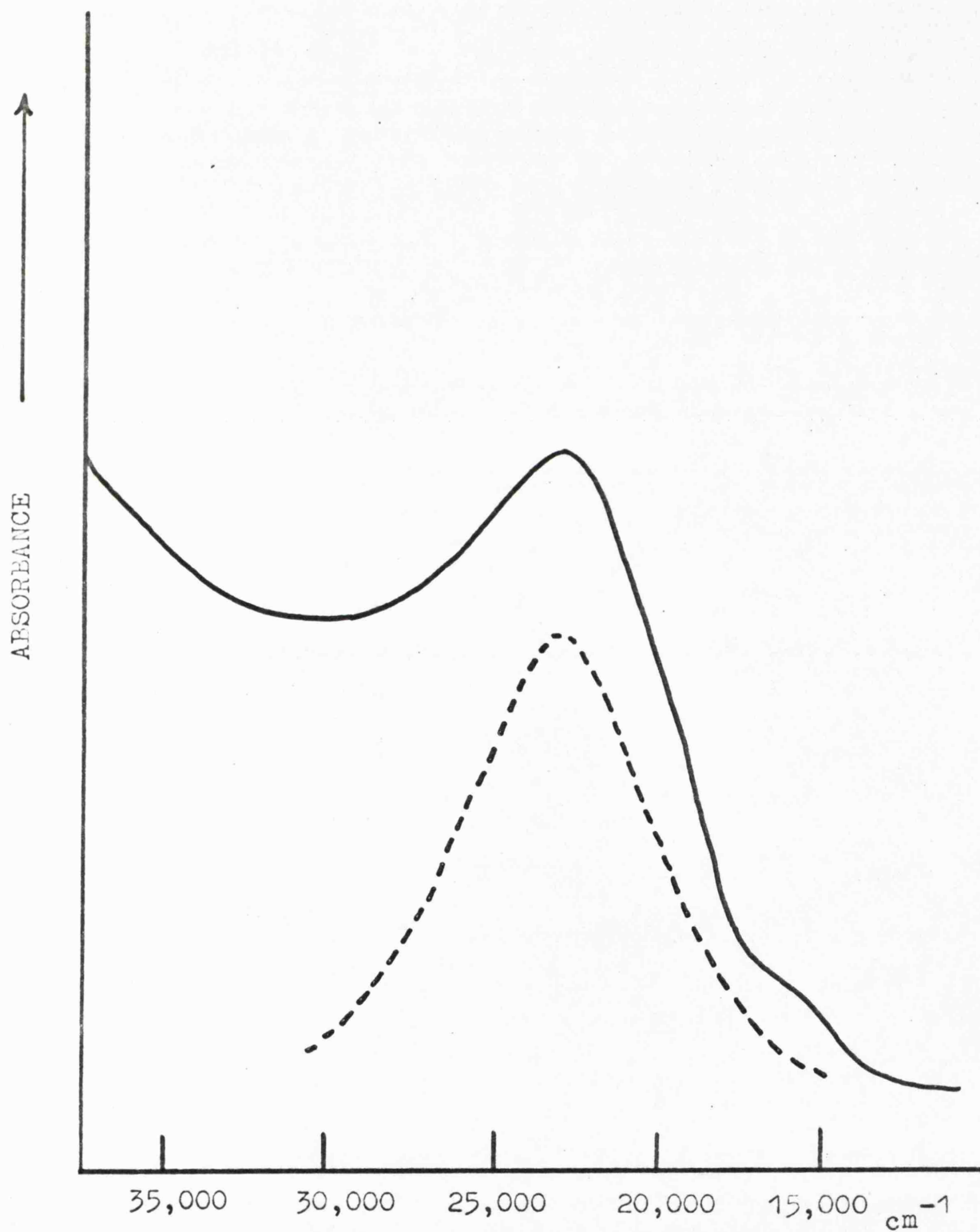


Figure VIII.11. Electronic spectrum, measured at 77°K, of irradiated 5.0 M aqueous H<sub>2</sub>SO<sub>4</sub>.

This absorption could be photobleached with an unfiltered tungsten lamp, or thermally annihilated at 150°K.

All subsequent optical absorption spectra of  $\gamma$ -irradiated samples of  $H_2SO_4$  containing impurity ions were measured against a 'blank' of the irradiated pure acid.

b)  $Ag_2SO_4$  in aqueous  $H_2SO_4$

Figure VIII.12 shows optical absorption spectra, measured at 77°K, of 0.05 M  $Ag_2SO_4$  in varying concentrations of  $\gamma$ -irradiated frozen aqueous sulphuric acid. As the concentration of the acid was increased absorption I having a maximum intensity at 345 nm ( $29,000\text{ cm}^{-1}$ ) was reduced in intensity, whilst the amplitude of absorption II ( $\lambda_{\text{max}} = 290\text{ nm}; 34,500\text{ cm}^{-1}$ ) was increased. From a comparison with the temperature profile of the ESR signals arising from the radiation products of  $Ag_2SO_4$  in aqueous  $H_2SO_4$ , we are tempted to assign absorption I to aquated silver atoms and absorption II to radical A. Radical B was formed in very low yields and consequently it is unlikely that we would be able to detect it by optical spectroscopy.

c)  $CdSO_4$  in  $H_2SO_4$

The optical absorption spectrum of  $\gamma$ -irradiated 0.05 M  $CdSO_4$  in 7.5 M aqueous  $H_2SO_4$  is shown in Figure VIII.13. The intense asymmetric absorption which developed on irradiation has a maximum at 290 nm ( $34,500\text{ cm}^{-1}$ ) and

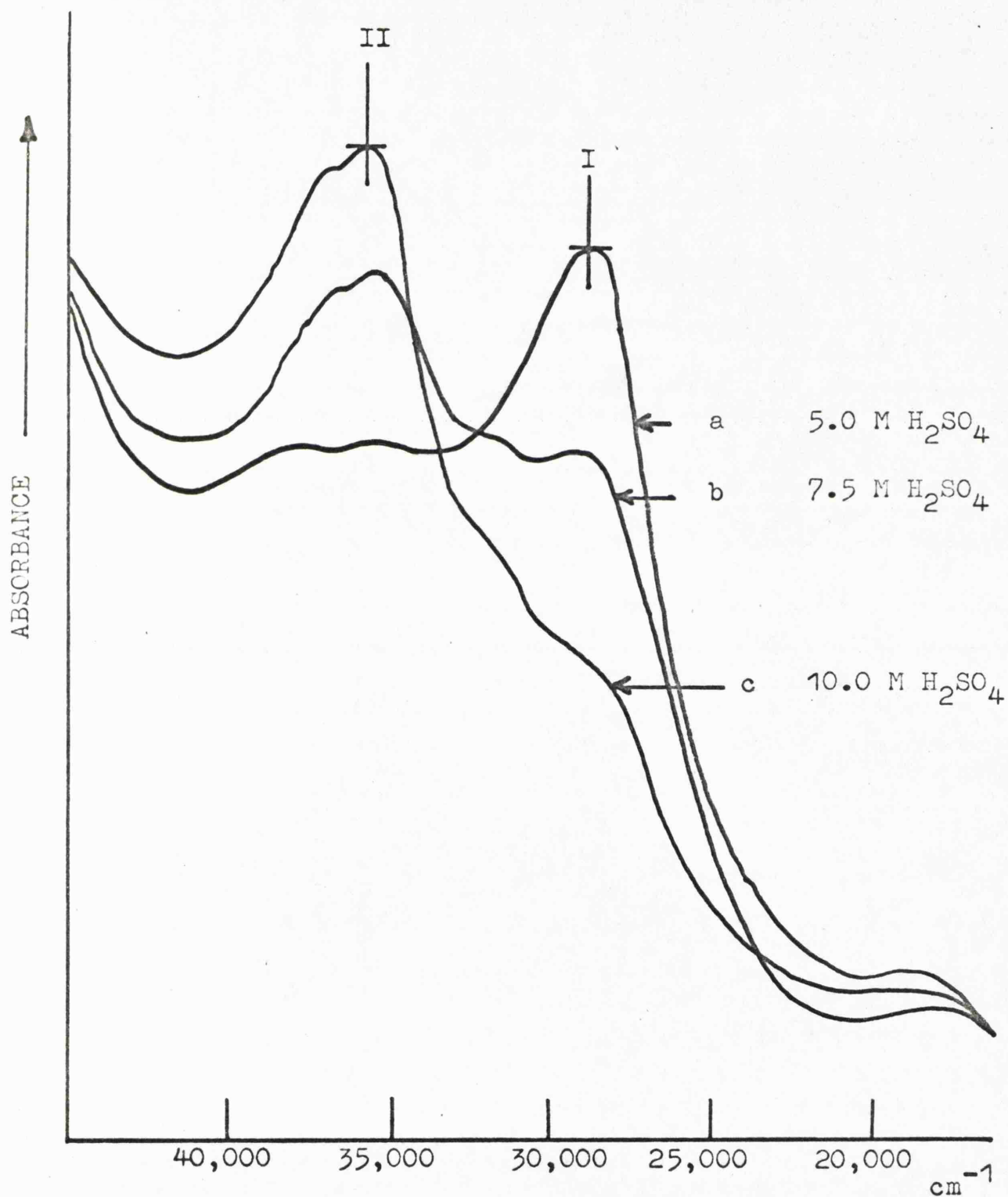


Figure VIII.12. Electronic spectra, measured at  $77^\circ\text{K}$ , of irradiated samples of  $0.05\text{ M Ag}_2\text{SO}_4$  in various concentrations of aqueous  $\text{H}_2\text{SO}_4$ .

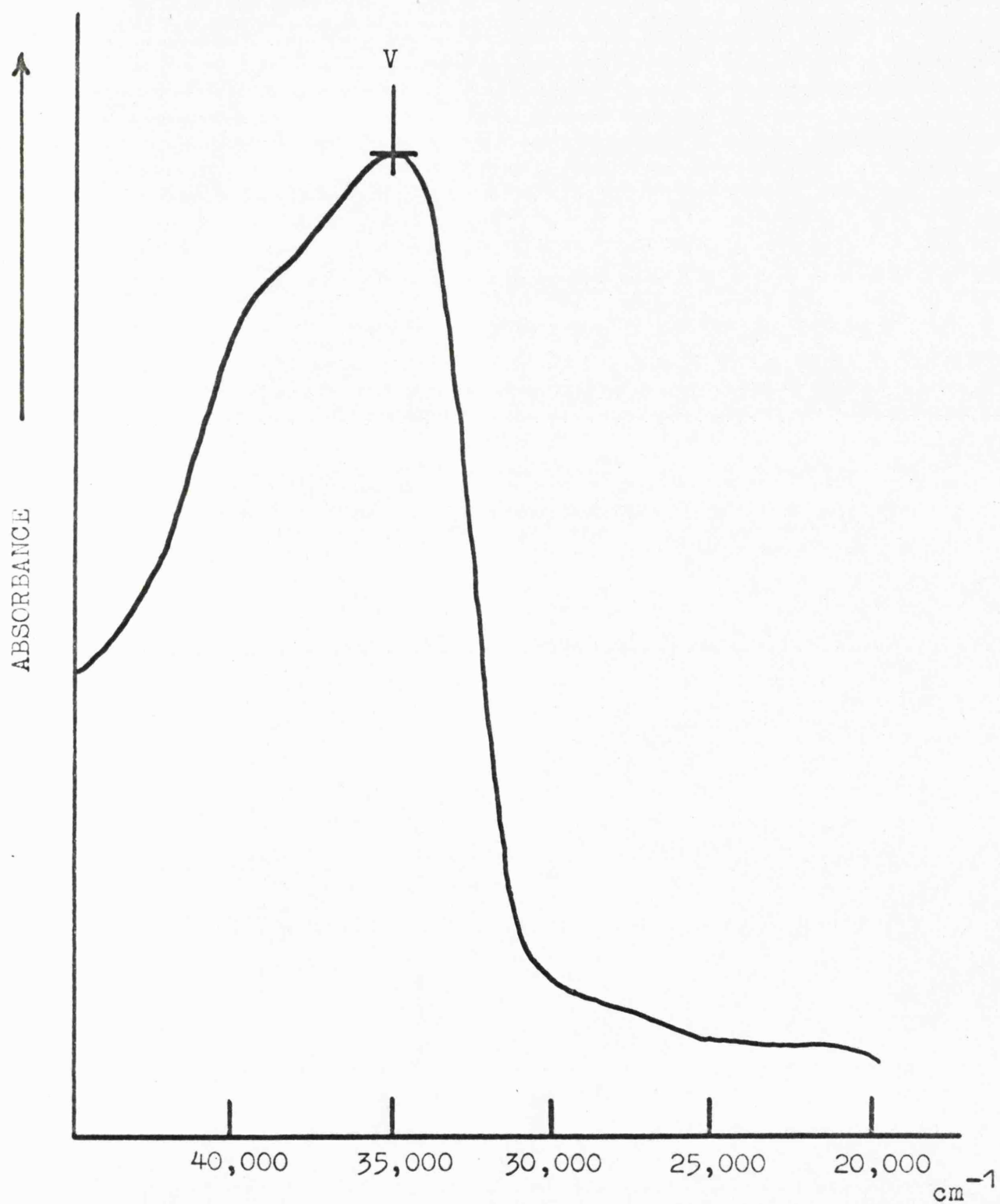


Figure VIII.13. Electronic spectrum, measured at 77°K, of 0.05 M CdSO<sub>4</sub> in 7.5 M aqueous H<sub>2</sub>SO<sub>4</sub>.

is ascribed to radical C.

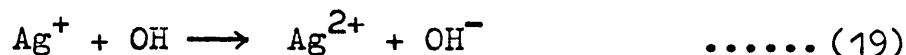
## DISCUSSION

### 1. The Identification of the Radiation Damage Centres in Alcoholic and Aqueous Acid Glasses containing Silver and Cadmium Ions.

#### a) Aquated silver atoms

Aquated silver atoms have been studied extensively in sulphuric acid environments. However, it is still difficult to reconcile the ESR results of Shields<sup>103</sup> with the optical absorption data published by Dainton and coworkers.<sup>111</sup>

Three transient species, giving rise to optical bands at 310 nm (32,300 cm<sup>-1</sup>), 270 nm (37,000 cm<sup>-1</sup>), and 360 nm (27,800 cm<sup>-1</sup>) have been detected in the pulse radiolysis of aqueous solutions containing argentous ions. The absorption of highest energy has been ascribed to argentic ions formed from the reaction:



whilst the peak at 310 nm (32,300 cm<sup>-1</sup>) has been associated with the  $5^2\text{P}_{\frac{1}{2}}$  or  $\frac{3}{2} \longleftarrow 5^2\text{S}_{\frac{1}{2}}$  transitions of silver atoms. The species giving rise to the remaining absorption at 360 nm (27,800 cm<sup>-1</sup>) remained unidentified.

Brown and Dainton<sup>111</sup> spectroscopically monitored the radiation-colouring of silver-containing vitreous 5.6 M sulphuric acid glasses at low temperatures. At 77°K the spectrum of the radiolysed glass was dominated by a strong absorption ( $\lambda_{\max} = 350 \text{ nm}; 28,600 \text{ cm}^{-1}$ ) which had a weaker shoulder at 313 nm ( $31,900 \text{ cm}^{-1}$ ). This band was suppressed by electron scavengers such as  $\text{N}_2\text{O}$  and  $\text{Fe}^{3+}$ . By analogy with the pulse radiolysis results, these authors assigned the 313 nm ( $31,900 \text{ cm}^{-1}$ ) absorption to trapped silver atoms and the lower energy band to a paramagnetic aggregated silver species, which they denoted by  $\text{Ag}^0(\text{Ag}^+)_n$ . Warming of the glass led to the decay of the 350 nm ( $28,600 \text{ cm}^{-1}$ ) band, whilst both the 313 nm ( $31,900 \text{ cm}^{-1}$ ) absorption and a new band, assigned to  $\text{Ag}^{2+}$  ions, at 275 nm ( $36,400 \text{ cm}^{-1}$ ) increased in intensity. However, the ESR spectrum of an irradiated 5.0 M sulphuric acid glass containing silver ions (Figure VIII.3c) is dominated by signals assigned to aquated silver atoms; these have the same temperature profile as the 350 nm ( $28,600 \text{ cm}^{-1}$ ) optical absorption (peak I in Figure VIII.12). Consequently, we have reassigned this band to aquated silver atoms and consider that the absorptions at 313 nm ( $31,900 \text{ cm}^{-1}$ ) and 275 nm ( $36,400 \text{ cm}^{-1}$ ) arise from  $\text{Ag}_2^+$  and argentic ions respectively. (These

species are discussed in detail in Section VIII B.)

b) Radical A

As the strength of the aqueous sulphuric acid environment was increased, the intensity of both the ESR features from aquated silver atoms and the 350 nm ( $28,600 \text{ cm}^{-1}$ ) optical absorption band decreased. In contrast, both the concentration of radical A and the intensity of the 290 nm ( $34,500 \text{ cm}^{-1}$ ) absorption were greater (Figure VIII.12). For the following reasons we have identified A as the  $\text{AgH}^+$  radical-ion.

i) It is reasonable to assume that the magnetic nucleus giving rise to the major isotropic doublet splitting in the ESR spectrum of this centre is  $^1\text{H}$  (Figure VIII.6) since in frozen  $\text{D}_2\text{SO}_4$  solution this principal doublet splitting collapsed to a triplet of approximately 45 gauss separation.

ii) Radical A contains a single silver atom. The use of isotopically enriched  $^{109}\text{Ag}_2\text{SO}_4$  resulted in a reduction in the ESR linewidth and a marked increase in spectral resolution. The spin-resonance data included in Table VIII.1 for this centre were derived from a spectrum of  $\gamma$ -irradiated 0.1 M  $^{109}\text{Ag}_2\text{SO}_4$  in 7.5 M aqueous  $\text{H}_2\text{SO}_4$  at  $100^\circ\text{K}$  (Figure VIII.14)

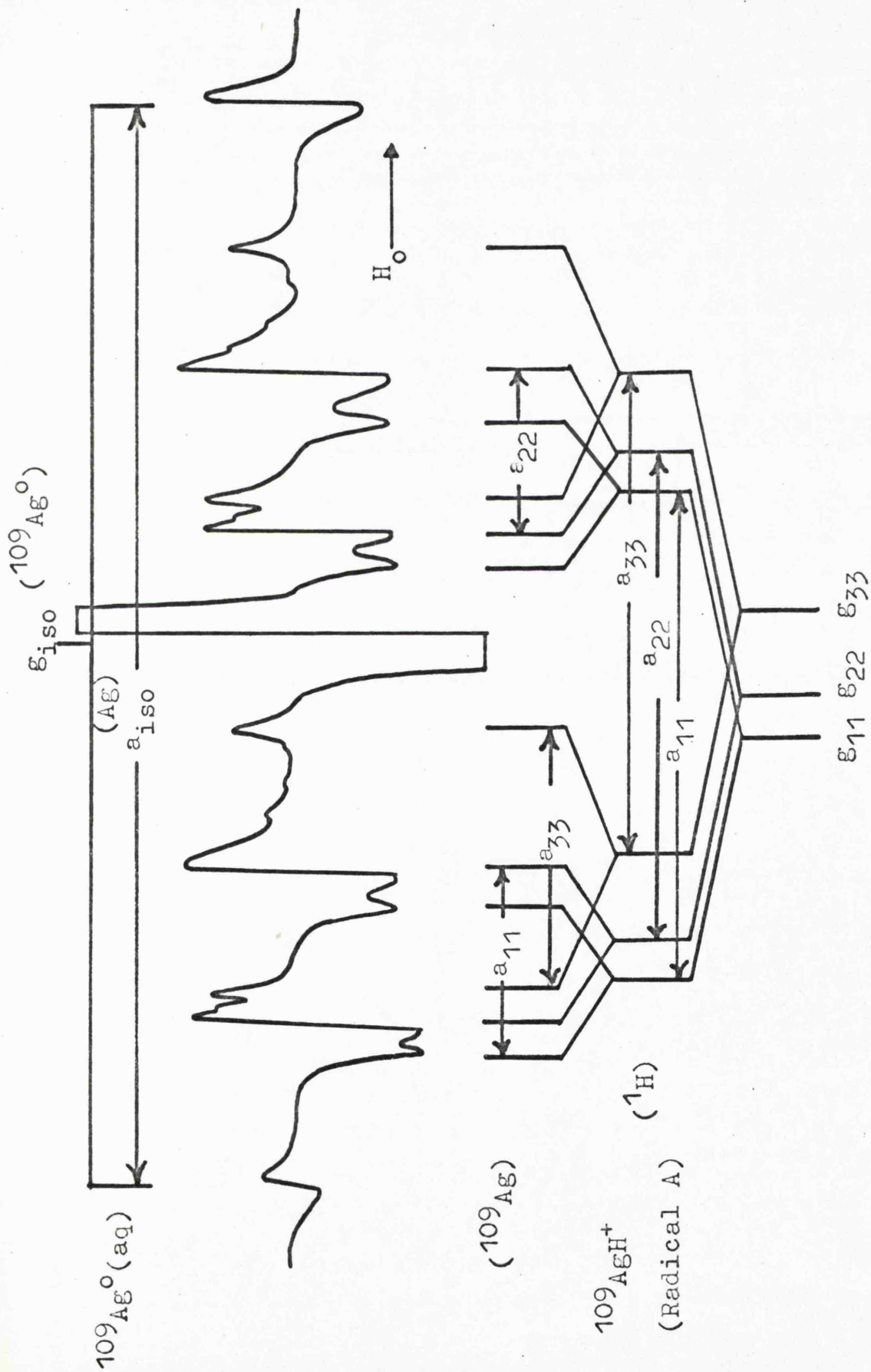


Figure VIII.14. ESR spectrum, measured at 100°K, of irradiated 0.1M  $^{109}\text{Ag}_2\text{SO}_4$  in 7.5 M aqueous  $\text{H}_2\text{SO}_4$ . 242

TABLE VIII.1. Electron Spin Resonance Data for the AgH<sup>+</sup> Ion and Related Species.

Radical	Nucleus	g-tensor (a)			Hyperfine coupling (a) in gauss				
		$g_{xx}$	$g_{yy}$	$g_{zz}$	$g_{av}$	$B_{xx}$	$B_{yy}$	$B_{zz}$	$A_{iso}$
(AGH) <sup>+</sup> (A)	<sup>109</sup> Ag	2.046	2.036	2.002	2.028	+12.8	+11.6	-24.4	-103.6
	<sup>1</sup> H					- 1.3	+ 0.7	+ 0.7	+302.3
Ag(aq)	<sup>109</sup> Ag				2.000				-702
(AG <sub>3</sub> CH <sub>3</sub> ) <sup>+</sup> (D)	<sup>109</sup> Ag				2.004				-120
(AG <sub>2</sub> CH <sub>2</sub> CH <sub>3</sub> ) <sup>+</sup> (E)	<sup>109</sup> Ag	2.000	2.000	2.004	2.002				-130

a. Derived from the Breit-Rabi equation.<sup>58</sup>

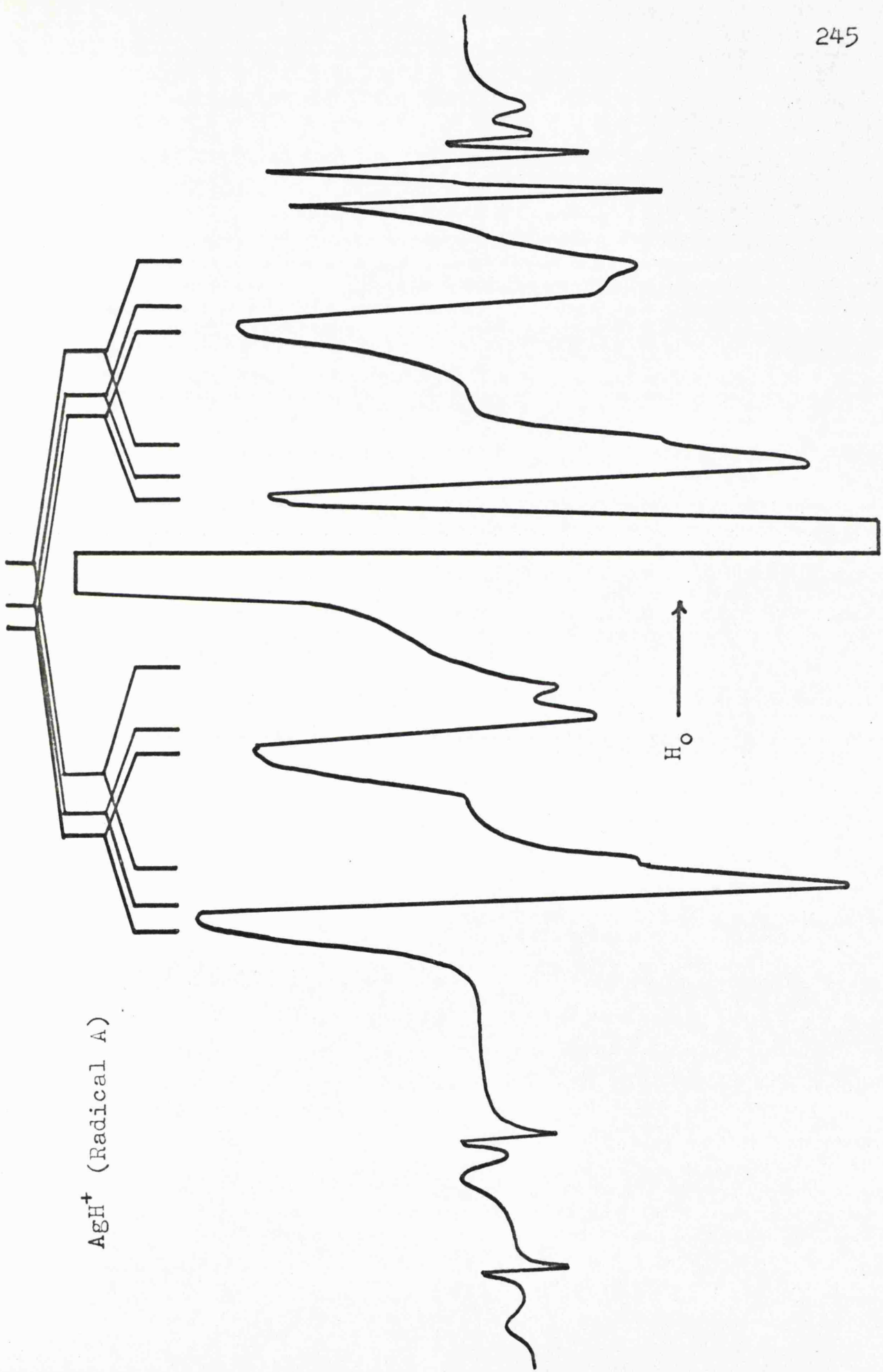
VIII.15 ). Confirmation of this analysis was obtained from the S-band spectrum shown in Figure VIII.15.

c) Radical B

The remaining detectable paramagnetic species (Radical B) present in an irradiated sample of 7.5 M  $\text{H}_2\text{SO}_4$  containing  $\text{Ag}^+$  ions gave rise to a pair of ESR doublets separated by approximately 650 gauss and centred on  $g = 1.9995$ . We are tempted to identify B as a matrix-isolated silver atom whose properties are only slightly modified by the acid environment. We base this conclusion on the following factors.

i) The remarkably small ESR linewidth of B ( $\Delta H_{\text{MS}} = 3.5$  gauss), compared to other silver containing radicals in this medium, reflects the complete absence of hyperfine and super-hyperfine interactions between the unpaired electron of this radical and the protons in the ligands and the matrix.

ii) Radiation-produced hydrogen atoms are thought to be trapped at interstitial sites in the glassy acid matrix<sup>112</sup> and consequently the nearest neighbouring proton, which can undergo nuclear spin-inversion, lies at a distance of not less than  $1.8\text{\AA}$ .<sup>108</sup> We have



AgH<sup>+</sup> (Radical A)

H<sub>2</sub>O →

Figure VIII.15. ESR spectrum, measured at 77°K and 3.1 Gc/s, of irradiated Ag<sub>2</sub>SO<sub>4</sub> in 7.5 N aqueous H<sub>2</sub>SO<sub>4</sub>.

detected analogous sympathetic proton spin-inversions for B, which would seem to suggest that this radical and hydrogen atoms occupy magnetically equivalent trapping sites in the rigid sulphuric acid.

iii) ESR signals from B were only detectable in environments having acid concentrations within the range 7.0 - 8.0 M. This peculiar sensitivity to the acid strength of the medium suggests that the structure of the glass is a controlling factor in the formation and stabilisation of B. Shields<sup>103</sup> has recently detected aquated silver atoms trapped in a variety of magnetically distinct sites in frozen solutions of  $\text{AgNO}_3$ . When the vitreous matrices were annealed the ESR spectrum was simplified as a small proportion of  $\text{Ag}^\circ$ , situated in slightly different crystal fields, was annihilated. Here also the structure of the matrix clearly controlled the nature and stability of the radiation-produced silver radicals.

We cannot completely rule out the possibility that B is a silver complex of the form  $\text{L} - \text{Ag}^\circ - \text{L}$ . The most

obvious possibility is the di-sulphato complex  $\text{Ag}^0(\text{SO}_4^{2-})_2$ , where the absence of protons in the ligand ions may account for the very narrow ESR lines of B. However, it is difficult to understand why the formation of this complex only occurs for sulphuric acid concentrations closely approaching 7.5 M. The concentration of  $\text{SO}_4^{2-}$  in aqueous  $\text{H}_2\text{SO}_4$ , albeit small, is almost independent of the acid strength within the range 4.0 - 10.0 M.<sup>113</sup>

d) Radical C

The pulse radiolysis of aqueous solutions containing  $\text{Cd}^{2+}$  ions gives rise to a transient absorption at about 300 nm ( $33,300 \text{ cm}^{-1}$ ) which grows simultaneously with the decay of the absorption of the solvated electron.<sup>114</sup> For this reason this band has been identified as the charge-transfer absorption of aquated  $\text{Cd}^+$  ions. The UV spectrum of an irradiated 5.0 M aqueous sulphuric acid glass containing 0.1 M  $\text{CdSO}_4$  was dominated by an intense asymmetric absorption with a maximum intensity at 290 nm ( $34,500 \text{ cm}^{-1}$ ) and a weaker shoulder at 250 nm ( $40,000 \text{ cm}^{-1}$ ). This absorption was suppressed by the addition of electron scavengers such as nitrate.

Figure VIII.7 shows the ESR spectrum at 77°K, of  $\gamma$ -irradiated 0.1 M  $\text{CdSO}_4$  in frozen 5.0 M aqueous  $\text{H}_2\text{SO}_4$ . This spectrum is dominated by an intense axially symmetric

absorption centred at low  $g$  and ascribed to radical C. The addition of suitable electron scavengers such as  $\text{NO}_3^-$  to the solutions prior to irradiation suppressed the formation of this centre. Its  $g$ -factors ( $g_{11} = g_{22} = 1.994$ ,  $g_{33} = 2.001$ ) are typical of an electron-excess centre and are in accord with the electron occupying an almost pure  $s$ -orbital. Therefore, we assign this ESR absorption and the optical band at 290 nm ( $34,500 \text{ cm}^{-1}$ ) to aquated  $\text{Cd}^+$  ions.

There are two magnetic isotopes of cadmium in natural abundance,  $^{111}\text{Cd}$  ( $I = \frac{1}{2}$ ,  $\gamma_N = -6.483 \times 10^{-4}$ , 12.86%) and  $^{113}\text{Cd}$  ( $I = \frac{1}{2}$ ,  $\gamma_N = -6.782 \times 10^{-4}$ , 12.34%), both of which have nuclear magnetic moments more than five times those of the  $^{109}\text{Ag}$  and  $^{107}\text{Ag}$  isotopes. Since the  $5s$ -orbital of  $\text{Cd}^+$  should be more confined than in  $\text{Ag}^0$  the hyperfine splittings expected for these isotopes are close to 5000 gauss (14.0 Gc/s), which are in fact larger than the microwave frequency of the ESR spectrometer (9.3 Gc/s). Figure VIII.16 shows the variation in the energy levels of the  $^{111}\text{Cd}^+$  or  $^{113}\text{Cd}^+$  ions with the applied magnetic field  $H_0$ . (Since  $S = I = \frac{1}{2}$ ,  $F = 1, 0$  and  $M_F = \pm 1, 0$ ). It is clear that, when the isotropic hyperfine splitting ( $A$ ) is greater than the frequency of the exciting incident radiation, only the transition

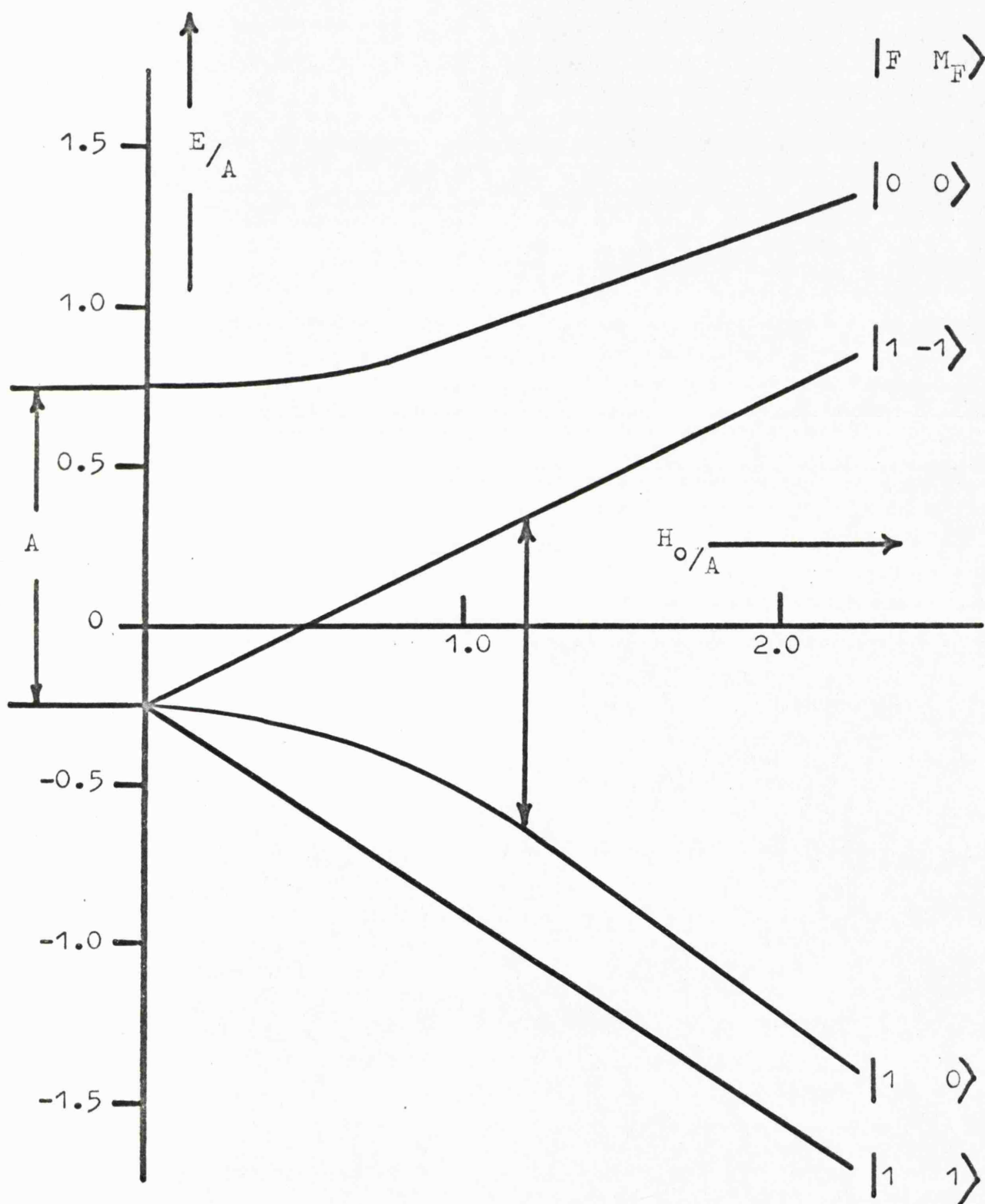


Figure VIII.16. The variation in orbital energy levels for a species with electron spin  $S = \frac{1}{2}$  and  $I = \frac{1}{2}$  in an applied magnetic field  $H_0$ .

$|F = 1, M_F = 0\rangle \longleftrightarrow |F = 1, M_F = -1\rangle$  can occur. This gives rise to the high-field component of the cadmium doublet. Therefore, we assign the very weak resonance at  $H_0 \cong 5000$  gauss in Figure VIII.7 to the overlapping high-field transitions of  $^{111}\text{Cd}^+$  and  $^{113}\text{Cd}^+$ . When the present investigation was complete Kasai<sup>27</sup> reported the matrix isolation of  $\text{Cd}^+$  ions in argon at  $4.2^\circ\text{K}$ . He detected a well-resolved doublet at  $H_0 \cong 5000$  gauss which he also assigned to the high-field transitions of the  $^{111}\text{Cd}^+$  and  $^{113}\text{Cd}^+$  cations.

Unlike argentous salts in this medium, the nature of the radiolysis products of cadmium salts in aqueous  $\text{H}_2\text{SO}_4$  were independent of the acid concentration.

e) Radical D

Radical D, formed when irradiated samples of argentous salts in methanol were annealed to  $100^\circ\text{K}$ , is almost certainly  $(\text{AgOCH}_3)^+$ . We base this conclusion on the following factors.

i) This radical was not formed when irradiated pure methanol was warmed to  $100^\circ\text{K}$ .

ii) No major proton hyperfine couplings were detected for this species. The ESR spectrum of D was unaffected, except for a small reduction in the linewidth, when studied in a  $\text{CD}_3\text{OD}$  matrix.

iii) The intensity of the ESR spectrum of this radical increased with the simultaneous loss of signals from the  $\text{CH}_2\text{OH}$  matrix radical.

f) Radical E

By analogous arguments to those outlined above for  $(\text{AgOCH}_3)^+$ , the axially symmetric spectrum, which was produced when a frozen solution of  $\text{AgClO}_4$  in  $\text{CH}_3\text{CH}_2\text{OH}$  was irradiated at  $77^\circ\text{K}$  and subsequently annealed, is ascribed to the corresponding species  $(\text{AgOCH}_2\text{CH}_3)^+$ .

g) Radical F

The principal products arising from the  $\gamma$ -irradiation of pure methanol and ethanol glasses at  $77^\circ\text{K}$  are  $\text{CH}_2\text{OH}$ ,  $\text{CH}_3\text{CHOH}$  and trapped electrons. The addition of  $\text{Cd}^{2+}$  ions to these glasses before irradiation suppressed electron trapping and resulted in the formation of a cadmium containing species, F. Radical F can be identified as a solvated  $\text{Cd}^+$  cation by a comparison of the spin-resonance parameters of this centre with those of  $\text{Cd}^+$  in aqueous  $\text{H}_2\text{SO}_4$  (Table VIII.2).

2. The Structure of the Radiation Damage Centres in Alcoholic and Aqueous Glasses containing Silver and Cadmium Ions

a) Aquated Silver Atoms

The  $\text{Ag}^0$  complex in aqueous  $\text{H}_2\text{SO}_4$  is characterised

TABLE VIII.2. Electron Spin Resonance Parameters  
for the Cd<sup>+</sup> Ion in a Variety of  
Matrices

Matrix	Hyperfine <sup>a</sup> tensor in gauss	g-tensor <sup>a</sup>			Ref.
		$g_{  }$	$g_{\perp}$	$g_{av}$	
Metaphosphate glass			$g_{iso} = 1.992$	119	
Argon	<sup>111</sup> Cd = -5137				
	<sup>113</sup> Cd = -5374		$g_{iso} = 2.0006$	27	
H <sub>2</sub> SO <sub>4</sub> (C)	$a_{iso} \cong -5250$	2.001	1.9940	1.9960	b
HClO <sub>4</sub>	$a_{iso} \cong -5190$		$g_{iso} = 1.9954$		b
CH <sub>3</sub> CH <sub>2</sub> OH (F)	$a_{iso} \cong -5100$	1.9924	1.9896	1.9905	b
CH <sub>3</sub> OH (F)	$a_{iso} \cong -5100$	1.9926	1.9895	1.9905	b

a. Derived using the Breit-Rabi equation <sup>58</sup>

b. This work

by a significant negative g-shift and a small delocalisation of electron density onto the ligands (~2%). If we assume that the silver atom is octahedrally co-ordinated in this solvent, then the vacant and higher-lying 5p-atomic orbitals of silver must be admixed into the  $\bar{a}_{1g}$  ground state to explain the form of the experimental g-tensor. In  $O_h$ -symmetry, the 5p-atomic orbitals which compose the  $\bar{t}_{1u}$ -molecular orbitals of the complex are degenerate and consequently an admixture of these orbitals into the ground state, by configurational interaction, will constitute the precondition of a Jahn-Teller distortion. The experimental results are most readily accounted for if we assume that the complex distorts to  $D_{4h}$ -symmetry (Figure VIII.17) by an extension along one polar axis.

It appears therefore, that it is necessary to invoke a small admixture of the antibonding  $a_{2u}$ -orbital into the  $\bar{a}_{1g}$  ground state of the complex, although we were unable to detect anisotropic hyperfine interactions in the ESR spectrum of this centre.

b) The  $AgH^+$  Radical-Cation

Table VIII.1 lists the spin-resonance data for the  $AgH^+$  radical in an aqueous sulphuric acid matrix. These results are most readily interpreted if we assume that the anisotropic contribution to the silver hyperfine coupling arises

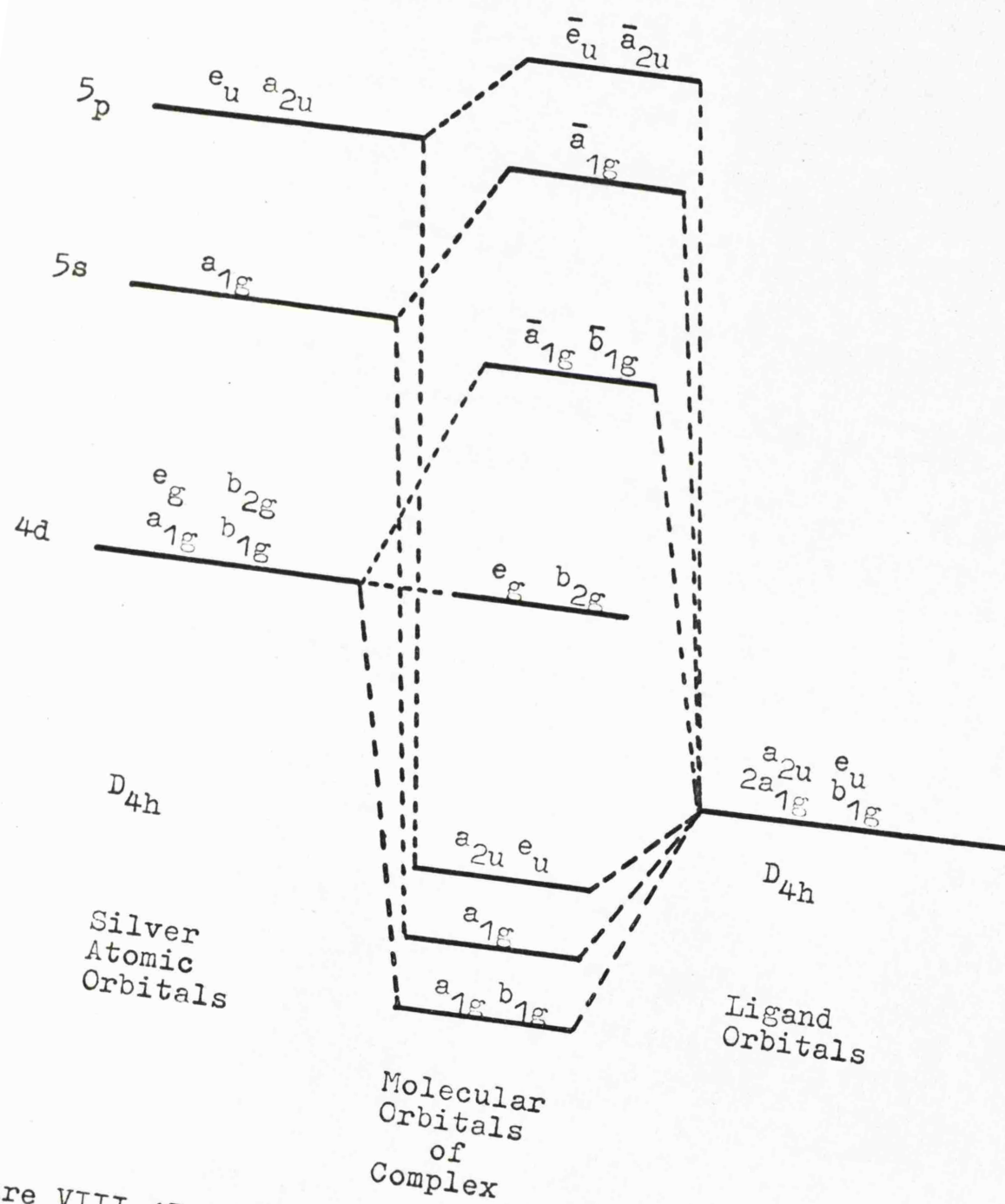


Figure VIII.17. Molecular orbital scheme for an  $Ag^0$  complex with a weak tetragonal distortion.

directly from spin-density in either the  $4d_{z^2}$ - or  $4d_{x^2-y^2}$ -orbital, for the radical is characterised by g-factors with significant positive deviations from the free-spin value. The anisotropic tensor has the form  $(+B, +B, -2B)$  and since  $\gamma_N$  for silver is negative we conclude that this anisotropy arises from electron density in the  $4d_{z^2}$ -level. The unpaired electron will therefore, occupy an antibonding orbital of  $a_1$ -symmetry constructed from the silver  $4d_{z^2}$ - and  $5s$ -orbitals overlapping with the  $1s$ -level of hydrogen. The orbital populations given in Table VIII<sup>3</sup> were derived on this basis. The deviations of the principal values of the g-tensor from 2.0023 will then arise through the magnetic coupling of the  $\bar{a}_1$ -level with the close but lower-lying  $\bar{a}_2$ - and  $\bar{b}_1$ -orbitals (we have assumed that the  $AgH^+$  complex possesses  $C_{2v}$ -symmetry in vitreous sulphuric acid matrices). Hence, we expect, and indeed find, that  $g_{xx} > g_{yy} > g_{zz} \cong 2.0023$ , where the z-direction is parallel to the Ag-H bond.

These results are in marked contrast to those reported in detail in Chapter III for the  $(Na^+---H)$  and  $(K^+---H)$  centres in barium sulphate, where the unpaired electrons are confined to the protons. However, as we emphasised previously, the latter centres are most probably hydrogen atoms trapped at sites adjacent to sodium and potassium

TABLE VIII.3. Molecular Parameters of the AgH<sup>+</sup> Ion and Related Species.

Radical	$a_{1s}^2(H)$	$a_{5s}^2(Ag)$	$a_{4d_z}^2(Ag)$
AgH <sup>+</sup>	0.55	0.14	0.31
Ag <sup>0</sup> (aq)		0.99	
(AgOCH <sub>3</sub> ) <sup>+</sup>		0.17	
(AgOCH <sub>2</sub> CH <sub>3</sub> ) <sup>+</sup>		0.18	

ions in the sulphate lattice, rather than ionised NaH or KH species.

c) Isolated Silver Atoms

The ESR data for matrix-isolated silver atoms in a variety of rigid polar and non-polar solvents, including 7.5 M aqueous sulphuric acid, are collated in Table VIII.4. Also included in this Table are the values for  $\text{Ag}^{\circ}$  in the gas phase.

The parameter  $\delta A$ , defined by the equation:

$$\delta A = \frac{A_{\text{iso}}^{\text{measured}} - A_{\text{iso}}^{\text{free atom}}}{A_{\text{iso}}^{\text{measured}}} \dots\dots(19)$$

is a measure of the perturbation of the trapped atom wavefunction's by the host matrix.  $\delta A$  in ice is small and positive and reflects the over-riding influence of Pauli exclusion forces in this environment. In contrast the  $\delta A$  values in 7.5 M aqueous  $\text{H}_2\text{SO}_4$  and pure ethanol are negative, which evidently indicates that the van der Waals interaction predominates in these vitreous matrices.

No adequate explanation has been given for the observation that the  $\delta A$  values have opposite signs in the two very similar polar solvents  $\text{CH}_3\text{CH}_2\text{OH}$  and  $\text{H}_2\text{O}$ . (their dipole moments are 1.7 D and 1.94D respectively). However, it is significant that  $\delta A$  appears to be a function of the

TABLE VIII.4.     Electron Spin Resonance Parameters  
for Trapped  $^{109}\text{Ag}^0$  in a Variety of  
Matrices

Matrix	Method of isolation	Isotropic hyperfine coupling in gauss	$g_{\text{iso}}$	$\delta A \times 10^2$	Ref.
Gas Phase	-	-706	2.00224	-	23
$\text{H}_2\text{O}$	a	-724	2.0020	+1.40	104
$\text{C}_{20}\text{H}_{42}$	a	-722	2.0016	+1.15	104
$\text{C}_{17}\text{H}_{36}$	a	-724	2.0004	+1.41	104
$\text{CH}_3\text{CH}_2\text{OH}$	a	-623	2.0004	-12.4	104
7.5 M $\text{H}_2\text{SO}_4$	b	-686	1.9996	-2.9	c

a. By deposition from the gas phase

b. By  $\gamma$ -irradiation

c. This work.

matrix structure. Negative values are obtained in glassy matrices such as aqueous  $\text{H}_2\text{SO}_4$  and ethanol, whilst a small positive shift was observed in a polycrystalline ice matrix.

The  $\Delta M_{\text{I}} = 0$  transitions of silver atoms trapped in 7.5 M aqueous  $\text{H}_2\text{SO}_4$  were accompanied by a pair of satellite lines, which must arise from the concurrent spin-inversion of the  $\text{Ag}^0$  5s-electron and neighbouring protons or silver nuclei. The separation between a satellite line and the central resonance feature has been shown to vary with the applied magnetic field strength, and is given by<sup>108</sup>

$$\Delta H_1 = \left( \frac{g_n}{g} \right) H_1 \quad \dots\dots(20)$$

where  $\Delta H_1$  is the magnetic resonance frequency of nucleus (i) in the applied magnetic field  $H_1$ .  $\Delta H_1$  ( $^{109}\text{Ag}$ ) at low-field was 5.25 gauss, which corresponds to an NMR frequency of 16.6 Mc/s in a magnetic field of about 2960 gauss. (Figure VIII.5). The calculated proton magnetic resonance frequency in this applied magnetic field would be 12.6 Mc/s, whereas both the  $^{109}\text{Ag}$  and  $^{107}\text{Ag}$  NMR frequencies are an order of magnitude smaller ( $< 1$  Mc/s). Consequently we can rule out the possibility that the species undergoing sympathetic nuclear spin-

inversion with silver atoms are  $^{109}\text{Ag}^+$  or  $^{107}\text{Ag}^+$  ions.

The ratio of the intensity of these satellite lines ( $T_1$ ) to that of the central line ( $T_0$ ) is given by the following equation<sup>108</sup>

$$\frac{T_1}{2T_0} = \frac{3}{20} \left( \sum_i \frac{g^2 \beta^2}{H_1^2 r_{ei}^6} \right) \dots\dots(21)$$

where  $H_1$  is the value of the applied magnetic field at which the principal hyperfine transition occurs, and  $r_{ei}$  is the distance between the electron and the nucleus ( $i$ ) undergoing sympathetic spin-inversion. The experimental transition probability ratio of the set of satellites and the principal transition line for trapped silver atoms was approximately 1:25. This corresponds to an average distance of  $\sim 1.82\text{\AA}$  between the  $^{109}\text{Ag}$  nucleus and the nearest neighbouring proton, which can be compared to the value of  $1.79\text{\AA}$  calculated for the trapped hydrogen atom - neighbouring proton separation in this environment.<sup>108,115</sup>

We consider these data adequate justification for concluding that trapped hydrogen atoms and silver atoms occupy magnetically equivalent sites in vitreous 7.5 M  $\text{H}_2\text{SO}_4$ .

d) The  $(\text{AgOCH}_3)^+$  and  $(\text{AgOCH}_2\text{CH}_3)^+$  Radical-Cations

The complete absence of detectable proton hyperfine couplings in the poorly resolved ESR spectra of the  $(\text{AgOR})^+$  radicals would seem to suggest that they have the structure  $\text{Ag}^+ - \text{O} - \text{R}$ , where approximately 0.8 of the unpaired-electron is confined to the bridging oxygen atom. This is not unexpected, for the higher electronegativity of oxygen compared to silver will produce a closer association of the  $\text{O} - \text{Ag} \sigma$ -bonding electrons with the former atom. The  $(\text{AgOR})^+$  radicals are more akin to solvated silver atoms than to the  $\text{AgH}^+$  centre formed in vitreous sulphuric acid. This is reflected in the g-tensors of the  $(\text{AgOR})^+$  species, where the principal values deviate little from 2.0023.

MECHANISM OF FORMATION

1. The Solvated  $\text{Ag}^0$  and  $\text{Cd}^+$  Radicals in Aqueous Sulphuric Acid

The primary radiation damage process in rigid samples of aqueous sulphuric acid is almost certainly electron ejection. In the absence of electron scavengers, rapid dissociative electron-capture by  $\text{H}_3\text{O}^+$  ions is thought to give rise to hydrogen atoms which are subsequently trapped at specific interstitial sites in the matrix.<sup>112</sup> However, even in strongly acid media, mobile electrons can react

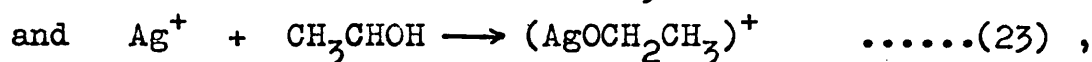
with suitable scavengers such as  $\text{Ag}^+$  and  $\text{Cd}^{2+}$  suppressing the formation of hydrogen atoms in favour of solvated silver atoms and  $\text{Cd}^+$  ions.

## 2. The $\text{AgH}^+$ Radical-Cation

The  $\text{AgH}^+$  radical may well be formed by the direct reduction of argentous ions by radiation-produced hydrogen atoms. However, it is more likely to result from the tautomeric rearrangement of a bisulphato-complex of the form  $(\text{AgOSO}_3\text{H})^-$ , produced by direct electron trapping. We are encouraged in this proposal by the observation that the radiolysis yield of  $\text{AgH}^+$  increased approximately linearly as the concentration of bisulphate ions in the acid environment increased. On the other hand, the yield of hydrogen atoms from a constant radiation dosage is known to be independent of the acid strength above approximately 4 M.

## 3. The $(\text{AgOCH}_3)^+$ and $(\text{AgOCH}_2\text{CH}_3)^+$ Cations

The appearance of spin-resonance features from these centres accompanied the loss of signals from the matrix  $\text{CH}_2\text{OH}$  and  $\text{CH}_3\text{CHOH}$  radicals. This observation suggests that reactions of the type,



must be occurring. The  $\text{CH}_3\text{OH}$  and  $\text{CH}_3\text{CH}_2\text{OH}$  precursors of

the matrix radicals may well have been part of the solvation shells of the silver ions involved in reactions (22) and (23).

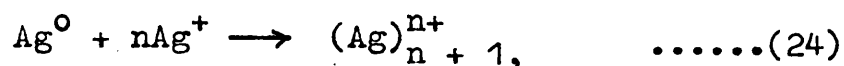
## SECTION B

### POLYNUCLEAR SILVER AND CADMIUM SPECIES IN ALCOHOLIC AND AQUEOUS ACID GLASSES

In 1959 Weyl<sup>116</sup> published a comprehensive monograph on the optical properties of vitreous media entitled "Coloured Glasses." In this review he attributed the characteristic yellow colouration exhibited by many silver-containing glasses to "the selective light absorption of the metal in a finely subdivided state." These 'chromophore' groups are very large and consist of a crystalline arrangement of several hundred silver atoms. Crystals of KCl doped with less than 0.05 mole % of argentous ions develop a yellow surface layer when heated in an atmosphere of hydrogen. This yellow colouration in the reaction zone has also been ascribed to colloidal silver metal, which could be precipitated along dislocation lines in the alkali halide crystal by heating.<sup>117</sup> The average size of the precipitated aggregates was determined by electron microscopy to be about  $1\mu$ .<sup>118</sup> Silver can also form atomic centres in KCl and atomic solutions in glasses, but in this state the characteristic

light absorption is absent. This 'frozen-in metal vapour' is actually a system of trapped free radicals and the aggregation of these atoms to form the chromophore group is a radical-annihilation process. As this process involves spin-pairing the precipitation of the  $(Ag)_{2n}$  aggregate must reduce the paramagnetism.

In this section we investigate, by ESR and optical spectroscopy, the formation of polynuclear silver species in acid and alcoholic glasses containing an excess of silver ions. Under these conditions the dominant annihilation process must be a reaction,



in which spin-pairing and the loss of paramagnetism is not a consequence of aggregation. We have attempted, wherever possible, to prepare the cadmium analogues of the polynuclear silver radicals to facilitate a comparison of their magnetic properties and structures.

#### EXPERIMENTAL RESULTS

##### 1. ESR Studies of Polynuclear Species Formed by $\gamma$ -Irradiation of Ag and Cd Salts in Various Matrices

###### a) $Ag_2SO_4$ in aqueous $H_2SO_4$

The  $\gamma$ -irradiation of vitreous samples of 0.1 M  $Ag_2SO_4$  in 5.0 M aqueous sulphuric acid at 77°K gave rise

to two detectable paramagnetic defect centres, aquated silver atoms and the matrix electron-deficient centre denoted by ' $\text{SO}_4^-$ .' When the acid matrix was carefully annealed to about  $120^\circ\text{K}$  both radicals decayed, the decomposition of the former giving rise to the  $\text{Ag}_2^+$  radical and the latter to the  $\text{Ag}^{2+}$  cation (see Figure VIII.18 ). ESR signals from  $\text{Ag}_2^+$  persisted up to approximately  $135^\circ\text{K}$  when they were replaced by those from two further radicals, labelled G and H in Figure VIII.19. Radical G was responsible for a narrow single line at  $g = 2.001$  whose intensity and linewidth were particularly sensitive to the incident microwave power level, broadening above 35 mW at  $160^\circ\text{K}$ . The radiolysis yield of radical G increased markedly if the sample was not thoroughly degassed before irradiation. This would seem to indicate that G was derived from dissolved gases in the samples, and was almost certainly the  $\text{CO}_2^-$  radical-ion.<sup>80</sup>

Radical H gave rise to a quintet of hyperfine lines centred upon  $g \cong 1.97$  and separated by approximately 150 gauss. Except for a small linewidth reduction, the use of silver enriched with the  $^{109}\text{Ag}$  isotope had little effect upon the ESR spectrum of this centre. Spin-resonance signals from H,  $\text{Ag}_2^+$  and  $\text{CO}_2^-$  persisted until the acid glass was warmed to  $200^\circ\text{K}$ , but their decomposition did not

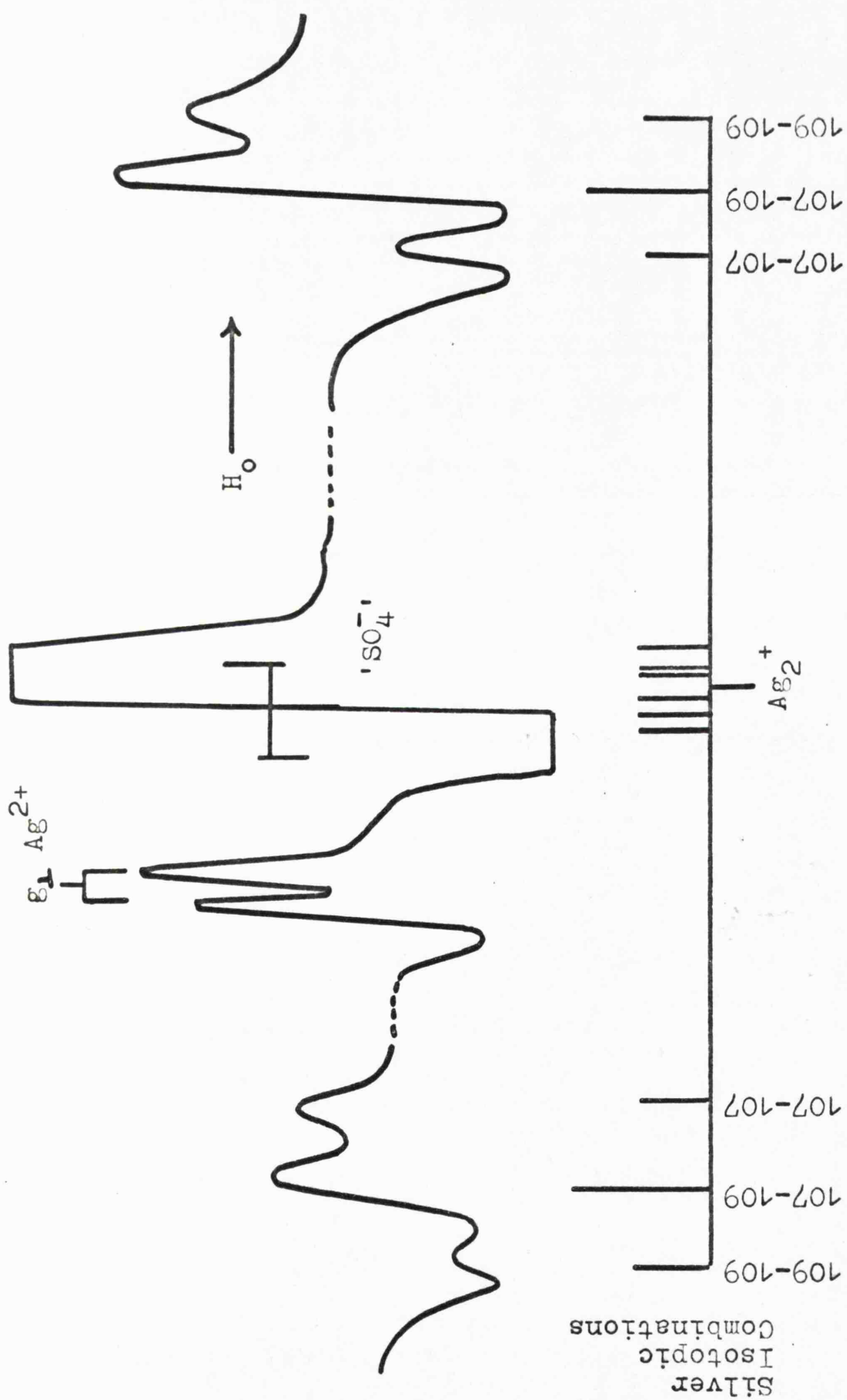


Figure VIII.18. ESR spectrum, measured at 120°K, of irradiated 0.1 M Ag<sub>2</sub>SO<sub>4</sub> in 5.0 M aqueous H<sub>2</sub>SO<sub>4</sub>.

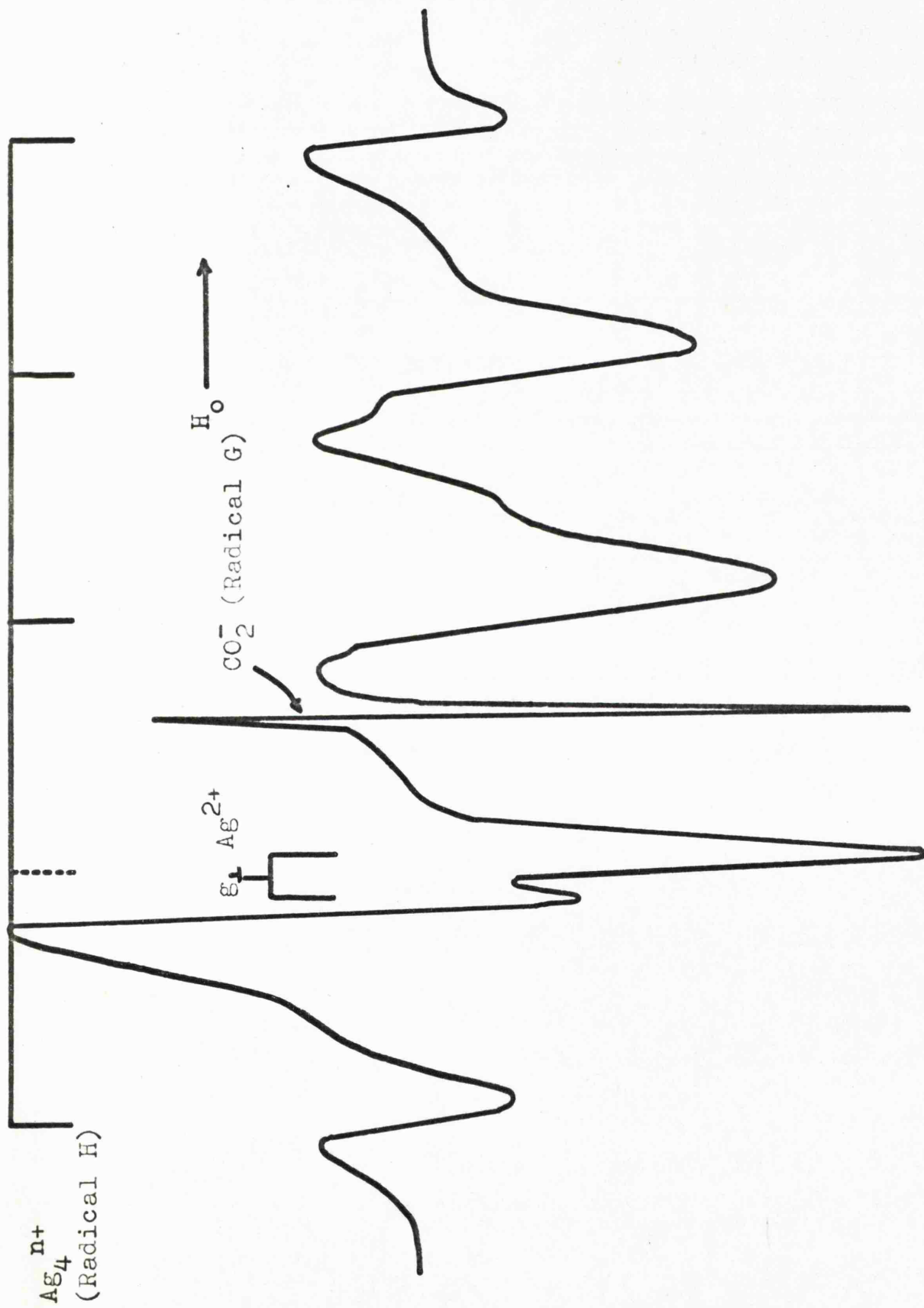


Figure VIII.19. ESR spectrum, measured at 140°K, of irradiated 0.1 M Ag<sub>2</sub>SO<sub>4</sub> in 5.0 M aqueous H<sub>2</sub>SO<sub>4</sub>.

result in the formation of further detectable paramagnetic species.

At 77°K the stable products from the  $\gamma$ -irradiation of 0.1 M  $\text{Ag}_2\text{SO}_4$  in 7.5 M aqueous sulphuric acid were aquated silver atoms,  $\text{AgH}^+$  radical-ions, ' $\text{SO}_4^-$ ,' and a fourth species which had the magnetic properties expected for isolated silver atoms which were only slightly perturbed by the medium. When the irradiated glass was annealed to 100°K, there was a significant increase in the concentration of aquated silver atoms, at the expense of  $\text{Ag}^0$  (Figure VIII.6). At 115°K the aquated silver atoms were sufficiently mobile for the occurrence of the primary reaction,



Consequently, the ESR spectrum of the warmed sample was dominated by signals from the  $\text{Ag}_2^+$  centre at this temperature (Figure VIII.20). Upon warming the matrix a further 10 deg.K, both the  $\text{Ag}_2^+$  cation and the matrix electron-deficient centre decayed. The decomposition of the latter species led to the formation of aquated argentic ions.<sup>103</sup> The  $\text{Ag}^{2+}$  ion was stable in this medium up to approximately 170°K, whereas the  $\text{AgH}^+$  cation did not decompose until the sample was heated above 180°K. The

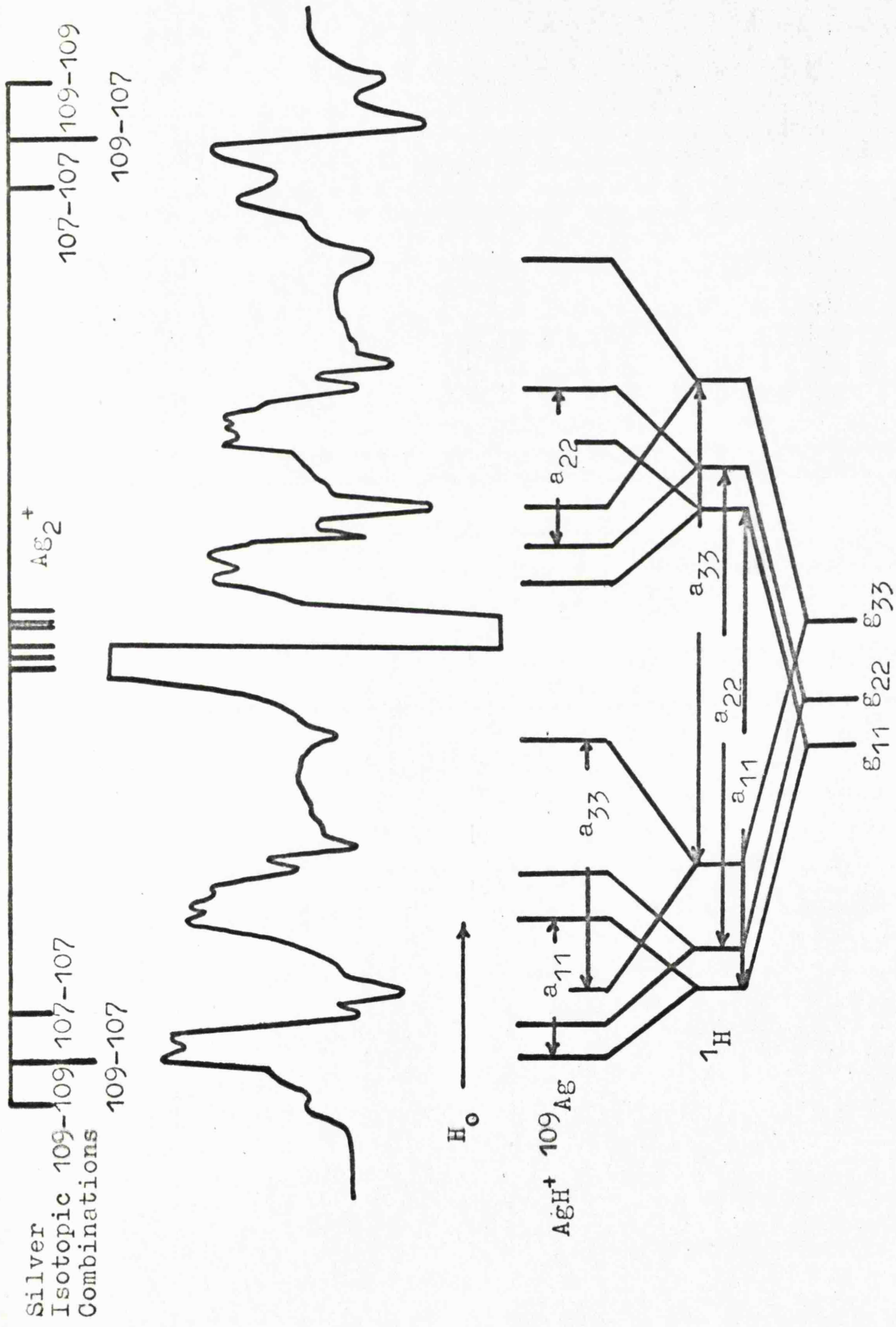


Figure VIII.20. ESR spectrum, measured at 115°K, of irradiated 0.1 M  $\text{Ag}_2\text{SO}_4$  in 7.5 M aqueous  $\text{H}_2\text{SO}_4$ .

ESR spectrum, measured at  $185^{\circ}\text{K}$ , of a  $\gamma$ -irradiated sample of  $0.1\text{ M Ag}_2\text{SO}_4$  in  $7.5\text{ M}$  aqueous sulphuric acid was characterised by signals from two paramagnetic species, the  $\text{CO}_2^-$  anion and a new radical labelled I in Figure VIII.21. The spectrum of I was extremely complex consisting of a basic hyperfine triplet separated by approximately 300 gauss, the high-field and low-field components of which were clearly resolved into three pairs of axially symmetric features. The central component of the triplet was poorly resolved at this temperature. When the glass was recooled to  $77^{\circ}\text{K}$ , there was a significant increase in the resolution of the spectrum of I, whereas the single feature attributed to  $\text{CO}_2^-$  broadened markedly and could not be detected above a microwave power level of 1 mW. Finally, as the vitreous acid was warmed to  $200^{\circ}\text{K}$  both  $\text{CO}_2^-$  and radical I decayed. When the experiment was repeated using silver enriched with  $^{109}\text{Ag}$  the spectrum of I altered significantly. Although it still consisted of a basic 300 gauss triplet, the low-field and high-field components collapsed to what appeared to be axially symmetric doublets. However, the spectrum was poorly resolved and so this analysis has to be regarded tentative.

Figure VIII.22 is the ESR spectrum of a  $\gamma$ -irra-

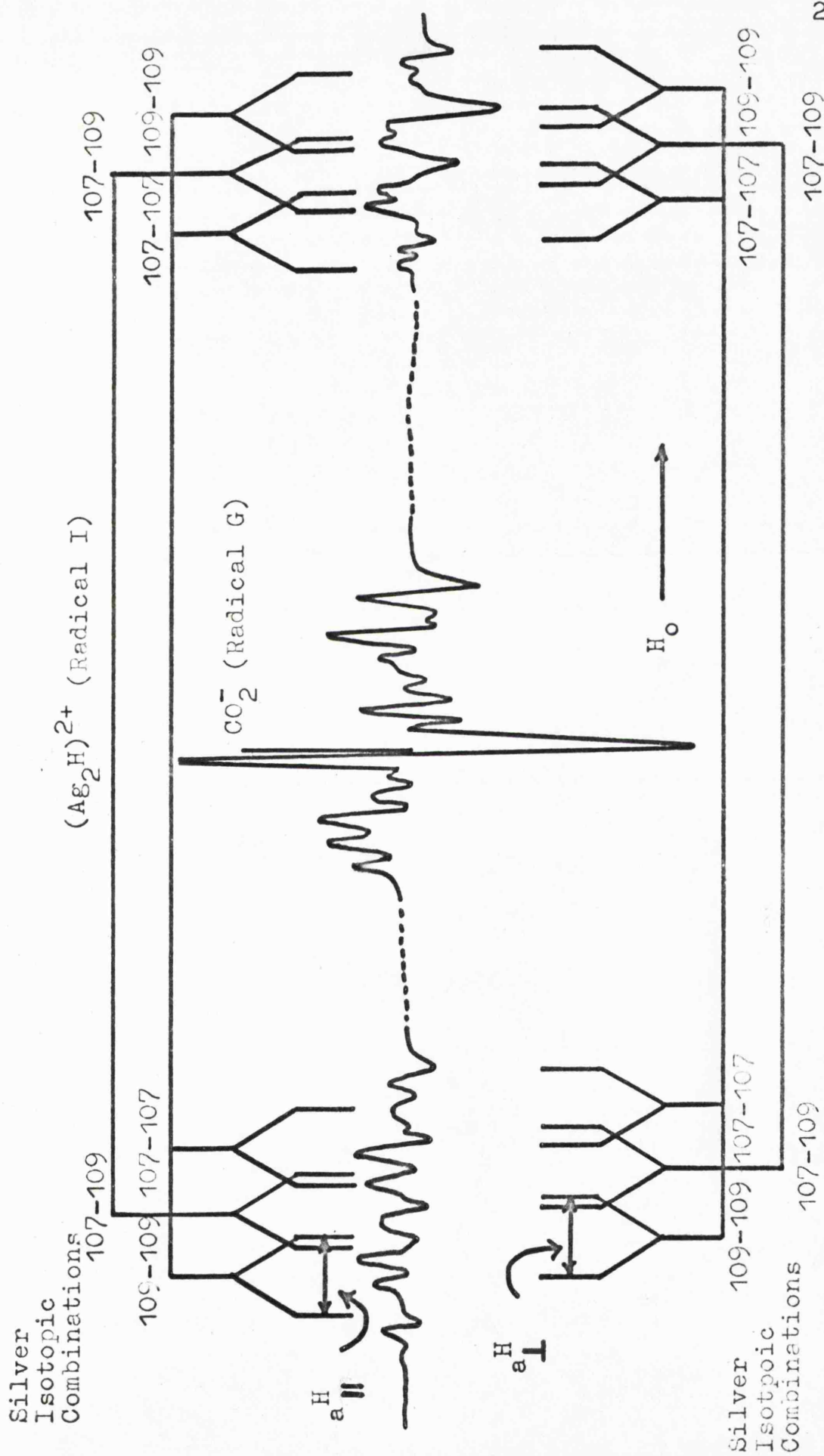


Figure VIII.21. ESR spectrum, measured at 185°K, of irradiated 0.1 M Ag<sub>2</sub>SO<sub>4</sub> in 7.5 M aqueous H<sub>2</sub>SO<sub>4</sub>. Only an analysis of the outermost features of radical I is shown for clarity.

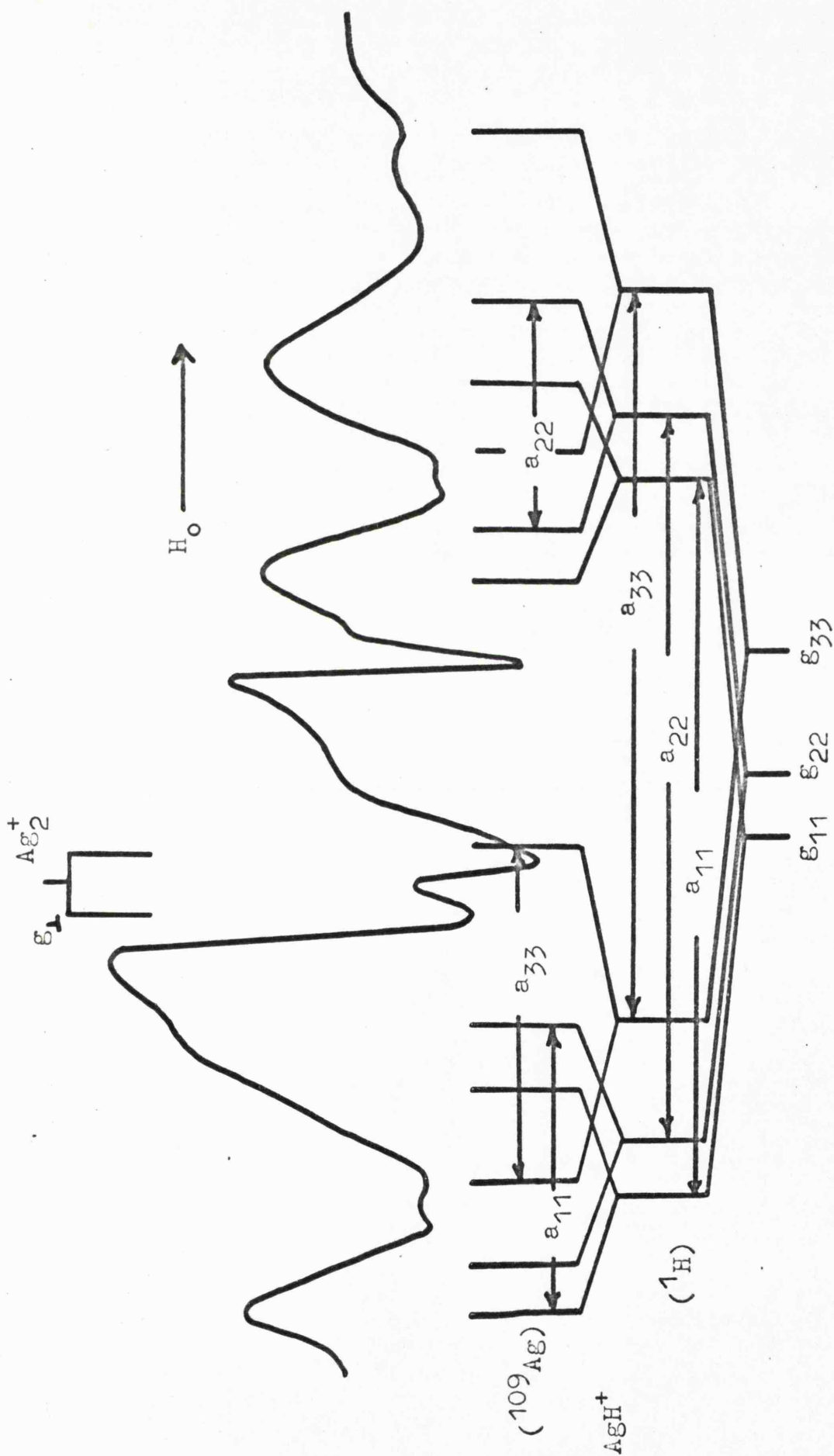


Figure VIII.22. ESR spectrum, measured at  $140^\circ\text{K}$ , of irradiated  $0.1 \text{ M Ag}_2\text{SO}_4$  in  $10.0 \text{ M}$  aqueous  $\text{H}_2\text{SO}_4$ .

diated sample of 0.1 M  $\text{Ag}_2\text{SO}_4$  in 10 M aqueous  $\text{H}_2\text{SO}_4$  which had been carefully warmed to  $140^\circ\text{K}$ . At this temperature the matrix hole-centre decayed giving rise to the intense absorption ascribed to the  $\text{Ag}^{2+}$  cation on the diagram, whereas the  $\text{AgH}^+$  cation was apparently unaffected by the annealing process.

At  $180^\circ\text{K}$  both  $\text{AgH}^+$  and  $\text{Ag}^{2+}$  decayed, but in this concentrated-acid matrix the decomposition of these radicals did not give rise to further paramagnetic species.

b)  $\text{CdSO}_4$  in aqueous  $\text{H}_2\text{SO}_4$

At  $77^\circ\text{K}$  the stable radical-products arising from the radiolysis of aqueous sulphuric acid solutions containing  $\text{Cd}^{2+}$  ions were ' $\text{SO}_4^-$ ' and aquated  $\text{Cd}^+$ . The latter centre was characterised by a strong axially symmetric absorption close to  $g = 1.99$  and a weaker feature at  $H_0 \cong 5100$  gauss which has been attributed to the overlapping high-field resonances corresponding to the magnetic  $^{111}\text{Cd}$  and  $^{113}\text{Cd}$  isotopes (see Section A). When the irradiated solutions were carefully annealed to  $120^\circ\text{K}$ , there was a marked reduction in the intensity of the  $\text{Cd}^+$  signal parallel with an increase in the amplitude of ESR features from a third paramagnetic centre, J in Figure VIII.23. Although J was almost

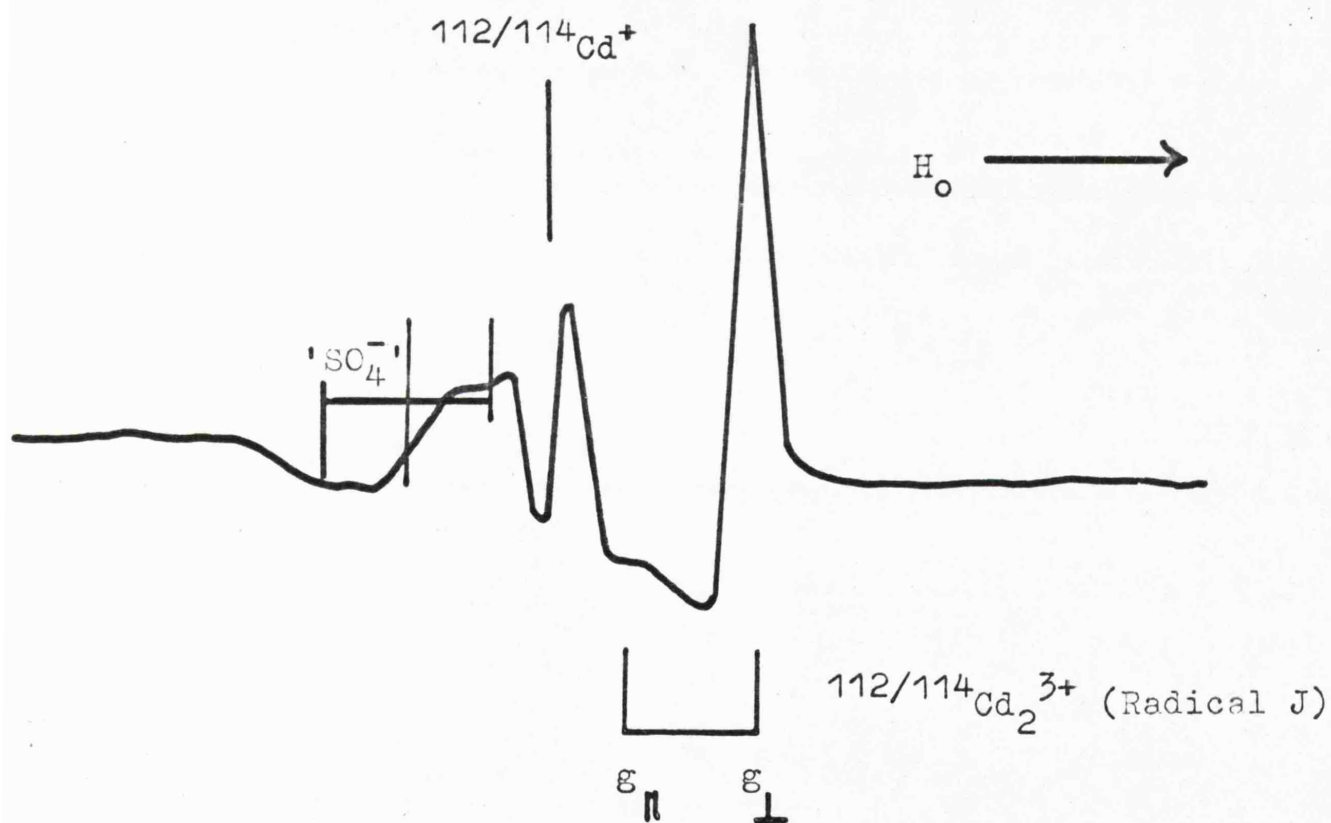


Figure VIII.23. ESR spectrum, measured at  $120^\circ\text{K}$ , of irradiated  $0.1\text{ M CdSO}_4$  in  $5.0\text{ M aqueous H}_2\text{SO}_4$ .

certainly a cadmium containing species, we could not detect Cd hyperfine features from this centre even under high resolution. At 130°K the matrix hole-centre decayed, but J was stable up to approximately 195°K.

c) CdSO<sub>4</sub> and Ag<sub>2</sub>SO<sub>4</sub> in aqueous H<sub>2</sub>SO<sub>4</sub>

Aquated Ag<sup>0</sup> and Cd<sup>+</sup>, and the matrix 'SO<sub>4</sub><sup>-</sup>' centre were the stable radical-products arising from the radiolysis of a sample of 5.0 M aqueous H<sub>2</sub>SO<sub>4</sub> containing 0.1 M Ag<sub>2</sub>SO<sub>4</sub> and 0.1 M CdSO<sub>4</sub>. At 120°K the Ag<sup>0</sup> and Cd<sup>+</sup> radicals were sufficiently mobile to diffuse, resulting in the formation of Ag<sub>2</sub><sup>+</sup>, radical J, and a third paramagnetic species, K. Radical K was responsible for a narrow pair of axially symmetric doublets centred upon g = 1.976 and separated by about 310 gauss. (Figure VIII.24). At 130°K the Ag<sub>2</sub><sup>+</sup> centre decayed, radical K was stable to approximately 145°K, but ESR signals from J could be detected above 190°K.

d) AgClO<sub>4</sub> in CH<sub>3</sub>OH and CH<sub>3</sub>CH<sub>2</sub>OH

When radiation-produced silver atoms were warmed to 110°K in alcoholic matrices, they reacted to give the (AgOR)<sup>+</sup> and Ag<sub>2</sub><sup>+</sup> radicals. These species subsequently disappeared at about 130°K resulting in the formation of a fourth silver-containing paramagnetic centre which was characterised, in CH<sub>3</sub>OH, CH<sub>3</sub>CH<sub>2</sub>OH, CH<sub>3</sub>OD, CH<sub>3</sub>CH<sub>2</sub>OD, CD<sub>3</sub>OD,

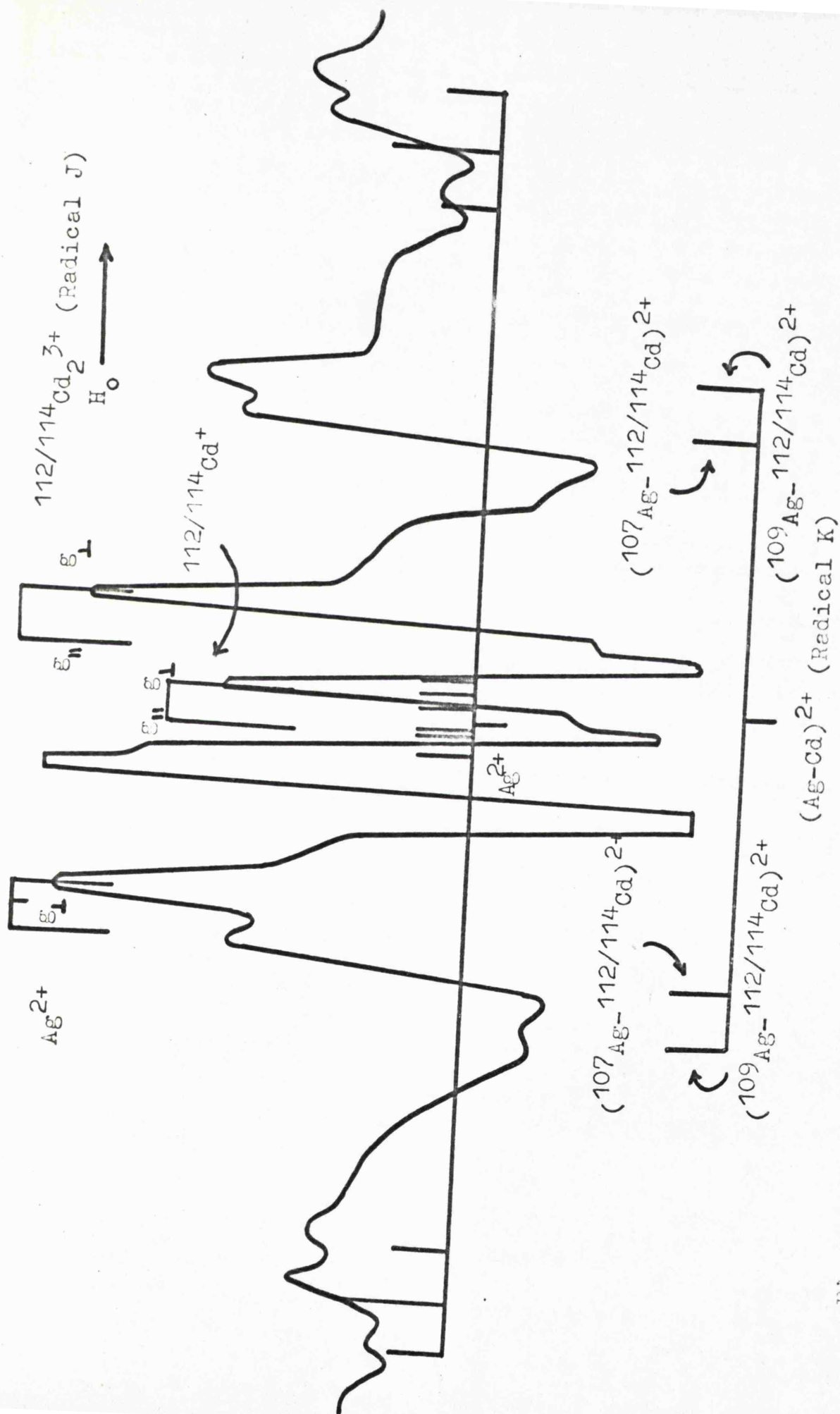


Figure VIII.24. ESR spectrum, measured at  $120^{\circ}K$ , of irradiated 5.0 M aqueous  $H_2SO_4$  containing 0.1 M  $Ag_2SO_4$  and 0.1 M  $CdSO_4$ .

and  $\text{CD}_3\text{CD}_2\text{OD}$ , by an ESR spectrum which was identical to that assigned to radical H in 5.0 M aqueous  $\text{H}_2\text{SO}_4$ . (Compare Figures VIII.25 and VIII.19). At  $140^\circ\text{K}$  radical H decayed. When the alcoholic matrices were subsequently melted, a mirror or black precipitate of metallic silver was formed.

e)  $\text{Cd}(\text{ClO}_4)_2$  in  $\text{CH}_3\text{OH}$  and  $\text{CH}_3\text{CH}_2\text{OH}$

Figure VIII.26 is an ESR spectrum, measured at  $135^\circ\text{K}$ , of a  $\gamma$ -irradiated frozen solution of cadmium perchlorate in methanol. The primary products of radiation damage,  $\text{CH}_2\text{OH}$ ,  $\text{CHO}$  and  $\text{Cd}^+$ , were unstable at this temperature and their decomposition resulted in the formation of a species whose spectral parameters closely resemble those of radical J in  $\text{H}_2\text{SO}_4$  (see Table VIII.5). Analogously, the thermal bleaching of the primary radical-products arising from  $\gamma$ -irradiated  $\text{Cd}(\text{ClO}_4)_2$  in  $\text{CH}_3\text{CH}_2\text{OH}$  resulted in the formation of radical J.

f)  $\text{AgClO}_4$  and  $\text{Cd}(\text{ClO}_4)_2$  in  $\text{CH}_3\text{OH}$  and  $\text{CH}_3\text{CH}_2\text{OH}$

When irradiated samples of methanol or ethanol containing  $\text{Ag}^+$  and  $\text{Cd}^{2+}$  ions were carefully annealed, the ESR spectra of the glasses altered significantly. At  $100^\circ\text{K}$  the primary paramagnetic centres decayed with the formation of  $\text{Ag}_2^+$ ,  $(\text{AgOR})^+$ , radical J, and a new species whose ESR spectrum was remarkably similar to that of K

H<sub>0</sub> →

Ag<sub>4</sub><sup>n+</sup> (Radical H)

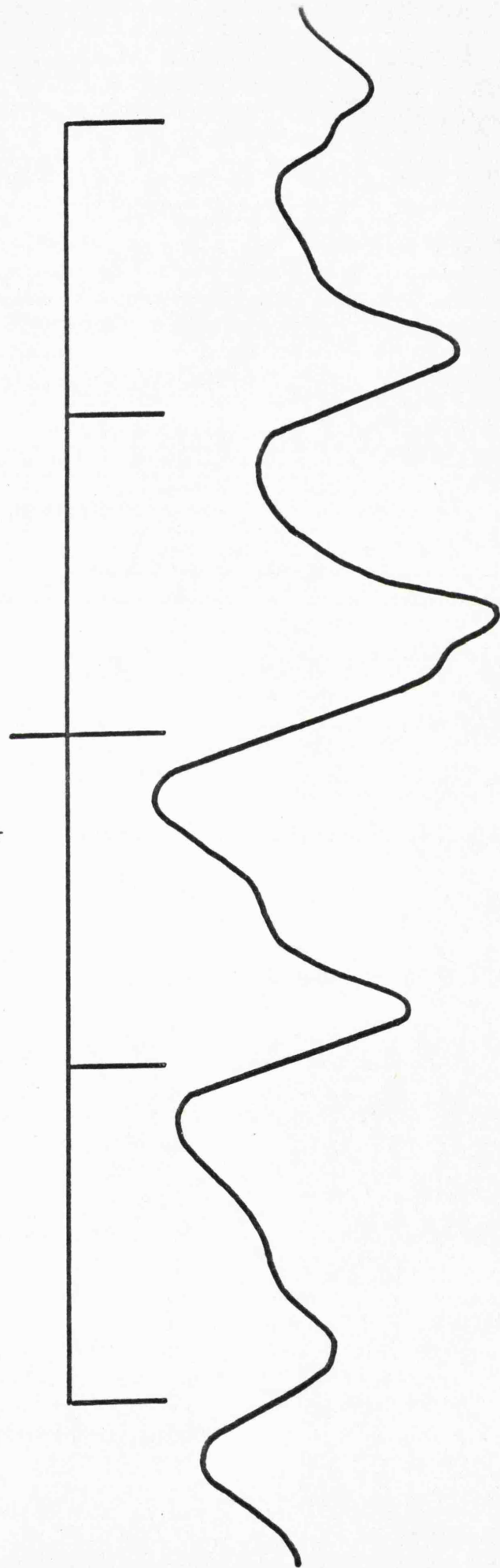


Figure VIII.25. ESR spectrum, measured at 130°K, of irradiated 0.1 M AgClO<sub>4</sub> in methanol, showing the five features arising from radical H.

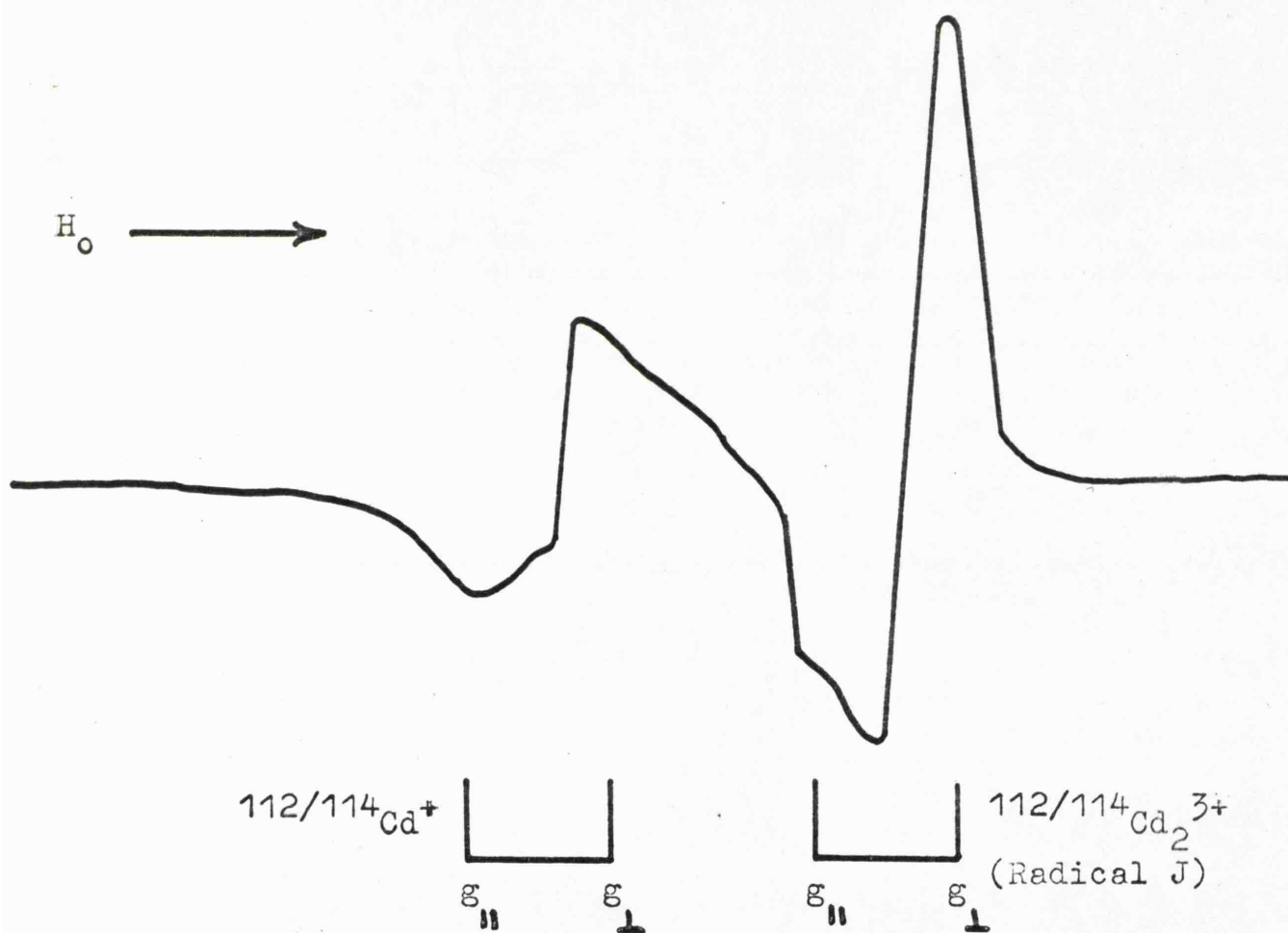


Figure VIII.26. ESR spectrum, measured at  $135^\circ\text{K}$ , of irradiated  $0.1\text{ M Cd}(\text{ClO}_4)_2$  in methanol.

in 5.0 M aqueous  $\text{H}_2\text{SO}_4$  (a pair of axially symmetric doublets separated by about 310 gauss and centred upon  $g = 1.973$ ).

## 2. The Electronic Spectra of Polynuclear Species Formed From Ag and Cd Salts in Various Matrices

### a) $\text{Ag}_2\text{SO}_4$ in aqueous $\text{H}_2\text{SO}_4$

Figure VIII.27 shows optical absorption spectra, measured at  $77^\circ$ ,  $120^\circ$  and  $170^\circ\text{K}$ , of a  $\gamma$ -irradiated sample of 0.05 M  $\text{Ag}_2\text{SO}_4$  in 7.5 M  $\text{H}_2\text{SO}_4$ . Aquated silver atoms are thought to be responsible for absorption (I) ( $\lambda_{\text{max}} = 345 \text{ nm}$ ;  $29,000 \text{ cm}^{-1}$ ) whilst (II) ( $\lambda_{\text{max}} = 290 \text{ nm}$ ;  $34,500 \text{ cm}^{-1}$ ) has been assigned to  $\text{AgH}^+$  cations. As the sample was annealed to  $120^\circ\text{K}$  the concentration of a new species, characterised by an absorption (IV) at 310 nm ( $32,300 \text{ cm}^{-1}$ ), increased at the expense of both  $\text{AgH}^+$  and aquated silver atoms. At  $170^\circ\text{K}$  the amplitude of absorption (IV) was markedly reduced, but there was a compensating increase in the intensity of a new absorption (III) at 265 nm ( $37,800 \text{ cm}^{-1}$ ). From a comparison with the temperature profiles of the ESR spectra, we assign absorption (IV) to  $\text{Ag}_2^+$  radicals whilst  $\text{Ag}^{2+}$  cations are considered to give rise to absorption (III).

### b) $\text{CdSO}_4$ in aqueous $\text{H}_2\text{SO}_4$

The optical absorption spectra, measured at  $77^\circ$

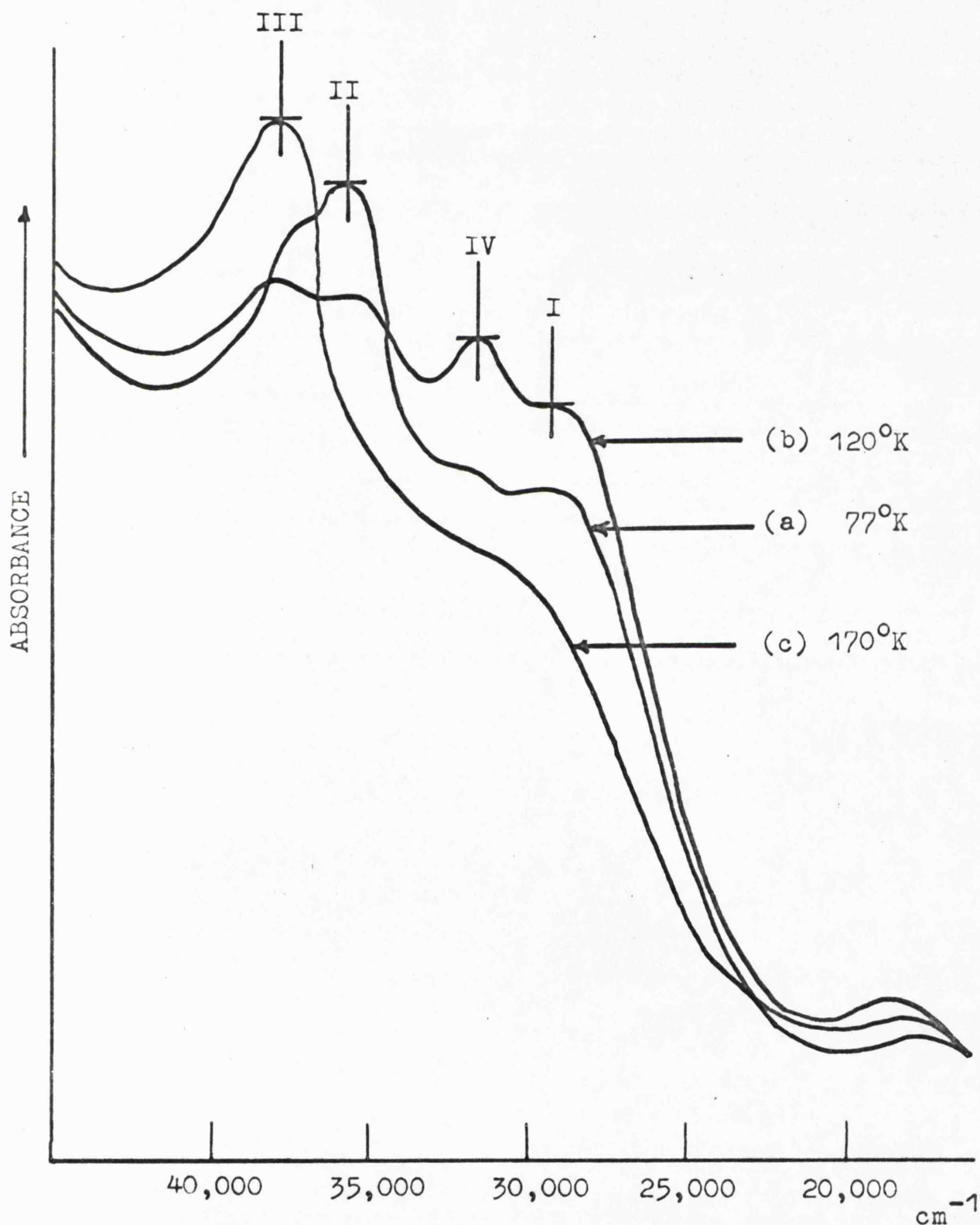


Figure VIII.27. Electronic spectra of an irradiated sample of 0.05 M  $\text{Ag}_2\text{SO}_4$  in 7.5 M  $\text{H}_2\text{SO}_4$  measured at various temperatures.

and 120°K, of a sample of  $\gamma$ -irradiated 0.05 M CdSO<sub>4</sub> in 7.5 M aqueous H<sub>2</sub>SO<sub>4</sub> are shown in Figure VIII.28. Absorption (V) ( $\lambda_{\text{max}} = 290 \text{ nm}$ ;  $34,500 \text{ cm}^{-1}$ ), previously assigned to aquated Cd<sup>+</sup> ions, decayed when the irradiated sample was warmed and a weaker absorption (VI) ( $\lambda_{\text{max}} = 240 \text{ nm}$ ;  $41,700 \text{ cm}^{-1}$ ) appeared. This high energy absorption persisted to 170°K and is assigned to radical J.

## DISCUSSION

### 1. The Identification of the Polynuclear Silver and Cadmium Species

#### a) Radical H

For the following reasons we tentatively identify H as an (Ag)<sub>4</sub><sup>n+</sup> centre.

i) It is reasonable to assume that the quintet of ESR features characteristic of this centre arise from the interaction of the unpaired electron with four silver atoms. The use of argentous salts enriched with the <sup>109</sup>Ag isotope resulted in a detectable reduction in the ESR linewidth of this species.

ii) High yields of radical H were obtained in those Ag<sup>+</sup> solutions from which metallic silver was the ultimate radiation product.

This suggests that H is an intermediate in the

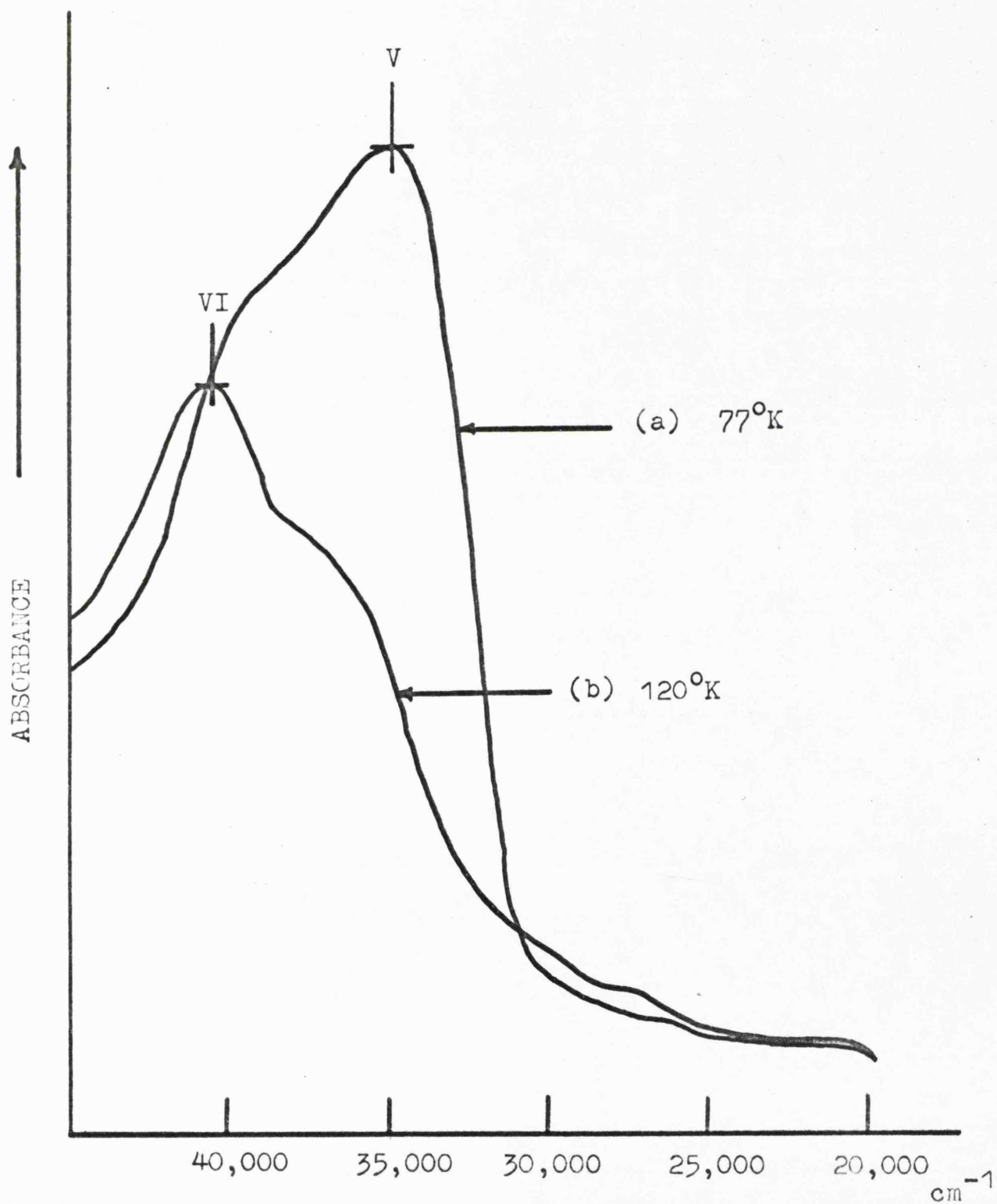


Figure VIII. 28. Electronic spectra of an irradiated sample of 0.05 M CdSO<sub>4</sub> in 7.5 M aqueous H<sub>2</sub>SO<sub>4</sub> measured at various temperatures.

aggregation process responsible for the annihilation of isolated silver radicals. The formation of  $\text{Ag}_2^+$  is almost certainly the primary stage in this process, and it is significant that the appearance of spin-resonance signals from H accompanied the loss of signals from  $\text{Ag}_2^+$ . It is also interesting that as a consequence of the decomposition of radical H, the alcoholic matrices developed a deep yellow colouration, prior to the precipitation of metallic silver, and this colour almost certainly arises from the chromophore groups discussed in the introduction to this section.

b) Radical I

Radical I, formed when a frozen 7.5 M aqueous sulphuric acid solution containing  $\text{AgH}^+$  radical-cations was carefully warmed to  $180^\circ\text{K}$ , is thought to be the  $(\text{Ag}_2\text{H})^{2+}$  cation. We base this conclusion on the following factors.

i) The ESR spectrum of radical I could best be interpreted in terms of an axially symmetric species containing two equivalent silver atoms. The spectrum consisted of a basic isotropic

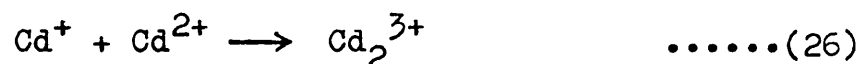
triplet of approximately 300 gauss, the low-field and high-field components of which were split into 1:2:1 axially symmetric triplets corresponding to the isotopic combinations  $^{109}\text{Ag} - ^{109}\text{Ag}$ ,  $^{109}\text{Ag} - ^{107}\text{Ag}$ , and  $^{107}\text{Ag} - ^{107}\text{Ag}$ . Each of these features was in turn split into a doublet by a third nucleus having  $I = \frac{1}{2}$ . The use of  $^{109}\text{Ag}$  isotopically-enriched argentous salts resulted in a marked simplification of this spectrum. The low-field and high-field components of the basic triplet collapsed to axially symmetric doublets.

ii) The minor doublet splitting of the silver isotopic components almost certainly arose from the interaction of the unpaired electron with a single  $^1\text{H}$  nucleus.

iii) There was an increase in the amplitude of the ESR spectrum of this centre as the  $\text{AgH}^+$  radical decayed. Furthermore, radical I was formed only in sulphuric acid matrices from which  $\text{AgH}^+$  was a primary radiation damage product.

c) Radical J

We were unable to detect hyperfine interactions involving the magnetic  $^{111}\text{Cd}$  and  $^{113}\text{Cd}$  cadmium isotopes in the ESR spectrum of this centre and consequently we can only offer a tentative identification for radical J. The appearance of ESR signals from J, with the simultaneous loss of features from the  $\text{Cd}^+$  centre, occurred at approximately  $115^\circ\text{K}$  in aqueous sulphuric acid and at  $100^\circ\text{K}$  in methanol or ethanol. At these temperatures the solvents are sufficiently mobile for the reaction:



to occur, and we therefore identify J as  $\text{Cd}_2^{3+}$ . We are encouraged in this assignment by the fact that the g-tensor of this radical closely resembles that of the isoelectronic  $\text{Ag}_2^+$  centre (see Table VIII.5).

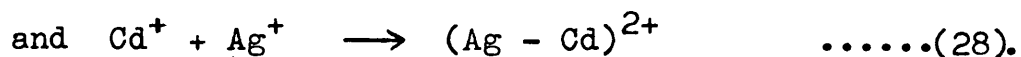
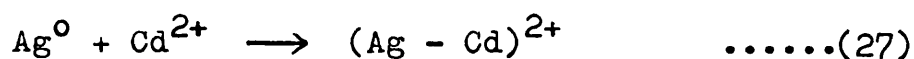
The absorption band at 240 nm ( $41,700 \text{ cm}^{-1}$ ), in the electronic spectrum of  $\gamma$ -irradiated  $\text{Cd}^{2+}$  in  $\text{H}_2\text{SO}_4$  almost certainly arises from this centre.

e) Radical K

Radical K was formed when irradiated acid and alcoholic glasses containing both silver and cadmium ions were carefully warmed. It has the expected spin-resonance parameters for a  $(\text{Ag-Cd})^{2+}$  ion, isoelectronic

with  $\text{Cd}_2^{3+}$  and  $\text{Ag}_2^+$  (see Table VIII.5). The axially symmetric doublets separated by approximately 310 gauss correspond to the isotopic combinations ( $^{107}\text{Ag} - ^{112/114}\text{Cd}$ ) $^{2+}$  and ( $^{109}\text{Ag} - ^{112/114}\text{Cd}$ ) $^{2+}$ . It is not surprising that we could not detect features arising from the corresponding combinations containing magnetic cadmium nuclei because the large cadmium hyperfine splittings are coupled with very large ESR linewidths in these matrices.

The  $(\text{Cd} - \text{Ag})^{2+}$  centre was probably formed from the reactions:

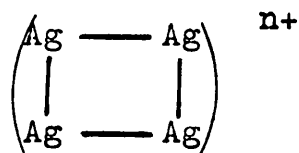


## 2. The Molecular and Electronic Structures of the Polynuclear Silver and Cadmium Containing Radicals

### a) The $(\text{Ag})_4^{n+}$ centre

The ESR spectrum of this centre was poorly resolved in both aqueous acid and alcoholic matrices. The spin-resonance features were extremely broad ( $\Delta H_{\text{MS}} \cong 30$  gauss), even when isotopically-enriched  $^{109}\text{Ag}$  salts were used, and there was considerable overlapping in the central region of the spectrum between features from this centre and those from the  $\text{Ag}^{2+}$  and  $\text{CO}_2^-$  radical-ions. Consequently, we have been unable to accomplish an unambiguous analysis of this

spectrum. The  $(\text{Ag})_4^{n+}$  radical may well have axial symmetry and contain four equivalent silver atoms, in which case the only possible configuration for this centre is



For this structure the intensity distribution of the five hyperfine features should be approximately 1:4:6:4:1. However, the actual distribution is closer to 1:2:4:2:1.

Alternatively, the ESR spectrum of this radical can be interpreted in terms of a species possessing totally symmetric g- and A-tensors and containing two pairs of inequivalent silver atoms. This analysis can be accounted for if the radical has a linear 'chain-like' structure. Since the most stable silver complexes have a linear L - Ag - L configuration, we prefer the latter alternative structure for the  $(\text{Ag})_4^{n+}$  aggregate and the spin-resonance parameters included in Table VIII.5 were derived accordingly.

In the  $(\text{Ag})_4^{n+}$  centre we cannot independently determine the value of n. However, the g-tensor of this centre is very similar to that of  $\text{Ag}_2^+$  where the

TABLE VIII.5. Magnetic Data for a Variety of Polynuclear Ag and Cd Containing Species in Alcoholic and Aqueous Acid Matrices

Radical	Matrix	g-tensor <sup>a</sup>			<sup>109</sup> Ag Hyperfine tensor in gauss			a <sub>s</sub> <sup>2</sup> (Ag)	Ref.
		g <sub>  </sub>	g <sub>⊥</sub>	g <sub>av</sub>	B <sub>  </sub>	B <sub>⊥</sub>	A <sub>iso</sub>		
Ag <sup>+</sup>	CH <sub>3</sub> CH <sub>2</sub> OH	2.001	1.974	1.983	-10	+5	-302	0.425	103
	H <sub>2</sub> SO <sub>4</sub>	2.001	1.974	1.983	-11	+5.5	-321	0.450	
	CH <sub>3</sub> OH	2.001	1.974	1.983	-10	+5	-303	0.430	
(Ag-Cd) <sup>2+</sup>	CH <sub>3</sub> OH	g <sub>iso</sub> = 1.973					-305	0.430	c
(Radical K)	H <sub>2</sub> SO <sub>4</sub>	g <sub>iso</sub> = 1.976					-319	0.450	c
<sup>112/114</sup> Cd <sup>3+</sup>	CH <sub>3</sub> OH	1.9970	1.9730	1.9810	-	-	-	-	c
(Radical J)	H <sub>2</sub> SO <sub>4</sub>	1.9995	1.9747	1.9829	-	-	-	-	c

TABLE VIII.5. (Continued)

	$g_{\parallel}$	$g_{\perp}$	$g_{av}$	$B_{\parallel}$	$B_{\perp}$	$A_{iso}$	$a_B^2(AG)$
$(Ag_2H)^{2+}$ (Radical I)	1.989	1.982	1.984	-2.1	+1.1	-313.3	0.440
	$^1H$ Hyperfine tensor in gauss						
				-2.0	+1.0	+25.0	$a_B^2(H) = 0.05$
$Ag_4^{n+}$ (Radical H)	$g_{iso} \approx 1.975$			(b) $A_{iso}(^xAg) \approx -156$			0.22
				$A_{iso}(^yAg) \approx -146$			0.21
	$g_{iso} \approx 1.975$			(b) $A_{iso}(^xAg) \approx -155$			0.22
				$A_{iso}(^yAg) \approx -142$			0.20

a. Derived using the Breit-Rabi equation.<sup>58</sup>

b. This data was derived assuming that the  $Ag_4^{n+}$  centre consisted of two pairs of inequivalent silver atoms,  $^xAg$  and  $^yAg$ .

c. This work.

unpaired electron occupies a bonding  $\sigma$ -orbital constructed from the 5s- and 5p-atomic orbitals of the silver atoms.<sup>103</sup> Consequently, n is probably 1 or 3 so that the unpaired electron in the  $(\text{Ag})_4^{n+}$  centre likewise occupies a bonding  $\sigma$ -orbital constructed from the silver 5s- and 5p-levels.

b) The  $(\text{Ag}_2\text{H})^{2+}$  centre

The spin-resonance parameters of the  $(\text{Ag}_2\text{H})^{2+}$  radical, included in Table VIII.5, reflect the close similarity between the unpaired electron distribution in this centre and that in the  $\text{Ag}_2^+$  cation. However, there is a superimposed residual coupling to a single proton in the former species. The most probable structure for an  $(\text{Ag}_2\text{H})^{2+}$  cation, in which the two silver atoms are entirely equivalent, is:  $(\text{Ag} - \text{H} - \text{Ag})^{2+}$ . In view of the higher electronegativity of hydrogen compared to silver one would have expected the unpaired electron to be more closely associated with the former atom, which would have resulted in proton hyperfine coupling constants considerably larger than the observed  $25 \pm 2$  gauss. The only alternative structure for this centre is:  $(\text{H} - \text{Ag} - \text{Ag})^{2+}$ , but here we would not have expected the silver atoms to remain equivalent, although a small proton coupling is probable.

It seems that further studies are needed before firm conclusions about the structure of this centre can be drawn.

c) The  $\text{Cd}_2^{3+}$  centre

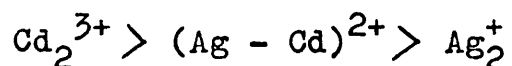
The  $\text{Cd}_2^{3+}$  centre, in both aqueous acid and alcoholic matrices, is characterised by an axially symmetric g-tensor whose principal values have significant negative deviations from the free-spin value. The unpaired electron occupies a bonding  $\sigma$ -orbital constructed from the 5s-atomic orbitals of the cadmium atoms. The principal contribution to the negative shift of  $g_1$  (1.975) from 2.0023 must involve promotion to vacant cadmium 5p-orbitals. We were unable to estimate the contribution of these higher lying levels to the bonding  $\sigma$ -orbital of  $\text{Cd}_2^{3+}$  as we could not detect hyperfine interactions involving the  $^{111}\text{Cd}$  and  $^{113}\text{Cd}$  magnetic nuclei in the ESR spectrum of this centre.

d) The  $(\text{Ag} - \text{Cd})^{2+}$  centre

Both the silver A-tensor and the g-tensor of the  $(\text{Ag} - \text{Cd})^{2+}$  centre are remarkably similar to those of the isoelectronic  $\text{Ag}_2^+$  cation. This is probably because the electronegativities of silver and cadmium are about equal. Therefore, we would expect the unpaired electron distribution in the heteronuclear diatomic  $(\text{Ag} - \text{Cd})^{2+}$  to be

close to those in  $\text{Ag}_2^+$  and  $\text{Cd}_2^{3+}$ .

We expect, and indeed find, the following order of stability for the three identified diatomic cations in both aqueous acid and alcoholic matrices:



The radical annihilation process is almost certainly aggregation and the rate of this process must be controlled by the mobility of the solvent shell about the expanding metal-ion cluster. The highly charged  $\text{Cd}_2^{3+}$  cation will bind the solvent molecules more strongly than  $(\text{Ag} - \text{Cd})^{2+}$  and will consequently have a higher kinetic stability. Similarly the  $(\text{Ag} - \text{Cd})^{2+}$  cation will be less labile than the singly charged  $\text{Ag}_2^+$  radical.

## REFERENCES

REFERENCES

1. A. Carrington and A.D. McLachlan, "Introduction to Magnetic Resonance," Harper & Row, New York, 1967.
2. M. Bersohn and J.C. Baird, "An Introduction to Electron Paramagnetic Resonance," Benjamin, New York, 1966.
3. C.P. Poole, "Experimental Techniques in Electron Spin Resonance," Wiley, New York, 1966.
4. P.B. Ayscough, "Electron Spin Resonance in Chemistry," Methuen, London, 1967.
5. H.G. Hecht, "Magnetic Resonance Spectroscopy," Wiley, New York, 1967.
6. M.T. Jones and W.D. Phillips, Ann.Rev.Phys.Chem., 1966, 17, 323.
7. A. Carrington and D.H. Levy, J.Phys.Chem., 1967, 71, 2.
8. E. Mueller, K. Rieker, K. Scheffler and A. Moosmayer, Angew.Chem.Intern.Ed.Engl., 1966, 5, 6.
9. N.M. Atherton, A.J. Parker and H. Steiner, Ann.Rept., 1966, 63, 62.
10. A. Horsefield, Ann.Rept., 1966, 64, 257.

11. P.W. Atkins and M.C.R. Symons, "The Structure of Inorganic Radicals," Elsevier, Amsterdam, 1967.
12. J.E. Geusic and L.C. Brown, Phys.Rev., 1958, 112, 64.
13. M.H.L. Pryce, Proc.Phys.Soc., 1950, A63, 25.
14. J.A. Weil and J.H. Anderson, J.Chem.Phys., 1958, 28, 864.
15. D.S. Schonland, Proc.Phys.Soc., 1959, 73, 788.
16. S. Subramanian, Ph.D. Thesis, Leicester, 1968.
17. F.K. Kneubühl, J.Chem.Phys., 1960, 33, 1074.
18. M.C.R. Symons, J.Chem.Soc., 1965, 2276.
19. H.M. McConnell and J. Strathdee, Mol.Phys., 1959, 2, 129.
20. C.A. Coulson, Volume Commemoratif Victor Henri, Contributions a l'Etude de la Structure Moleculaire, 1948, 15.
21. J.A. Brivati, N. Keen and M.C.R. Symons, J.Chem.Soc., 1962, 237.
22. J.A. Brivati, J.M. Gross, M.C.R. Symons and D.J.A. Tinling, J.Chem.Soc., 1965, 6504.
23. N.F. Ramsey, "Molecular Beams," Clarendon Press, Oxford, 1955, and "Nuclear Moments," Wiley, New York, 1953.
24. C.C.J. Roothan and E. Clementi, University of Chicago.

25. R.E. Watson and A.J. Freeman, Phys.Rev., 1961, 123, 521.
26. R.E. Watson and A.J. Freeman, Phys.Rev., 1961, 124, 117.
27. P.H. Kasai, Phys.Rev.letters, 1968, 21, 67.
28. J.R. Morton, J.R. Rowlands and D.H. Wiffen, Natl. Phys.Lab.Gr.Brit.Circ.No.BPR.13.
29. A.G. Walton, "The Formation and Properties of Precipitates," Interscience, New York, 1967.
30. P. Kusch, Phys.Rev., 1955, 100, 1188.  
R. Berringer and M.A.S. Heald, Phys.Rev., 1954, 95, 1474.
31. F.J. Adrian, J.Chem.Phys., 1960, 32, 972.
32. C.K. Jen, V.A. Bowers, E.L. Cochran and S.N. Foner, Phys.Rev., 1962, 126, 1749.
33. P.W. Atkins, Ph.D. Thesis, Leicester, 1964.  
H.W. Wardale. Ph.D. Thesis, Leicester, 1967.
34. G. Walton and G.H. Walden, J.Amer.Chem.Soc., 1946, 68, 1750.
35. G. Walton and G.H. Walden, J.Amer.Chem.Soc., 1946, 68, 1742.
36. R.A. Serway and S.A. Marshall, J.Chem.Phys., 1967, 46, 1949.

37. S.A. Marshall, A.R. Reinberg, R.A. Serway and J.A. Hodges, Mol.Phys., 1964, 8, 223.
38. R.S. Eachus and M.C.R. Symons, J.Chem.Soc., A, 1968, 790.
39. G.W. Chantry, A. Horsefield, J.R. Morton and D.H. Whiffen, Mol.Phys., 1962, 5, 589.
40. A.D. Walsh, J.Chem.Soc., 1953, 2296.
41. R. Livingston and H. Zeldes, J. Chem.Phys., 1964, 41, 4011.
42. S.J. Strickler and M. Kasha, "Molecular Orbitals in Chemistry and Biology," Academic Press, New York, 1964.
43. H. Schäfer and A. Sieverts, Z.anorg.Chem., 1941, 246, 149.
44. D.E. Wood and T.M. Pietrzak, J.Chem.Phys., 1967, 46, 2973.
45. W.B. DeMore and N. Davidson, J.Amer.Chem.Soc., 1959, 81, 5869.
46. E.J. Jones and O.R. Wulf, J.Chem.Phys., 1937, 5, 873.
47. M.C.R. Symons, Advan. in Chem., 1968, 82, 1.
48. A. Horsefield, J.R. Morton and D.H. Wiffen, Mol.Phys., 1961, 4, 475.
49. J. Cunningham, Intern.Symp. on Free Radicals, 5th, Uppsala, 1961.

50. C. Jaccard, Phys.Rev., 1961, 124, 60.
51. J.R. Byberg, S.J.K. Jensen and L.T. Muus, J.Chem. Phys., 1967, 46, 131.
52. J.E. Bennett and D.J.E. Ingram, Proc.Phys.Soc., 1956, 1, 109.
53. R.F. Curl, J.Chem.Phys., 1962, 37, 779, and Mol. Phys., 1965, 9, 585.
54. P.W. Atkins, J.A. Brivati, N.Keen, M.C.R. Symons and P.A.T. Trevalion, J.Chem.Soc., 1962, 4785.
55. R.D. Burbank and F.N. Bensey, J.Chem.Phys., 1953, 21, 602.
56. P.W. Atkins and M.C.R. Symons, J.Chem.Soc., 1964 4363.
57. T. Cole, J.Chem.Phys., 1961, 35, 1169.
58. G. Breit and I. Rabi, Phys.Rev., 1931, 38, 2082.
59. J.R. Morton, J.Chem.Phys., 1966, 45, 1800.
60. R.S. Eachus and M.C.R. Symons, J.Chem.Soc., A, 1968, 2433.
61. M. Hampton, F. Herring, W. Lin and C.A. McDowell, Mol. Phys., 1966, 10, 565.
62. G.F. Kokoszka and F.E. Brickman, Chem.Comm., 1968, 349.
63. R.W. Fessenden and R.H. Schuler, J.Chem.Phys., 1966, 45, 1845.

64. A.D. Walsh, J.Chem.Soc., 1953, 2266.
65. R.A. Serway and S.A. Marshall, J.Chem.Phys., 1966, 45, 4098.
66. V.V. Gromov and J.R. Morton, Can.J.Chem., 1966, 44, 527.
67. P.W. Atkins, J.A. Brivati, A. Horsfield, M.C.R. Symons and P.A. Trevalion, Proc. Int. Symp. on Free Radicals, 6th, Cambridge, 1963.
68. P.W. Atkins, A. Horsfield and M.C.R. Symons, J.Chem.Soc., 1964, 5220.
69. G.W. Chantry, A. Horsfield, J.R. Morton, J.R. Rowlands and D.H. Wiffen, Mol.Phys., 1962, 5, 233.
70. R.S. Eachus, unpublished results.
71. R.S. Eachus, P.R. Edwards, S. Subramanian and M.C.R. Symons, J.Chem.Soc., A, 1968, 1704.
72. T.G. Kastner and W. Känzig, J.Phys.Chem. Solids, 1957, 3, 178.
73. T.E. Hasty, W.B. Ard and W.G. Moulton, Phys.Rev., 1959, 116, 1459.
74. J.E. Bennett, D.J.E. Ingram, M.C.R. Symons, P. George and J.S. Griffith, Phil.Mag. 1955, 46, 443.
75. J.C. Fayet and B. Thieblemont, Suppl.J. De Physique, 1967 28 (8-9), Ce, 93.

76. H.G. Heal, Can.J.Chem., 1959, 37, 979.
77. W.H. Zachariasen, Z.Krist., 1929, 71, 501.
78. C. Ramasatry and S.B.S. Sastry, J.Phys.Chem. Solids, 1968, 29, 399.
79. W. Buser and H. Hännisch, Helv.Chim.Acta., 1952, 35, 2547.
80. P.W. Atkins, N. Keen and M.C.R. Symons, J.Chem. Soc., 1962, 2873.
81. L.G. Harrison, R.J. Adams and R.C. Catton, J.Chem. Phys., 1966, 45, 4023.
82. W. Känzig and M.H. Cohen, Phys.Rev. Letters, 1959, 3, 509.
83. D. Schoemaker, Phys.Rev., 1966, 149, 693.
84. R.D. Brown and J.B. Peel, Aust.J.Chem., 1968, 21, 2599; 2605; 2618.
85. Z.G. Szabo, Acta.Chim.Acad.Sci.Hung., 1953, 3, 139.
86. D.F.C. Morris, J.Inorg.Nucl.Chem., 1958, 6, 295.
87. T. Cole, Proc.Nat.Acad.Sci., 1960, 46, 506.
88. I. Norman and G. Porter, Proc.Roy.Soc., 1955, A230, 399.
89. M.M. Rochkind and G.C. Pimentel, J.Chem.Phys, 1967, 46, 4481.

90. A. Arkel and I. Schwager, J.Amer.Chem.Soc., 1967, 89, 5999.
91. G. Porter and F.J. Wright, Z.Electrochem., 1957, 56, 782.
92. C. Gottfried and C. Schusterius, Z. Krist., 1932, 84, 65.
93. J.R. Byberg, J. Chem.Phys., 1967, 47, 861.
94. P.W. Atkins and D. Kivelson, J.Chem.Phys., 1966, 44, 163.
95. M.C.R. Symons, J.Phys.Chem., 1967, 71, 12.
96. R.S. Eachus, P.R. Edwards, S. Subramanian and M.C.R. Symons, Chem.Comm., 1967, 1036.
97. E.D. Morris and H.S. Johnston, J.Amer.Chem.Soc., 1968, 90, 1918.
98. A. Carrington, P.N. Dyer and D.H. Levy, J.Chem. Phys., 1967, 47, 1756.
99. T. Amano, E. Hirota and Y. Morino, J. Mol. Spectroscopy, 1968, 27, 257.
100. R.D. Spratley and G.C. Pimentel, J.Amer.Chem.Soc., 1966, 88, 2394.
101. F.J. Adrian, J.Chem.Phys., 1967, 46, 1543.
102. M.B.D. Bloom, R.S. Eachus and M.C.R. Symons, to be published.

103. L. Shields and M.C.R. Symons, Mol.Phys. 1966, 11, 57.  
L. Shields, J.Chem.Phys., 1966, 44, 1685.  
L. Shields, Trans. Faraday Soc., 1966, 62, 1042.
104. R.A. Zhitnikov, N.V. Kolesnikov and V.S. Kosyakov, Soviet Phys. - JETP, 1963, 16, 839.  
R.A. Zhitnikov and N.V. Kolesnikov, Soviet Phys. - JETP., 1964, 19, 65.
105. H.J. Bower, M.C.R. Symons and D.J.A. Tinling, "Radical Ions," ed. E.T. Kaiser and L. Kevan, Interscience, New York, 1968, 417.
106. J.C. Russell, Can.J.Chem., 1967, 45, 839.
107. R. Livingston, H. Zeldes and E.H. Taylor, Disc. Faraday Soc., 1955, 19, 166.
108. G.T. Tramell, H. Zeldes and R. Livingston, Phys. Rev., 1958, 110, 630.
109. P.J. Sullivan and W.S. Koski, J.Amer.Chem.Soc., 1962, 84, 1; 1964, 85, 384.
110. R.S. Alger, T.H. Anderson and L.A. Webb, J.Chem. Phys., 1959, 30, 695.
111. D.H. Brown and F.S. Dainton, Trans. Faraday Soc., 1966, 62, 1139.
112. J. Zimbrick and L. Kevan, J. Chem.Phys., 1967, 47, 5000.

113. T.F. Young, Rec.Chem.Prog., 1951, 12, 81.
114. G.E. Adams, J.H. Baxendale and J.W. Boag, Proc. Chem.Soc., 1963, 241.
115. W. Köhnlein and J.H. Venable, Nature, 1967, 215, 618.
116. W.A. Weyl, "Coloured Glasses," Dawsons of Pall Mall, London, 1959.
117. W. Gomes, Trans. Faraday Soc., 1963, 59, 1648.
118. J. Van der Vorst and K.B. Dekeyser, Phil.Mag., 1956, 1, 882.
119. T. Feldmann, A. Treinin and V. Voltera, J. Chem. Phys., 1965, 42, 5366.